INVESTIGATIONS INTO STATIC AND DYNAMIC ASPECTS OF VOLTAGE STABILITY

A THESIS SUBMITTED

IN PARTIAL FULFILLMENT OF THE REQUIREMENTS

FOR THE DEGREE OF

DOCTOR OF PHILOSOPHY

By

Kailash N. Srivastava

to the

DEPARTMENT OF ELECTRICAL ENGINEERING

INDIAN INSTITUTE OF TECHNOLOGY

KANPUR-208016 INDIA

DECEMBER 1994

dedicated

to

my Late Father

EE - 1994 - D - SRI - INV

Certificate

It is certified that this work entitled **INVESTIGATIONS INTO STATIC AND DYNAMIC ASPECTS OF VOLTAGE STABILITY**, by *Kailash N. Srivastava* has been carried out under my supervision and that this work has not been submitted elsewhere for a degree.

(Dr Suresh C. Srivastava)
Associate Professor
Department of Electrical Engineering
Indian Institute of Technology
Kanpur–208016 India

THESIS SUPERVISORS

During the initial period from December 27, 1991 to April 29, 1994, this work for the award of the Ph D degree submitted by Mr K.N Srivastava was carried out under the co-supervision of Prof. S.C Srivastava and Prof P.K Kalra. Thereafter, Prof S C. Srivastava served as the sole supervisor

Dean of Academic Affairs

Synopsis

Name of Student Kailash N Srivastava Roll no 9110466
Degree for which submitted Ph D Department Electrical Engineering

Thesis Title **INVESTIGATIONS INTO STATIC AND DYNAMIC ASPECTS OF VOLTAGE STABILITY**

Name of thesis supervisor Dr Suresh C Srivastava

Month and year of thesis submission: December 1994

Voltage stability has been defined [1] as the ability of the system to maintain voltage so that when load admittance is increased, load power also increases and both power and voltage remain controllable Voltage collapse is the process by which voltage instability leads to very low voltage profile in a significant part of the system resulting into partial or total blackout. oltage stability studies have been carried out for variation (increase) in system loading or for contingency conditions

Most of the works have considered voltage stability as static phenomena due to slow variation of voltage over a long time until it reaches near to maximum loadability or collapse point Load flow equations have been used as model and to explain the phenomena, singularity of Newton-Raphson load flow Jacobian has been observed [2–4]. Minimum singular value and condition number of the load flow Jacobian [5–7] have been popularly used as indicators to predict static voltage stability in A C systems Several other techniques such as optimisation method [8], multiple load flow solutions [9] etc have been used to predict extreme loading conditions and static voltage stability margin

From the literature survey, it appears that most of the works [10, 11] on voltage stability analysis of AC-DC systems have represented AC systems by their Thevenin equivalent The concept of minimum singular value and condition number has not been applied to combined AC-DC systems considering the detailed representation of AC systems

One of the recent concerns of maximising voltage stability margin has led the researchers to find out new objectives for rescheduling real and reactive output of the sources An optimal generation scheduling scheme with respect to maximisation of minimum singular value of the Jacobian has been presented in ref [12] Traditionally, optimal power flow (OPF) is run for generation rescheduling in view of minimisation of the total fuel cost of generation or minimisation of the system transmission loss From the literature survey it appears that the effect of the various optimal power flow schemes on the voltage stability margin has not been explored

One important outcome of the studies reported in the literature is the general consensus that bifurcations in underlying mathematical models of a power system are closely linked with various types of instabilities This is especially true for voltage collapse precipitated by the slow variation in a system parameter such as load etc A bifurcation is a qualitative change in the phase portrait of a dynamical system that occurs as a system bifurcation parameter is varied

Bifurcations and chaos have been demonstrated by several researchers [13] in simple models of power system Hopf bifurcation phenomena has been studied in ref [14–16]. A fourth order generator model along with excitation system have been considered in ref [15] and it has been shown that a complex pair of eigenvalue associated with excitation system results in Hopf bifurcation Most of the works [17, 18] showing chaotic invariant set have considered only the load dynamics along with swing equations and have observed only the period doubling route to chaos

The literature survey reveals that the detailed model of induction motor with speed dependent generalised loading and speed governing control loop has not been considered Also the dynamics of various other dynamic elements such as OLTC and SVS have not been investigated

The bifurcation and chaos are unwanted phenomena in the power system Hopf bifurcation reduces the stability margin, especially the subcritical Hopf bifurcation in which the operating point is stable but its region of attraction is reduced by the surrounding unstable periodic orbit A power system though being dynamically stable can exhibit a bounded behaviour when the stable operating print is perturbed to attracting region of chaos The chaotic systems have continuous broad band spectrum and can introduce harmonics especially low frequency harmonics in the system, even in the absence of any harmonic source

One of the simplest ways to avoid bifurcation and chaos is to move the system out of the chaotic region by restricting the parameter to enter this region However, it reduces the system loadability Recently new devices for the control of voltage and power have been developed [19] The prominent amongst these components are static var compensators (SVC), static phase angle regulator (PAR) and controllable services capacitors (CSC) The effectiveness of these devices for controlling bifurcation and chaos has not been explored

Therefore, the motivation behind the work reported in this thesis are

(i) To extend the concept of minimum singular value and condition number of load flow Jacobian to combined AC-DC systems considering the detailed representation of AC system and also to AC systems having voltage dependent loads

(ii) To explore the effect of different generation rescheduling schemes on the static voltage stability margin considering voltage dependent capabilities of synchronous machine

(iii) To observe various types of local bifurcations such as static and Hopf bifurcations and their effect on stability considering the dynamic models of generator and loads, to determine critical loading and control parameters' values and to ascertain the predominant states causing Hopf bifurcation using participation analysis

(iv) To observe various types of global bifurcations and chaos considering the OLTC, SVS, load and generator dynamics and possibility of voltage collapse due to these phenomena

(v) To study the effectiveness of FACTS devices in eliminating dynamic bifurcation and chaos

A brief description of the work reported in the thesis is given below

Chapter 1 introduces various aspects of voltage stability and presents the state-of-art survey on the subject

In Chapter 2 the minimum singular value and condition number of load flow Jacobian has been used to predict static voltage stability of integrated AC systems considering voltage dependent characteristics of loads and extended, for the first time, to combined AC-DC systems considering detailed representation of AC systems. The effect of control mode switching in the DC link and bus type switching in handling the reactive power limits of generators on the static voltage stability has also been demonstrated

In Chapter 3 four different schemes of generation rescheduling such as minimisation of total cost of generation, system transmission loss, maximisation of minimum singular value and a

new scheme have been used to maximise the static voltage stability margin Voltage dependent capabilities of synchronous machines have been considered in the model The new proposed scheme of generation rescheduling has consistently resulted into maximum voltage stability margin for various loading conditions

Chapter 4 investigates the local bifurcations namely static and Hopf bifurcation in various sample power systems Effect of static bifurcation on power system stability has been demonstrated by studying the associated unstable manifold of type-1 unstable equilibrium points on the stability boundary Center manifold theory has been used for studying the stability of Hopf bifurcation and determining critical values of parameters The effect of local bifurcations on the stability in parameter space has also been studied

Chapter 5 presents the sample system study results on observance of various types of global bifurcations such as period doubling bifurcation, bifurcation of periodic orbit to torus, chaos via period doubling bifurcations & via torus breakdown and boundary crisis Lyapunov exponents and dimension of the attractor have been determined Broad band frequency spectrum has been observed under chaotic oscillations Occurrence of voltage collapse due to subcritical Hopf bifurcation and boundary crisis has been demonstrated

Chapter 6 demonstrates the application of FACTS devices such as PAR, SVC and CSC for control of bifurcation and chaos A first order delay model of these devices have been considered It has been found that the dynamic bifurcations and chaos can be eliminated with proper selection of control signals and the controller gain parameters

Chapter 7 concludes the main findings in this thesis and gives suggestions for further work in this area

References

[1] IEEE system dynamic performance subcommittee, *Voltage Stability of Power Systems Concepts, Analytical Tools and Industry Experience*, IEEE document 90TH0358-2-PWR-1990

[2] P W Sauer and M A Pai, *Power System Steady-State Stability and the Load Flow Jacobian*, IEEE Trans on Power Systems, Vol 5, No 4, Nov 1990, pp 1374-1383

[3] V A. Venikov, V A Stroev, V I Idelchick and V A Torasov, *Estimation of System Steady State Stability in Load Flow Calculations*, IEEE Transactions on Power Apparatus and

Systems, Vol 94, May/June 1975, pp 1034-1040

[4] H G Kwatny, A K. Pasrıja and L Y Bahar, *Statıc Bıfurcatıon ın Electrıc Power Networks Loss of Steady-State Stabılıty and Voltage Collapse*, IEEE Trans on Cırcuıts and Systems, Vol 33, No 10, October 1986, pp 981-991

[5] M A Paı and M G O' Grady, *Voltage Collapse Analysıs wıth Reactıve Generatıon and Voltage Dependent Constraınts*, Journal of Electrıc Machınes and Power Systems, Vol 17, No 6, 1989, pp 379-390

[6] P A Lof, T Smed, G Anderson and D J Hıll, *Fast Calculatıon of a Voltage Stabılıty Index*, IEEE Trans. on Power Systems, Vol. 7, No 1, Feb 1992, pp 54-64

[7] A Tıranuchıt, L M Ewerbrıng, R A Duryea, R J Thomas and F T Luk, *Towards a Computatıonally Feasıble On-Lıne Voltage Instabılıty Index*, IEEE Trans on Power System, Vol 3, No 2, May 1988, pp 669-675

[8] T. Van Cutsem, *A Method to Compute Reactıve Power Margıns wıth respect to Voltage Collapse*, IEEE Trans on Power Systems, Vol 6, No 1, Feb 1991, pp 145-156

[9] Y Tamura, K Iba and S Iwamoto, *Relatıonshıp between Instabılıty and Multıple Load Flow Solutıons ın Electrıc Power Systems*, IEEE Trans on Power Systems, Vol 102, No 2, May 1983, pp 1115-1125

[10] Y Yoshıda, *Development of a Calculatıon Model of AC Voltage Stabılıty ın HVDC Transmıssıon System*, Electrıcal Engg ın Japan, Vol 94, No 2, 1974, pp 77-85.

[11] T Hayashı, *Analysıs of Voltage Instabılıty of AC-DC Interconnected System*, Electrıcal Engg ın Japan, Vol 101, No 4, 1981, pp 46-53

[12] A Tıranuchıt and R.J Thomas, *A Posturıng Strategy agaınst Voltage Instabılıtıes ın Electrıc Power Systems*, IEEE Trans on Power Systems, Vol 3, No 1, Feb 1988, pp 87-93

[13] P Varaıya, F Wu and H D Chıang, *Bıfurcatıon and Chaos ın Power System A Survey*, EPRI TR-100834, August 1992, Fınal Report

[14] E H. Abed and P Varaıya, *Nonlınear Oscıllatıons ın Power Systems*, Int Jr of Electrıc Power and Energy Systems, Vol 6, No 1, Jan 1984, pp 37-43

[15] C Rajagopalan, P W Sauer and M A Pai, *Analysis of Voltage Control Systems exhibiting Hopf Bifurcation*, Proceedings of 28th IEEE Conference on Decision and Control, Tampa, FL, pp 332-335, 1989

[16] V Ajjarapu and B. Lee, *Bifurcation Theory and its Application to Nonlinear Dynamical Phenomena in an Electric Power System*, IEEE Trans on Power Systems, Vol 7, No 1, Feb 1992, pp 424-431

[17] H D Chiang, C C Liu, P Varaiya, F F Wu and M G Louby, *Chaos in a Simple Power System*, IEEE Trans on Power Systems, Vol 8, No 4, Nov 1993, pp 1407-1417

[18] H O Wang, E H Abed and A M A Hamdan, *Bifurcation, Chaos and Crises in Voltage Collapse of a Model Power System*, IEEE Trans on Circuits and Systems—I Fundamental Theory and Applications, Vol 41, No 4, March 1994, pp 294-302

[19] N G Hingorani, *Flexible AC Transmission*, IEEE Spectrum, Vol 30, No 4, April 1993, pp 40-45

Acknowledgement

On the completion of this thesis, I take this opportunity, with pleasure, to place on record my profound sense of gratitude and indebtedness to my supervisor, Dr S C Srivastava, for his invaluable guidance, unfailing support, and constant encouragement that he has bestowed on me and also for his tremendous patience with which he has lived with my follies My association with him been extremely remarkable and fruitful. I must say, I have all the pride in working with him

I am extremely grateful to Professors L P. Singh, S S Prabhu, Sachchidanand, S Pushpavanam, A Ghosh, M R M Rao, U B Tewari and R Arora for their keen interest evinced in me and also for the useful discussions that I had with them I must acknowledge the kind gesture of Professor S S Prabhu with which he always found time off his busy schedule whenever I approahed him for any discussion I will always recall the thought provoking discussions with Dr P K Kalra in the beginning days of my stay

My interaction with various researchers through *email* has been extremely helpful and I must acknowledge the courtesy and interest with which they always responded to me The prominent amongst them are Professors M A Pai, P Varaiya, E H Abed, F M A Salam, C A Canizares, D J Hill, Ian Dobson, M Pavella, Thierry Van Cutsem, J. Guckenheimer, E J Doedel, M Begovic, T J Overbye, R A. Schlueter, Mani Venkatasubramanian, and Mr P A Lof I must place on record the kind gesture and interest with which Professors E J Doedel, J Guckenheimer and C A Canizares provided me some of the softwares that proved very handy in the studies

The financial support received from the Central Board of Irrigation and Power, New Delhi vide grant no GIA no F-98-P and from the Council of Scientific and Industrial Research, New Delhi vide grant no CSIR/3(7005-A)/94-Pool is gratefully acknowledged

My association and interaction with my fellow researchers M/s S N Singh, S K Joshi and D M Vinod Kumar have been of immense purpose Without their unfailing support and help, it would have been hard for me to bring out this thesis in the form it appears today My

association with the other research-fellows, M/s Nagoree, Shanker, Kannan and Gautam will be memorable

Me and my family will always cherish the affection and attention received from Dr S C Srivastava, Professor L P Singh, Professor U B Tewari and members of their family during our stay over this campus The cooperation received from my friends, namely Mr R K Mishra and Mr K Singh of UPSEB Panki, and their family is gratefully acknowledged

Finally, I express my sincere feelings to my mother, wife and children for their patience, cooperation and understanding during the course of this thesis

(Kailash N. Srivastava)

Contents

List of Figures

List of Tables

Chapter 1

Introduction

1.1 General

A modern interconnected power system network can be described as highly nonlinear and stressed system. Being one of the most complex man made dynamical system, its stability and control has always been challenging The power system stability may be broadly defined as the property of the system that enables it to remain in a state of operating equilibrium under normal operating conditions and to regain an acceptable state of equilibrium after being subjected to a disturbance [176, 189] Instability in a power system may be manifested in many different ways depending upon the system configuration and operating mode Traditionally, the problem of stability has been one of maintaining synchronous operation — *rotor angle stability* However, due to economic and environmental pressures the power system of today is being operated close to the maximum loadability limit, and is facing the problem of maintaining the required bus voltage [92, 130, 146] — *voltage stability*

1.1.1 Voltage Stability, Voltage Collapse and Voltage Security

Some of the terms related to voltage stability have been formally defined in IEEE report [73] and by Concordia [82] which are given below

- *Voltage stability* is the ability of a system to maintain voltage so that when load admittance is increased, load power will increase, and so that both power and voltage are controllable
- *Voltage collapse* is the process by which voltage instability leads to very low voltage profile in a significant part of the system

- *Voltage security* is the ability of a system, not only to operate stably, but also to remain stable (as far as the maintenance of system voltage is concerned) following any reasonable credible contingency or adverse system change.

Voltage stability encompasses a wide range of phenomena. It has been treated as fast phenomena by engineers involved with induction motor loads or HVDC links It has also been viewed as slow phenomena by those involved with on load tap changer dynamics of transformers

1.1.2 (Voltage) Angle Vs Voltage (Magnitude) Stability

The problem of rotor angle instability is well understood and documented [7, 14, 25, 109, 176] However, the voltage instability has recently attracted the attention of researchers world wide and is an active area of research

Just as real power is the key variable to rotor angle instability analysis, reactive power is central to voltage stability analysis Deficit of reactive power either locally or globally leads to poor voltage profile and with increase in loadings it may lead to voltage collapse

Imbalances in active power input to the generators and their electrical power outputs are balanced by the changes in angular momentum of the rotor resulting into change in the average system frequency, whereas the imbalances in the reactive power result into change in the bus voltage profile affecting the energy stored in shunt capacitors and reactors Usually the R/X ratio of the transmission system is very small Because of low resistances of the network the flow of active energy between the generators and the loads is lightly damped However, because of large reactance of the transmission system, the flow of reactive power is highly damped, causing the voltage instability to start as a local phenomenon The angle instability leads to loss of synchronism and operation of protective relays causing disconnection of loads and/or system breaking into separate subsystems The problem of angle instability has now been overcome due to improvements in the design philosophy of machines and control strategy such as power system stabilisers, fast excitation system etc The loss of voltage (magnitude) stability follows upon a change in either the reactive power supply or demand beyond the ability of the system to accommodate it by changes in bus voltage magnitude resulting into stalling of induction motors and/or disconnection of equipments due to protective relay operation leading to cascade tripping The power factors of the generators affect the voltage stability Under voltage instability conditions, some of the existing controls may prove counter productive

1.2 State-of-the-Art

Voltage collapse was identified and analysed for simple power systems even in the first half of this century as given in text books [1,3,4] However, only recently the problem of voltage stability has become serious operating concern The voltage stability studies have been carried out on *static* as well as on *dynamic considerations* A large number of papers exist in the area of voltage stability and it is difficult to present a detailed review of all of them Hence, only a representative survey of literature relevant to the work carried out in the present thesis is presented in this section

Mercede et al [48] and Chow et al [67] presented a framework for analysis and prediction of voltage stability problems Depending upon the nature of disturbance and the subsystem dynamics, the voltage instability may be regarded as slow or fast phenomena [121] A special issue on the subject [129] contains some of the state-of-the-art papers

The static or steady state voltage stability has often been regarded as *viability* problem suitable for static power flow[1] The ability to transfer reactive power from production sources to consumption nodes during steady state operating conditions is a significant aspect of voltage stability A 1987 CIGRE report [42] recommends analysis methods and power system planning approaches based on static models The singularity of power flow Jacobian has been linked to steady state stability [6,36,78] and its positive definiteness has been proved to be the sufficient condition for an operating point to be small disturbance stable [41,56] Various indices for prediction of steady state voltage stability margin has been presented in CIGRE report [169]

It has been observed that when the operating point reaches the nose point of $P-V$ or $Q-V$ curve, the sensitivity of bus voltage to the load power becomes alarmingly high and at the nose of $P-V$ or $Q-V$ curve, $\frac{dV}{dP}$ or $\frac{dV}{dQ}$ becomes infinity [8] The concept of load flow Jacobian sensitivity has been used by Flatabo et al [69, 134] and has been applied on the Norwegian system for maintaining required security level The sensitivity of total reactive power generation to variation in real and reactive load has also been proposed as security index by Carpentier [28] and Begovic et al [102] Carpentier has termed this index as Voltage Collapse Proximity Indicator (VCPI) Another sensitivity based indirect criteria which relates the change in generator voltage E with corresponding change in load bus voltage $V_j(\frac{dE}{dV})$ has been proposed by Venikov [8] and used by Borremans et al [27] for voltage stability studies At the point of voltage instability, $\frac{dE}{dV}$ becomes zero, meaning thereby the load voltage can not be controlled by

[1] *Load flow* and *power flow* have been interchangeably used in this thesis

generators, a fact which has been mathematically proved by Hiskens et al. [56,84]. The deficit of reactive power has been cited as one of the important reasons responsible for voltage instability by Lachs [31]. Tamura et al. [24] observed that voltage instability is closely related to multiple load flow solutions which are caused by the nonlinear nature of load flow equations. A heavily loaded system has two very close power flow solutions. One is the higher voltage power flow solution which is usually obtained by the conventional power flow calculations and the other is the lower voltage solution which is obtained by the methods proposed in ref. [10]. When these two solutions coalesce, a saddle node bifurcation occurs. The proximity of these two solutions have been used by many researchers as an index for voltage stability margin. Use of energy based measures has been suggested to determine the closeness of multiple solution [68,90,91,155]. Use of P–V and Q–V curves have also been made to assess the vulnerability of an operating point to voltage collapse [49,53,75,94,97,103,116,126,181]. Using a conventional power flow programme, the maximum power transfer can be found by a binary search without computing an entire P–V curve. Near the nose point, the Newton-Raphson algorithm may diverge. To overcome this difficulty, the continuation power flow method has been introduced by Ajjarapu et al. [100], Canizares et al. [166] and Iba et al. [86].

The divergence of power flow solution has been used as one of the indicators for assessing voltage instability [37,71]. However, the divergence of power flow may also be due to the load flow Jacobian being ill-conditioned. The proximity of load flow Jacobian to singularity can be better measured in terms of its minimum singular value [51,52,58,113,141–143,179]. A fast algorithm based on parallel processing for computation of minimum singular value has been suggested by Tiranuchit et al. [52]. A minimum singular value based security index for scheduling real and reactive power output of sources has also been suggested by Tiranuchit et al. [51]. Lof et al. [113,141] presented a fast algorithm based on inverse iteration to compute minimum singular value and tested it on a large system. Prediction of static voltage stability has also been made by Lof et al. [142,179] using minimum singular value of power flow Jacobian and considering voltage dependent reactive capability of generators. Pai et al. [58] considered an exponential type voltage dependent load model and considered a new index called condition number for static voltage stability prediction. Begovic et al. [81] demonstrated that by minimising the weighted sum of the absolute values of control actions subject to equality constraints (real and reactive power balance equations) and inequality constraints (limits on the state variables, real and reactive power generations) voltage stability could be improved.

Eigenvalue analysis has been used to assess static voltage stability and sensitivity analysis has

been carried out to determine critical group of buses responsible for voltage collapse [64,93,110, 148,175] Participation analysis has also been carried out to determine participation of various states in different modes of power system model by Hamdan [135] and Rajagopalan et al [61] The concept of coherency among load buses with respect to voltage dynamics was introduced by Begovic et al [65] and Vargas et al [159] An algorithm for approximate assessment of minimum singular value [65] and eigenvalue [159] of Jacobian was presented based on partial state information about network obtained from coherent clusters of load buses Ajjarapu et al [162] have presented a scheme to improve voltage stability margin by use of fixed capacitors at appropriate locations However, the use of fixed capacitors may prove detrimental to voltage stability in some operating conditions (example 11 2 of ref [8] and example 14 1 of ref [176])

The prevailing approach to real time control of voltage collapse (as opposed to system planning) consists of security monitoring coupled with algorithms for allocation of resources for minimising risk of voltage collapse [102,140,152] A related problem is that of maintaining maximum distance (in parameter space) to the set of parameter values at which bifurcation from the nominal operating point occurs The development of voltage stability indices is essential to studies of this kind [67,107,132,133,153,163,178] Dobson [106] has studied the geometry of saddle node bifurcation and presented a method to avoid saddle node bifurcation [107] Overbye [182,183] has also presented a method to restore power flow solvability

On dynamic considerations, the problem of voltage instability has been studied by solving set of nonlinear differential algebraic equations [63,112,131,143] It has been shown that when the Jacobian associated with the algebraic system becomes singular, the system model breaks down and the load bus voltages can no longer be controlled [63,84,118,173] The eigenvalue analysis has also been carried out using dynamic models of power systems for analysis of voltage instability [61,87,115,125,144,160,186,190]

Voltage stability analysis of an AC-DC system has been studied both as a steady state as well as dynamic phenomena In steady state analysis, the converters are assumed to act very fast Dynamic voltage stability analysis of a two terminal HVDC link and a AC system are presented in ref [5,12] The influence of the short-circuit ratio (SCR), DC line resistance and control parameters on the voltage stability characteristics of the systems is highlighted In the analysis, the authors have assumed constant current and constant extinction angle (CEA) control at the rectifier and inverter terminals respectively The converter control is assumed to be of proportional type Hammad et al [30,35] and Franken et al [70] have used the concept of voltage stability factor (VSF) for steady state voltage stability analyses The VSF was defined

as the ratio of the incremental change in converter bus voltage to the incremental change in capacitive susceptance at the same bus Effect of short circuit ratio (SCR) of both rectifier and inverter AC system on voltage stability of HVDC link has been investigated by Srivastava et al [96]

With developments and increased understanding of the nonlinear dynamic system theory along with availability of inexpensive computing facility, it is being increasingly used to study the power system behaviour [161] Varaiya et al [117] presented a survey of nonlinear dynamical phenomena covering bifurcation and chaos They demonstrated that even the simplest representation of a power system can exhibit both local and global bifurcations Saddle node bifurcation was hypothesised by some researchers as the only cause of voltage collapse [36, 54, 66, 101] However, later work demonstrated the possible role of other bifurcations such as Hopf bifurcation, chaos and boundary crisis in power system voltage instability leading to voltage collapse [60, 76, 88, 122, 127, 139, 154, 191] Abed et al [26] demonstrated the effect of variable damping, frequency dependence of electrical torque, transmission line resistance and excitation control on the classical swing equation dynamics and observed the emergence of periodic orbit through Hopf bifurcation Alexander [33] demonstrated the existence of subcritical and supercritical Hopf bifurcations for different values of resistance to reactance (R/X) ratio of transmission lines A fourth order generator model along with excitation system have been considered by Rajagopalan et al [60] and it has been shown that a complex pair of eigenvalues associated with the excitation system results in Hopf bifurcation Ajjarapu et al [101] have considered a dynamic load model as suggested by Walve [40] along with generator swing dynamics and demonstrated multiple Hopf bifurcations and existence of a series of period doubling bifurcation leading to chaotic oscillations in a sample 3-bus system Hopf bifurcation has been demonstrated in synchronous motor dynamics [83]. Chen et al [47] demonstrated degenerate Hopf bifurcation in power system Frequency domain approach has been adopted by Kwatny et al [74] to study Hopf bifurcation in power system Kopell et al [17] have demonstrated the presence of chaotic invariant set in a 3 generator power system network described by swing equations using Melnikov's method Nayfeh et al [76,88] investigated a single machine (quasi) infinite bus system in which periodic orbits became unstable through a series of period doubling bifurcations that led to chaos A single generator under excitation control may exhibit chaos as demonstrated by Salam [22] Salam et al [23, 29] demonstrated that in multimachine system even the classical swing equations could exhibit complex chaotic motion called Arnold diffusion Using the same

model of power system as in [101], chaotic dynamics have been studied using Lyapunov exponents by Chiang et al [127] and voltage collapse through boundary crisis was demonstrated by Abed et al [122] and by Wang et al. [191] Lee et al. [139] investigated in detail the period doubling route to chaos using the same model of power system Liu et al [177] proposed a technique to detect chaotic behaviour by computing largest Lyapunov exponents through measured values of state variables A new bifurcation term, *singularity induced bifurcation* (SIB) was introduced and applied to power system voltage stability by Venkatasubramanian [118]

Voltage stability has also been called to be load stability [8] as the load characteristics have profound effect on the system dynamics [185] Dynamics of induction motor especially large induction motors have been reported to be crucial for voltage stability studies [99,185] Effect of various load characteristics including synchronous and induction motor loads on voltage stability have been studied [55,56,58,62,79,87,114,125,150,160,170,172,184,188] Canizares [167] have demonstrated the effect of load model on the bifurcation characteristic of the system model

The classical stability simulation of Swedish blackout on 27th December 1983 could not explain the system behaviour that led to cascade tripping This prompted the researchers to develop new load models for voltage stability studies such as by Hill [136], Walve [40], Xu et al [192] and Hill et al. [174] Probabilistic load models have also been considered in [43,149,164]

The effect of on load tap changer (OLTC) is to restore the load However it has been found to aggravate the voltage instability [15,32,57,89,119] Instability due to OLTC controls may lead to the possibility of either hunting or voltage collapse [44]. The behaviour of SVC has been studied by Hiskens et al [111] under voltage collapse

Recently, the system stability has also been linked to its structural stability [185] The structurally unstable set form the bifurcation surfaces In order to eliminate bifurcation and chaos, Chiang et al [127] suggested that the system parameters should be restricted to enter the range where these phenomena would be present This, however, limits system loadability It has been demonstrated by Tan et al [154] that by varying damping the bifurcation and chaos can be controlled Wang et al [157] employed a feedback law using generator speed deviation as feedback signal to control stability and amplitude of bifurcated solution

1.3 Objective of the Thesis

From the survey of literature presented in section 1 2, it appears that most of the works on voltage stability analysis of AC-DC system [5,12,35,70,96] have represented AC system by their

Thevenin equivalent. Though the concept of minimum singular value and condition number of power flow Jacobian has been successfully used in literature to assess static voltage stability of AC systems, it has yet to be applied to AC-DC systems considering the detailed representation of AC systems

One of the recent operating concerns in the power system network is to maximise the voltage stability margin A limited research efforts have been made to achieve this objective through rescheduling of real and reactive power output of the sources Tiranuchit et al [51] have used maximisation of minimum singular value as the objective for optimal rescheduling Modern energy management system (EMS) run the traditional optimal power flow (OPF) for rescheduling of sources in view of minimisation of the total fuel cost of generation or minimisation of the system transmission loss In all these formulations, fixed reactive power limits of generators have been considered Also, the effect of these optimal power flow schemes on the voltage stability margin has not been explored in the literature

One important outcome of the studies reported in the literature is the general consensus that bifurcations in underlying mathematical models of a power system are closely linked with various types of instabilities A power system is usually designed to operate at a stable fixed point and a well designed power system should not exhibit any bifurcation under normal operating range of parameters Regions of the state space, where these bifurcations and the associated instabilities in behaviour occur, are reached only under disturbances or unanticipated loading conditions Nevertheless, the study of these bifurcations are important because the region of stable operating point is determined by the location of bifurcation The detailed model of induction motors with speed dependent generalized loading and speed governing loop along with excitation system dynamics has not been considered Also the dynamics of OLTC and SVS have not been investigated for bifurcation studies

Recently new devices for the control of voltage and power have been developed [108,137,138] The prominent amongst these components are static var compensators (SVC), static phase angle regulator (PAR) and controllable series capacitors (CSC) The effectiveness of these FACTS (Flexible AC Transmission System) devices for controlling bifurcation and chaos has not yet been explored

Therefore the motivation behind the work reported in this thesis was

(i) To extend the concept of minimum singular value and condition number of load flow Jacobian to combined AC-DC systems considering the detailed representation of AC system and also to AC systems having voltage dependent loads

(ii) To study the effect of different generation rescheduling schemes on increasing the static voltage stability margin considering the voltage dependent capability of the synchronous machines and to explore a new computationally attractive scheme for generation rescheduling that maximises voltage stability margin especially under stressed condition

(iii) To observe various types of local bifurcations such as static and Hopf bifurcations and their effect on stability considering the dynamic models of generators and loads, to determine critical loading and control parameter values and to ascertain predominant states using participation analysis causing Hopf bifurcation

(iv) To observe various types of global bifurcations and chaos considering OLTC, SVS, load and generator dynamics and possibility of voltage collapse due to these phenomena and also to explore other routes to chaos than the period doubling route in power system models

(v) To study the effectiveness of FACTS devices in eliminating dynamic bifurcation and chaos

1.4 Outline of the Thesis

The present chapter introduces the problem of voltage stability, presents a brief survey of literature in the area of voltage stability & collapse and lays down the motivation of the research work presented in this thesis

In Chapter 2 the minimum singular value and condition number of the load flow Jacobian has been used to predict static voltage stability of integrated AC system considering voltage dependent characteristic of loads and extended them, for the first time, to combined AC-DC systems considering detailed representation of AC system The effect of control mode switching in the DC link and bus type switching in handling the reactive power limits of generators on static voltage stability has also been demonstrated

In Chapter 3 four different schemes of generation rescheduling using objective functions as minimisation of total cost of generation, system transmission loss, maximisation of minimum singular value and a new scheme in which slack bus reactive power injection is minimised, have been used to maximise the static voltage stability margin Voltage dependent capabilities of synchronous machines have been considered in the model

Chapter 4 investigates the local bifurcation namely static and Hopf bifurcations in sample power systems Effect of static bifurcation on power system stability has been demonstrated by

studying the associated unstable manifold of type-1 unstable equilibrium points on the stability boundary Center manifold theory has been used for studying the stability of Hopf bifurcation and determining critical values of parameters The effect of local bifurcations on the stability in parameter space has also been studied The hard limiters in excitation and speed governing control loop has been represented by a new approach using tanhyperbolic function

Chapter 5 presents the system study results on observance of various types of global bifurcations such as period doubling bifurcation, bifurcation of periodic orbit to torus, chaos via period doubling bifurcations and via torus breakdown and boundary crisis Lyapunov exponents and dimension of the attractor have been determined Broad band frequency spectrum has been observed under chaotic oscillations Occurrence of voltage collapse due to subcritical Hopf bifurcation and boundary crisis has been explored

Chapter 6 demonstrates the application of FACTS devices such as CSC, PAR and SVC for control of bifurcation and chaos A first order delay model of these devices have been considered The control signals have been selected through participation analysis and the effect of varying controller gain parameters on elimination of dynamic bifurcations have been observed

Chapter 7 concludes the main findings of the thesis and gives a few suggestions for further work in this area

Chapter 2

Static Voltage Stability Prediction of Integrated AC and AC/DC Systems

2.1 Introduction

Voltage stability, in most of the works, have been studied as *static phenomena* due to the reason that in many incidents of voltage collapse, it has been characterised as slow variation of voltage over a long time until it reaches close to the collapse point Moreover, the static consideration provides several conceptual observations about the phenomena

Several researchers such as Venikov et al [6], Kwatny et al [36] and Sauer et al [78] have linked the singularity of power flow Jacobian to the steady state stability limit Wu et al [41] and Hiskens et al [56] demonstrated that the sufficient condition for an operating point to be small disturbance stable is the positive definiteness of the power flow Jacobian Kwatny et al [36] demonstrated that the static bifurcation of load flow equations are associated with either divergence type instability or loss of causality A generic assumption in considering the power flow equations as the static model for voltage stability studies is that there is some underlying dynamics, the fixed point of which is given by the power flow equations [106] In fact, the power flow solution is a subset of the fixed point of any generic dynamic model of the power system However, the power flow Jacobian is topologically diagonally dominant and almost symmetrical matrix This implies that the possibility of instability is associated with a real eigenvalue or singularity of the power flow Jacobian Assessment of singularity of power flow Jacobians by observing the divergence of power flow solution may sometimes be misleading as the solution may also diverge due to many other reasons In view of this, other indices such as minimum

singular value and condition number have been used to determine the singularity of the power flow Jacobian

Tiranuchit et al [51,52] presented an approach to predict the occurrence of voltage collapse using singular value decomposition of the load flow Jacobian and an efficient algorithm to compute the singular value using parallel processing Lof et al [113, 141] presented a fast method based on inverse iteration scheme to compute minimum singular value of the Jacobian suitable for large size systems Pai et al [58] extended the concept of singular value decomposition for detecting voltage collapse, considering an exponential type voltage dependent loads and Q-limits of the generators, and also proposed the condition number as a new indicator

Voltage stability analysis of HVDC links has also been studied as static [35, 70, 96] and dynamic [5, 12] phenomena But in all these studies, the AC system has been represented by Thevenin equivalent

From the literature survey, it appears that the minimum singular value and condition number of the load flow Jacobian have been effectively used for the prediction of point of static voltage instability in AC system and are yet to be applied to combined AC-DC systems Moreover, in all the voltage stability studies of AC-DC systems, the AC systems have been represented as Thevenin equivalent sources and detailed representation of combined AC-DC systems has not been considered Hence, the motivation behind the work presented in this Chapter is to extend the concept based on minimum singular value and condition number of the load flow Jacobian to combined AC-DC systems considering the detailed representation of the AC system and also to AC systems having polynomial type voltage dependent load characteristics

The effect of considering reactive power limit of synchronous machines and control mode switching in DC link on occurrence of the voltage instability has also been investigated Studies have been conducted on IEEE-14 bus AC system, and its three modified configurations to include a DC link, IEEE-30 bus AC system and a 156-bus Indian system having a DC link

2.2 Singularity of Jacobian as a Condition of Voltage Collapse

The singularity of the power flow Jacobian has been utilised to determine the point of voltage collapse To illustrate the validity of this concept, consider a 2-bus system as shown in Fig 2 1 with an infinite source connected to bus-1 The real and reactive power loads ($P\&Q$) at bus-2

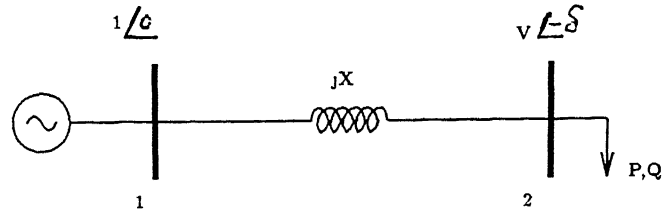

Figure 2 1 Sample AC system

are given by the following equations

$$P = \frac{V}{X} \sin \delta \tag{2 1}$$

$$Q = \frac{V}{X} \cos \delta - \frac{V^2}{X} \tag{2 2}$$

The contours of P and Q in the (V, δ) plane will look like those shown in Fig 2 2 The intersection of the contours of P and Q in the (V, δ) plane yields the steady state operating point, that is, the load flow solutions It is seen from Fig 2 2 that for a load $Q = Q_1$ and $P = P_1$, there are two solutions of voltages V_1 and V_2 Keeping $Q = Q_1$ constant, as P is increased from P_1 to P_2, V_1 decreases to V_3 and V_2 increases to V_4 If P is further increased to P_3 both the solutions coalesce at V_5 This point corresponds to static bifurcation (saddle-node) point At this point, the gradient vectors of P and Q will be collinear, that is,

$$\nabla P = \alpha \nabla Q \tag{2 3}$$

where α is a scalar quantity The power flow Jacobian for the sample system in Fig 2 1, assuming bus-1 as slack, will be

$$J = \begin{bmatrix} \frac{\partial P}{\partial \delta} & \frac{\partial P}{\partial V} \\ \frac{\partial Q}{\partial \delta} & \frac{\partial Q}{\partial V} \end{bmatrix} = \begin{bmatrix} \nabla P^T \\ \nabla Q^T \end{bmatrix} \tag{2 4}$$

Equations (2 3) and (2 4) imply that the load flow Jacobian will be rank deficient at $P = P_3$ and $Q = Q_1$ which describe the voltage collapse point Thus, the singularity of Jacobian implies the point of static voltage instability

This concept can be similarly extended to larger systems Assume a system having $(n + 1)$ buses, $(n + 1)^{th}$ being the slack bus The load flow equations can be written as,

$$\mathbf{F}(\lambda, \mathbf{X}, \mathbf{N}) = 0 \tag{2 5}$$

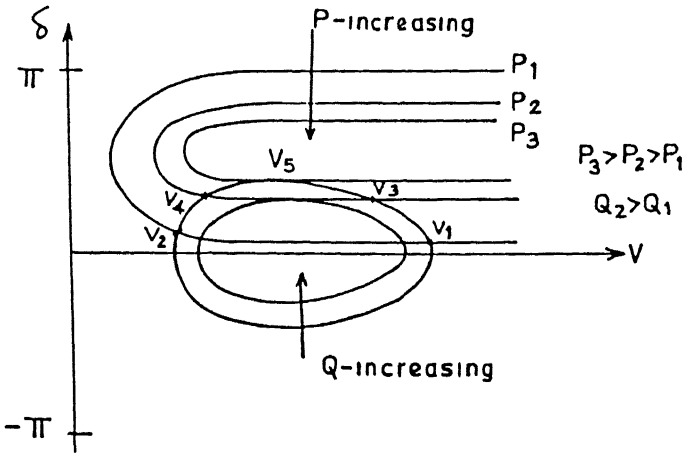

Figure 2 2 Loci of P and Q

where $\lambda = [P_1, \quad , P_n, Q_1, \quad , Q_n] \in R^{2n}$

$\mathbf{X} = [V_1, \quad , V_n, \delta_1, \quad , \delta_n] \in R^{2n}$

$\mathbf{F} = [F_1, \quad , F_{2n}] \in R^{2n}$

$\mathbf{N}$ = Network parameter such as $[\mathbf{Y_{bus}}]$

The intersection of the contours of $\mathbf{F}$ in $\mathbf{X} \in R^{2n}$ will yield a load flow solution for a given N If there exist at least two elements of $\mathbf{F}$, say F_i and F_j such that either they do not intersect or they intersect at one point only, the gradient vector associated with them will be collinear, that is

$$\nabla F_i = \alpha \nabla F_j \tag{2 6}$$

Equation (2 6) denotes the linear dependence of two rows of the Jacobian, which implies that the load flow Jacobian is rank deficient or singular One approach to test the singularity of the Jacobian for increased loading or different operating conditions in the system is to check the divergence of the solution This approach, however, sometimes gives erroneous results as the load flow may also diverge due to numerical solution difficulties A more effective index to check the singularity of the Jacobian is through calculation of the minimum singular value or condition number as described below

2.2.1 Minimum Singular Value as a Measure of Proximity to Singularity

Consider a matrix $A \in R^{n \times n}$ Let ΔA be the perturbation matrix such that $(A + \Delta A)$ is singular The notion of singularity is intimately related to the ability to compute its inverse If A is non singular, the following holds good

$$(A + \Delta A)^{-1} = (I + A^{-1}\Delta A)^{-1} A^{-1} \tag{2.7}$$

The term $(I + A^{-1}\Delta A)$ can be shown to have an inverse if $\|A^{-1}\Delta A\| < 1$, which is guaranteed if $\|\Delta A\| < 1/\|A^{-1}\|$ since $\|A^{-1}\Delta A\| < \|A^{-1}\|\|\Delta A\|$ for some suitable matrix norm $\| \|$ Hence, a measure of the nearness of matrix A to singularity is the number $\|A^{-1}\|^{-1}$

Define $\|A\|^2 = \lambda_{max}(A^T A) = \sigma^2_{max}(A)$ where $\lambda_{max}(A^T A)$ maximum eigenvalue of $A^T A$ In terms of singular values, $\|A^{-1}\| = \sigma_{max}(A^{-1})$ The singular value decomposition is given by $A = U\Sigma V^T$ where U and V are orthonormal matrices $(UU^T = I, VV^T = I)$ and $\Sigma = diag[\sigma_1, \quad , \sigma_n]$ with $\sigma_{max} = \sigma_1 \geq \sigma_2 \geq \quad \geq \sigma_n = \sigma_{min}$ Therefore, $A^{-1} = V\Sigma^{-1}U^T$ and $\|A^{-1}\|^{-1} = \sigma_{min}(A)$ Hence, minimum singular value is a measure of proximity of a matrix A to singularity

The minimum singular value of a power flow Jacobian matrix J can be computed by applying inverse iteration scheme [113, 141] The following are the steps applied for computation of minimum singular value

(i) Perform LU factorisation of J

(ii) To start the iteration scheme, choose the right singular vector v such that $\|v\| \neq 0$ To perform computations on the power flow Jacobian matrix J for minimum singular value, the components of v corresponding to bus angles were set as zero, and those for bus voltages were taken as 1 This choice results in better convergence [141]

(iii) For k^{th} iteration, solve $J^T u^k = v^k$, for the left singular vector u^k

(iv) Compute minimum singular value $\sigma^k_{min} = \frac{\|v^k\|_2}{\|u^k\|_2}$

(v) If $\|\sigma^k_{min} - \sigma^{k-1}_{min}\| \leq tol$, stop

(vi) If convergence is not achieved in step (v), the right singular vector v^k is updated for $(k+1)^{th}$ iteration by solving $Jv^{k+1} = u^k$

(vii) Compute the minimum singular value $\sigma^k_{min} = \frac{\|u^k\|_2}{\|v^{k+1}\|_2}$

(viii) If $\|\sigma_{min}^{k+1} - \sigma_{min}^{k}\| \leq tol$ stop, else go to step (iii)

This method converges rapidly when the ratio of σ_{n-1}/σ_n is much larger than 1

2.2.2 Condition Number to Test Singularity of Jacobian

The condition number of a matrix J is defined [19] as the ratio of its maximum singular value to minimum singular value

$$k(J) = \frac{\sigma_{max}(J)}{\sigma_{min}(J)} \tag{2.8}$$

A small value of $k(J)$ refers to a well conditioned matrix which is not very sensitive to perturbations On the other hand, if a matrix is highly sensitive to perturbation, it is said to be ill-conditioned and is characterised by a very large value of $k(J)$ The condition number $k(J)$ can be used to measure the nearness to singularity of the power flow Jacobian When Jacobian is singular, σ_{min} will be zero and $k(J)$ becomes infinite

For computing $k(J)$, σ_{max} is also needed in addition to σ_{min} The σ_{max} can be computed by applying inverse iteration scheme for finding the largest eigenvalue of the matrix using the following steps

(i) Choose left singular vector u such that $\|u\|_2 \neq 0$ In this work, each component of u is taken as 1

(ii) For k^{th} iteration, find the right singular vector v^k such that $v^k = J^T u^k$

(iii) Compute maximum singular value $\sigma_{max}^{k} = \frac{\|v^k\|_2}{\|u^k\|_2}$

(iv) If $\|\sigma_{max}^{k} - \sigma_{max}^{k-1}\| \leq tol$, stop

(v) If convergence is not achieved in step (iv), the left singular vector u is updated for $(k+1)^{th}$ iteration by solving $u^{k+1} = Jv^k$

(vi) Compute the maximum singular value $\sigma_{max}^{k} = \frac{\|u^{k+1}\|_2}{\|v^k\|_2}$

(vii) If $\|\sigma_{max}^{k} - \sigma_{max}^{k-1}\| \leq tol$ stop, else go to step (ii)

This method will converge rapidly when the ratio of σ_1/σ_2 is much larger than 1

2.3 Problem Formulation

2.3.1 AC System with Voltage Dependent Load Model

Voltage stability of a system is greatly affected by its load characteristics In power flow simulations loads are often modelled as function of the bus voltage magnitude Usually frequency is assumed to be constant at its rated value Steady state composite load characteristics of equivalent consumption nodes are often approximated by the polynomials [168]

$$P_L = a_0 + a_1 V + a_2 V^2 \tag{2 9}$$

$$Q_L = b_0 + b_1 V + b_2 V^2 \tag{2 10}$$

where P_L, Q_L and V are expressed in per unit and a_0, a_1, a_2, b_0, b_1, b_2 are the load coefficients By appropriately choosing coefficients in equations (2 9) and (2 10), a variety of load characteristics can be modelled The composition of loads may be different at each of the buses in a system However, a typical example of complex consumption is taken from ref [168] for the purpose of the present study as given below

$$P_L = 0\,83 - 0\,3V + 0\,47V^2 \tag{2 11}$$

$$Q_L = 6\,7 - 15\,3V + 9\,6V^2 \tag{2 12}$$

The above model has been utilised to represent loads at each of the buses in the AC system At nominal voltage ($V = 1$ pu), $P_L = Q_L = 1$ pu Since the real and reactive complex consumption of a load node is the function of voltage at that bus, the load flow Jacobian elements corresponding to derivatives of P and Q with respect to V will be modified If H, L, M and N are the submatrices of the AC system load flow Jacobian corresponding to $\frac{\partial P}{\partial \delta}$, $\frac{\partial P}{\partial V}V$, $\frac{\partial Q}{\partial \delta}$, and $\frac{\partial Q}{\partial V}V$ terms, the Newton-Raphson (N-R) equations with voltage dependent loads will be of the form

$$\begin{bmatrix} \Delta P \\ \Delta Q \end{bmatrix} = \begin{bmatrix} H & L' \\ M & N' \end{bmatrix} \begin{bmatrix} \Delta \delta \\ \frac{\Delta V}{V} \end{bmatrix} \tag{2 13}$$

where only diagonal elements of the submatrices L' and N' are modified as follows (say corresponding to bus-p)

$$L'_{pp} = L_{pp} + (a_1 V_p + 2a_2 V_p^2) \tag{2 14}$$

$$N'_{pp} = N_{pp} + (b_1 V_p + 2b_2 V_p^2) \tag{2 15}$$

The off-diagonal elements remain unaltered

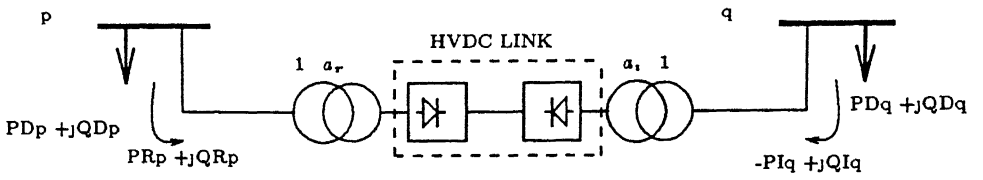

Figure 2 3 Sample HVDC link

2.3.2 AC/DC System

For steady state voltage stability analysis of an AC-DC system, the steady state performance equations of DC link can be integrated in the AC power flow equations

Consider a monopolar HVDC link connected between two AC buses p and q, as shown in Fig 2 3 The performance equations can be written as

$$V_{dR} = V_{dI} + R_d I_d \tag{2 16}$$

$$V_{dR} = k_1 a_R V_p \cos\alpha_R - k_2 X_c I_d \tag{2 17}$$

$$V_{dI} = k_1 a_I V_q \cos\gamma_I - k_2 X_c I_d \tag{2 18}$$

$$P_{Rp} = V_{dR} I_d \tag{2 19}$$

$$P_{Iq} = V_{dI} I_d \tag{2 20}$$

$$S_{Rp} = |P_{Rp} + jQ_{Rp}| = k k_1 a_R V_p I_d \tag{2 21}$$

$$S_{Iq} = |-P_{Iq} + jQ_{Iq}| = k k_1 a_I V_q I_d \tag{2 22}$$

$$Q_{Rp} = \left(S_{Rp}^2 - P_{Rp}^2\right)^{1/2} \tag{2 23}$$

$$Q_{Iq} = \left(S_{Iq}^2 - P_{Iq}^2\right)^{1/2} \tag{2 24}$$

where k, k_1 and k_2 are constants and their value are taken [18] as $k = 0\ 995$, $k_1 = \frac{3\sqrt{2}}{\pi}$, $k_2 = \frac{3}{\pi}$

In the above equations, V_p and V_q are rectifier and inverter side AC bus voltages, V_{dR} and V_{dI} are the DC voltages on rectifier and inverter sides, a_R & a_I the rectifier and inverter side

converting transformer tap ratio, α_R the firing angle of rectifier, γ_I the extinction angle of inverter, P_{Rp} & Q_{Rp} the real and reactive power drawn by the rectifier from AC bus, P_{Iq} & Q_{Iq} the real power injection into AC bus and reactive power drawn by the inverter from AC bus respectively and I_d the DC line current $S_{Rp} = |P_{Rp} + \jmath Q_{Rp}|$ and $S_{Iq} = |-P_{Iq} + \jmath Q_{Iq}|$ are the apparent powers drawn by the converters R_d is the DC line resistance and X_c the commutating reactance The following choice of base quantities have been made to define p u system for interfacing equations of DC link with equations for AC system

For AC system S_B three-phase power base
V_B line to-line voltage base
I_B (current base) $= \frac{S_B}{\sqrt{3}V_B}$
For DC system $S_B^{dc} = S_B$, $V_B^{dc} = V_B$, $I_B^{dc} = \sqrt{3}I_B$

The above performance equations (2 16) to (2 24) involve seven DC variables

$$X_{dc} = [V_{dR}, V_{dI}, I_d, a_R, a_I, \alpha_R, \gamma_I] \tag{2 25}$$

Only three equations out of equations (2 16) to (2 24) are independent Hence, in order to have a unique solution, four variables should be prespecified In the normal operation of an HVDC link, one terminal controls the voltage and the other the current in the DC link Usually under normal operation, the inverter controls the voltage and the rectifier controls the current in the DC link When the AC voltage at the rectifier goes down, the rectifier may hit minimum α_R In such situation, the voltage is controlled by the rectifier and the current by the inverter When the inverter is controlling DC voltage, the possible combinations of variables to be prespecified, result into four possible control modes C_1 to C_4 as given in Table 2 1 When the rectifier is controlling the voltage three control modes C_5 to C_7 are possible depending on the combination of variables given in Table 2 1 In this formulation the tap ratios a_R and a_I are treated as continuous variables Equations (2 14) to (2 24), with any combination of the four prespecified variables as in Table 2 1, will be a polynomial in V_p and V_q

A DC link in an integrated AC-DC system may exist in any of the following configurations

Case–A a DC link forming a part of an AC system with no AC line in parallel
Case–B a DC link forming a part of an AC system with an AC line in parallel
Case–C a DC link acting as an asynchronous tie between two AC systems

Table 2 1 Control Modes of HVDC Link

Control Mode	Specified Variables
C_1	$\alpha_R, \gamma_I, V_{dI}, P_{dI}$
C_2	$a_R, \gamma_I, V_{dI}, P_{dI}$
C_3	$\alpha_R, \gamma_I, a_I, P_{dI}$
C_4	$a_R, a_I, \gamma_I, P_{dI}$
C_5	$a_R, \alpha_R, a_I, P_{dI}$
C_6	$\alpha_R, \gamma_I, \alpha_R, P_{dI}$
C_7	$\alpha_R, a_I, V_{dI}, P_{dI}$

The AC-DC power flow model used in the present study is due to Smed et al [95] Since the converters have been considered as loads on AC buses, the elements of the mismatch vector at buses p and q will be modified as follows

$$\Delta P_p = \Delta P_p^{ac} - P_{Rp}(V_p, V_q, X_{dc}) \tag{2 26}$$

$$\Delta Q_p = \Delta Q_p^{ac} - Q_{Rp}(V_p, V_q, X_{dc}) \tag{2 27}$$

$$\Delta P_q = \Delta P_q^{ac} + P_{Iq}(V_p, V_q, X_{dc}) \tag{2 28}$$

$$\Delta Q_q = \Delta Q_q^{ac} - Q_{Iq}(V_p, V_q, X_{dc}) \tag{2 29}$$

where ΔP^{ac} and ΔQ^{ac} are the real and reactive power mismatches without considering the DC link

The modifications in the Newton-Raphson (N-R) load flow equations to include the DC link for the three possible configurations is described below

Cases–A and B: Since the real and reactive power consumed by the converters are functions of only AC bus voltage magnitudes, the load flow Jacobian elements corresponding to the derivatives of P and Q with respect to V will be modified If H, L, M and N are the submatrices of the AC system load flow Jacobian corresponding to the $\frac{\partial P}{\partial \delta}$, $\frac{\partial P}{\partial V}V$, $\frac{\partial Q}{\partial \delta}$, and $\frac{\partial Q}{\partial V}V$ terms, the N-R equations for the AC-DC system will be of the form

$$\begin{bmatrix} \Delta P \\ \Delta Q \end{bmatrix} = \begin{bmatrix} H & L' \\ M & N' \end{bmatrix} \begin{bmatrix} \Delta \delta \\ \frac{\Delta V}{V} \end{bmatrix} \tag{2 30}$$

where the modified elements of the submatrix L' will be

$$L'_{pp} = L_{pp} + V_p \frac{\partial P_{Rp}}{\partial V_p} \tag{2 31}$$

$$L'_{pq} = L_{pq} + V_q \frac{\partial P_{Rp}}{\partial V_q} \tag{2 32}$$

$$L'_{qp} = L_{qp} - V_p \frac{\partial P_{Iq}}{\partial V_p} \tag{2 33}$$

$$L'_{qq} = L_{qq} - V_q \frac{\partial P_{Iq}}{\partial V_q} \tag{2 34}$$

The submatrix N' is also modified on similar lines The attractive feature of this formulation is that only four mismatch equations and upto eight elements of the Jacobian have to be modified and no new variables or equations are added to the solution vector when a DC link is considered in the power system network

Case–C: Consider two AC systems (systems A and B) connected by a DC link The methodology described for Cases–A and B for modifying the N-R load flow equations can also be extended to this case Both the systems have to be handled simultaneously, that is, two slack buses, one in each system, are required to be considered If H_A, L_A , M_A , and N_A represent the Jacobian submatrices of AC system A and H_B, L_B , M_B , and N_B for the system B, the modified N-R load flow equations for the two AC systems and the DC link combined will be

$$\begin{bmatrix} \Delta P_A \\ \Delta P_p \\ \Delta Q_A \\ \Delta Q_p \\ \Delta P_B \\ \Delta P_q \\ \Delta Q_B \\ \Delta Q_q \end{bmatrix} = \left[\begin{array}{cc|cc} H_A & L'_A & & \\ & & & L'_{Aq} \\ M_A & N'_A & & \\ & & & N'_{Aq} \\ \hline & & H_B & L'_B \\ & L'_{Bq} & & \\ & & M_B & N'_B \\ & N'_{Bq} & & \end{array}\right] \begin{bmatrix} \Delta\delta_A \\ \Delta\delta_p \\ \Delta V_A/V_A \\ \Delta V_p/V_p \\ \Delta\delta_B \\ \Delta\delta_q \\ \Delta V_B/V_B \\ \Delta V_q/V_q \end{bmatrix} \tag{2 35}$$

where $N'_{Aq} = V_q \frac{\partial Q_{Rp}}{\partial V_q}$

$L'_{Aq} = V_q \frac{\partial P_{Rp}}{\partial V_q}$

$L'_{Bp} = -V_p \frac{\partial P_{Iq}}{\partial V_p}$

$N'_{Bq} = V_p \frac{\partial Q_{Iq}}{\partial V_p}$

The elements of N'_A, N'_B, L'_A and L'_B will be similar to those defined for Cases–A and B For predicting the voltage collapse, the singularity of the Jacobian, as defined in equation (2 30) for Cases–A and B and in equation (2 35) for Case–C of the combined AC-DC systems, can be studied

2.4 Computational Procedure

2.4.1 AC System

Voltage collapse study for the real and reactive loads at all the buses were increased simultaneously by a loading factor α ($\alpha \geq 1$) till the load flow Jacobian approached to singularity The load flow was solved for each loading condition The minimum singular value and condition number were computed for each load flow solution In each iteration of the load flow, Q-limits of the generators were checked When a Q-limit of the generator bus violated, it was converted to a PQ type bus

2.4.2 AC/DC System

For voltage collapse study, the load flow of AC-DC systems was solved at different loading values increased gradually only at the inverter side AC bus and also in another case, simultaneously at all the buses The minimum singular value and the condition number were computed for each load flow solution To solve the load flow using the N-R method initial estimates of the DC variables are required The initial estimates for the DC variables X_{dc} were obtained from the specified value of P_{Iq} corresponding to the rated DC voltage of the HVDC link and assuming a converter power factor of 0 9 and an inverter operating under minimum extinction angle

For each of the AC-DC systems, the maximum and minimum limits of transformer taps on both inverter side (a_I) and rectifier side (a_R) were taken as 0 9 pu and 1 1 pu respectively The firing angle was assumed to vary from $\alpha_{min} = 5\,\text{deg}$ to $\alpha_{max} = 15\,\text{deg}$ and extinction angle from $\gamma_{min} = 10\,\text{deg}$ to $\gamma_{max} = 20\,\text{deg}$ Resistance of DC line was considered as $6\ 006 \times 10^{-3}$ pu and commutating reactance as 0 0061 pu All AC bus voltages were set to 1 0 pu except at PV buses for which specified values were considered In each iteration of the load flow, Q-limits of the generators and operating limits of the DC variables were checked When Q-limit of a generator bus violated, it was converted to PQ type bus and in the case of limit violation of DC variables, they were fixed to their respective limiting values, which changes the control mode

of the operation accordingly. A scheme for checking the limits of the DC variables and control mode switching is given in the flow chart presented in Fig 2 4 The main steps for estimating the voltage collapse point are given in Fig 2 5

2.5 Results and Discussions

The system studies were conducted on HP-9000/735 computer system to test the potential of the proposed method to predict the point of voltage collapse of AC systems as well as AC-DC systems

2.5.1 AC System

The studies were conducted on three sample systems namely IEEE-14 bus (Appendix–G), IEEE-30 bus (Appendix–I) and an Indian 156-bus systems (Appendix–J) For each of the three systems, the base case loads were assumed to have the same composition at all the buses as given by equations (2 11) and (2 12) 156-bus UPSEB system has a DC link between 26 and 113 buses The link has been modelled as a constant power source at bus-26 (P_G = 10 0 pu, Q_G = 0 0 pu) and a constant PQ load at bus-113 (P_L = 1021 pu, Q_L = 0 0) The following studies were carried out on all the three systems by simultaneously varying loads at all the buses by a loading factor α ($\alpha \geq 1$)

Case–1 Considering constant P, Q load model and without checking Q-limits of generators
Case–2 Considering constant P, Q load model and the generators' Q-limits
Case–3 Considering voltage dependent P, Q load model and without checking Q-limits of generat
Case–4 Considering voltage dependent P, Q load model and the generators' Q-limits

The variation of minimum singular value and condition number of load flow Jacobian with increase in loading have been observed for all the three systems The variation for the above four case studies of σ_{min} for IEEE-14 bus, 30-bus and 156-bus systems have been plotted in Figs 2 6, 2 7 and 2 8 respectively and the variation of the condition numbers are shown in Figs 2 9, 2 10 and 2 11 respectively From these figures it is found that the σ_{min} reduces close to zero while the condition number $k(J)$ increases sharply and goes to infinity near the point of voltage instability A sharp change in the value of σ_{min} and condition number has been observed at a loading when any of the generators in the system hits its reactive power limit This also reduces the maximum loadability of the system This can be clearly observed by comparing Figs 2 6 to

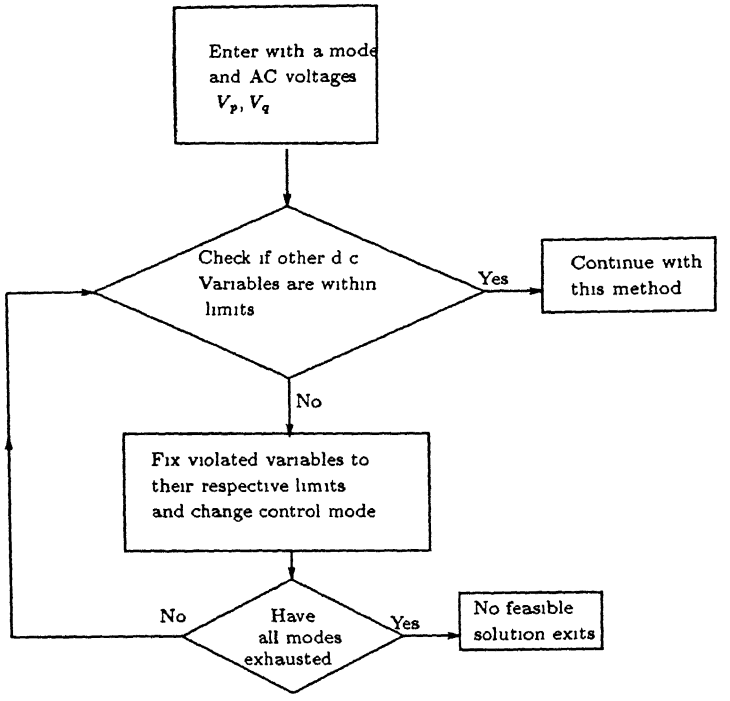

Figure 2 4 Flow chart for checking the limits of the DC variables

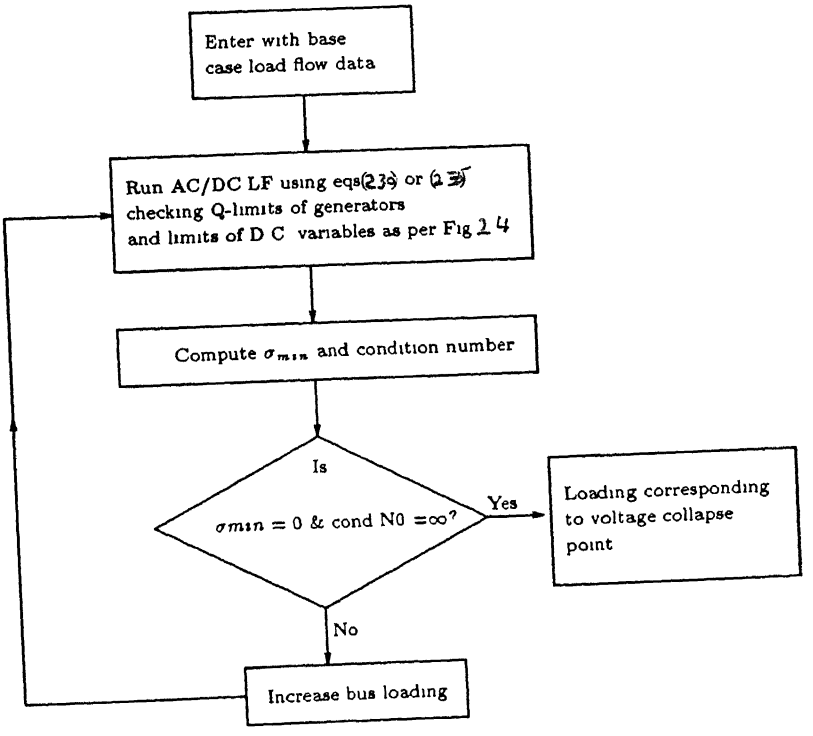

Figure 2 5 Flow chart for voltage collapse prediction

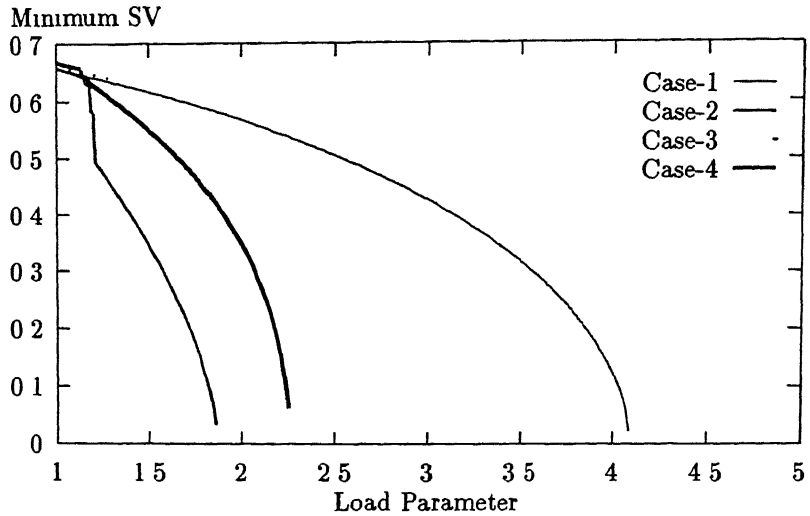

Figure 2 6 Plot of σ_{min} for IEEE-14 bus system

2 8 for Case–1 and Case–2 or for Case–3 and Case–4 in each system Further it has been found that with voltage dependent loads, the system maximum loadability increases (compare Case–1 with Case–3 or Case–2 with Case–4) This is due to the fact that the voltage dependent loads reduce as the bus voltage decreases

2.5.2 AC/DC System

To test the potential of the proposed method to predict the voltage collapse of an AC-DC network, four sample AC-DC systems were considered

System A an IEEE 14-bus system (Appendix–G) modified to replace line 20 (Fig G 1) by a DC link

System B an IEEE 14-bus system with a DC link in parallel with line 20 (Fig G 1)

System C an IEEE 14-bus system with the rectifier end connected to bus 14 of the IEEE-14 bus system and inverter end connected to bus 1 of a sample 2-bus system (Fig 2 12)

System D a 156-bus Indian system representing UP State power system network with a DC link (Fig J 1)

The study was carried out on all the above four systems by keeping the DC power from inverter fixed in one case and by varying it in the other case. In addition to this, the following studies

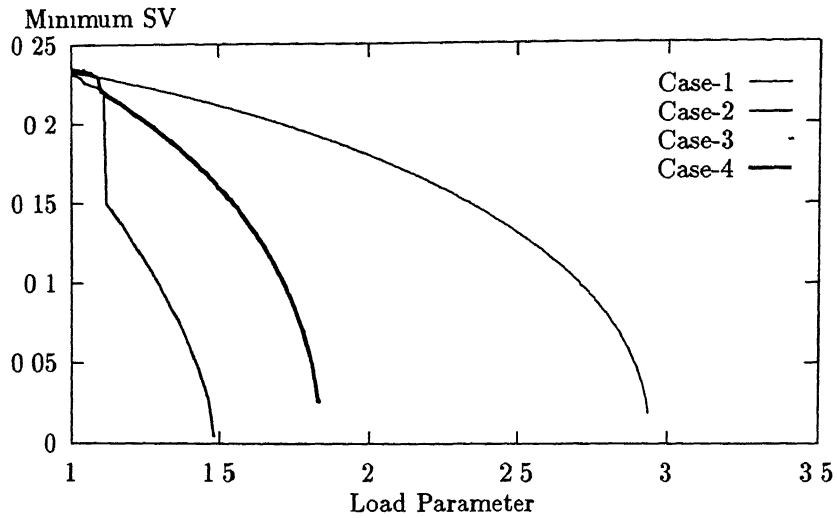

Figure 2 7 Plot of σ_{min} for IEEE-30 bus system

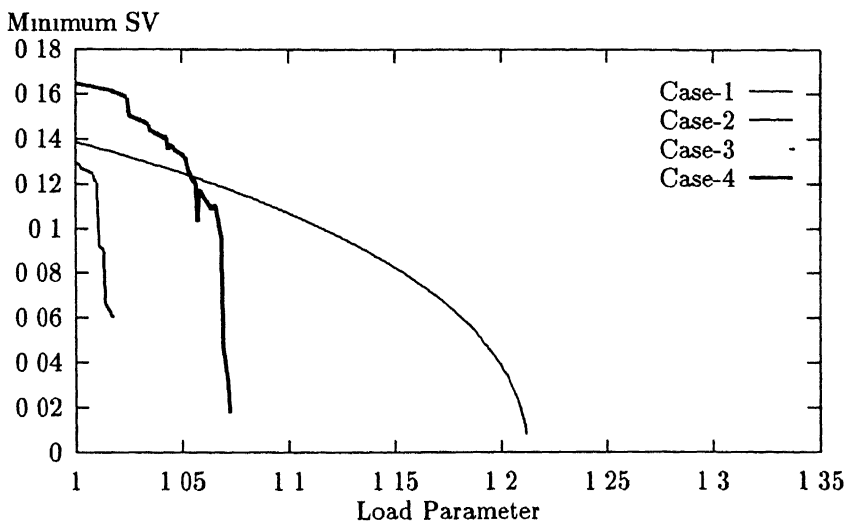

Figure 2 8 Plot of σ_{min} for 156-bus Indian system

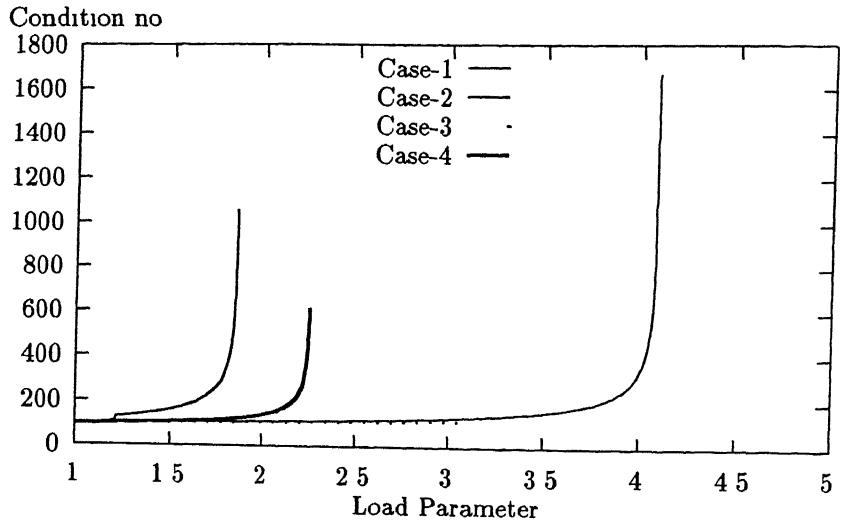

Figure 2 9 Plot of $k(J)$ for IEEE-14 bus system

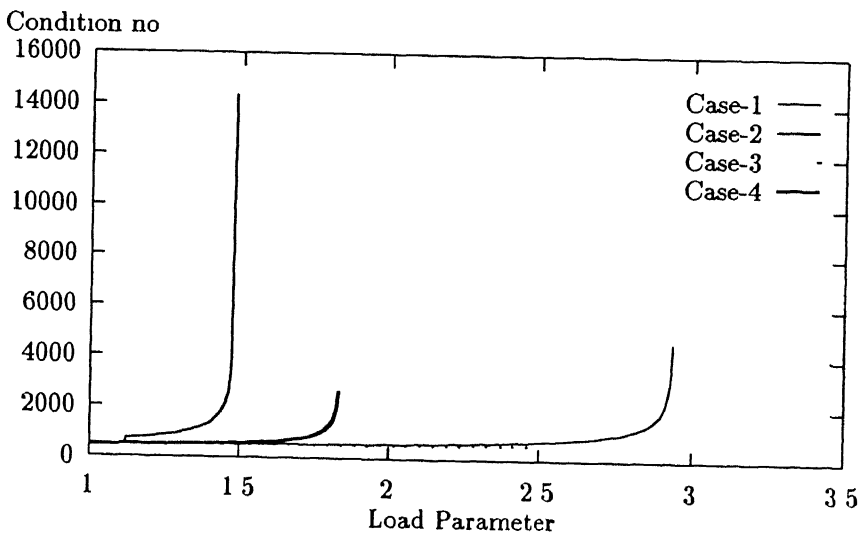

Figure 2 10 Plot of $k(J)$ for IEEE-30 bus system

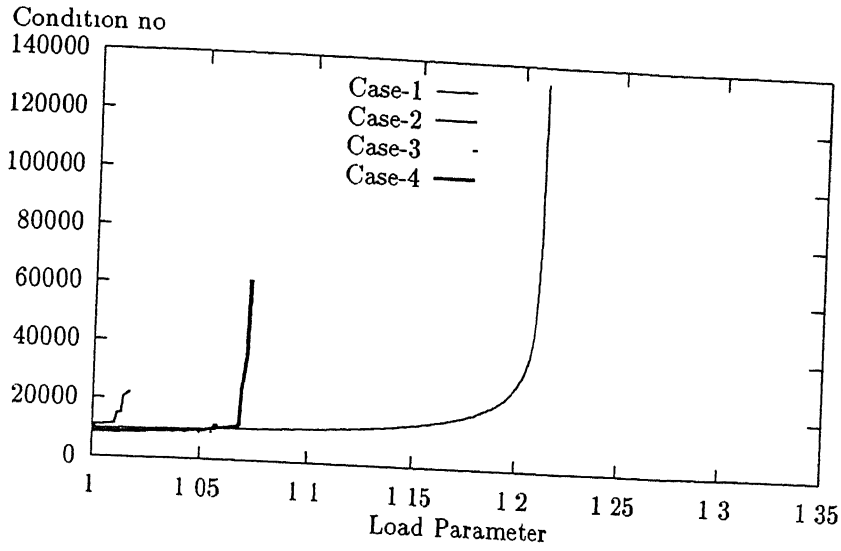

Figure 2 11 Plot of $k(J)$ for 156-bus Indian system

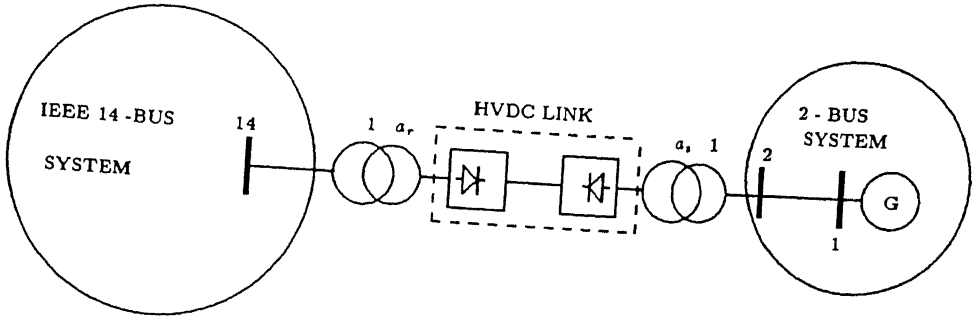

Figure 2 12 IEEE-14 bus extended system (System C)

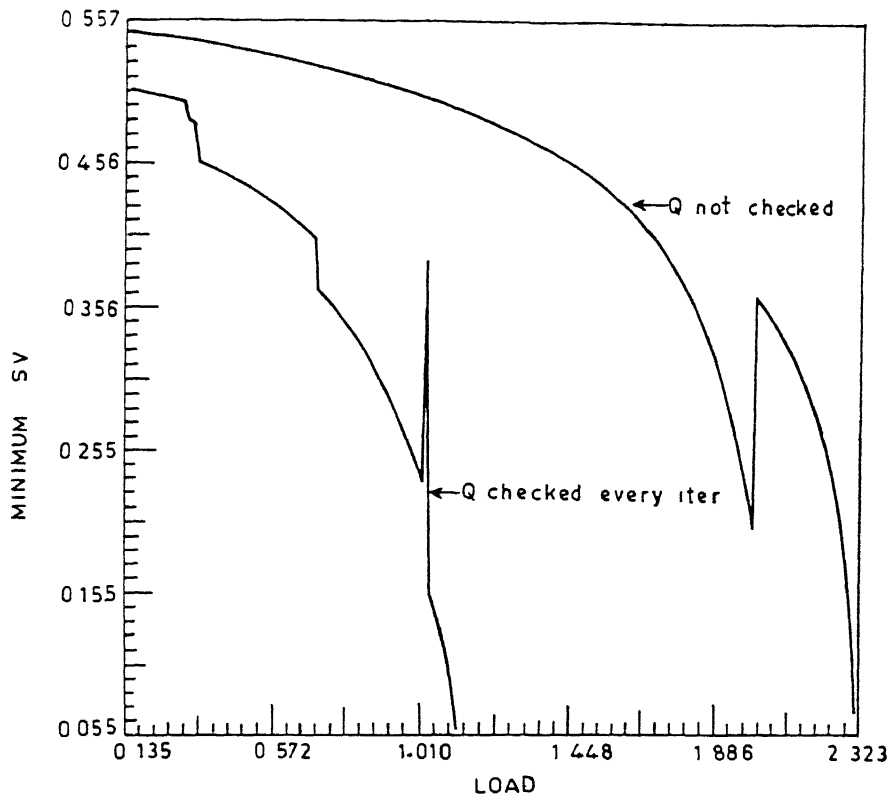

Figure 2 13 System A effect of Q-limit check and load variation on σ_{min}

also performed on System A

Variation of the load at the inverter bus without checking Q-limit

Variation of the load at the inverter bus with generator Q-limit checked at each iteration of the load flow

Simultaneous variation of the load at all the buses, considering the generators' Q-limits

he results of the studies conducted for system A are given in Figs 2 13 to 2 21, and those for stem B in Figs 2 22 to 2 24, for system C in Figs 2 25 to 2 27 and for system D in Figs 2 28 30 repectively

In system A, the load was increased at the inverter bus 14 from its base value of 0 135 pu the minimum singular value became quite close to zero It is seen from Fig 2 13 that when generator Q-limit is checked, the maximum loading corresponding to the voltage collapse at inverter bus reduces Moreover, the generators are found to be constrained at their upper power limits Thus, the reduction in the maximum loading is due to a deficit in the power generations At a load of 1 99 pu when Q-limit of the generators are not checked 1 01 pu when it is checked, a sudden discontinuity is observed in Fig 2 13 At this however, it is noted that the voltage control shifts to the rectifier from the inverter and

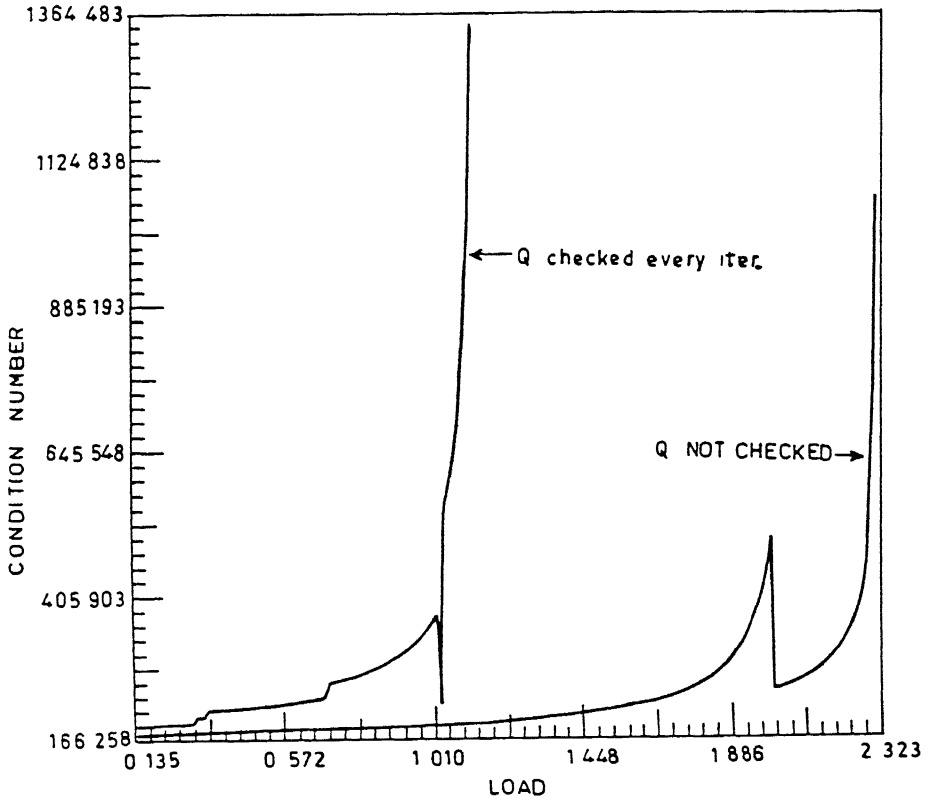

Figure 2 14 System A effect of Q-limit check and load variation on $k(J)$

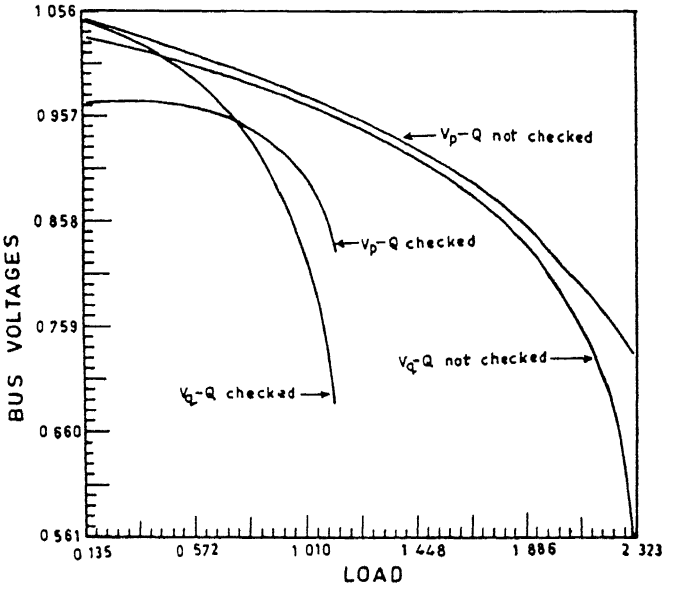

Figure 2 15 System A effect of Q-limit check and load variation on the bus voltage

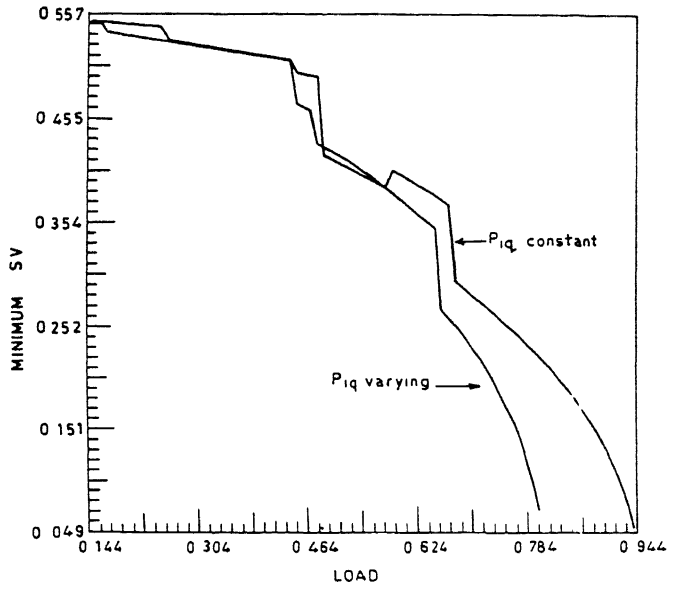

Figure 2 16 System A effect of DC power and load variation on σ_{min}

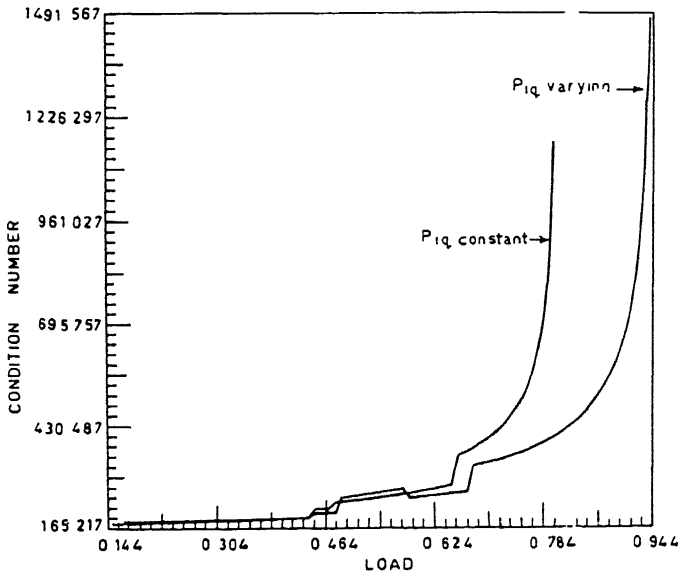

Figure 2 17 System A effect of DC power and load variation on $k(J)$

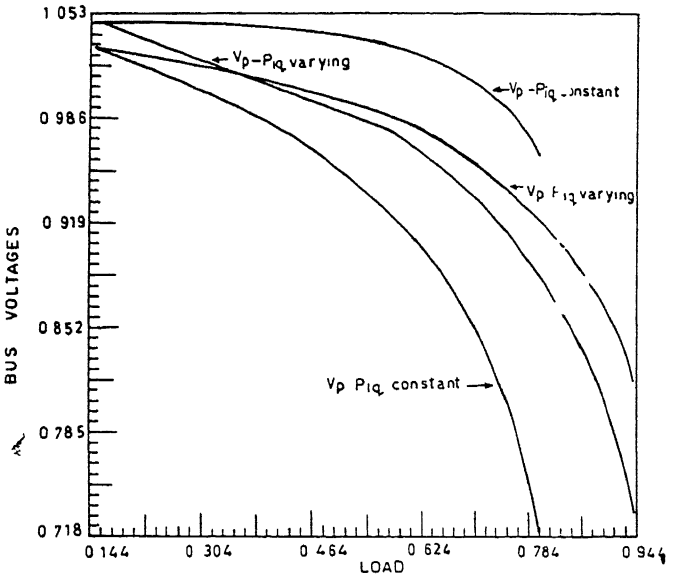

Figure 2 18 System A· effect of DC power and load variation on the bus voltages

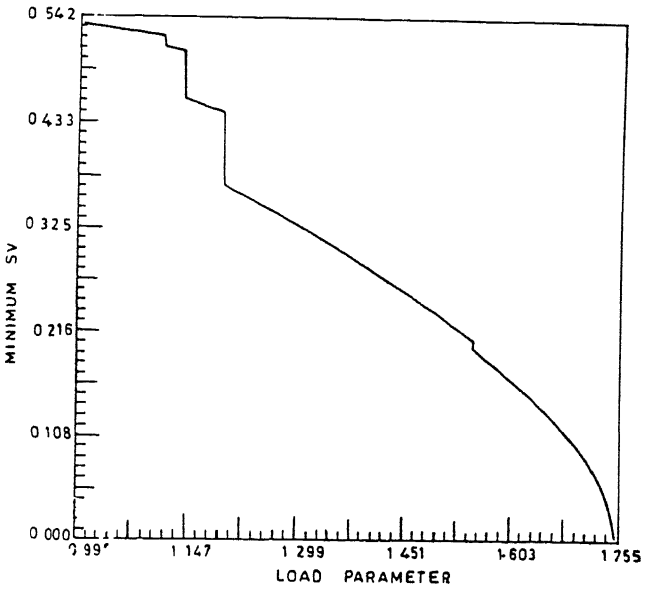

Figure 2 19 System A effect of simultaneous load variation on σ_{min}

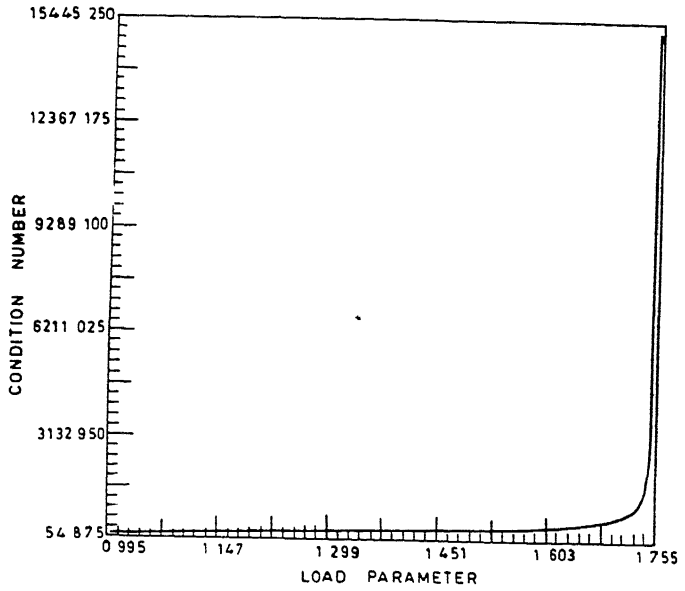

Figure 2 20 System A: effect of simultaneous load variation on $k(J)$

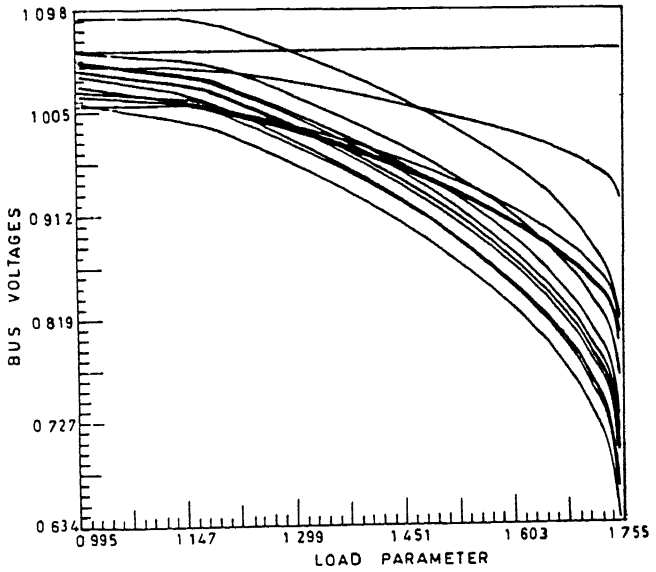

Figure 2 21 System A effect of simultaneous load variation on the bus voltages

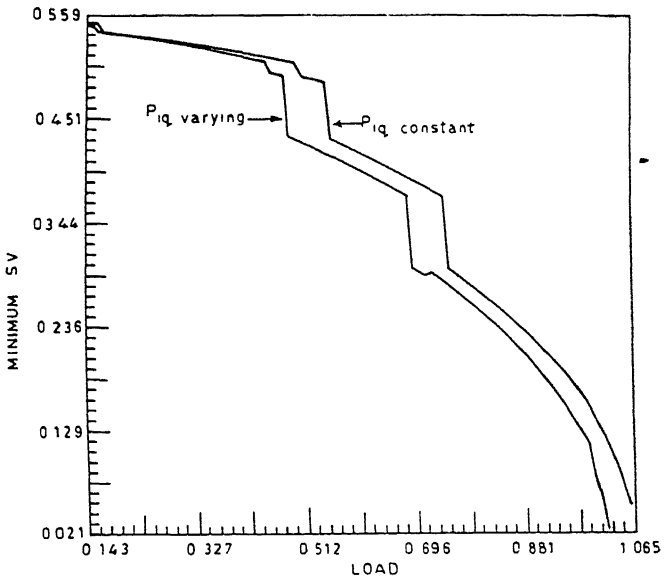

Figure 2 22 System B effect of DC power and load variation on σ_{min}

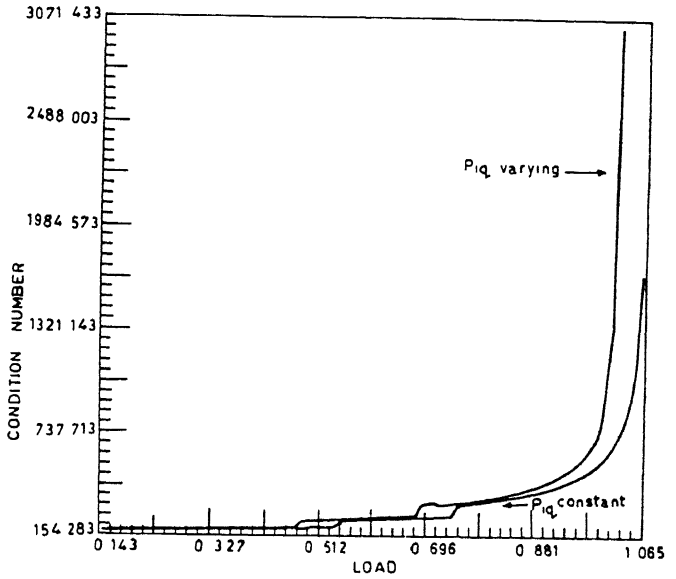

Figure 2 23 System B effect of DC power and load variation on $k(J)$

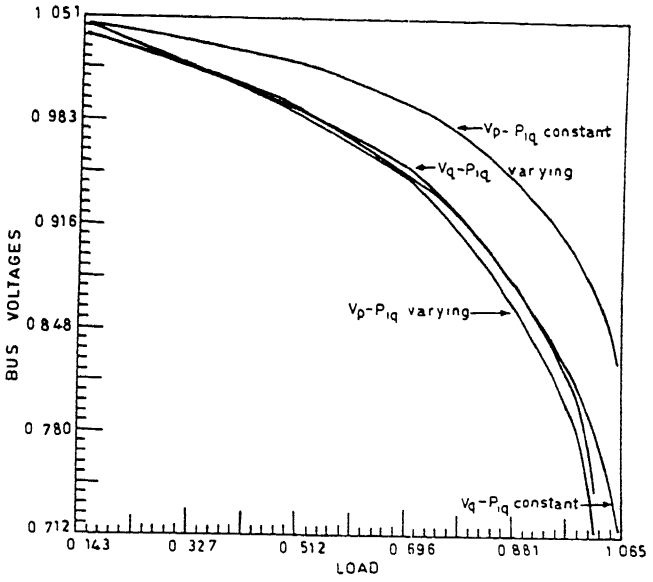

Figure 2 24 System B effect of DC power and load variation on the bus voltages

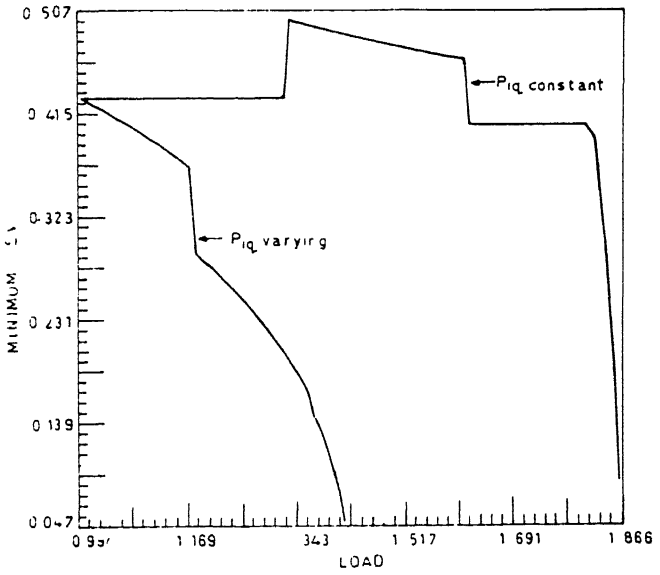

Figure 2 25 System C effect of DC power and load variation on σ_{min}

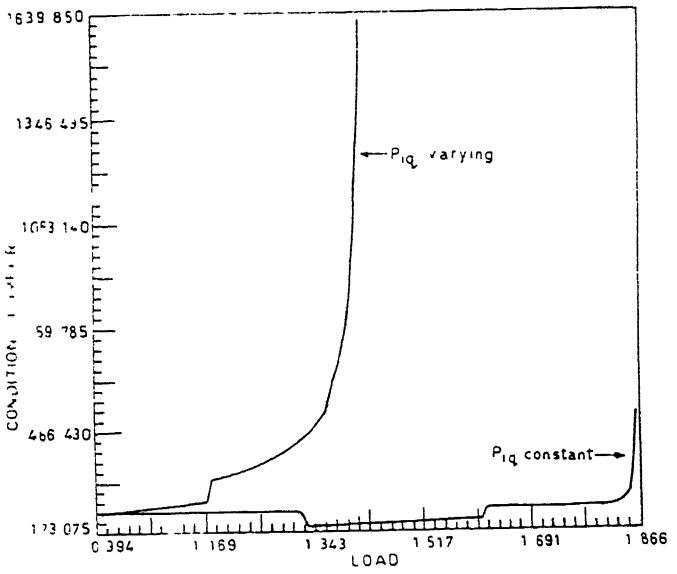

Figure 2 26 System C effect of DC power and load variation on $k(J)$

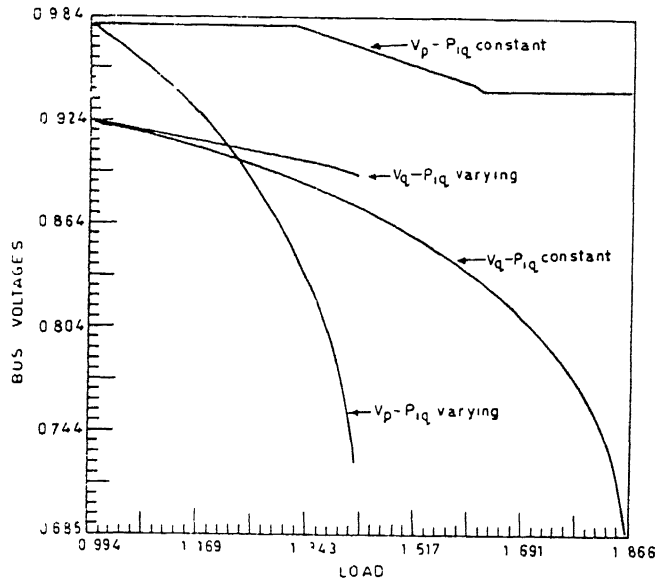

Figure 2 27 System C effect of DC power and load variation on the bus voltages

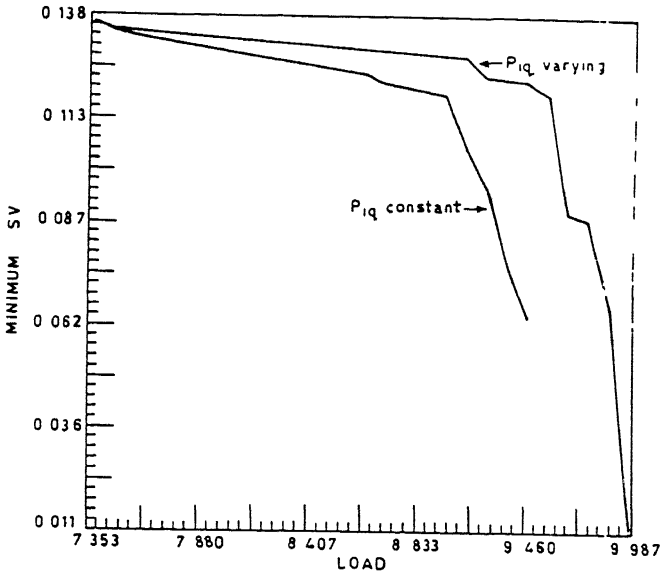

Figure 2 28 System D effect of DC power and load variation on σ_{min}

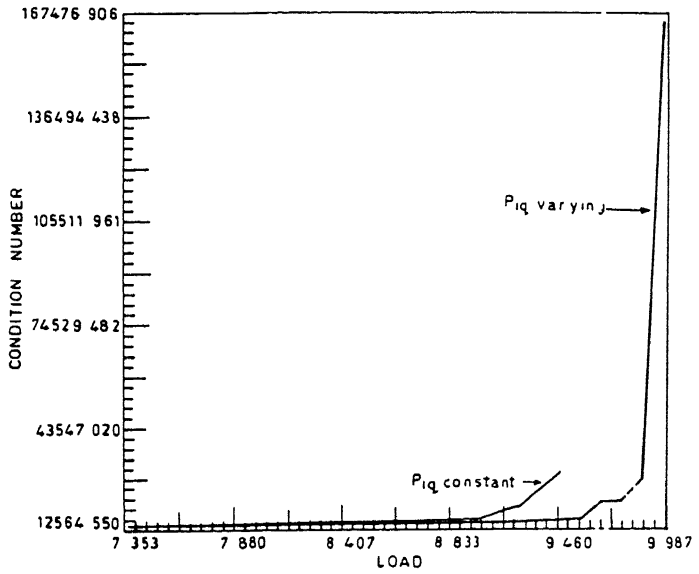

Figure 2 29 System D effect of DC power and load variation on $k(J)$

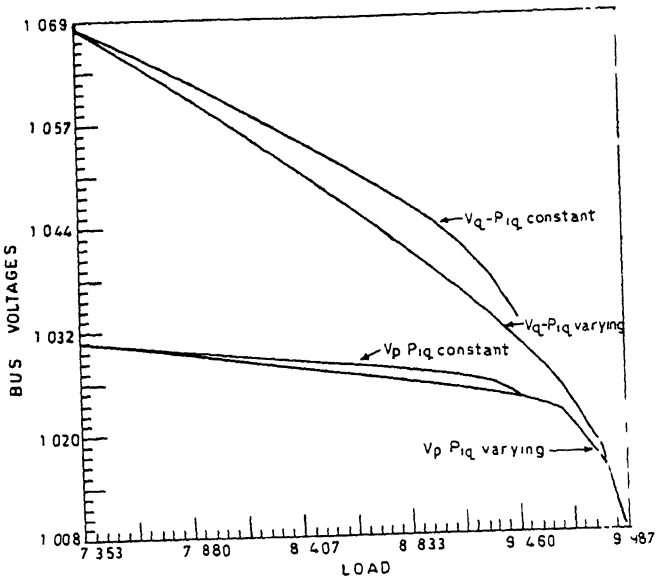

Figure 2 30 System D effect of DC power and load variation on the bus voltages

the current control shifts to the inverter from the rectifier Discontinuities are also observed in Fig 2 13 when the reactive power outputs of the generators reach their limiting values During control mode shift (control mode C_3 to mode C_6), the elements of the Jacobian change and when a generator hits its Q-limit, one row and one column are added to the Jacobian due to switching of a PV type bus to a PQ type bus, and the minimum singular value decreases more rapidly From Fig 2 14, it is seen that the condition number is more sensitive and approaches infinity at the maximum loading point Fig 2 15 shows the variation of AC bus voltages at the rectifier and inverter ends The lowest bus voltage is observed at the inverter end in both the cases

The study on system A was also performed by increasing the load at the inverter AC bus while the inverter end DC power was kept constant in one case and in the other case, was varied by the same amount as the load change It is seen from Fig 2 16 that a load of 0 944 pu can be supported when the DC power is kept fixed and 0 800 pu when it is also varied The reason for the higher maximum loading in the first case is due to the supply of the additional power through line 13 which is connected to bus 7 having Q-support (shunt capacitors) Also in this case, the lowest voltage as observed from Fig 2 18 is at bus 14 when the inverter end DC power

is varied by the same amount as the load The increase in the load is being met by the DC power transmitted through the DC line from bus 13. Since there is no Q-support at either bus 13 or at bus 12, which is connected to bus 13 through line 19, the voltage decrease at the rectifier end (bus 13) is faster than in the previous case. Fig 2 17 shows that the condition number increases to a very large value at the collapse point.

In the next set of studies on system A, the loads at the load buses were increased by a factor α ($\alpha \geq 1$) α was varied from 1.0 and the collapse was observed at $\alpha = 1\ 755$ (Fig 2 19) There are exactly four discontinuities corresponding to each of the four generators hitting their Q-limit Fig 2 20 shows a large value of the condition number at the collapse point and Fig 2 21 indicates that all the bus voltages (except the slack) approach the nose of the P-V curve simultaneously

The study was conducted on system B with the inverter end DC power fixed in one case and varying (by the same amount as the load at the inverter bus) in the other case Fig 2 22 shows that the minimum singular value assumes a sufficiently low value for the maximum loading of 1 065 pu and 1 028 pu when the DC power is kept fixed and varying respectively It can be noted that the maximum loading has increased in system B as compared to system A due to additional power support provided by the AC link in parallel with the DC link in system B The condition number approaches infinity at the maximum loading, as seen from Fig 2 23 The lowest voltage is seen at the inverter bus when the DC power is varied, for the same reasons mentioned for system A (Fig 2 24 In a similar set of studies on system C, it is seen from Fig 2 27 that if the DC power is kept fixed the voltage collapse takes place in the 2-bus AC system and the 14-bus AC system remains almost unaffected However, the discontinuity in the curve is due to control mode change (from mode C_3 to mode C_6) But when the DC power is also varied by the same amount as the load at the inverter bus, that is, assuming that the increase in load is met by the power flow in the DC link, the collapse of bus voltages takes place in the 14-bus AC system as the power flow in the bus system remains almost unaffected. Fig 2 25 shows that the minimum singular value goes sufficiently close to zero at the maximum loading and Fig 2 26 indicates that the condition number is sufficiently large at this point

Studies were carried out on the 156-bus Indian system (system D) for the conditions studied in systems B and C In this system a DC link (see Fig J 1) exists between buses RHND(S) and NCR for transportation of 1000 MW of power from RHND(S) to NCR (Dadri) bus NCR has a real power load of 735 MW (7.35 pu) The load flow for the 156-bus Indian system was run without considering the DC link and it was found that the load flow did not converge The

convergence of the load flow was possible only when the DC link was considered From Fig 2 28, it is seen that the maximum loading at the inverter bus is 9 987 pu when the increase in the load is met by the DC power, and when the DC power is kept fixed, the maximum load at which the collapse occurs is 9 565 pu From Fig 2 29, it is seen that the condition number is very large at the collapse point Fig 2 30 shows that the lowest voltage is observed at the rectifier end when the DC power is varied and at the inverter end when DC power is kept fixed The variation of voltage magnitude at the rectifier end is only about 5% when the DC power is varied This confirms the observation in ref [40] that the drop in bus voltage magnitude can not be taken as a voltage collapse indicator

2.6 Conclusion

From the works presented in this chapter, the following conclusions are drawn

(i) The concept of minimum singular value and condition number of load flow Jacobian can be used to predict the static voltage stability of an integrated AC-DC network as well as the AC system having a polynomial type voltage dependent loads

(ii) At maximum loadability point, the condition number approaches to infinity and the minimum singular value approaches to zero A sharp change in the values of condition number and minimum singular value of Jacobian is observed when Q-limits of generators are violated or control mode switching in a DC link takes place

(iii) Considering the static model, it has been found that if the load is varied at only one bus in an integrated AC-DC system, the collapse of voltage takes at the bus at which the load is being increased However, with simultaneous changes in the loadings at all the buses, all the bus voltages approach the nose point of the P-V curve simultaneously.

(iv) Consideration of reactive power output limits of synchronous machines reduces the loading at which the system becomes voltage unstable Thus it reduces the maximum loadability of the system

(v) The voltage dependent characteristic of loads enhances the voltage stability of the system

Chapter 3

Effect of Generation Rescheduling on Voltage Stability Margin

3.1 Introduction

Maintaining the required voltage stability margin has become one of the recent concerns of power utilities Extensive works exist in the area of steady state voltage stability and margin predictions [168, 169, 189] Some of the indices suggested for the static voltage stability are reactive power sensitivity to bus voltage [69, 134], stability margin in terms of real or reactive power [116, 181], VCPI (Voltage Collapse Proximity Indicator) derived from the sensitivity of total reactive power generation to real or reactive load increase [28,102], VIPI (Voltage Instability Proximity Indicator) based on the closeness of multiple load flow solutions [24, 68], minimum singular value, eigenvalue or condition number of power flow Jacobian [51, 52, 58, 113, 141, 142, 179]

Tiranuchit et al [51] proposed an optimal generation scheduling scheme to maximise the minimum singular value of the Jacobian using a linear programming technique Generators and condensers were modelled by their fixed reactive power limits and their voltage dependent capabilities were not considered Begovic et al [81] demonstrated that by using optimal power flow strategy to minimise the weighted sum of the absolute values of the control actions, the voltage stability can be improved

Traditionally generation scheduling is performed in view of the minimisation of total fuel cost of generation or system transmission loss These schemes form a part of modern energy management system Ref [85] presents a review of various optimal power flow strategies being

used in practice However, effect of these conventional optimal power flow schemes on the voltage stability margin has not been reported in the literature Hence, in this Chapter, the following O P F schemes for generation rescheduling have been considered and their relative impact on voltage stability margin has been studied

(1) Minimisation of the total fuel cost of the generation

(2) Minimisation of the total system transmission loss

(3) Maximisation of the minimum singular value of the Jacobian

(4) A new scheme which minimises the reactive power injection at the slack bus

The voltage stability margin has been compared for the above four formulations in terms of minimum singular value of power flow Jacobian as well as the total system reactive power margin in each case for IEEE-14 bus, IEEE-30 bus and 156-bus Indian System The reactive power margin has been computed by estimating the closest distance of an operating point to the static bifurcation set in reactive parameter space [132]

In addition, the voltage dependent real and reactive power capability of the synchronous machines (generators and condensers) have been considered

3.2 Generator and Synchronous Condenser Model

One of the major factors responsible for the long term voltage instability is the heating of armature and field circuit of synchronous machines [189] This underlines the need for their appropriate modelling The synchronous machines for the present study have been modelled as constant voltage source behind the synchronous reactance The real and reactive power outputs of a salient pole generator ignoring armature resistance is given as follows [2]

$$P_G = \frac{V_t E_q}{X_d} \sin\delta + \frac{V_t^2}{2}\left[\frac{1}{X_q} - \frac{1}{X_d}\right] \tag{3 1}$$

$$Q_G = \frac{V_t E_q}{X_d} \cos\delta - V_t^2\left[\frac{\cos^2\delta}{X_d} + \frac{\sin^2\delta}{X_q}\right] \tag{3 2}$$

where E_q is the induced emf, V_t the terminal voltage, δ is the phase angle between V_t and E_q X_d, X_q are the d-axis and q-axis synchronous reactances

The corresponding equations for power angle characteristic of a cylindrical rotor machine having synchronous reactance X_s can be written as

$$P_G = \frac{V_t E_q}{X_s} \sin\delta \tag{3 3}$$

$$Q_G = \frac{V_t E_q}{X_s} \cos\delta - \frac{V_t^2}{X_s} \tag{3 4}$$

The machine real and reactive power outputs (P_G and Q_G) and the other variables such as E_q and δ are physically constrained because of limits on maximum electrical and mechanical stress and temperature rise to which the machine can be subjected to

The maximum real power output $P_{G_{max}}$ of the generator is usually constrained by turbine rating Also, it is not desirable to reduce the real power output of generator in certain power plants below a minimum value $P_{G_{min}}$ unless it is taken off-line For example, in a fossil fuel plant, constant boiler temperature must be maintained to prevent slagging These operating limits on the real power output of generators can be expressed as

$$P_{G_{min}} \leq P_G \leq P_{G_{max}} \tag{3 5}$$

The synchronous condensers are connected in a network to meet the lagging and leading VAR requirement Neglecting all losses, their real power output and the load angle δ can be assumed to be zero The reactive power output of a synchronous condenser is, thus, given by

$$Q_G = \frac{V_t E_q}{X_d} - \frac{V_t^2}{X_d} \tag{3 6}$$

3.2.1 Rotor Heating Limit

If the effect of the saturation is ignored, the field current of a synchronous machine (both generator and condenser) is proportional to the induced emf E_q Therefore, the maximum allowable rotor current can be mapped to a maximum allowable induced emf $E_{q_{max}}$ Thus, the rotor heating limit can be expressed as,

$$E_q \leq E_{q_{max}} \tag{3 7}$$

3.2.2 Underexcitation Limit

Stability considerations impose a limit on the reactive power that a generator can absorb while operating in leading power factor mode Under AVR action, the leading power factor operation causes increase in the load angle Hence, it is possible to map the underexcitation limit of a generator to a suitable maximum limit on the load angle

$$\delta \leq \delta_{max} \tag{3 8}$$

For stable synchronous operation of the condenser with the rest of the network, synchronising power $\frac{dP}{d\delta}$ must be greater than or equal to zero Under these conditions, if the excitation voltage is allowed to be negative, the maximum reactive power that can be absorbed by the condenser is given as follows [2]

$$Q_{min} = -\frac{V_t^2}{X_q} \tag{3 9}$$

3.2.3 Stator Heating Limit

The real and reactive power output of a generator is also limited by maximum allowable armature current $I_{a_{max}}$

$$I_a = \frac{\sqrt{(P_G^2 + Q_G^2)}}{V_t} \leq I_{a_{max}} \tag{3 10}$$

The reactive power output of a synchronous condenser is also limited by maximum allowable armature current

$$Q_G \leq V_t I_{a_{max}} \tag{3 11}$$

The equations (3 1) and (3 2) for the salient pole or equations (3 3) and (3 4) for the cylindrical rotor together with equations (3 5), (3 7), (3 8) and (3 10) represent the generator operating capability under steady state Though it is possible to overload the generators [9], the overload capability of the generators has not been considered in this thesis

Since the terminal voltages of synchronous machines are not usually allowed to exceed a specified maximum value $V_{t_i}^{max}$, the following additional constraints will apply

$$V_{t_i} \leq V_{t_i}^{max} \tag{3 12}$$

3.3 Generation Rescheduling Schemes

The voltage dependent model of synchronous generators and condensers, as discussed in section 3 2, can be integrated in the power flow programme The nonlinear real and reactive power balance equations at any bus i can be written as follows

$$P_i(\theta, V) = P_{G_i}(\delta, E_q) - P_{L_i} \tag{3 13}$$

$$Q_i(\theta, V) = Q_{G_i}(\delta, E_q) - Q_{L_i} \tag{3 14}$$

where P_i and Q_i refer to the real and reactive power injections at bus-i, P_{L_i} and Q_{L_i} the loads, V and θ the bus voltage magnitude and angle vectors Since in this formulation, a large number of variables are constrained, the load flow for determining the base case operating point has been formulated as an optimisation problem The following objective function has been minimised to obtain the load flow solution subject to equality constraints (power balance) equations (3 13) and (3 14) and inequality constraints as given in equations (3 1) to (3 12)

$$Minimise \quad \sum_{i \in N_{pv}} W_{V_i} \left(V_{t_i} - V_{t_i}^{max} \right)^2 \tag{3 15}$$

where W_{V_i} is a weighing factor and N_{pv}, the set of PV buses in the network

Four different formulations of the generation rescheduling have been attempted in the present work considering voltage magnitude and angle at all the system buses and the internal nodes of the generators and the synchronous condensers as optimisation variables The objective functions considered for the generation rescheduling schemes are described below

3.3.1 Minimisation of the Total Fuel Cost (OBJ-I)

The cost characteristics of a generator-i is a function of its real power output and can be approximated by a quadratic function as below·

$$C(P_{G_i}) = \frac{1}{2} a_i {P_{G_i}}^2 + b_i P_{G_i} + c_i \tag{3 16}$$

The total fuel cost of the generation for a system can be given as

$$C_T = \sum_{i \in N_g} C(P_{G_i}) \tag{3 17}$$

where N_g is the set of thermal generating plants in the system In the present formulation, scheduling of hydrogenerators have not been considered

3.3.2 Minimisation of the Total Transmission Loss (OBJ-II)

The total real power transmission loss of the system is taken as the sum of the real power injections P_{inj_i} at all the buses Thus, for a N bus system, the real power system transmission loss P_{loss} can be given as,

$$P_{loss} = \sum_{i=1}^{N} P_{inj_i} \tag{3 18}$$

P_{inj_i} can be expressed in terms of bus voltages and angles as follows

$$P_{inj_i} = \sum_{j=1}^{N} y_{ij} V_i V_j \cos(\theta_i - \theta_j - \gamma_{ij}) \tag{3 19}$$

where $y_{ij}\angle\gamma_{ij}$ is the ij^{th} element of Y_{bus}

3.3.3 Maximisation of Minimum Singular Value (OBJ-III)

The power balance equations (3 13) and (3 14) can be linearised around an operating point to yield the following Newton-Raphson power flow relationship

$$\begin{bmatrix} \Delta P \\ \Delta Q \end{bmatrix} = \underbrace{\begin{bmatrix} P_\theta & P_V \\ Q_\theta & Q_V \end{bmatrix}}_{=J} \begin{bmatrix} \Delta\theta \\ \frac{\Delta V}{V} \end{bmatrix} \tag{3 20}$$

The Jacobian matrix J is composed of the four submatrices P_θ, P_V, Q_θ and Q_V The system voltages are infinitely sensitive to bus injections if the Jacobian is singular i e when $\det\{J\} = 0$ Using Schur complement [141] and assuming P_θ to be non-singular, it can be shown that

$$\det\{J\} = \det\{P_\theta\} \det \underbrace{\{Q_V - Q_\theta P_\theta^{-1} P_V\}}_{=J_R} \tag{3 21}$$

If both the active power injections, ΔP and the changes in the bus voltage angle $\Delta\theta$ in equation (3 20) are set to zero, the relationship between changes in reactive power injections and voltage magnitudes can be described by the submatrix Q_V and written as

$$[\Delta Q] = [Q_V]\left[\frac{\Delta V}{V}\right] \tag{3 22}$$

However, there also exists considerable coupling between change in reactive power injections and change in bus voltage angles especially during stressed system conditions [189] One way of considering it is to consider the full Jacobian matrix J From equation (3 21), it is seen that in order for the Jacobian J to be singular, the reduced matrix J_R must be singular if the submatrix P_θ is non-singular

Upon setting $\Delta P = 0$ in the equation (3 20), the change in reactive power injections can be related to change in bus voltage magnitudes as follows

$$[\Delta Q] = \left[Q_V - Q_\theta P_\theta^{-1} P_V\right]\left[\frac{\Delta V}{V}\right] \tag{3 23}$$

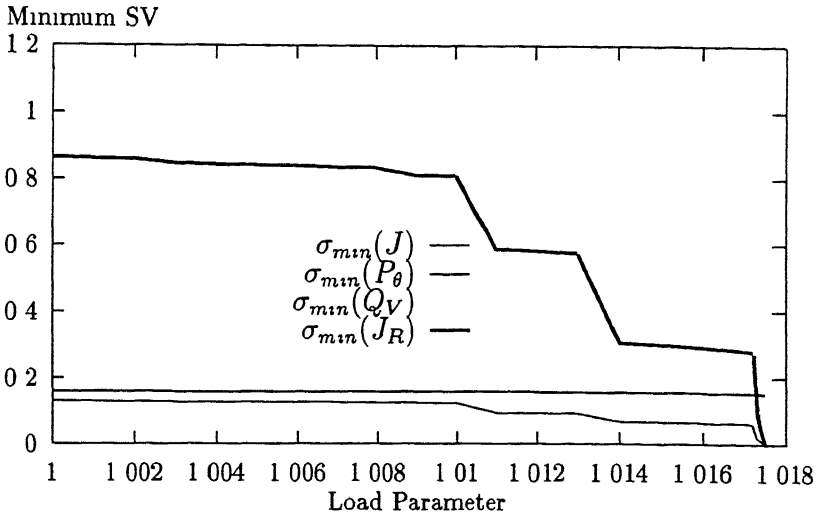

Figure 3 1 Plot of σ_{min} of J, J_R, P_θ and Q_V for increase in system loading

In order to observe whether the matrices J, J_R , Q_V and P_θ become singular simultaneously for increase in loading, their minimum singular values were plotted as a function of loading parameter α ($\alpha \geq 1$) for 156-bus Indian System as shown in Fig 3 1 The real and reactive loads at all the buses were increased simultaneously by the factor α, retaining the base case power factor of loads at all the buses It was observed that out of the four matrices, the minimum singular value of J and J_R approached zero corresponding to $\alpha = 1\ 0175$ Only these two matrices become singular when the loading in the system was increased, while the matrices P_θ and Q_V did not become singular at the loading corresponding to the static bifurcation set Similar observation has also been noted by Lof et al [141] In the present formulation, minimum singular value of matrix J_R has been maximised

Though the matrix J is highly sparse, the matrix J_R is dense The following algorithm [113] can be used for sparse formulation to compute σ_{min} of J_R

(i) Find LU factorisation of J

(ii) To start the iteration scheme, choose the right singular vector v such that $\|v\| \neq 0$ To perform computations, the components of v corresponding to bus angles were set as zero, and those for bus voltages were taken as 1 This choice result in better convergence [141] Set $k = 1$

(iii) For k^{th} iteration, solve $J^T u^k = v^k$, for the left singular vector u^k

(iv) Set $u_i = 0$ for all i corresponding to the active power injections

(v) Compute $\sigma_{min}(J_R) = \frac{\|v^k\|_2}{\|u^k\|_2}$

(vi) If $\|\sigma^k_{min} - \sigma^{k-1}_{min}\| \leq tol$, stop

(vii) If convergence is not achieved in step (vi), the right singular vector v^k is updated for $(k+1)^{th}$ iteration by solving $Jv^{k+1} = u^k$

(viii) Set $v_i = 0$ for all i corresponding to the node angles

(ix) Compute $\sigma_{min}(J_R) = \frac{\|u^k\|_2}{\|v^{k+1}\|_2}$

(x) If $\|\sigma^{k+1}_{min} - \sigma^k_{min}\| \leq tol$ stop, else go to step (iii)

3.3.4 Minimisation of Slack Bus Reactive Injection (OBJ-IV)

Tiranuchit et al [51] observed that the effect of maximising the minimum singular value of power flow Jacobian is to reduce the slack bus reactive power injection and call upon the other reactive sources to inject more reactive power This can be achieved by a simpler formulation utilising a new objective function as given below in that the slack reactive injection is also minimised along with the load flow objective

$$Minimise \quad \sum_{i \in N_{pv}} W_{V_i} \left(V_{t_i} - V_{t_i}^{max}\right)^2 + W_Q Q_{inj_s} \tag{3 24}$$

where W_Q is weighing factor associated with the slack bus reactive power injection Q_{inj_s} If subscript s stands for slack bus, Q_{inj_s}, can be expressed as

$$Q_{inj_s} = \sum_{j=1}^{N} y_{sj} V_s V_j \sin(\theta_s - \theta_j - \gamma_{sj}) \tag{3 25}$$

3.4 Estimation of System Reactive Power Margin

For a given reactive loading vector Q^0_L, assume that the resulting operating state is stable When Q_L is varied, the operating state may change For some $Q_L = Q^*_L$, let the load flow Jacobian is singular In reactive parameter space set of all Q_L, such that the Jacobian is singular, define a boundary of the feasible region say Ω for stable operation Ω typically consists

of hypersurfaces and their intersections The saddle node bifurcation instability, when the reactive loads encounters Ω, can result in catastrophic collapse of the system voltages and blackouts [54, 66] One of the ways to monitor the proximity of an operating point to voltage collapse is to measure the closest distance of the operating point Q_L^0 to Ω Although the geometry of Ω is not known, Ω has been assumed to be convex in the present study In particular, it is useful to calculate a critical reactive load power Q_L^* in Ω for which $\|Q_L^* - Q_L^0\|_2$ is a local minimum [13, 97, 107, 132, 133, 163] The line segment Q_L^0 to Q_L^* represents a worst case reactive load variation and $\|Q_L^* - Q_L^0\|_2$ measures the proximity of Q_L^0 to Ω This problem has been formulated as an optimisation problem whereas it was solved by using Newton-Raphson method in ref [132, 163] A sequential quadratic programming algorithm has been used to find Q_L^* such that $\|Q^* - Q_L^0\|_2$ is a minimum while satisfying the power balance equations (3 13) and (3 14), implying that the load flow Jacobian J in equation (3 20) is singular

3.5 Results and Discussions

The studies were conducted on the following three sample AC system using HP 9000/735 computer system

System–A IEEE-14 bus system given in Appendix–G
System–B IEEE-30 bus system given in Appendix–I
System–C 156-bus Indian system given in Appendix–J

Sequential quadratic programming algorithm was used for the optimisation in each of the four generation scheduling formulations

The numerical values of X_d, X_q and $E_{q_{max}}$ for the generators and synchronous condensers were taken from [7] in accordance with their capacity The maximum allowable load angle δ_{max} was taken to be 70 deg for all the generators in the three systems The studies were carried out by varying real and reactive loads at all the buses simultaneously by a factor α ($\alpha \geq 1$) The weighing factors W_{V_i} in equations (3 15) and (3 24) were taken as 1 0 in each of the system studies and W_Q in equation (3 24) was selected as 0 1 The value of W_Q was decided through experimentation and was taken as the one resulting into the maximum voltage stability margin (VSM) The study results of the three systems are given below

Table 3 1 Voltage Stability Margin for System–A

Loading Factor	VSM	LFLOW	OBJ-I	OBJ-II	OBJ-III	OBJ-IV
$\alpha = 1\ 0$	Q-margin (L_1)	1 081325	1 074358	0 998987	1 080723	1 078052
	Q-margin (L_2)	0 371041	0 368844	0 341533	0 370492	0 370179
	σ_{min}	0 6008	0.5984	0 5914	0 6035	0 6014
$\alpha = 2\ 0$	Q-margin (L_1)	0 332611	0 349178	0 454444	0 539591	0 538171
	Q-margin (L_2)	0 105002	0 112257	0 146889	0 173682	0 173885
	σ_{min}	0 2810	0.2478	0 2952	0 3399	0 3345

3.5.1 System–A

There are 3 generators and 2 condensers in this system. Generator # 1 at bus-1 was taken as the slack Two sets of results were obtained corresponding to the base case loadings (loading factor $\alpha = 1\ 0$) and the stressed conditions at higher loading ($\alpha = 2\ 0$) Loads at all the buses were raised to two times their base values in the stressed condition The reactive power margins (both L_1 and L_2 norm) using the method described in section 3 4 and the minimum singular value σ_{min} of final Jacobian submatrix J_R obtained in each of the cases were computed and are given in Table 3 1 It is seen from the Table 3 1 that at base case loading amongst the four objectives, OBJ-III yields a maximum of σ_{min} and reactive power margin (both L_1 and L_2 norm) which are very close to the results obtained from OBJ-IV and OBJ-I However, none of them could improve the reactive power margin available at base case condition though the minimum singular value has increased slightly with OBJ-III and OBJ-IV At higher loading, though OBJ-III resulted in maximum σ_{min}, but provides (slightly) less reactive power margin (both L_1 and L_2 norm) in comparison to OBJ-IV The voltage stability margin, however, has substantially increased by using either of the objectives from the unoptimised case The optimum real and reactive power outputs were obtained using the four objectives and their values are given in Table 3 2 along with load flow values at $\alpha = 2\ 0$

It is found that OBJ-III which maximises the minimum singular value does not yield a maximum of reactive power margin, for example at a loading ($\alpha = 1\ 0$) much lower than critical loading The correlation between minimum singular value and reactive power margin is lost because at lower loading, a singular value which is minimum may not remain so when loading is increased

Table 3 2 Real and Reactive Power Outputs (in p u) for System–A ($\alpha = 2\ 0$)

P_G&Q_G	LFLOW	OBJ-I	OBJ-II	OBJ-III	OBJ-IV
P_{G_1}	5 3130	4 1762	4 3112	4 8080	4 7510
P_{G_2}	0 4000	0 8466	0 7143	0 4636	0 4168
P_{G_3}	0 2000	0 7287	0 7096	0 5124	0 6027
Q_{G_1}	1 4288	1 4332	1 0497	0 8511	0 8093
Q_{G_2}	0 8767	0 4658	0 6740	0 8729	0 8983
Q_{G_3}	0 9826	0 6402	0 7121	0 9095	0 8451
Q_{G_4}	0 4188	0 4224	0 4346	0 4400	0 4412
Q_{G_5}	0 3982	0 3950	0 4071	0 4163	0 4159

3.5.2 System–B

There are 3 generators and 3 condensers in this system Generator # 1 at bus-1 was taken as the slack Two sets of studies were performed One corresponding to normal (base case) loading at $\alpha = 1\ 0$ and the other for a higher loading corresponding to $\alpha = 1\ 6$ Value of α higher than 1 6 could not be considered as it resulted into divergence of the load flow Table 3 3 presents the values of voltage stability margin (Q-margin and σ_{min}) obtained through load flow and with the different objectives described in the earlier section At normal loading, though OBJ-III results in a maximum of σ_{min}, the proposed new OBJ-IV yields the maximum reactive margin Also at higher loading condition, the OBJ-IV turns out to yield a reactive margin which is almost same as with OBJ-III At normal (low) loading condition, the generation rescheduling does not help in increasing the voltage stability margin However, distinct improvement in the margin is observed during stressed conditions The generator outputs obtained with the four objectives along with load flow results at $\alpha = 1\ 6$ is presented in Table 3 4

3.5.3 System–C

The data for this system has been slightly changed from one given in Appendix–J At bus-24 a synchronous condenser has been assumed to be present, and generators are placed at bus-1 to 23 The loading in this system already corresponds to the stressed condition Since the generator cost coefficients were not available for this system, the studies were confined to generation rescheduling using only OBJ-II, OBJ-III and OBJ-IV From the studies conducted on System–A and System–B (Table 3 1 and Table 3 3), it was found that minimum singular

Table 3 3 Voltage Stability Margin for System–B

Loading Factor	VSM	LFLOW	OBJ-I	OBJ-II	OBJ-III	OBJ-IV
$\alpha = 1\ 0$	Q-margin L_1	0 710141	0 723411	0 725283	0 727966	0 716998
	Q-margin L_2	0 194651	0 184339	0 186435	0 188566	0 193180
	σ_{min}	0 2171	0 2081	0 2130	0 2191	0 2175
$\alpha = 1\ 6$	Q-margin L_1	0 314804	0 338730	0 336078	0 339490	0 339442
	Q-margin L_2	0 071728	0 077342	0 076710	0 077504	0 077496
	σ_{min}	0.1242	0 1277	0 1275	0 1285	0 1285

Table 3 4 Real and Reactive Power Outputs (in p u) for System–B ($\alpha = 2\ 0$)

P_G&Q_G	LFLOW	OBJ-I	OBJ-II	OBJ-III	OBJ-IV
P_{G_1}	4 4310	2 2250	2 0087	2 0648	2 1868
P_{G_2}	0 4000	1 3618	1 4230	1 3414	1 2253
P_{G_3}	0 2000	1 2061	1 3473	1 3739	1 3736
Q_{G_1}	−0 1896	0 0441	0 1218	0 0297	0 0018
Q_{G_2}	1 5745	0 9642	0.8660	0 9981	1 0433
Q_{G_3}	1 3142	0 8807	0 8552	0 8119	0 8123
Q_{G_4}	0 2545	0 2565	0 2564	0 2568	0 2568
Q_{G_5}	0 3792	0 3817	0 3812	0 3825	0 3824
Q_{G_6}	0 2519	0 2542	0 2541	0 2546	0 2546

Table 3.5: Real and Reactive Power Outputs (in p.u.) for System–C ($\alpha = 1$)

Bus No.	Real Power Output				Reactive Power Output			
	LFLOW	OBJ-II	OBJ-III	OBJ-IV	LFLOW	OBJ-II	OBJ-III	OBJ-IV
1	7.6781	4.5391	4.2247	3.3033	2.2162	0.8752	0.7374	0.6205
2	0.3000	0.5250	0.5250	0.5250	0.1735	0.0495	0.0493	0.0729
3	3.6000	1.7519	3.2493	3.8033	1.1045	0.4242	0.4107	0.4343
4	1.8000	2.5666	2.2618	3.2040	0.7143	0.5152	0.4629	0.6575
5	0.9900	0.2500	0.9647	1.2491	0.1740	0.0321	0.0393	0.0656
6	1.0000	2.5000	2.5000	2.5000	0.5643	0.2644	0.2431	0.3273
7	2.5000	0.5407	0.7555	1.0444	0.6937	0.5852	0.5604	0.5415
8	2.3000	2.4673	3.3752	3.4925	0.6544	0.0043	−0.0556	−0.0789
9	1.4000	2.1623	2.5000	2.5000	0.5597	0.0935	0.3395	0.6459
10	1.8000	3.6900	3.6900	3.6900	0.7562	0.0487	0.0357	0.0436
11	0.6000	1.7495	1.3160	1.9650	0.1152	0.1018	0.0442	0.2343
12	1.8000	2.3968	2.3429	3.5713	0.2848	0.1782	0.1737	0.4873
13	1.2000	1.3233	1.0926	1.9287	0.1598	0.1059	0.0904	0.2738
14	5.5000	4.0470	2.8844	2.3046	0.3171	−0.5780	−0.6928	−0.7728
15	0.2000	1.0266	0.9513	1.0263	0.1456	0.0952	0.0766	0.0984
16	0.1800	0.1583	0.6222	0.8886	0.0007	−0.0083	0.0338	0.1036
17	0.3200	0.3557	0.9641	0.9434	0.0190	0.0047	0.0613	0.0870
18	0.2000	0.4706	0.8161	0.9372	0.0462	0.0499	0.1146	0.1653
19	16.0000	10.0083	9.2007	6.1192	0.9829	−1.8605	−2.0563	−2.2953
20	9.0000	8.4574	7.3400	5.5835	0.6687	−0.5604	−0.7087	−0.8798
21	1.5000	3.6900	3.6900	3.6900	0.4244	−0.1579	−0.1935	−0.0287
22	4.5400	7.0455	6.5446	7.8172	−0.6074	−0.7161	−0.9026	−0.4167
23	1.0000	2.5000	2.5000	2.5000	0.3707	−0.3328	−0.3536	−0.3312
24	—	—	—	—	−0.3754	−0.3846	−0.3846	−0.1626

value σ_{min} can act as a reliable indicator of voltage stability margin during stressed condition of the network and it gives similar information as the Q-margin. However, at light loading condition (away from saddle node bifurcation points), the correlation between Q-margin and σ_{min} is lost. Since the base case loading of the System–C corresponds to a stressed condition, effect on voltage stability margin for this system has been analysed in terms of σ_{min} only. The source real and reactive power outputs (in p.u.) obtained from the three rescheduling schemes and their base values are presented in Table 3.5.

Fig. 3.2 presents the variation of σ_{min} in each case as the loading is increased in the system. Loading has been increased upto $\alpha = 1.38$ beyond which the load flow did not converge. From

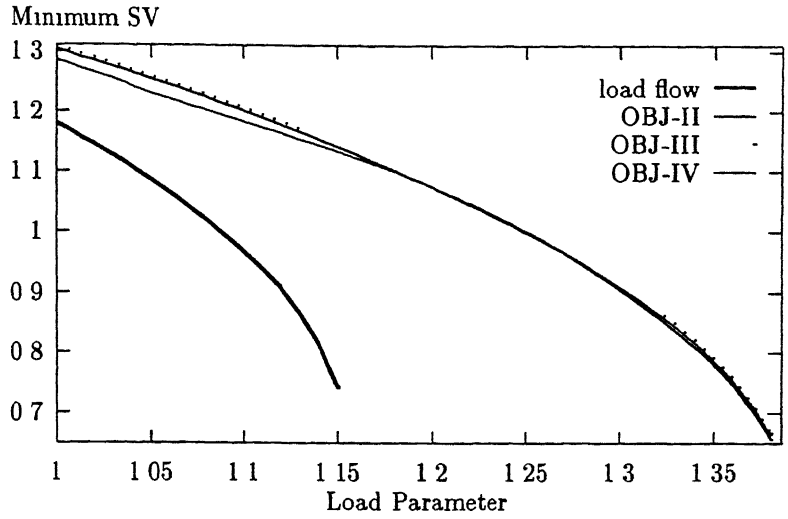

Figure 3 2 Effect of load variation on σ_{min} for 156-bus Indian System

this figure, it can be observed that at all the loadings, the voltage stability margin is enhanced using either of the three (OBJ-II, OBJ-III or OBJ-IV) schemes from the unoptimised case

3.6 Conclusion

The studies presented in this Chapter reveal the following

(i) The generation rescheduling using any of the four objectives in stressed condition of system increases the voltage stability margin which can be measured either in terms of system Q-margin or the minimum singular value of the power flow Jacobian

(ii) At light load conditions, the rescheduling of generation using any of the schemes is unable to increase the Q-margin σ_{min}, however, is slightly increased with OBJ-III or OBJ-IV In such cases, any correlation between σ_{min} of the power flow Jacobian and Q-margin is lost

(iii) Amongst the four objectives tried out, the new OBJ-IV has consistently resulted into better results than other objectives which is close to that obtained with OBJ-III However, computationally it is less expensive in comparison to OBJ-III Hence the new objective (OBJ-IV) of minimising the slack bus reactive injection along with load flow objective can be effectively used for voltage stability margin enhancement

Chapter 4

Observance of Local Bifurcations

4.1 Introduction

An electric power system is a complex nonlinear dynamical system and its behaviour can be described by nonlinear algebraic and differential equations The behaviour of a power system may undergo qualitative changes under system disturbances and parameter variations In dynamical systems' lingo, this qualitative change in the phase portrait of a system, when a system parameter is quasistatically varied is known as *bifurcation* The parameter under variation is called *bifurcation parameter* It is found in the literature [117, 161] that bifurcations in underlying dynamical model of a power system are closely linked with its instability This is especially true for voltage collapse precipitated by slow variation in a system parameter such as load. This chapter deals with the *local bifurcations* namely static and Hopf bifurcation A local bifurcation means bifurcations occurring in the neighbourhood of the fixed operating point[1]

The region of attraction of stable operating point (s e p) is decided by unstable operating points.(u e p) and closed orbits (especially the type-1) lying on the stability boundary of the stable operating point Following the instability, the unstable trajectory is determined by the unstable manifold of the controlling unstable operating point [128]

In this Chapter, the study of the unstable manifold of the unstable operating point has been conducted to differentiate between angle and voltage stability The studies have been conducted on the two sample systems, one being a 3-bus system and the other a 9-bus system having multiple generators Further, Hopf bifurcation theory has been used to determine the

[1]Fixed operating point, fixed point, equilibrium point and singular point have been used interchangeably in this thesis It simply means a point in the state space where the velocity vector vanishes i e $\dot{x} = 0$

critical values of control system and load parameters A detailed nonlinear dynamical model of generator along with its excitation control system and turbine governing system loop and induction motor load have been considered The hard limiters in the excitation control loop and turbine speed governing loop have been modelled using a new approach in an analytic form and the load torque as nonlinear function of speed The analysis have been carried out on two sample systems, one consisting of a single generator (2-bus system) and the other containing multiple generators (10-bus system) Finally, the stability region in the parameter space has been characterised considering the saddle-node bifurcation and Hopf bifurcation

Since the phenomena of bifurcation and chaos are relatively new to the power system field, some of the basic definitions and concepts of these phenomena have been briefly explained in this Chapter and also in Chapter 5

4.2 Local Bifurcation

4.2.1 General

Consider an autonomous dynamical system described by the following parameterised vector field

$$y = g(y, \lambda), \quad y \in R^n, \quad \lambda \in R^p \tag{4 1}$$

where g is a C^r function on some open set in $R^n \times R^p$ The degree of differentiability will be determined by the need for the number of terms to be retained in Taylor expansion of equation (4 1) Usually C^5 will be sufficient Let equation (4 1) has a fixed point at $(y, \lambda) = (y_0, \lambda_0)$, i e

$$g(y_0, \lambda_0) = 0 \tag{4 2}$$

Two questions immediately arise·

1 Is the fixed point stable or unstable ?

2 How is stability or instability affected if λ is varied ?

To check the stability of a fixed point, the first step is to examine the linear vector field obtained by linearising equation (4 1) about the fixed point $(y, \lambda) = (y_0, \lambda_0)$ The linear vector field is given by

$$\xi = D_y g(y_0, \lambda_0)\xi, \quad \xi \in R^n \tag{4 3}$$

where $\xi = y - y_0$, $D_y g = \left\{\frac{\partial g}{\partial y}\right\}$ is Jacobian matrix

If the fixed point is hyperbolic (i e none of the eigenvalues of $D_y g(y_0, \lambda_0)$ lie on the imaginary axis), the stability of (y_0, λ_0) of equation (4 1) is determined by the linear equation (4 3)

If the fixed point is hyperbolic, then varying λ slightly does not alter the nature of the stability of the fixed point If $D_y g(y_0, \lambda_0)$ is hyperbolic and is invertible, then by implicit function theorem, there exists a unique C^r function $y(\lambda)$, such that

$$g(y(\lambda), \lambda) = 0 \tag{4 4}$$

for λ sufficiently close to λ_0 with $y(\lambda_0) = y_0$

Now by continuity of the eigenvalues with respect to parameters, for λ sufficiently close to λ_0, $D_y g(y(\lambda), \lambda)$ has no eigenvalue on the imaginary axis Therefore, for λ sufficiently close to λ_0, the hyperbolic fixed point (y_0, λ_0) of equation (4 1) persists and its stability type remains unchanged To summarise, in a neighbourhood of λ_0 an isolated fixed point of equation (4 1) persists and always has the same stability type However, if the fixed point (y_0, λ_0) of equation (4 1) is not hyperbolic i e when $D_y g(y_0, \lambda_0)$ has some eigenvalues on the imaginary axis, radically new dynamical behaviour can occur for λ very close to λ_0 , for example fixed points can be created or destroyed and time-dependent behaviour such as periodic, quasiperiodic or even chaotic dynamics can be created In certain sense, the more are the eigenvalues on the imaginary axis, the more exotic the dynamics will be

4.2.2 A Zero Eigenvalue

If $D_y g(y_0, \lambda_0)$ has a single zero eigenvalue with the remaining eigenvalues having non zero real parts, the following three types of bifurcations may occur.

4 2.2.1 Pitchfork Bifurcation

Consider a vector field

$$x = f(x, \mu) = \mu x - x^3, \quad x \in R^1, \quad \mu \in R^1 \tag{4 5}$$

The fixed points of equation (4 5) are $x = 0$ and $x^2 = \mu$ as shown in Fig 4 1 At $\mu = 0$, the associated Jacobian matrix is singular

For $\mu < 0$, there is one fixed point i e $x = 0$ which is stable For $\mu > 0$, $x = 0$ is still a fixed point, but two new fixed points have been created at $\mu = 0$ and are given by $x^2 = \mu$

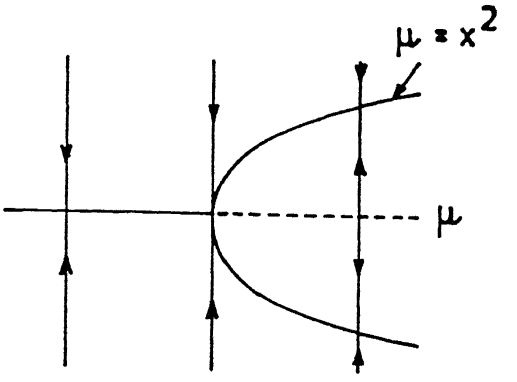

Figure 4 1 Pitchfork Bifurcation

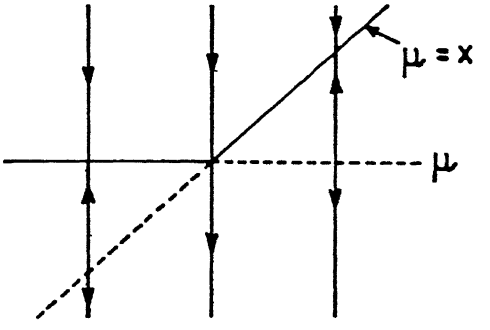

Figure 4 2 Transcritical Bifurcation

In the process, $x = 0$ has become unstable for $\mu > 0$, while other two fixed points are stable This type of bifurcation in which the original branch changes its stability character and a pair of fixed points are born when the Jacobian matrix is singular, is called *pitchfork bifurcation*

4.2.2.2 Transcritical Bifurcation

Consider a vector field

$$x = f(x, \mu) = \mu x - x^2, \quad x \in R^1, \quad \mu \in R^1 \tag{4 6}$$

The fixed points of equation (4 6) are $x = 0$ and $x = \mu$ as shown in Fig 4 2

At $\mu = 0$, the associated Jacobian matrix is singular For $\mu < 0$, there are two fixed points $x = 0$ is stable and $x = \mu$ is unstable The two fixed points coalesce at $\mu = 0$ and for $\mu > 0$, $x = 0$ is unstable and $x = \mu$ is stable Thus, an exchange of stability has occurred at $\mu = 0$ This type of bifurcation is called *transcritical bifurcation*

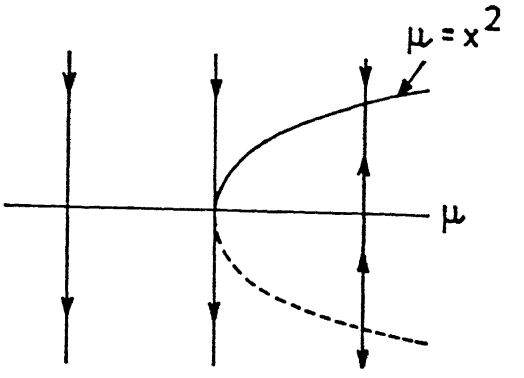

Figure 4 3 Saddle-node Bifurcation

4.2.2.3 Saddle–node Bifurcation

Consider a vector field

$$\dot{x} = f(x, \mu) = \mu - x^2, \quad x \in R^1, \quad \mu \in R^1 \tag{4 7}$$

The fixed points of equation (4 7) are $\mu = x^2$ This represents a parabola in the μ–x plane as shown in Fig 4 3 For $\mu < 0$, equation (4 7) has no fixed point For $\mu > 0$, there exists two fixed points, one of them being stable and the other unstable At $\mu = 0$, the associated Jacobian matrix is singular This particular type of bifurcation where on one side of a parameter value there is no fixed point and on the other side there exists two fixed points is referred to as a *saddle-node bifurcation*

4.3 A Pair of Pure Imaginary Eigenvalues

When the matrix $D_y g(y_0, \lambda_0)$ has a pair of purely imaginary eigenvalues, a Hopf bifurcation (HB) arises and is characterised by emergence of a periodic orbit (limit cycle) around an equilibrium point At Hopf bifurcation, the number of fixed points are preserved The Hopf bifurcation is said to be *subcritical* when unstable periodic orbit emerges around stable fixed point as shown in Fig 4 4 The Hopf bifurcation is said to be *supercritical* when stable periodic orbit emerges around unstable fixed points as shown in Fig 4 5 The nature of Hopf bifurcation (subcritical/supercritical) can be determined by solving the set of nonlinear differential equations

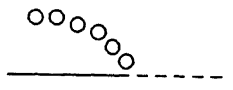

Figure 4 4 Subcritical Hopf Bifurcation

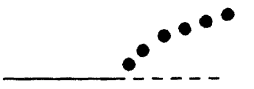

Figure 4 5 Supercritical Hopf Bifurcation

4.3.1 Determination of Static Bifurcation

Occurrence of transcritical bifurcation in power systems have been shown in very few literatures [105, 165] Transcritical and pitch fork bifurcations are non generic whereas the saddle-node bifurcation (SNB) is generic

The saddle-node bifurcation in a power system model occurs when the number of solutions to the load flow equations changes under parameter variation The singularity of $D_y g(y_0, \lambda_0)$ has been popularly used to identify SNB At SNB, a stable operating point and a saddle coalesce to form an unstable equilibrium at which the Jacobian is singular and has a zero eigenvalue A zero eigenvalue of $D_y g(y_0, \lambda_0)$, also arises when a type-2 and a type-1 equilibrium coalesce to form a *fold bifurcation* (FB) or *limit point* (LP)

Several researchers such as Alvarado et al [53] and Canizares et al [103,126] have presented a method called *Point of Collapse* (POC) method to determine SNB In POC method, the parameter λ is regarded as a variable and the condition of zero eigenvalue of the Jacobian is appended to the set of nonlinear equations Thus, if v is right eigenvector corresponding to the zero eigenvalue of the Jacobian, the SNB or LP can be obtained by solving the following equations considering $\lambda \in R^1$,

$$g(y, \lambda) = 0 \tag{4 8}$$

$$D_y g(y, \lambda) v = 0 \tag{4 9}$$

$$\|v\| \neq 0 \tag{4 10}$$

The POC method can also be formulated in terms of the left eigenvector One of the major limitations of the POC method is that it yields only (y, λ) corresponding to a SNB or LP In the neighbourhood of the SNB or LP, the equation (4 8) can not be solved by Newton Raphson

method as the Jacobian becomes ill-conditioned To overcome this difficulty, the continuation method [50] which is a modification of Newton-Raphson method has been used by Ajjarapu et al [100] and Iba et al [86] In the present work AUTO86 software [34] has been used for numerical analysis which also utilises the continuation method The continuation method involves a predictor step and a corrector step which have been described below

Predictor Step: Let a solution y_0 corresponding to λ_0 is known Prediction of the next solution can be made by taking an appropriately sized step in a direction tangent to the solution path Thus, the first task in the predictor process is to calculate the tangent vector This tangent calculation is derived by first taking the derivative of both sides of the equation (4 8)

$$d[g(y,\lambda)] = [g_y, g_\lambda] \begin{bmatrix} dy \\ d\lambda \end{bmatrix} = 0 \tag{4 11}$$

On the left side of this equation is a matrix of partial derivatives multiplied by a vector of differential The above equations involve $(n+1)$ variables

Thus one more equation is needed to have a unique solution for the tangent vector This problem can be overcome by choosing a non-zero magnitude (say unity) for one of the components of the tangent vector (Let $d\lambda = 1$) This results in

$$\begin{bmatrix} g_y & g_\lambda \\ 0 & 1 \end{bmatrix} \begin{bmatrix} dy \\ d\lambda \end{bmatrix} = \begin{bmatrix} 0 \\ 1 \end{bmatrix} \tag{4 12}$$

The AUTO86 software usually chooses the largest component of the tangent vector to have a non-zero magnitude The corresponding parameter is called continuation parameter

Once the tangent vector has been found by solving equation (4 12) the predicted solution (y^*, λ^*) can be obtained as follows

$$\begin{bmatrix} y^* \\ \lambda^* \end{bmatrix} = \begin{bmatrix} y_0 \\ \lambda_0 \end{bmatrix} + \alpha \begin{bmatrix} dy \\ d\lambda \end{bmatrix} \tag{4 13}$$

The software has the capability to choose variable magnitude of step size α to improve the convergence

Corrector Step: Once the prediction has been made, a method of correcting the approximate solution is needed This is achieved by specifying the value of the parameter λ at its predicted value The new set of equations would be,

$$\begin{bmatrix} g(y,\lambda) \\ \lambda - \lambda^* \end{bmatrix} = 0 \tag{4 14}$$

The equation (4 14) is solved using Newton-Raphson method with predicted solution as initial guess The convergence of this equation yields a point say (y_1, λ_1) on the branch and repeating the above process the solution curve in $(n+1)$ dimensional space $R^n \times R^1$ is traced Along the solution branch, the eigenvalues of matrix $g_y(y_0, \lambda_0)$ is monitored to detect the local bifurcations such as saddle-node and Hopf bifurcations

4.3.2 Determination of Hopf Bifurcation

For determination of Hopf bifurcation, BIFOR2 program [11] has been used It makes use of center manifold theory [11,21,80] The structure of orbit near $(y, \lambda) = (y_0, \lambda_0)$ is determined by the vector field in equation (4 1) restricted to the centre manifold This restriction results in a p-parameter family of vector fields on a two-dimensional center manifold However BIFOR2 program utilised in the present work, caters to one parameter only

On the center manifold, the vector field in equation (4 1) has the following form [11,80]

$$\begin{bmatrix} Z_1 \\ Z_2 \end{bmatrix} = \begin{bmatrix} Re\lambda(\mu) & -Im\lambda(\mu) \\ Im\lambda(\mu) & Re\lambda(\mu) \end{bmatrix} \begin{bmatrix} Z_1 \\ Z_2 \end{bmatrix} + \begin{bmatrix} f^1(Z_1, Z_2, \mu) \\ f^2(Z_1, Z_2, \mu) \end{bmatrix} \tag{4 15}$$

$$(Z_1, Z_2, \mu) \in R^1 \times R^1 \times R^1$$

where, f^1 and f^2 are nonlinear functions in Z_1 & Z_2 and $\lambda(\mu) = \alpha(\mu) + \jmath\omega(\mu)$ are the eigenvalues of the vector field linearised about the fixed point If $\alpha(\mu) = 0$ and $\omega(\mu) \neq 0$, the fixed point is not hyperbolic The dynamical system undergoes a Hopf bifurcation [11,21,38,80] and a periodic orbit emerges In order to analyse the dynamics, the equation (4 15) needs to be simplified and cast into its Poincare-normal form [11,80] as follows,

$$Z_1 = \alpha(\mu)Z_1 - \omega(\mu)Z_2 + (a(\mu)Z_1 - b(\mu)Z_2)({Z_1}^2 + {Z_2}^2) + O(|Z_1|^5, |Z_2|^5) \tag{4 16}$$

and

$$Z_2 = \omega(\mu)Z_1 + \alpha(\mu)Z_2 + (a(\mu)Z_1 + b(\mu)Z_2)({Z_1}^2 + {Z_2}^2) + O(|Z_1|^5, |Z_2|^5) \tag{4 17}$$

For the sake of simplicity, it is desirable to work in polar coordinates ($r\angle\theta = Z_1 + \jmath Z_2$) and the equations (4 16) and (4 17) will assume the following form,

$$r = \alpha(\mu) + a(\mu)r^3 + O(r^5) \tag{4 18}$$

$$\theta = \omega(\mu) + b(\mu)r^2 + O(r^4) \tag{4 19}$$

Upon Taylor series expansion of coefficients around $\mu = 0$, the equations (4 18) and (4 19) yield,

$$r = \alpha'(0)\mu r + a(0)r^3 + O(\mu^2 r, \mu r^3, r^5) \tag{4 20}$$

$$\theta = \omega(0) + \omega'(0)\mu + b(0)r^2 + O(\mu^2, \mu r^2, r^4) \tag{4 21}$$

Neglecting higher order terms, the dynamics of equation (4 1) in Poincare-normal form can be given as follows

$$r = \alpha'(0)\mu r + a(0)r^3 \tag{4 22}$$

$$\theta = \omega(0) + \omega'(0)\mu + b(0)r^2 \tag{4 23}$$

The value of $r > 0$ and μ for which $r = 0$ and $\theta \neq 0$ correspond to periodic orbits of equations (4 22) and (4 22) Therefore, for $-\infty < \mu\alpha'(0)/a(0) < 0$ and μ sufficiently small, the periodic orbit for equations (4 22) and (4.23) is given as follows

$$(r(t), \theta(t)) = \left[\sqrt{\frac{-\mu\alpha'(0)}{a(0)}}, \left(\omega(0) + \left\{\omega'(0) - \frac{b(0)\alpha'(0)}{a(0)}\right\}\mu\right)t + \theta_0\right] \tag{4 24}$$

where θ_0 is the initial phase angle The periodic orbit is asymptotically stable for $a(0) < 0$ (supercritical) and unstable for $a(0) > 0$ (subcritical)

4.3.3 Determination of Unstable Manifold

Consider a type-1 unstable equilibrium point (u e p) say $\hat{x}$ Let λ_μ be the only eigenvalue with a positive real part and its eigenvector be η_μ The one dimensional unstable manifold $W^u(\hat{x})$ of $\hat{x}$ can be broken by removing $\hat{x}$ from the manifold, into two half manifolds $W^u_+(\hat{x})$ and $W^u_-(\hat{x})$ Each part in itself is an invariant manifold consisting of a single trajectory as shown in Fig 4 6 Calculation of each part involves following two major steps [45,59,128]

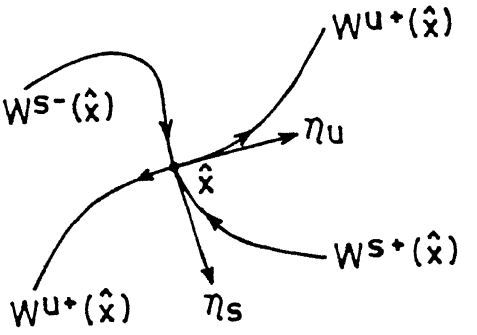

Figure 4 6 Half-manifolds at an equilibrium point

Locating a point on $W_+^u(\hat{x})$: Near the controlling (u e p) $W_+^u(\hat{x})$ can be approximated to the first order, by the unstable eigenvector η_μ Therefore, in order to derive $W_+^u(\hat{x})$, a point close to $\hat{x}$ that lies on η_μ can be chosen More specifically, for some small $\alpha > 0$, choose the point

$$x_\alpha = \hat{x} + \alpha\eta_\mu \tag{4 25}$$

Care should be taken when choosing α If α is too large, x_α might not lie close enough to $W_+^u(\hat{x})$ in which case the trajectory through x_α is not a good approximation to $W_+^u(\hat{x})$ α is chosen to locate a point x_α on $W_+^u(\hat{x})$, as follows

(1) Given a small enough $\epsilon > 0$, create a ball around $\hat{x}$ such that $\mid x - \hat{x} \mid < \epsilon$ holds

(2) Give the initial α $(\alpha > \epsilon)$

(3) Obtain $x_\alpha = \hat{x} + \alpha\eta_\mu$

(4) Integrate the system from x_α in reverse time by a specified number of steps

(5) If the system trajectory remains in the ball, stop Otherwise, let $\alpha = \frac{1}{2}\alpha$ and go to Step 3

Integrating on $W_+^u(\hat{x})$: Removal of $\hat{x}$ from $W^u(\hat{x})$, splits $W^u(\hat{x})$ into two segments The larger segment of $W_+^u(\hat{x})$ is found by integration from x_α in forward time The smaller segment is the line segment connecting $\hat{x}$ and x_α

Similarly $W_-^u(\hat{x})$ can be computed by considering the reverse direction of the eigenvector In order for an (u e p) to be on stability boundary, one of the two half manifolds should converge to the stable equilibrium point (s e p)

4.4 Power System Model for Bifurcation Studies

4.4.1 Generator Model

Different models of the generator [7,25,176] used in the studies are given as follows,

4.4 1.1 Second Order Generator Model

In this model, the generator is represented by a constant emf source behind the transient reactance and modelled by the swing equation

$$\frac{d\delta}{dt} = \omega \tag{4 26}$$

$$M_g \frac{d\omega}{dt} = P_M - P_{ge} - D\omega \tag{4 27}$$

where δ is generator's internal bus voltage angle, ω the speed deviation, M_g the moment of inertia of generator, P_{ge} the electrical power output of the generator, D the damping constant and P_M is the mechanical power input to the generator

4 4 1.2 Third Order Generator Model

This model ignores the saliency and accounts for the changes in the flux linkage of the field winding although the changes in the flux linkages of other windings are ignored Therefore, there is one more state equation for the third order generator model, in addition to the swing equations (4 26) and (4 27)

$$\frac{T'_{do}}{X_d - X'_d}\frac{dE'_q}{dt} = \left[\frac{E_{fd} - E'_q}{X_d - X'_d} - \frac{Q_{ge}}{E'_q}\right] \tag{4 28}$$

where E'_q is the voltage behind the d-axis transient reactance X'_d, T'_{do} is the d-axis transient open circuit field time constant, X_d is the d-axis steady state reactance, E_{fd} the voltage applied to the field and Q_{ge} is the reactive power output at the internal node of the generator

4.4 1 3 Fourth Order Generator Model

If the effect of saliency is considered, the changes in flux linkages of the field windings have to be accounted for along the d- and q-axes Therefore, two more additional state equations (4 29) and (4 30) along with the swing equations (4 26) and (4 27) have to be considered

$$T'_{do}\frac{dE'_q}{dt} = E_{fd} + (X_d - X'_d)I_d - E'_q \tag{4 29}$$

$$T'_{qo}\frac{dE'_d}{dt} = -(X_q - X'_q)I_q - E'_d \tag{4 30}$$

along with the voltage equation,

$$\begin{bmatrix} E'_q - V_q \\ E'_d - V_d \end{bmatrix} = \begin{bmatrix} R_a & -X'_d \\ X'_q & R_a \end{bmatrix} \begin{bmatrix} I_q \\ I_d \end{bmatrix} \tag{4 31}$$

where, T'_{qo} is the q-axis open circuit transient time constant, R_a the armature resistance, X_q the steady state q-axis reactance, X'_q the q-axis transient reactance, E'_d the voltage behind X'_q, I_d & I_q the d- and q- axes armature current and V_d & V_q are the generator terminal voltage along d- and q-axes

4.4.2 Load Model

The load characteristics are known to have profound effect on the system dynamics [184, 185] The classical models of load such as constant P and Q, constant current or constant impedance have been reported to be insufficient and inappropriate to capture voltage dynamics [40, 114] Different load models used for the bifurcation studies are as follows

4.4 2.1 Load Model–I

This load model considers a composite load consisting of a dynamic induction motor ($P_{IM} + jQ_{IM}$) in parallel with a static constant P, Q load ($P_s + jQ_s$) The model of induction motor has been taken from ref [40] and expressed as a function of rate of change of its terminal voltage magnitude and angle The model is given as follows

$$P_s = P_1 \tag{4 32}$$

$$Q_s = Q_1 \tag{4 33}$$

$$P_{IM} = P_0 + K_{p\omega}\theta + K_{pv}(V + TV) \tag{4 34}$$

$$Q_{IM} = Q_0 + K_{q\omega}\theta + K_{qv}V + K_{qv_2}V^2 \tag{4 35}$$

where $P_0 + jQ_0$ is the constant part of induction motor load, $K_{p\omega}$, K_{pv}, T, $K_{q\omega}$, K_{qv} and K_{qv_2} are load coefficients

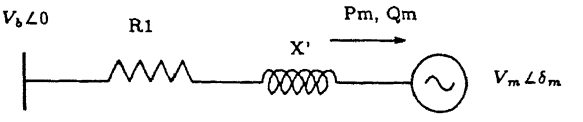

Figure 4 7 Model of induction motor

4.4.2.2 Load Model–II

This model also represents a composite load consisting of static and dynamic components The equations describing the load $(P_d + jQ_d)$ using this model [104, 150] are as follows

$$P_d = \ell\, pf + D\theta + aV \tag{4 36}$$

$$Q_d = \ell\, \sqrt{1 - pf^2} + b\theta + kV \tag{4 37}$$

where ℓ is nominal MVA demand at the load bus, pf the power factor and D, a, b and k are the dynamic load parameters

The model–I and model–II tacitly ignore the stator/network transients and if stator transients are included, these models are not be valid [150]

4.4.2.3 Load Model–III

This model represents a third order induction motor model that ignores stator transients If $V_m\angle\delta_m$ be the voltage behind the stator resistance R_1 and transient reactance X' of the motor as shown in Fig 4 7, ω_R its rotor speed, the equation governing its dynamics can be written as [99]

$$\frac{T'_o}{X_s - X'}\frac{dV_m}{dt} = \left[\frac{Q_m}{V_m} - \frac{V_m}{X_s - X'}\right] \tag{4 38}$$

$$\frac{d\delta_m}{dt} = \omega_R - \omega_s + \frac{P_m(X_s - X')}{V_m^2 T'_o} \tag{4 39}$$

$$M_m\frac{d\omega_R}{dt} = P_m - T_L\,\omega_R \tag{4 40}$$

where M_m = Moment of inertia of induction motor

T'_o = Open circuit transient time constant

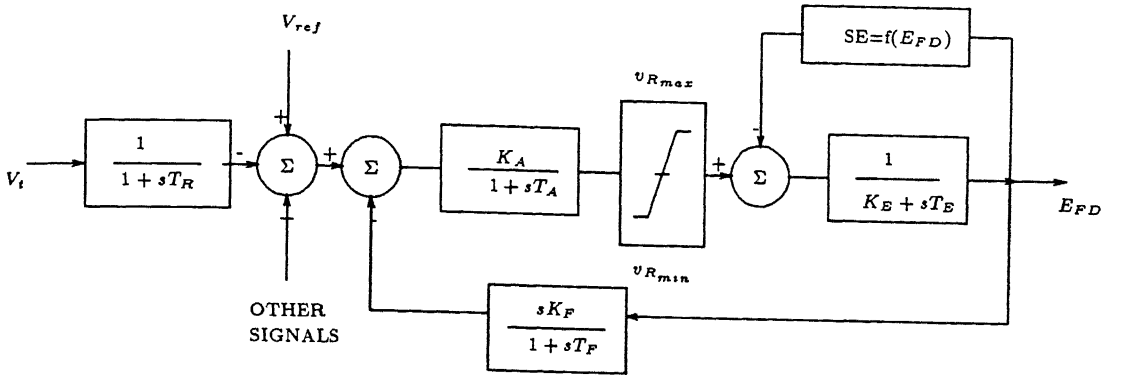

Figure 4 8 IEEE type–1 exciter

X_s & X' = Steady state and transient reactance

P_m & Q_m = Real and reactive power drawn at the internal node of the motor

ω_R = Rotor speed

$T_L = A_0 + B_0\omega_R + C_0\omega_R^2$, speed dependent load torque

$\omega_s = \omega_0 + \phi_s$, where ω_0 is the synchronous speed and ϕ_s is the phase angle of the terminal voltage

4.4.3 Exciter Model

IEEE type-1 exciter [7,25] as shown in Fig 4 8 has been considered in this study and equations governing the dynamics is given as follows

$$T_e\frac{dE_{fd}}{dt} = V_a - (K_e + S_E)E_{fd} \tag{4 41}$$

$$T_f\frac{dV_f}{dt} = K_f E_{fd} - V_f \tag{4 42}$$

$$T_a\frac{dV_a}{dt} = K_a(V_{ref} - V_t - V_f) - V_a \tag{4 43}$$

and $V_a^{min} < V_a < V_a^{max}$

where $S_E = A_{ex}\exp(B_{ex}E_{fd})$ is a saturation function

V_a = Regulator amplifier output voltage

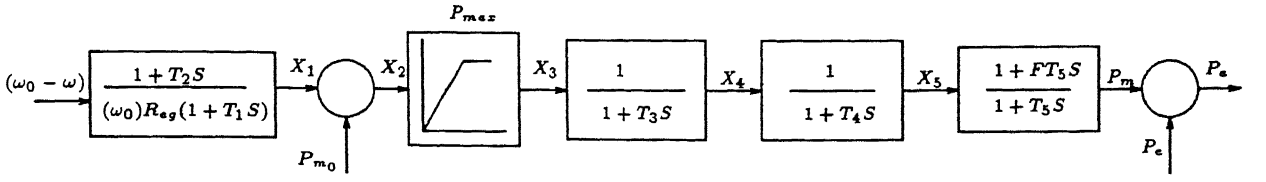

Figure 4 9 General purpose speed governing system

K_a = Regulator amplifier output gain

T_a = Regulator amplifier output time constant

V_f = Stabilising circuit output voltage

K_f = Stabilising circuit output gain

T_f = Stabilising circuit output time constant

K_e = Exciter gain

T_e = Exciter time constant

V_{ref} = Reference voltage setting

V_t = Terminal voltage

4.4.4 Speed Governor Model

A general purpose governor model [7] as shown in Fig 4 9 has been used and its model can be described by the following equations,

$$T_1 \frac{dX_1}{dt} = \left[\frac{\omega_0 - \omega - T_2 \frac{d\omega}{dt}}{\omega_0 R_{eg}} - X_1 \right] \tag{4 44}$$

$$X_2 = X_1 + P_{M0} \tag{4 45}$$

$$X_3 = X_2 \tag{4 46}$$

$$P_{max} > X_3 > 0 \tag{4 47}$$

$$T_3 \frac{dX_4}{dt} = X_3 - X_4 \tag{4 48}$$

$$T_4 \frac{dX_5}{dt} = X_4 - X_5 \tag{4 49}$$

and

$$T_5 \frac{dP_M}{dt} = X_5 + FT_5 \frac{dX_5}{dt} - P_M \tag{4 50}$$

where R_{eg} = Turbine steady state regulator setting or droop

P_{max} = Maximum turbine output

T_1 = Governor response time constant

T_2 = Hydro reset or pilot valve time constant

T_3 = Servo or hydro gate time constant

T_4 = Steam valve bowl time constant (zero for hydrogovernor)

T_5 = Steam reheat time constant or half hydro water starting time constant

$F = pu$ shaft output ahead of reheater (-2 0 for hydro units)

4.4.5 Hard Limiter Model

The hard limiters used in the excitation control as well as in turbine speed governing control loop for providing ceiling to amplifier output voltage and generator real power output The presence of hard limiters make the nonlinear equations non-analytic Thus the model can not be straightaway analysed for Hopf bifurcation using BIFOR2 [8] which is based on the assumption that the function is C^r $(r \geq 5)$ i e analytic in nature In order to overcome this difficulty, a new model of the limiters is proposed representing them by *tanhyperbolic* function

A typical hard limiter is shown in Fig 4 10 having input variable as X and output as Y It is seen that if X is between $-X_{LIMIT}$ and X_{LIMIT}, $Y = X$ i e the slope of the curve is unity and when $X > X_{LIMIT}$ or $X < -X_{LIMIT}$, $Y = \pm X_{LIMIT}$ i e the slope is zero In order to approximate the hard limiter, a function of the following form has been selected

$$Y = X_{LIMIT} \tanh\left(\frac{X}{X_{LIMIT}}\right) \tag{4 51}$$

This function has unity slope at $X = 0$ and saturates when $X > X_{LIMIT}$ or $X < -X_{LIMIT}$ In order to establish the validity of this function, a sample study was conducted on the excitation

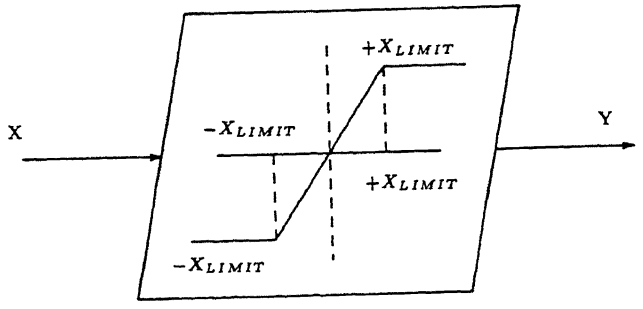

Figure 4 10· A typical hard limiter

system for $X_{LIMIT} = 3\,5$ pu and the signal $YvsX$ has been plotted in Fig 4 11 and 4 12 for the sake of comparison It can be observed that the new function as given by equation (4 51) closely approximate the hard limiter Hence, tanh function has been used to the model hard limiter action which is smooth and analytic

4.5 Case Studies

4.5.1 Static Bifurcations

Static bifurcations arise when number of fixed points changes if a system parameter is varied In order to illustrate the occurrence of static bifurcations and its implications, studies were conducted on a 3-bus and a 9-bus sample systems derived from ref [66] and [7], respectively and also presented in Appendices–B and E respectively The studies were assisted by AUTO86 software [34] on HP-9000/735 computer systems and are presented below

4.5.1.1 3–Bus System

The topology and data for 3-bus system is shown in Fig B 1 in Appendix–B It consists of an infinite bus, a generator and a load bus The generator is modelled by using its second order model equations (4 26) and (4 27) and load by load model-I given by equations (4 32) to (4 35) With this formulation, the resulting equations become purely a system of ordinary differential

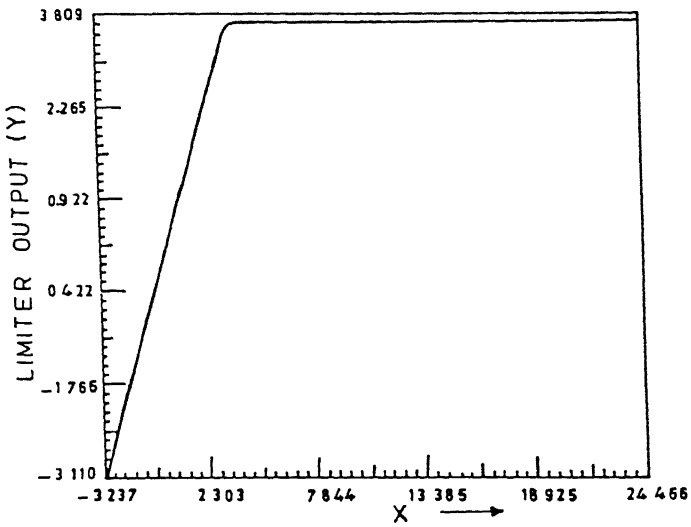

Figure 4 11 Hard limiter output

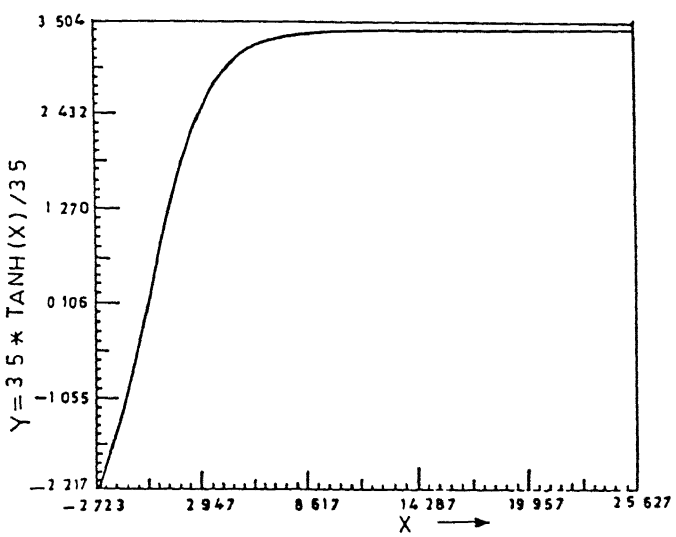

Figure 4 12 Tanh limiter output

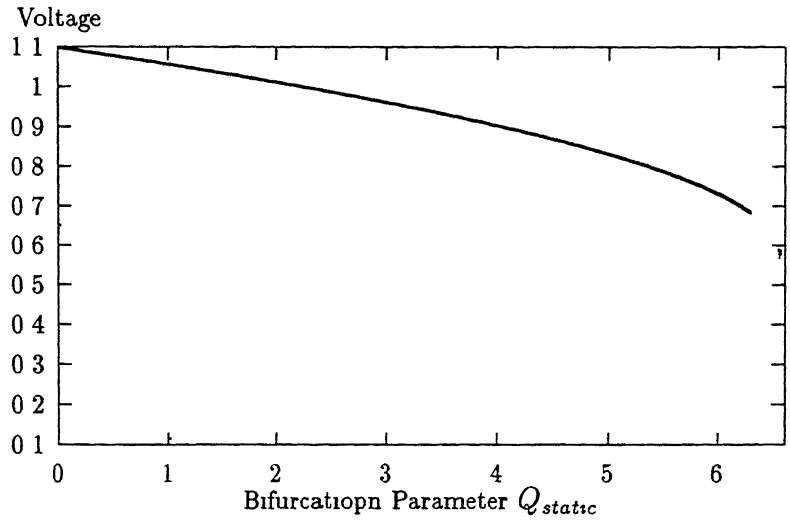

Figure 4 13 Variation of voltage magnitude V vs bifurcation parameter Q_1 for 3-bus system

equations The static reactive load component Q_1 was taken as bifurcation parameter The bifurcation diagram has been plotted showing variation of load bus voltage V versus the bifurcation parameter Q_1 is given in Fig 4 13 The following bifurcations are observed from Fig 4 13

- HB at $Q_1 = 6\ 272709$ and $6\ 542023$
- SNB at $Q_1 = 6\ 543211$
- LP at $Q_1 = 0\ 7841441$ and $1\ 978656$

From Figs 4 13, it is seen that there are different numbers and types of fixed points in different regions of the parameter They are listed as below.

Region A ($0 \leq Q_1 \leq 0\ 7841441$) one stable and one type-1 unstable fixed points

Region B ($0\ 7841441 \leq Q_1 \leq 1\ 978658$) one stable, two type-1 unstable and a type-2 unstable fixed points

Region C ($1\ 978658 \leq Q_1 \leq 6.272709$) one stable, one type-1 unstable fixed points

Region D ($6\ 272709 \leq Q_1 \leq 6\ 542023$) one type-2 unstable and one type-1 unstable fixed points

Region E ($6\ 542023 \leq Q_1 \leq 6\ 543211$) one stable and one type-1 unstable fixed points

All along the bifurcation parameter, it is seen from the bifurcation diagrams of Fig 4 13 that unstable equilibrium points exist along with stable equilibrium point In view of this, the stable equilibrium point is not globally asymptotically stable, and its boundary of region of attraction is given by the union of the stable manifolds of type-1 equilibrium points

Concentrating in the region B, it is found that there exist two type-1 unstable equilibrium points One type-1 u e p is characterised by high voltage and the other one by low voltage It will be of interest to know about the unstable manifold because for a type-1 u e p , the critical unstable trajectory can be approximated, after a finite time, by the unstable manifold of the type-1 controlling u e p [128] Since the dimension of unstable manifold of a type-1 u e p is one, the unstable mode relative to critical unstable trajectory whose corresponding controlling u e p is type-1, is uniquely defined by the one-dimensional unstable manifold For a type-2 (or higher type) controlling u e p , the critical unstable trajectory can be approximated, after a finite time, by the unstable manifold of the controlling u e p But the dimension of the unstable manifold of a type-k u e p is k This causes the unstable mode relative to the critical unstable trajectory, whose corresponding controlling u e p is type-2 (or higher), not to be uniquely defined by the corresponding unstable manifold [128]

Figs 4 14 and 4 15 show the half unstable manifold, $W^u_-(\hat{x})$ computed in the reverse direction of the eigenvector associated with the real positive eigenvalue for the high voltage u e p at $Q_1 = 1\ 0$ pu From Figs 4 14 and 4 15 it is evident that the half manifold for this u e p converged to the stable equilibrium point (s e p) Thus, this type-1 u e p will be on the boundary of the region of s e p

Fig 4 16 and 4 17 show the plot of the other half manifold, $W^u_+(\hat{x})$ in the forward direction of the eigenvector It is seen that the state variables $\delta = (x[1])$ and $\omega = (x[2])$ in Fig 4 16 associated with the generator becomes unbounded while the variables $\theta = (x[3])$ and $V = (x[4])$ in Fig 4 17 remain bounded Therefore, a post-fault trajectory for which this type-1 u e p is the controlling one, will be accompanied by angle instability (or synchronous instability) only The voltage instability would not be observed in this case

Figs 4 18 and 4 19 show the plot of half manifold in the reverse direction of the eigenvector associated with the positive real eigenvalue of low voltage type-1 u e p corresponding to the same parameter value $Q_1 = 1\ 0$ pu , as studied earlier for the case of high voltage u e p It is established from the Figs 4 18 and 4 19 that the u e p will be on the stability boundary of s e p as it converged to the s e p Figs 4 20 and 4 21 show the plot of the other half manifold of this u e p determined in the direction of the eigenvector It is seen from Fig 4 20 that the

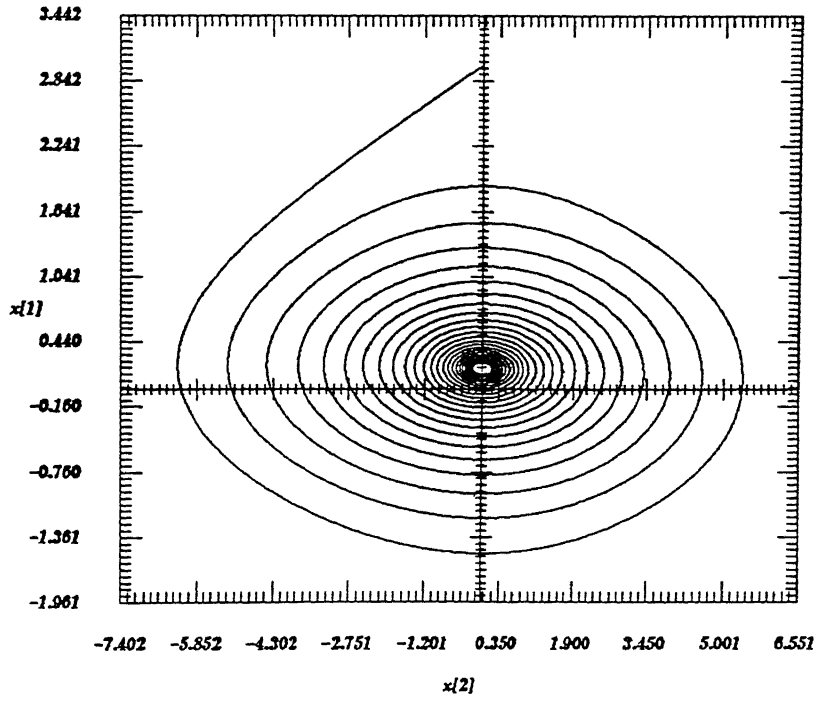

Figure 4 14: $W^u_{-}(\hat{x})$ plot of δ and ω for high voltage u e p of 3-bus system

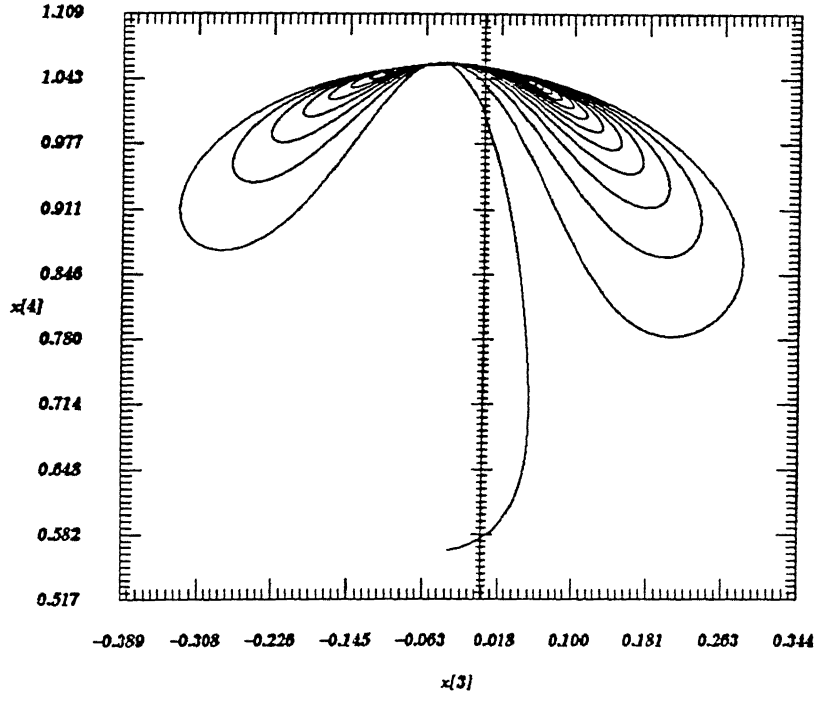

Figure 4 15 $W^u_{-}(\hat{x})$ plot of θ and V for high voltage u e p of 3-bus system

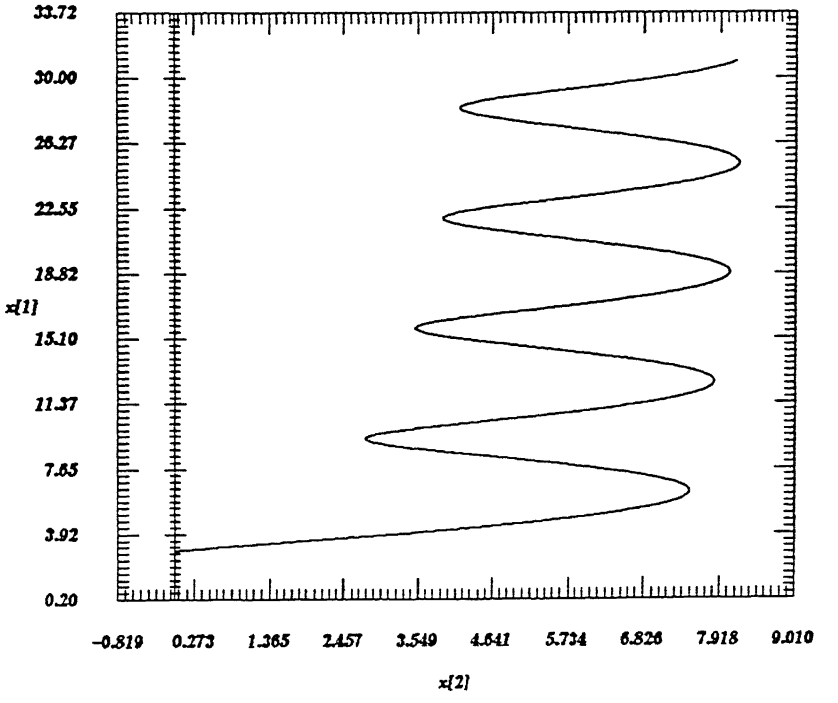

Figure 4 16 $W^u_+(\hat{x})$ plot of δ and ω for high voltage u e p of 3-bus system

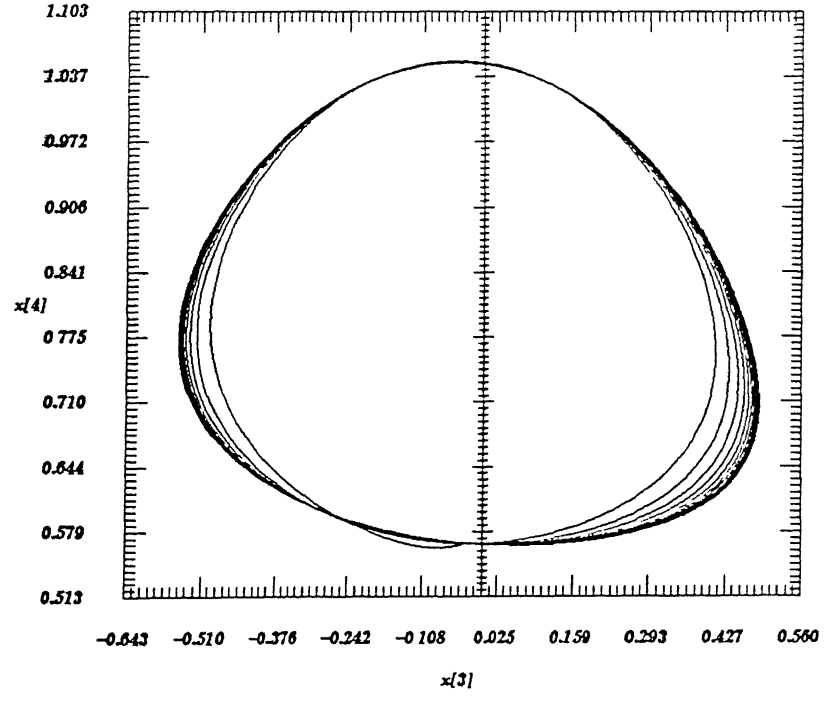

Figure 4 17 $W^u_+(\hat{x})$ plot of θ and V for high voltage u e p of 3-bus system

$\delta = (x[1])$ and $\omega = (x[2])$ variables remain bounded while in Fig 4.21 the variables $\theta = (x[3])$ and $V = (x[4])$ become unbounded If this type-1 u e p is the controlling u e p , the fault-on trajectory will be accompanied by collapse of the voltage

However for parameter value $Q_1 = 1\ 0$ pu. both the type-1 u e p would exist Therefore, the system will be vulnerable to angle as well as voltage stability in the region B

In region A, the system will be prone to angle instability For $Q_1 > 1.978658$, the system will be threatened by only voltage stability However, for $Q_1 > 1\ 978658$, several types of global bifurcations would exist which have been explored in the next Chapter (Chapter 5)

4.5.1.2 9–Bus System

The single line diagram and data of 9-bus system is presented in Fig. E and Appendix–E respectively The network was slightly modified to take the line 5-4 out The existing static load of $(125 + j50)$ MVA was reduced to $(100 + j30)$ MVA This change in loading was done since the load flow was not converging after the line 5-4 was taken out

The system consists of 3 generators The generator at bus-1 was taken as the reference bus and those at bus-2 and 3 were modelled by swing equations (4 26) and (4 27) All the base case loads have been modelled as constant impedance type. These constant impedance loads were clubbed with the Y_{bus} of the system An additional load represented by the load model–II (equations (4 36) to (4 37) has been considered at bus-5

This formulation results in a nonlinear system of ordinary differential equations consisting of six state variables viz the internal machine voltage angle δ and speed deviation ω for the two generators (generator # 2 & 3) and voltage magnitude V and angle θ at bus-5 Using AUTO86 software [34], the dynamics was studied on HP-9000/735 computer system, by varying ℓ The power factor was assumed to be unity and the other parameters of the dynamic load D, a, b and k were taken to be 0 05 (sec), 0 0, 0 0 and 0 1 (sec), respectively

The bifurcation diagram for variation in parameter ℓ has been drawn as shown in Fig 4 22 (load bus voltage magnitude V vs ℓ) Some of the important points on the bifurcation diagram are as given below·

- SNB at $\ell = 1\ 195323$
- HB at $\ell = 1\ 116463$ and 1 192705
- LP at $\ell = 0\ 2351554$ and 0 6105376

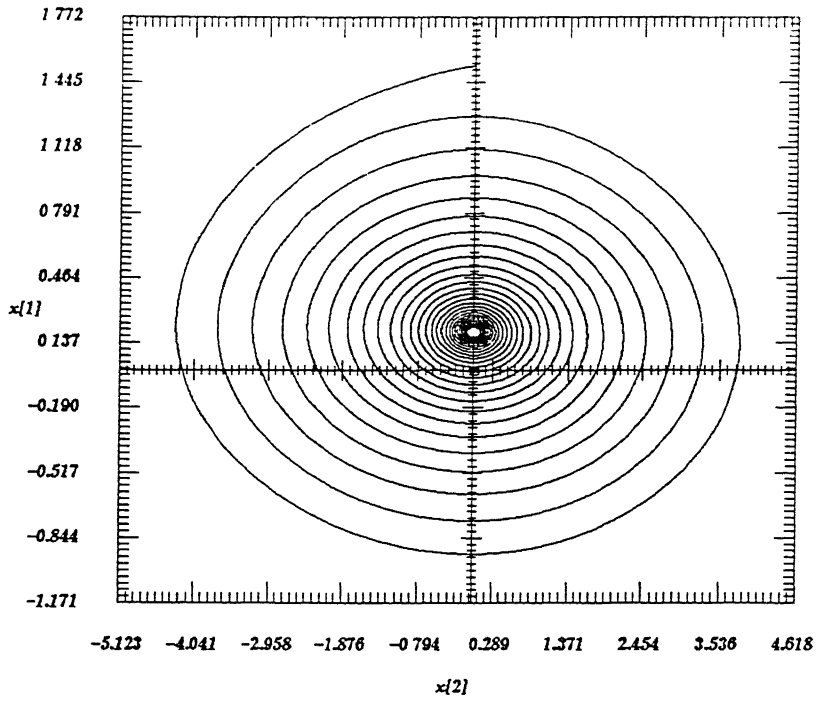

Figure 4 18· $W^u_-(\hat{x})$ plot of δ and ω for low voltage u e p of 3-bus system

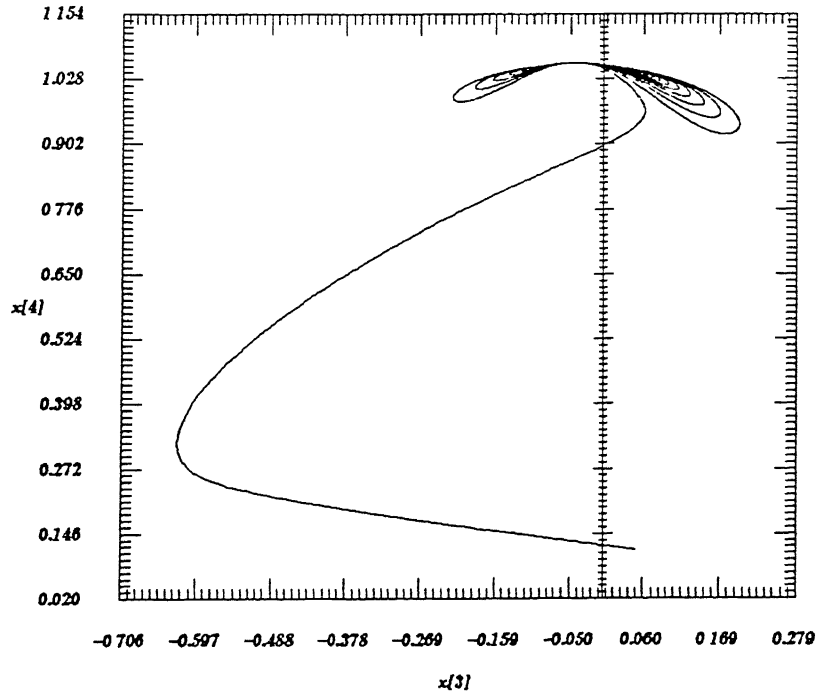

Figure 4 19 $W^u_-(\hat{x})$ plot of θ and V for low voltage u e p of 3-bus system

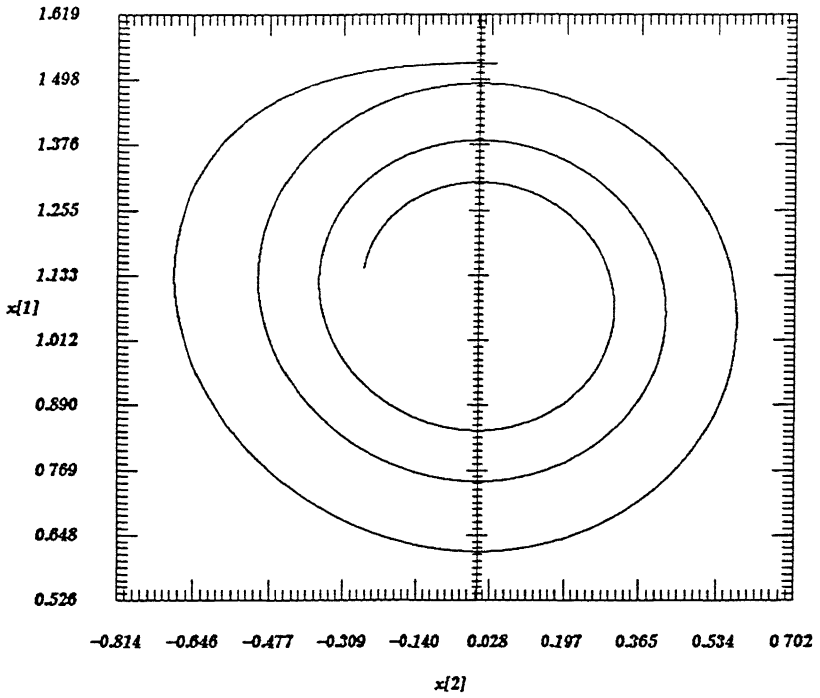

Figure 4 20 $W^u_+(\hat{x})$ plot of δ and ω for low voltage u e p of 3-bus system

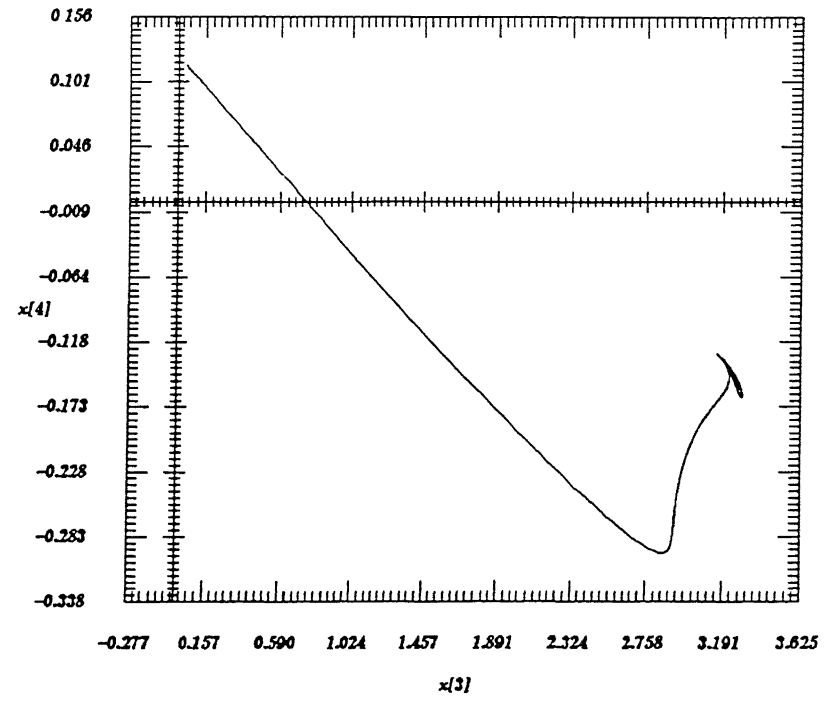

Figure 4 21 $W^u_+(\hat{x})$ plot of θ and V for low voltage u e p of 3-bus system

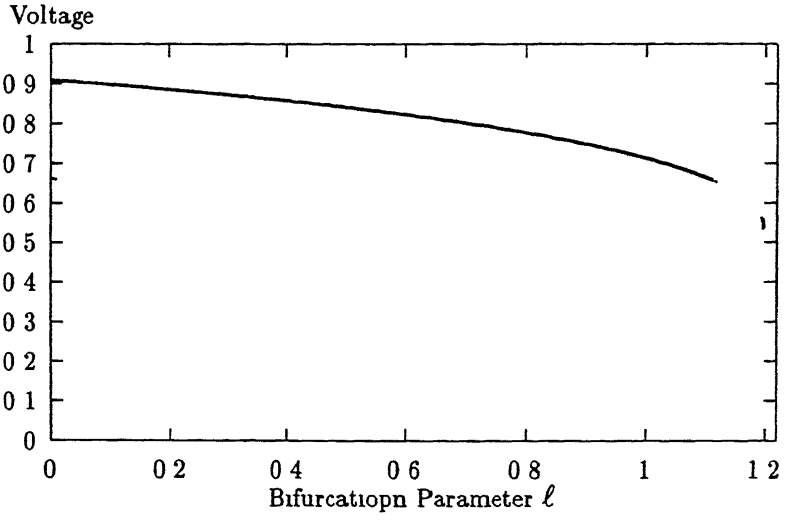

Figure 4 22 Variation of voltage magnitude V vs bifurcation parameter ℓ for 9-bus system

It may be seen from the bifurcation diagram in Fig. 4 22 that for $\ell < 0\ 2351554$ and $\ell > 0\ 6105376$ there is only one type-1 u e p These two u e.ps are markedly different One is characterised by high voltage and the other by low voltage The low voltage u e p coalesces with s e p to form SNB

The one-dimensional manifold of both the type-1 u e p corresponding to parameter $\ell = 0\ 4$ has been studied Figs 4.23 to 4 25 show the plot of one dimensional half unstable manifold for high voltage u e p. computed in the reverse direction of the eigenvector corresponding to real positive eigenvalue It is seen from Figs 4 23 to 4 25 that this half manifold converged to the s e p indicating that this u e.p is on the boundary of the region of attraction of the s e p Figs 4 26 to 4 28 show the plot of the other half manifold for this u e p computed in the forward direction of the eigenvector It is clear from these figures that not only the synchronous machines loose angle instability but also the system voltages collapse

The one dimensional half unstable manifold of the low voltage small angle u e p computed in the reverse direction of the value converged to the s e p (Figs 4 29 to 4 31), thus, confirming that this u e p is also on the boundary of the region of attraction of s e p The other half unstable manifold computed in the forward direction of the eigenvector as shown in Figs 4 32 to 4 34, indicate that load voltage collapses and the synchronism amongst generators is also lost Therefore, as noted above for this system, the voltage and angle instability will occur together

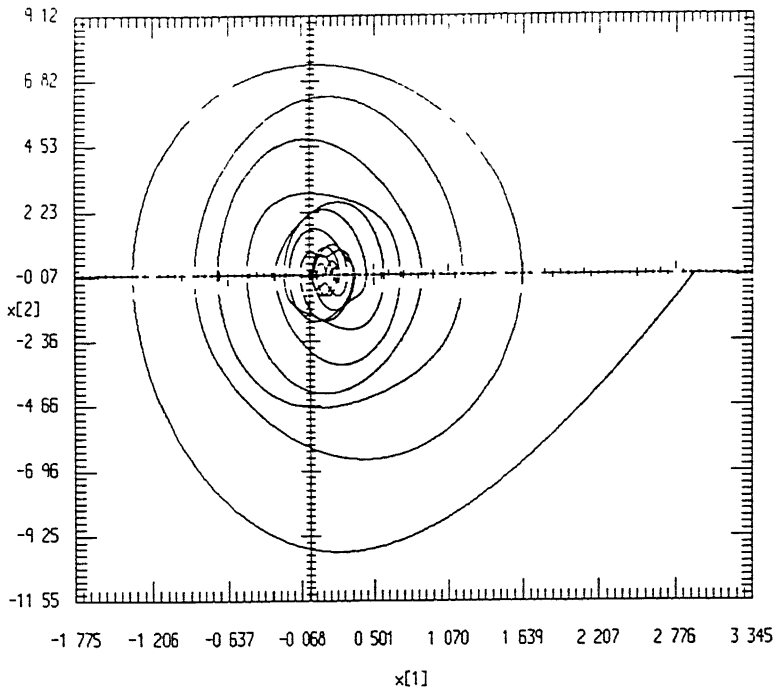

Figure 4 23 $W^u_-(\hat{x})$ plot of $\delta_2 = x[1]$ and $\omega_2 = x[2]$ for high voltage u e p. of 9-bus system

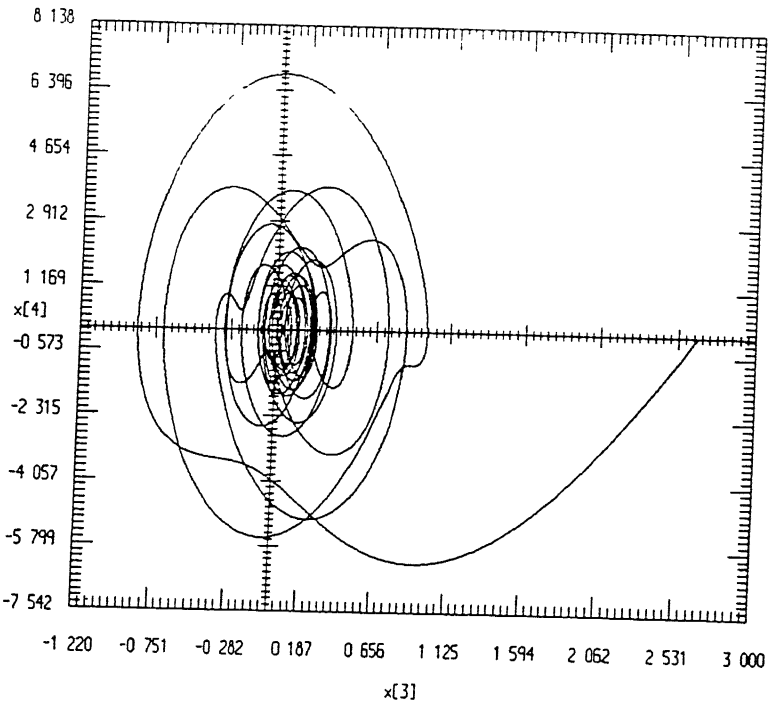

Figure 4 24 $W^u_-(\hat{x})$ plot of $\delta_3 = x[3]$ and $\omega_3 = x[4]$ for high voltage u e p of 9-bus system

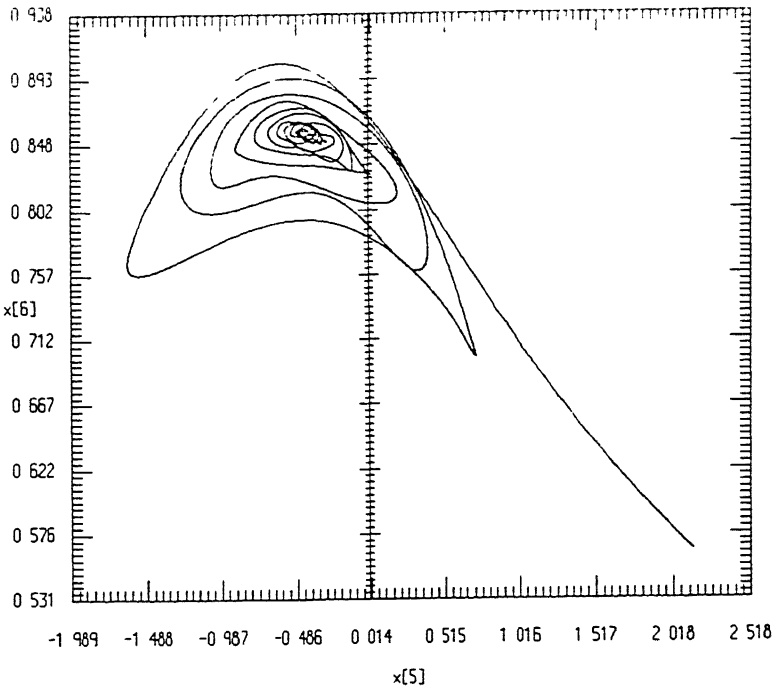

Figure 4 25 $W^u_-(\hat{x})$ plot of $\theta = x[5]$ and $V = x[6]$ for high voltage u e p of 9-bus system

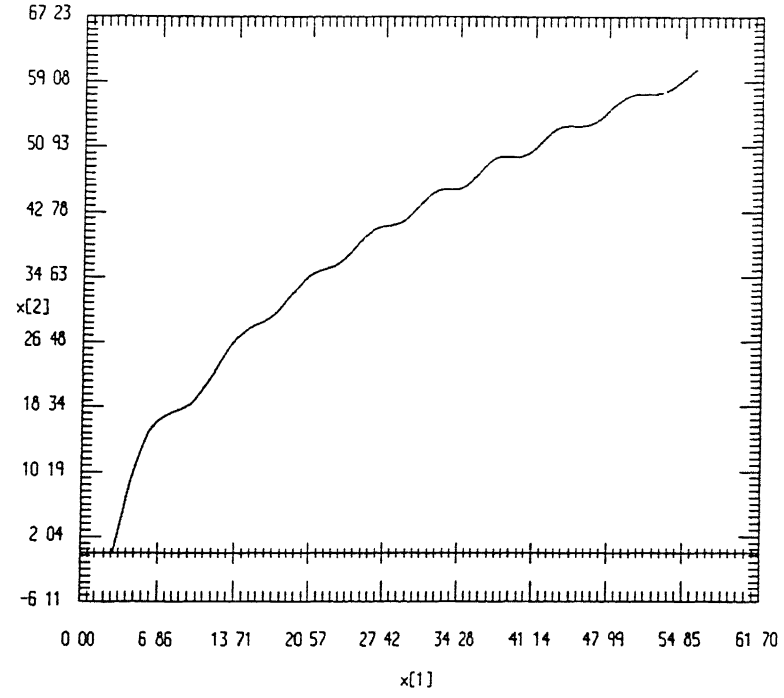

Figure 4 26 $W^u_+(\hat{x})$ plot of $\delta_2 = x[1]$ and $\omega_2 = x[2]$ for high voltage u e p of 9-bus system

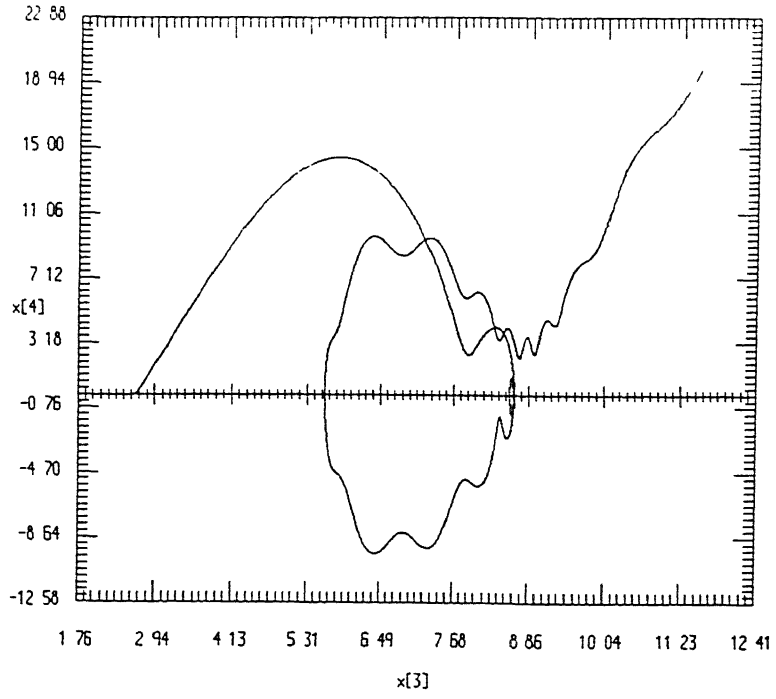

Figure 4 27 $W^u_+(\hat{x})$: plot of $\delta_3 = x[3]$ and $\omega_3 = x[4]$ for high voltage u e p of 9-bus system

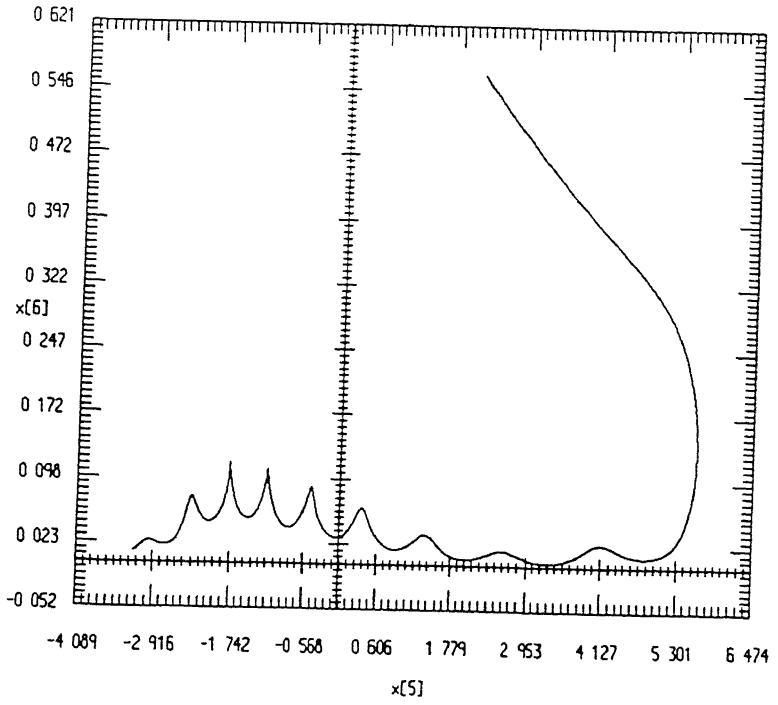

Figure 4 28 $W^u_+(\hat{x})$ plot of $\theta = x[5]$ and $V = x[6]$ for high voltage u e p of 9-bus system

4.5.2 Dynamic Bifurcation

Dynamic bifurcations arise when the stability characteristic of the equilibrium points changes Hopf bifurcation is such an example of the (local) dynamic bifurcation This section presents the study of Hopf bifurcation on two sample systems, one consisting of two buses (a generator and a induction motor load bus) as shown in Fig A.1 and the other a 10-bus system as shown in Fig F 1 The 10–bus system is derived from the 9–bus system of Appendix–E An induction motor was connected to bus-6 The studies were assisted by BIFOR2 program [11] on HP-9000/735 computer system for the following cases

Case–I: For different combinations of induction motor load torque coefficients (A_0, B_0, C_0), BIFOR2 program was used to find out critical value of generator AVR amplifier gain K_a The bifurcation parameter λ for this study was taken as $K_a^{1/2}$ which ensures positive value of gain

Case–II: For the base value of AVR amplifier gain and different combination of load torque coefficients (A_0, B_0), BIFOR2 program was used to find out critical value of torque coefficient C_0 The bifurcation parameter λ for this study was taken as $C_0^{1/2}$.

The results of the above two Cases for the two sample test systems are given below

4.5.2.1 Results of 2–Bus System

For both Case–I and Case–II studies on 2–bus system, the fourth order model of generator (equations (4 26) (4 27) (4 29) and (4 30)) together with AVR (equations (4 41) to (4 43)), speed governing control system (equations (4 44) to (4 50)) and load model-III (equations (4 38) to (4 40)) were used The hard limiters were represented as described in section 4 4 5 The reference voltage to AVR was selected as 1 1 pu and reference setting of governor was considered as 1 048 pu The various data used in the system studies are given in Appendix–A

For Case–I study, different values of all the load coefficients (A_0, B_0, C_0) were fixed between 0 1 to 0 8 The corresponding values of critical gain K_a obtained from BIFOR2 and some of the other parameters are given in Table 4 1 For Case–II studies, the different values of load coefficients A_0 and B_0 were selected in the range of 0 00 to 0 81, the K_a was fixed at 10 00 and critical values of C_0 and some of the other parameters obtained from BIFOR2 are listed in Table

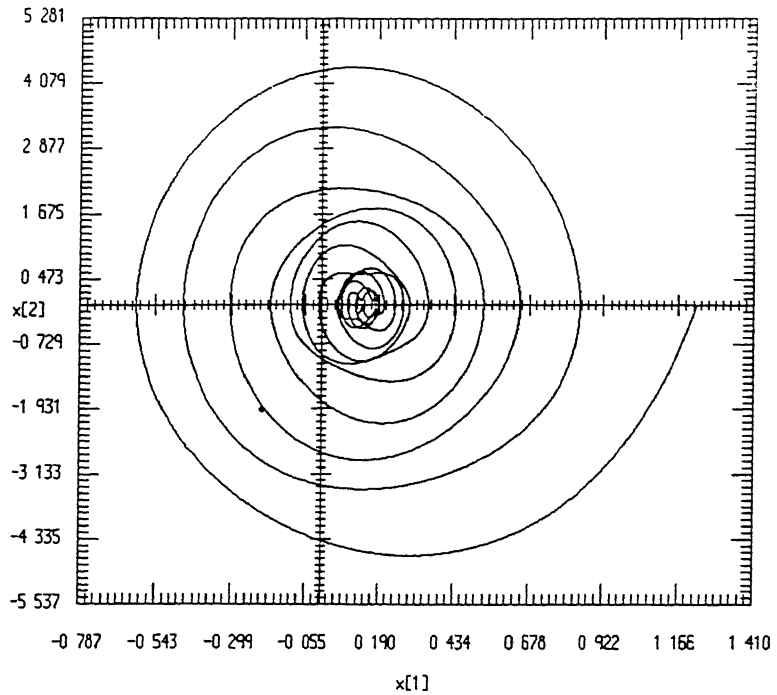

Figure 4 29 $W^u_-(\hat{x})$ plot of $\delta_2 = x[1]$ and $\omega_2 = x[2]$ for low voltage u e p of 9-bus system

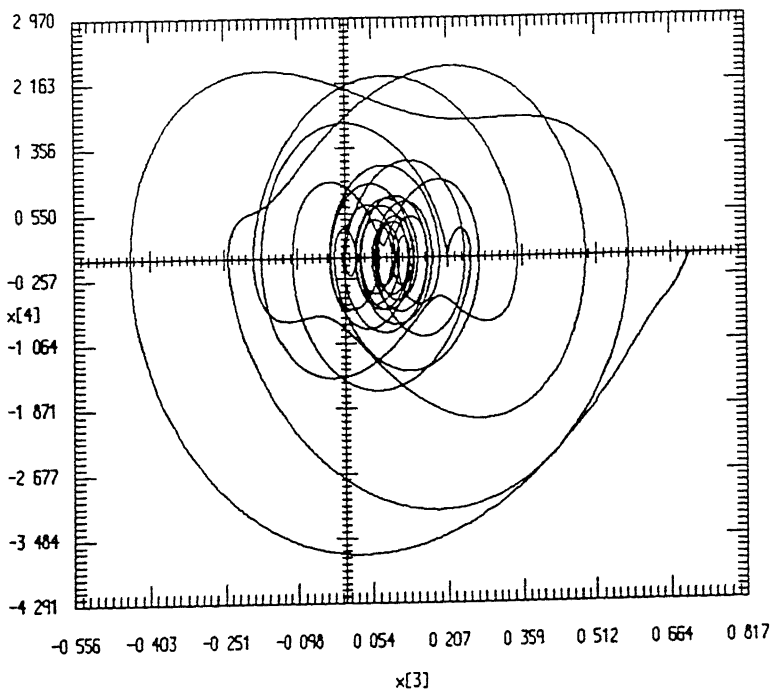

Figure 4 30 $W^u_-(\hat{x})$ plot of $\delta_3 = x[3]$ and $\omega_3 = x[4]$ for low voltage u e p of 9-bus system

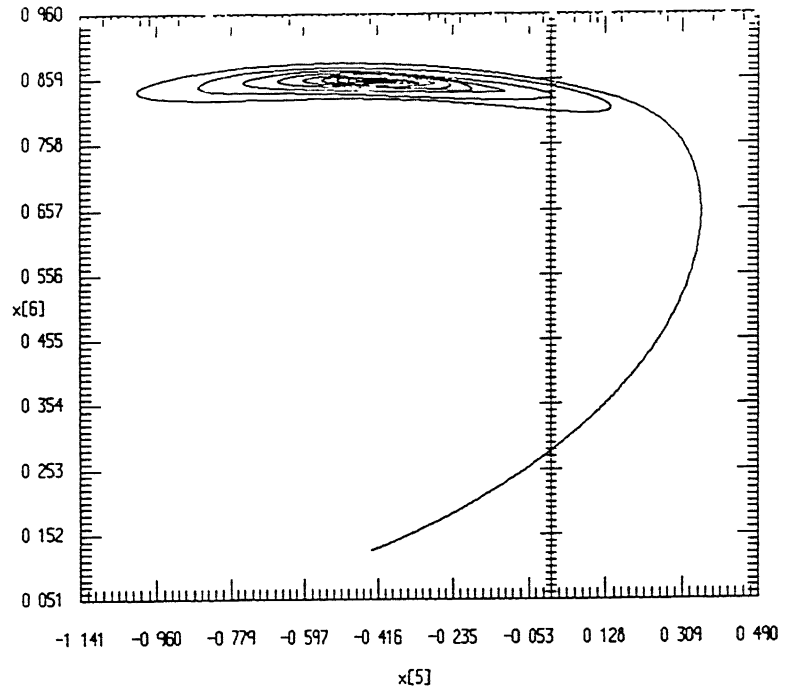

Figure 4 31 $W^u_-(\hat{x})$ plot of $\theta = x[5]$ and $V = x[6]$ for low voltage u e p of 9-bus system

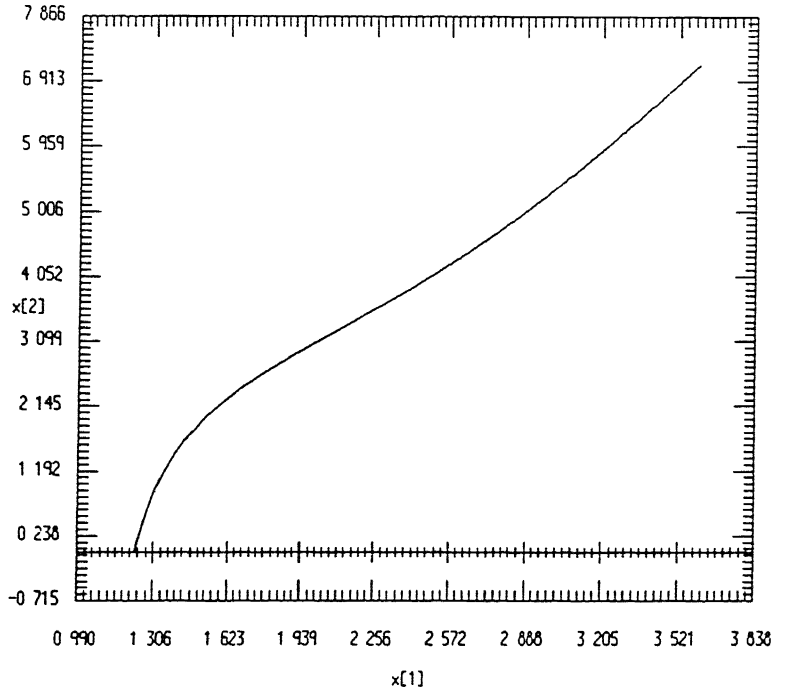

Figure 4 32 $W^u_+(\hat{x})$ plot of $\delta_2 = x[1]$ and $\omega_2 = x[2]$ for low voltage u e p of 9-bus system

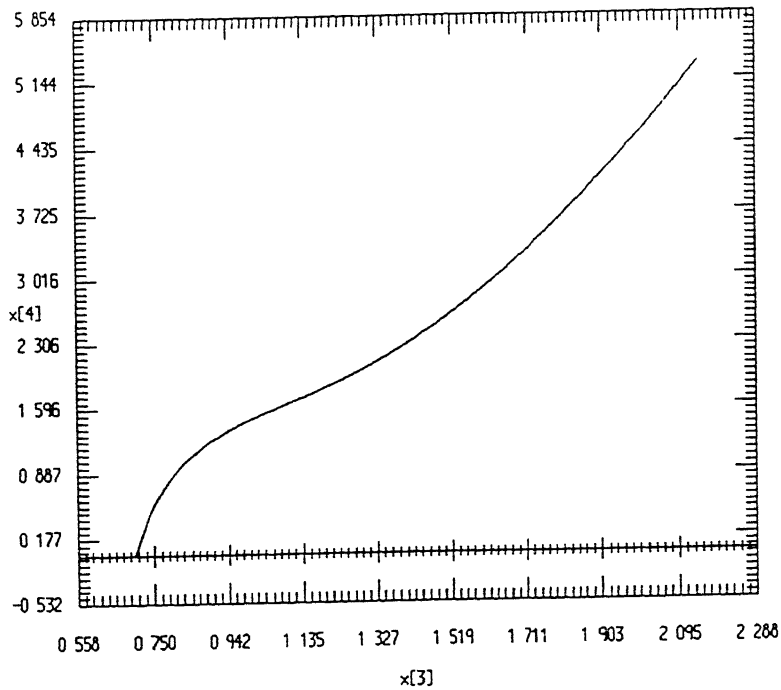

Figure 4 33 $W^u_+(\hat{x})$ plot of $\delta_3 = x[3]$ and $\omega_3 = x[4]$ for low voltage u e p of 9-bus system

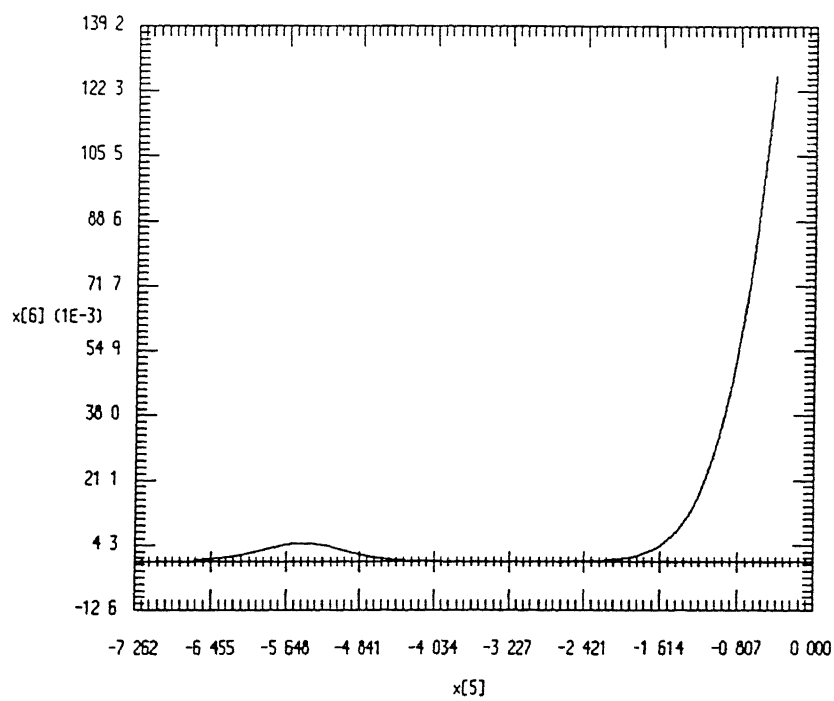

Figure 4 34 $W^u_+(\hat{x})$ plot of $\theta = x[5]$ and $V = x[6]$ for low voltage u e p of 9-bus system

Table 4 1: Case–I results of 2-bus system

Load Coefficients $A_0 = B_0 = C_0$	Critical gain K_a	$a(0)$	$b(0)$	$\alpha'(0)$ $\times 10^{-3}$	$\omega'(0)$ $\times 10^{-2}$	$\omega(0)$ $\times 10^{-2}$
0 1	15.9949	−161 972	−76 562	0 2483	0 1681	0 6903
0 2	15.6009	−040 397	−18 514	0 2585	0 1696	0 6884
0 3	14.8591	−016 647	−07 218	0 2756	0.1717	0 6823
0 4	13.6547	−007 857	−03 130	0 2999	0 1747	0 6683
0 5	11.9119	−003 641	−01 302	0 3314	0 1782	0 6416
0 6	09.6294	−001 391	−00 477	0 3689	0 1825	0 5969
0 7	06.8670	−000 182	−00 186	0 4018	0 1877	0 5255
0 8	03.4227	−000 416	−00 248	0 3111	0 1997	0 3906

Table 4 2: Case–II results of 2-bus system

Load Coefficients $A_0 = B_0$	Critical value of C_0	$a(0)$	$b(0)$	$\alpha'(0)$ $\times 10^{-3}$	$\omega'(0)$ $\times 10^{-2}$	$\omega(0)$ $\times 10^{-2}$
0 0	2 1130	−1 7651	−0 6821	0 8892	0 1043	0 6044
0 1	1.8505	−1 7384	−0 6580	0 8671	0 1038	0 6047
0 2	1.5885	−1 7142	−0 6351	0 8378	0 1023	0 6049
0 5	0 8061	−1 6570	−0 5738	0 6803	0 0878	0.6051
0 7	0 2883	−1 6323	−0 5392	0 4463	0 0595	0.6048
0 8	0 0309	−1 6242	−0 5237	0 1534	0.0208	0.6046
0 81	0 0053	−1 6237	−0 5222	0 0635	0 0086	0.6046

4 2. It can be observed that the critical values of K_a in Case–I and that of C_0 in Case–II studies which result into Hopf bifurcation lie in their normal operating range Further for periodic orbit to exist, $\mu\alpha'(0)/a(0)$ should be strictly less than zero This implies that the periodic orbit will exist if $\mu = \lambda - \lambda_0 > 0$, i e for Case–I study, if $K_a > K_{a_{critical}}$ and for Case–II if $C_0 > C_{0_{critical}}$

It is seen that either when loading increases or exciter amplifier gain increases, a complex pair of eigenvalues moves towards imaginary axis At critical value of parameters the stationary point looses stability via Hopf bifurcation An eigenvalue sensitivity analysis using the techniques given in [72, 176], was performed to ascertain as to which of the states caused this instability Participation factors of state variables in the critical mode were computed Their magnitude for a typical case study (corresponding to $A_0 = B_0 = 0.1$ and $C_0 = 1\ 5130$) are given in Table 4 3 The study reveals that the unstable modes correspond to E'_q and E_{fd} states

Table 4 3 Magnitude of participation factor 2-bus system

0 02407(ω_R)	0 01918(V_m)	0 00186(δ_m)	0 47605(E'_q)	0 00006(E'_d)	0 47715(E_{fd})
0 00099(V_f)	0.05506(V_a)	0 00915(ω)	0 00049(X_1)	0 00049(X_4)	0 00040(P_m)

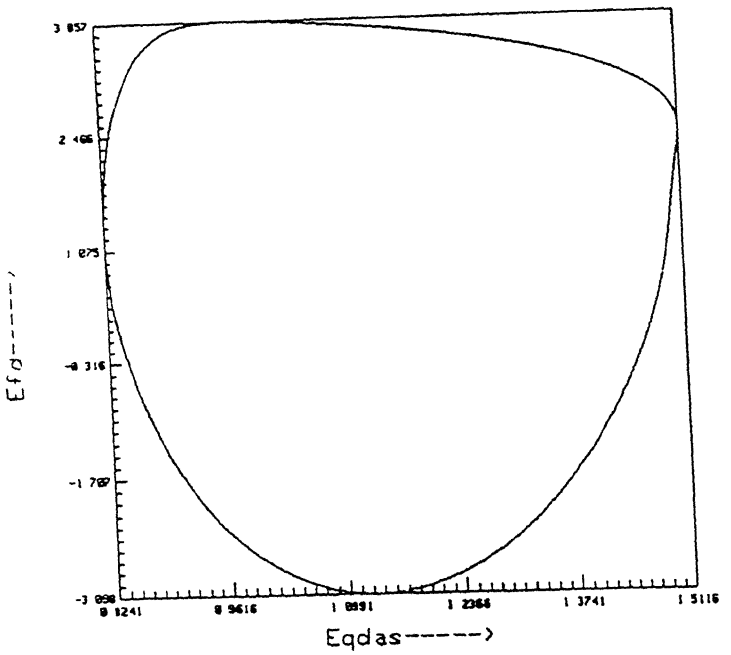

Figure 4 35 2-bus system plot of limit cycle projected on E'_q and E_{fd} plane

For validation of BIFOR2 results, numerical simulation was done using Runge-Kutta-Merson method for solving the system of ODE and a typical plot of limit cycle between state E'_q and E_{fd} is given in Fig 4 35

4.5.2.2 Results of 10–Bus System

The generators were modelled by third order model (equation (4 26) to (4 28)) along with AVR, speed governing control loop and hard limiters. A dynamic load model at bus 6 was considered represented by load model–III

For Hopf bifurcation studies on the 10–bus system, reference voltages to AVR were selected as 1 02774 pu, 1 08087 pu and 1 090037 pu for generators # 1, 2 and 3, respectively The reference power settings of speed governing system were taken as 1 425, 1 03 and 1 05 pu for generators #

Table 4 4 Case–I results of 10-bus system

Generator Exciter No	Critical gain K_a	$a(0)$ $\times 10^{-1}$	$b(0)$ $\times 10^{-1}$	$\alpha'(0)$ $\times 10^{-4}$	$\omega'(0)$ $\times 10^{-5}$	$\omega(0)$ $\times 10^{-2}$
1	11 5588	−0 5999	−0 3424	0 2203	0 4068	0 4466
2	10 1675	−0 5480	−0 3461	0 0229	102 30	0 4492
3	10 4850	−0 5392	−0.3177	0 7825	03 372	0 4489

Table 4 5 Case–II results of 10-bus system

Load Coefficients $A_0 = B_0$	Critical value of C_0	$a(0)$ $\times 10^{-1}$	$b(0)$ $\times 10^{-1}$	$\alpha'(0)$ $\times 10^{-4}$	$\omega'(0)$ $\times 10^{-4}$	$\omega(0)$ $\times 10^{-2}$
0 01	0 1836	−0 5455	−0 3121	0 2980	0 4537	0 4474
0 02	0 1634	−0 5482	−0 3161	0 3165	0 4602	0 4474
0 03	0 1431	−0 5454	−0 3061	0 1626	0 1287	0 4474
0 04	0 1229	−0 5528	−0 3247	0 3110	0 4398	0 4474
0 05	0 1027	−0.5503	−0 3265	0 2790	0 4436	0 4474
0 06	0 0825	−0 5501	−0 3209	0 2400	0 3643	0 4474
0 07	0 0623	−0 5507	−0 3232	0 1271	0 1130	0 4474
0 08	0 0421	−0 5517	−0 3240	0 1461	0 1935	0 4474
0 09	0 0218	−0 5482	−0 3163	0 1153	0 1753	0 4474
0 10	0 0016	−0.5510	−0 3296	0 0515	0 1660	0 4474

1, 2 and 3, respectively Since static loads were represented as constant impedances, the Ward reduction method was used to reduce the system to a 4–bus system containing only generators' and motor's internal nodes. This reduction eliminates the algebraic variables and resulting are a set of nonlinear ordinary differential equations only One set of results was obtained for Case–I pertaining to the load coefficients ($A_0 = B_0 = C_0 = 0\ 1$) and the result of BIFOR2 are presented in Table 4 4 For Case–II, seven sets of results were obtained for load coefficients (A_0, B_0) varying between 0 01 to 0 10 and results of BIFOR2 are presented in Table 4 5

From these results it can be observed that the periodic orbits will exist for $K_a > K_{a_{critical}}$ as computed by BIFOR2 for Case–I study and $C_0 > C_{0_{critical}}$ for Case–II study As the coefficients $a(0) < 0$ in all sets of studies, the bifurcation will be supercritical Participation analysis reveals that the dominant states that caused this instability correspond to E'_q and E_{fd} The magnitude of participation factors of the critical mode for a typical case study (corresponding

Table 4 6 Magnitude of participation factor 10-bus system

0 01035(E'_{q_1})	0 35172(E'_{q_2})	0 11256(E'_{q_3})	0 00037(δ_2)	0 00007(δ_3)	0 00389(ω_2)
0 00000(ω_3)	0 00317(ω_1)	0 00994(E_{fd_1})	0 36805(E_{fd_2})	0 11315(E_{fd_3})	0 00010(V_{f_1})
0 00071(V_{f_2})	0 00022(V_{f_3})	0 00029(V_{a_1})	0 09934(V_{a_2})	0 03052(V_{a_3})	0 00008(X_{11})
0 00008(X_{51})	0 00004(P_{M_1})	0 00008(X_{12})	0 00005(X_{13})	0 00020(X_{42})	0.00012(X_{43})
0 00067(X_{51})	0 00039(X_{53})	0 00072(P_{M_2})	0 00045(P_{M_3})	0 00002(δ_m)	0.00060(V_m)
0 00047(ω_R)					

to $A_0 = B_0 = 0\ 01$ and $C_0 = 0\ 18211$) are given in Table 4.6

For validation of results, numerical simulation was performed using Runge-Kutta-Merson method for solving the system of ODE and a typical plot of limit cycle between E'_{q_2} and E_{fd_2} & E'_{q_3} and E_{fd_3} are shown in Figs 4 36 and 4 37, respectively

4.6 Effect of Local Bifurcation on the Region of Stability in Parameter Space

Further studies were done to observe the effect of static and dynamic bifurcations on the region of stability in parameter space on the 3–bus and 9–bus systems studied in section 4 5 1 Both real P_1 and reactive loads Q_1 at the load node 2 and 5 for the 3 bus and 9 bus systems respectively, have been considered as bifurcation parameters and locus of saddle-node bifurcation and Hopf bifurcation has been drawn on $P - Q$ plane using AUTO86 [34] Fig 4 38 shows the locus of saddle-node and Hopf bifurcations for 3 bus system in $P - Q$ plane and Fig. 4.39 for the 9 bus system It is seen that the effect of dynamic bifurcations such as Hopf bifurcation is to further reduce the region of stable operating parameters It is seen from Fig 4 38 that Hopf bifurcation occurs for 3-bus system when power factor of load is low while for 9-bus system (Fig. 4 39) it occurs when power factor is high

4.7 Conclusion

From the studies presented in this chapter the following conclusions are drawn

(1) A power system may exhibit static and dynamic bifurcations even for variations of operating parameters in their normal range

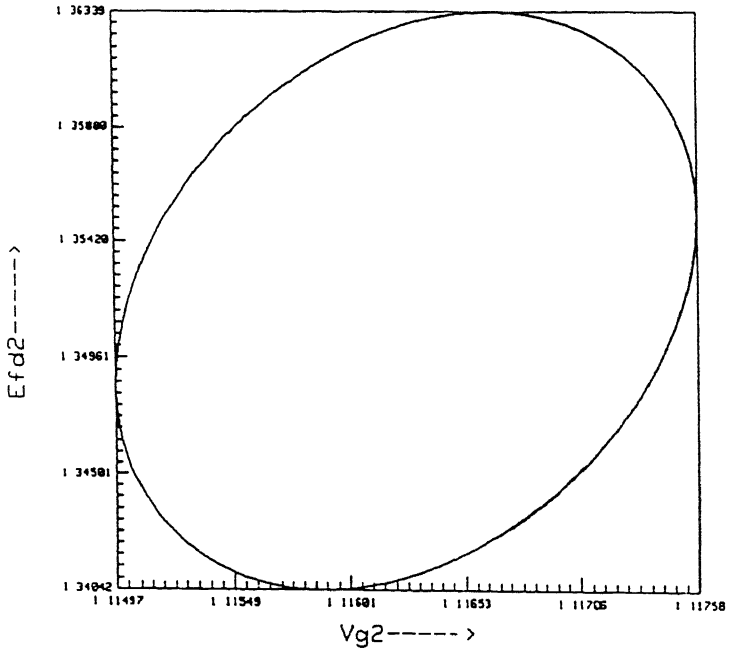

Figure 4 36 10-bus system plot of limit cycle projected on E'_{q_2} and E_{fd_2} plane

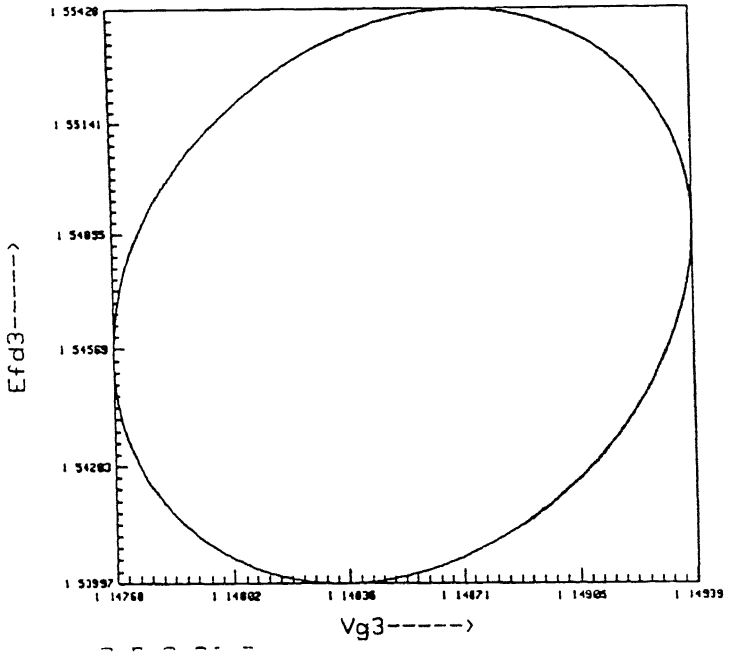

Figure 4 37 10-bus system plot of limit cycle projected on E'_{q_3} and E_{fd_3} plane

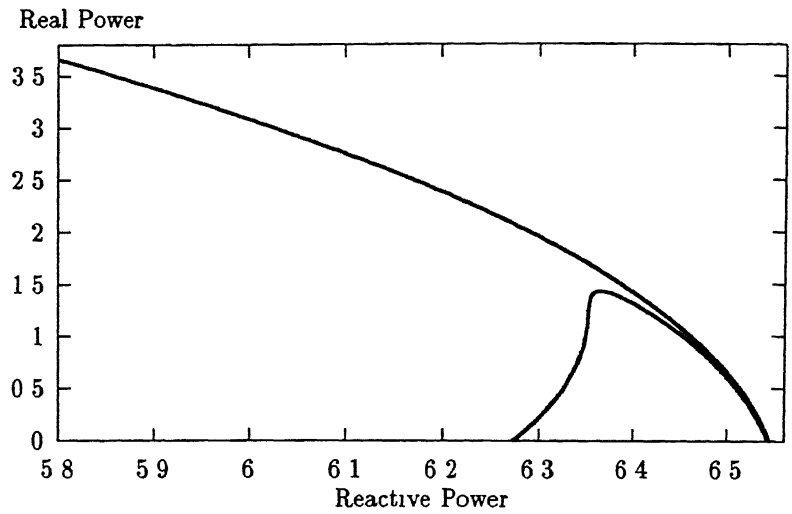

Figure 4 38 Loci of saddle–node and Hopf bifurcation for 3-bus system

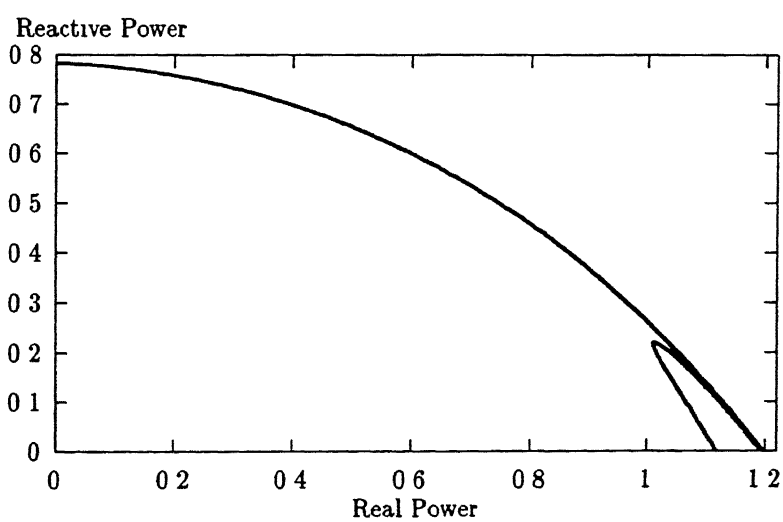

Figure 4 39 Loci of saddle–node and Hopf bifurcation for 9-bus system

(ii) For the same value of bifurcation parameter, the system may become unstable either purely due to angle instability or purely due to voltage instability or both may occur simultaneously depending upon disturbance

(iii) When a system undergoes Hopf bifurcation, the system looses linear stability. However, for small perturbations, the system becomes oscillatory It is shown that for certain choices of motor load torque coefficients A_0, B_0 and C_0 or AVR gain K_a values, the power system may undergo oscillatory type instability that is essentially bifurcation of a stationary point into a periodic orbit.

(iv) The eigenvalue sensitivity reveals that the states responsible to cause Hopf bifurcation are E'_q and E_{fd} when AVR, speed governor and motor dynamics are considered in the model along with the generator dynamics

(v) The effect of Hopf bifurcation is to further reduce the stable operating range of parameter

(vi) Hopf bifurcation may occur both at low or high power factor loadings

Chapter 5

Observance of Global Bifurcations

5.1 Introduction

Global bifurcations emerge out of periodic orbit and characterises a qualitative change in phase portrait not restricted to small neighbourhood of an equilibrium point When viewed in a continuous time-setting, the bifurcation of limit cycles such as *period doubling bifurcation* (PDB), *cyclic fold bifurcation* (CFB) and *bifurcation to torus* (TRB) are the global bifurcation as they involve considerations over a large domain in phase space [161] Other global bifurcations may also arise in the study of system dynamics A periodic solution may collide with a saddle equilibrium in a *saddle connection bifurcation* A strange attractor may collide with a saddle equilibrium or periodic orbit and disappear in a *boundary crisis* Examples of some of these global bifurcations in electric power system models are given in ref [118,120,154,191] In mathematical literatures [21,38,80], the global bifurcations refer to the homoclinic and hetroclinic bifurcations which are still an active area of research Kopell et al [17] and Salam [22,23] have studied the homoclinic bifurcations in a model of power systems using Melnikov's method

PDB route to chaos and boundary crisis has been studied in ref [120, 122, 127, 154, 191] considering load and generator dynamics However, phenomena of voltage collapse is also greatly influenced by the on load tap changer (OLTC) and static var system (SVS) dynamics

In this Chapter, extensive studies have been done to observe different types of dynamic bifurcations such as PDB, CFB, TRB, chaos and boundary crisis (blue sky bifurcation) on three sample systems namely 3-bus, 9-bus and 19-bus systems The effect of OLTC and SVS dynamics have been considered along with load and generator dynamics Existence of new dynamic bifurcations in power system models such as stable and unstable torus & chaos via

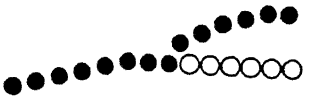

Figure 5 1 Period doubling bifurcation

torus breakdown and voltage collapse due to some of these phenomenon has been explored To study the stability of the dynamic bifurcations and chaos behaviour, Floquet multipliers, Lyapunov exponents and dimension of the attractor have been computed

5.2 Bifurcation of Periodic Orbit

5.2.1 General

The bifurcation of a periodic orbit (in continuous time setting) involves consideration over a large domain in phase space Under variation of the bifurcation parameter, a periodic orbit may undergo any of the following types of bifurcations

5.2.1.1 Period Doubling Bifurcation (PDB)

In some of the systems, the stable limit cycle out of supercritical Hopf bifurcation may soon become unstable with another stable limit cycle of twice the period generated Emergence of a stable periodic orbit of twice the time period around another periodic orbit is known as *period doubling bifurcation* as shown in Fig 5 1 This acts as a gateway to chaos The original periodic orbit becomes unstable after bifurcation The PDB may also emerge out of unstable periodic orbit resulting into an unstable periodic orbit of twice the time period The original unstable orbit may or may not remain unstable Local analysis is generally not enough to predict the PDB

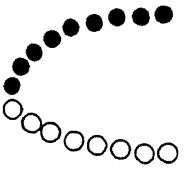

Figure 5 2 Cyclic fold bifurcation

5 2 1.2 Cyclic Fold Bifurcation (CFB)

This type of bifurcation arises when two periodic orbits coalesce Thus on one side of parameter at bifurcation point no periodic orbit exists and on the other side there exist two periodic orbits This is called *fold bifurcation* or *limit point* When a stable and an unstable periodic orbit coalesce, the resulting bifurcation is called *cyclic fold bifurcation* or saddle-node bifurcation of periodic orbits as shown in Fig 5 2

5.2.1.3 Torus Bifurcation (TRB)

This type of bifurcation occurs at a point when a periodic orbit becomes quasiperiodic This generates frequencies of oscillations incommensurate or irrational to each other

5.2.2 Stability of Periodic Orbit

Consider an n^{th} order autonomous parameterised vector field defined by the state equation

$$x = f(x, \lambda) \tag{5 1}$$

where f is a C^r $(r \geq 1)$ function on some open set in $R^n \times R^p$ $(x, \lambda) = (x_0, \lambda_0)$ at which $f(x, \lambda) = 0$ is a fixed point of the vector field The equation (5 1) undergoes Hopf bifurcation (HB) if a complex pair of eigenvalues of the matrix[1] $D_x f(x, \lambda)|_{(x_0, \lambda_0)}$ become purely imaginary A periodic orbit is, thus, born It may be stable or unstable A periodic orbit is characterised by a point x^* having a time period T such that the trajectory $\phi_t(x)$ emanating from x^* returns back to x^* in T time The system of equation (5 1) can be integrated for fixed λ from 0 to T to yield a point x such that $x(T)$ is equal to $\phi_T(x^*)$

[1]The matrix $D_x f(x, \lambda) = \{\frac{\partial f}{\partial x}\}$

In order for x^* to lie on the periodic orbit and T to be time period

$$x^* - \phi_T(x^*) = F(x^*, T) = 0 \tag{5 2}$$

The equation (5 2) is a system of n nonlinear equations in $(n+1)$ unknown variables At every iteration one component of x is fixed such that it lies on the periodic orbit, thereby reducing the number of unknowns by one The stability of a periodic orbit can be determined by the eigenvalues of the solution of variational equations, which can be calculated by appending the variational equations to the equations describing the dynamics

$$\begin{bmatrix} x \\ \Phi \end{bmatrix} = \begin{bmatrix} f(x) \\ D_x f(x)\Phi \end{bmatrix} \tag{5 3}$$

where $\Phi_t(x_0, t_0) = D_{x_0}\phi_t(x_0, t_0)$

The above (n^2+n) equations are integrated over the time period for initial conditions $x(t_0) = x_{t_0}$ and $\phi_{t_0} = I$ and the eigenvalues of the solution of variational equations are determined These eigenvalues are called *Floquet multipliers* A periodic solution is stable if all the eigenvalues lie within the unit circle except one that will be on the unit circle The stability of a periodic solution changes when some Floquet multiplier crosses the unit circle when λ is varied If one multiplier which was earlier within the unit circle passes through the unit circle at -1 on the real axis, the original stable periodic orbit becomes unstable and a branch of periodic solutions with a two fold period branches off at this point With respect to the orientation of parameter variation the branching can be either *supercritical* or *subcritical* This bifurcation is usually called as period doubling bifurcation (PDB) If the original branch of the periodic solution is unstable, the new branch of the periodic solutions with two fold period will also be unstable Second important bifurcation takes place when a multiplier intersects the unit circle through $+1$ This case corresponds to a limit point (LP) when two periodic solutions coalesce If a stable periodic orbit coalesces with an unstable periodic orbit, it is called cyclic fold bifurcation (CFB)

Another bifurcation from a branch of periodic solution occurs when two complex conjugate eigenvalues intersect the unit circle The originally stable branch of periodic solution becomes unstable and a stable or unstable torus (TRB) may appear at the bifurcation point Torus is a quasiperiodic motion However, if the periodic orbit is unstable, the torus will be unstable

5.3 Chaos

5.3.1 Route to Chaos

Chaos is seemingly a random behaviour in a deterministic system One fundamental characteristic of chaos is its extreme sensitivity to initial conditions Given two different initial conditions arbitrarily close to each other, the trajectories emanating from these two points diverge from each other with a wide separation. The transition to chaos may occur in one of the following four different ways

5.3 1 1 Period Doubling (Sub-harmonic Cascade) Route to Chaos

The period doubling route to chaos is the most widely known and studied route to chaos In this, a periodic orbit undergoes period doubling bifurcation in that the one original periodic orbit becomes unstable and a new periodic orbit of two fold period is born A complete period doubling cascade is an infinite sequence of period doubling bifurcations after which the dynamics become chaotic

5.3.1.2 Quasi-periodic route to Chaos

This route of chaos typically follows the sequences of bifurcations given below as the parameter is monotonically varied

$$\text{Steady state} \Longrightarrow \text{Periodic} \Longrightarrow \text{Quasi-periodic } (T^2) \Longrightarrow \text{Quasi-periodic } (T^3) \Longrightarrow \quad \text{Chaos}$$

The main property of this route to chaos is that chaos is observed after a short sequence (finite) of bifurcation with continuous changes of the attractors

5.3.1.3 Intermittent Transition to Chaos

Generally speaking, a signal (the value of a variable changing in time) is said to be intermittent if it is subject to infrequent variations of large amplitude On this route, a limit cycle becomes unstable as the parameter increases through a critical value. At the critical value a stable and an unstable limit cycle coalesce For very small increase of the parameter past its critical value, the same cycle persists but is occasionally and rarely interrupted by busts which are not small As the parameter is further increased, the busts occur more frequently but do not change much in magnitude, thus the dynamical system becomes chaotic

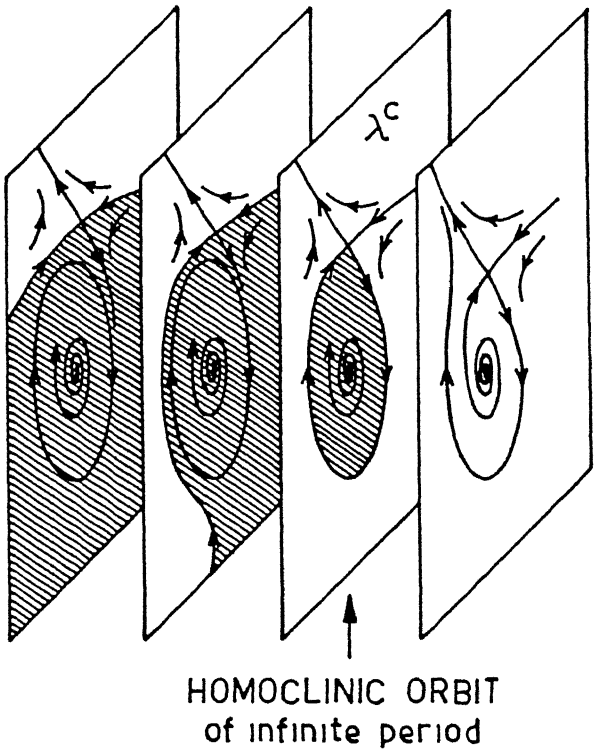

Figure 5 3 Blue sky bifurcation

5.3 1.4 Subcritical Instability

On this route a familiar attractor, i e a fixed point, periodic or quasiperiodic attractor, becomes unstable as the bifurcation parameter is slowly varied through a critical value The system jumps rapidly to a strange attractor which is not a continuous extension of the familiar attractor

5.3.2 Blue Sky Bifurcation

Thompson and Stewart [38] refer to a type of global bifurcation in stable space involving the discontinuous disappearance of a limit cycle as a blue sky catastrophe (Fig 13 5, page 271 of ref [38]) and reproduced as Fig 5 3 This is not a local bifurcation However, it does possess the feature of the saddle-node bifurcation, namely the disappearance of the attractor by collision with a saddle, in this case a saddle equilibrium point As seen from Fig 5 3, the blue sky bifurcation for a periodic orbit is the sudden disappearance of a limit cycle through collision with a saddle equilibrium point Prior to the critical parameter value λ_c at which the collision occurs, a saddle equilibrium coexists with the limit cycle At λ_c the limit cycle and a branch of both the stable and unstable manifolds of the saddle point coincide, forming a homoclinic connection Past λ_c, the limit cycle no longer exists Collision with a saddle fixed point as a typical mechanism by which a limit cycle can abruptly vanish from state space This blue

sky bifurcation can take place in two forms, the disappearance of a stable limit cycle and the disappearance of an unstable limit cycle Moreover, it is a global, discontinuous and catastrophic bifurcation It also serves as a prototype of a blue sky bifurcation for a strange attractor or a boundary crisis of a strange attractor

One type of global bifurcation involving a strange attractor is the sudden death of the attractor [120] Such a blue sky bifurcation occurs commonly for strange attractors of differential equations Like the blue sky bifurcation for a limit cycle, a chaotic blue sky bifurcation involves a collision with an object of saddle type and is analogous to the blue sky disappearance of a limit cycle as discussed above The chaotic blue sky bifurcation is also known by another term, namely the boundary crisis of a strange attractor The term crisis was introduced in [16,20] and applies to sudden qualitative changes in strange attractors with quasistatic changes in parameters A crisis involves the sudden destruction of a strange attractor through collision

5.3.3 Lyapunov Exponents and Dimension

Lyapunov exponents (LE) characterise the asymptotic orbital instability of dynamic systems As n^{th} order dynamical system has n Lyapunov exponents Each exponent $\lambda(x, v)$ is a real number and is a measure of the divergence rate of trajectories in the direction of a vector v The positive, zero and negative Lyapunov exponents denote stretching, marginal and contracting directions in the phase space Some of the informations derived from Lyapunov exponents are as follows,

(i) For conservative systems the sum of all Lyapunov exponents is zero

(ii) The attractor is a stable fixed point if all the LEs are negative

(iii) If all LEs are negative except one which is zero, system undergoes periodic motion More than one zero (other negative) indicate quasiperiodic motion or torus for multidimensional cyclic motion

(iv) If one of the LEs is positive, one being zero and all other negative, the system undergoes chaotic oscillation Two positive, one zero and other negative LEs indicate the presence of *Superchaos*

The Lyapunov exponents are defined as [59]

$$\lambda_i = \lim_{t\to\infty} \frac{1}{t} \ln \mid m_i(t) \mid, \quad i = 1, \quad , n \tag{5 4}$$

where $m_i(t)$ are the eigenvalues of $\Phi_t(x_0, t_0)$

The obvious way to find the Lyapunov exponents [59] is to integrate $\Phi_t(x_0, t_0)$ for T time and if T is large, the LE can be approximated as

$$\lambda_i \approx \frac{1}{T} \ln \mid m_i(t) \mid, \quad i = 1, \quad , n \tag{5 5}$$

However, there are two problems with this approach First, for a chaotic trajectory, $\lambda_i > 0$ and $\Phi_t(x_0, t_0)$ is unbounded as $t \to \infty$. Second, as $t \to \infty$, each column of $\Phi_t(x_0, t_0)$ tends to line up with the eigenvector associated with the largest eigenvalue $m_1(t)$ It follows that $\Phi_t(x_0, t_0)$ is ill conditioned and its eigenvalues may not be reliably computed

A more robust algorithm [59] is based on the concept that almost every perturbation in the linearised system evolves on the average as $e^{(\lambda_1 t)}$ Thus to find λ_1 , choose a time interval $T > 0$, an iteration count K, and any initial condition $u^{(0)}$, normalised to 1 Calculate the solution to variational equation for $t = kT$ normalising every T seconds as follows

$$x^{(k)} = \delta x(kT, u^{(k-1)}, (k-1)T) \tag{5 6}$$

$$u^{(k)} = \frac{x^{(k)}}{\|x^{(k)}\|} \tag{5 7}$$

for $k = 1, \quad , K$

where $\delta x(t, u, \tau) = \Phi_{t-\tau}(\phi_\tau(x_0), \tau)u$ is the solution at time t starting from initial condition u at time τ Then,

$$\delta x(kT, u^{(0)}, 0) = \|x^{(1)}\| \ . \ \|x^{(k)}\| u^{(k)} \tag{5 8}$$

and for K large enough

$$\lambda_1 \approx \frac{1}{kT} \ln \|\delta x(kT, u^{(0)}, 0)\| \tag{5 9}$$

$$\approx \frac{1}{kT} \ln \prod_{k=1}^{K} \|x^{(k)}\| \tag{5 10}$$

$$\approx \frac{1}{kT} \sum_{k=1}^{K} \ln \|x^{(k)}\| \tag{5 11}$$

Similarly, the area spanned by almost any n-linearly independent vectors evolves in the linearised system on the average as $e^{(\lambda_1 + \ + \lambda_n)t}$. Hence, $(\lambda_1 + \ . + \lambda_n)$ can be found by following the time evolution of almost any n-linearly independent vectors $(x_1, \quad , x_n)$ However, as the evolution goes on, these vectors $x_1, \quad , x_n)$ tend to align in the same direction This effect can be avoided by orthonormalising every T time using modified Gram-Schmidt orthonormalisation [59] At

each step in the iteration, the area is given by $\|v_1^{(k)}\|$ $\|v_n^{(k)}\|$ where $\|v\|$ is the orthonormalised vector If k is large

$$\lambda_1 + \quad . + \lambda_n = \frac{1}{kT}\sum_{k=1}^{K} \ln \|v_1^{(k)}\| \quad \|v_n^{(k)}\| \tag{5 12}$$

$$= \frac{1}{kT}\sum_{k=1}^{K} \ln \|v_1^{(k)}\| + \quad + \frac{1}{kT}\sum_{k=1}^{K} \ln \|v_n^{(k)}\| \tag{5 13}$$

$$= \lambda_1 + \quad + \lambda_{n-1} + \frac{1}{kT}\sum_{k=1}^{K} \ln v_n^{(k)}\| \tag{5 14}$$

$$\lambda_n = \frac{1}{kT}\sum_{k=1}^{K} \ln \|v_n^{(k)}\| \tag{5 15}$$

Thus by following the evolution, of volume elements with dimensions from 1 to n, each of the Lyapunov exponents can be determined

Let $\lambda_1 \geq \lambda_2 \geq \quad \lambda_n$ be the Lyapunov exponents of an attractor of a continuous time dynamical system Let j be the largest integer such that $\lambda_1 + \quad + \lambda_j \geq 0$ The Lyapunov dimension as defined by Kaplan et al [59] can be estimated

$$D_L = j + \frac{\lambda_1 + \quad + \lambda_j}{|\lambda_{j+1}|} \tag{5 16}$$

If no such j exists, as is the case for a stable hyperbolic equilibrium point, D_L is defined to be 0 For an attracting limit cycle, the generic situation is $(\lambda_1 = 0 > \lambda_2 > \quad > \lambda_n)$ Thus, the Lyapunov dimension of a generic attracting limit cycle is 1 Similarly, the Lyapunov dimension of a generic attracting K-periodic behaviour is K If the attractor is chaotic, D_L is almost always a non-integer In a three-dimensional chaotic system with Lyapunov exponents $(\lambda_+ > 0 > \lambda_-$, the Lyapunov dimension is given as

$$D_L = 2 + \frac{\lambda_+}{|\lambda_-|} \tag{5 17}$$

5.4 System Model

For the studies in this chapter, the transmission lines have been modelled by their lumped π equivalent The generators and load models have been taken same as those described in section 4 4 2 in Chapter 4 The models for OLTC and SVS utilized in the present work are presented below

5.4.1 OLTC Model

The dynamic characteristics of tap changer and the operating practices vary from country to country [168] There is always a small voltage deadband within which tap changer is not activated

In the present work, the dynamics of OLTC has been represented by a discrete time model which changes the tap setting n at each time step $(k+1)$ as follows [98]

$$n\{(k+1)\} = \begin{cases} n(k\Delta t) + \Delta n & \text{if } V > V^o + \epsilon \\ n(k\Delta t) & \text{if } |V - V^o| \leq \epsilon \\ n(k\Delta t) - \Delta n & \text{if } V < V^o - \epsilon \end{cases} \tag{5 18}$$

with $n_{min} \leq n(k+1) \leq n_{max}$

where V = controlled secondary voltage

V^o = corresponding set point

ϵ = dead band

Δn = OLTC step size

Δt = time interval

k = an integer time step

5.4.2 SVS Model

SVS has been modelled by a first order time delay block as shown in Fig 5 4. The equation describing the dynamics of SVS can be written as

$$T_{svs}\frac{dB}{dt} = K_{svs}(V_{ref} - V) - B \tag{5 19}$$

with $B_{min} \leq B \leq B_{max}$

where B = shunt susceptance

K_{svs} = SVS gain

V_{ref} = reference voltage

T_{svs} = SVS time constant

The action of limiter has been realised by using *tanh* function as discussed in Chapter 4 (equation (4 51))

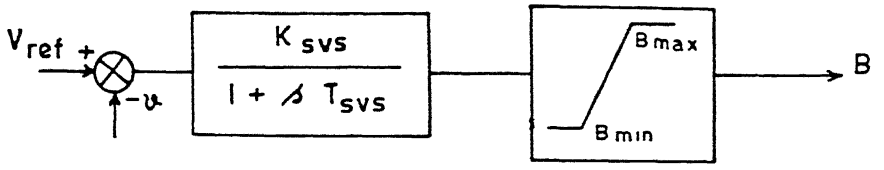

Figure 5 4 SVS Model

5.5 Case Studies

The studies were conducted on four sample systems viz a 3-bus system with SVS (Appendix–C, a 4-bus system with OLTC (Appendix–D, a 9-bus system (Appendix–E) and 19-bus UPSEB system (Appendix–H) The systems in Appendices–C and D are derived from that in the ref [66] A transmission line between the two generators is added and through network reduction, the terminal node of the finite generator at bus-1 was eliminated The data for the reduced network retaining the internal node of the generator # 1 are given in Appendices–C & D The studies were performed on HP9000/735 computer systems and assisted by AUTO86 software [34] and INSITE software [59]

5.5.1 3–Bus System with SVS

The generator at bus-3 was taken as infinite bus and the generator at bus-1 was represented by swing equations (4 26) and (4 27) described in Chapter 4 The effect of SVS dynamics were studied using its models given in section 5 4 2 The load at bus-2 was assumed to be consisting of two parts, one being the static load of polynomial type and the other being an induction

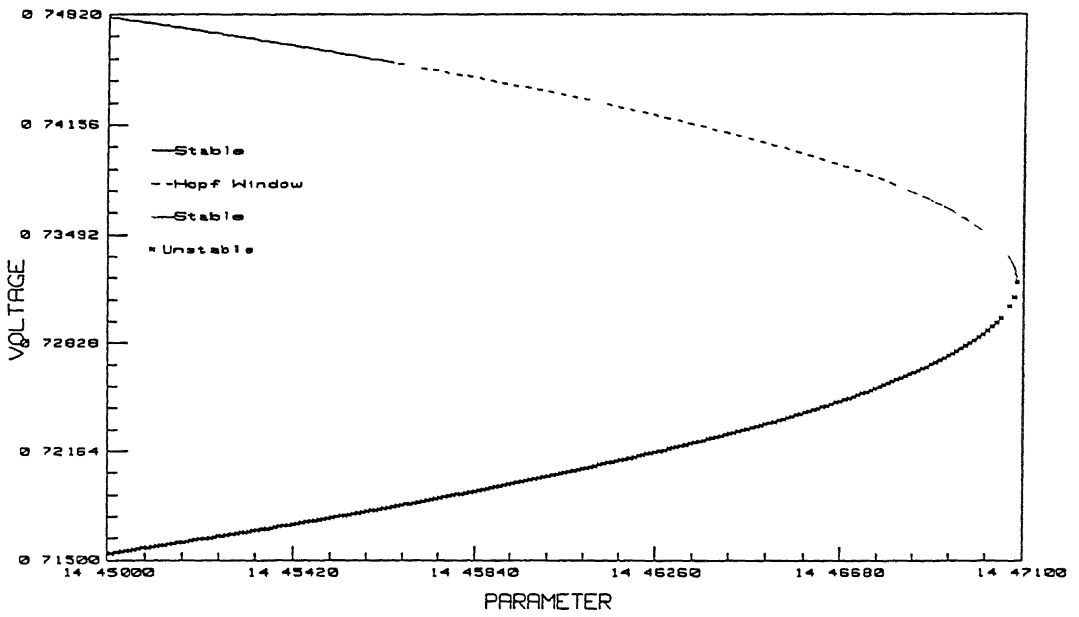

Figure 5 5 3-bus system with SVS bifurcation diagram

motor load The real and reactive power components of static load were taken as follows

$$P_s = P_1 + P_V V^{\eta} \tag{5 20}$$

$$Q_s = Q_1 + Q_V V^{\xi} \tag{5 21}$$

where P_1, Q_1 = constant real and reactive load demand

P_V, Q_V = coefficients of voltage dependent terms

η, ξ = exponents

The model of induction motor considered in this study is the same as described by the equations (4 34) and (4 35) in Chapter 4 and also in ref [40]

The system shown in Appendix-C was considered for the present study The bifurcation diagram has been drawn as shown in Fig 5 5 considering Q_1 as the parameter There are two Hopf bifurcations, subcritical HB at $Q_1 = 14\ 4548$ and supercritical HB at $Q_1 = 14\ 4782$ and a saddle-node bifurcation for $Q_1 = 14\ 479395$ Figs 5 6 and 5 7 show the movement of real part of complex eigenvalue and the largest real eigenvalue respectively After supercritical HB the critical mode corresponds to the real eigenvalue and causes the saddle-node bifurcation

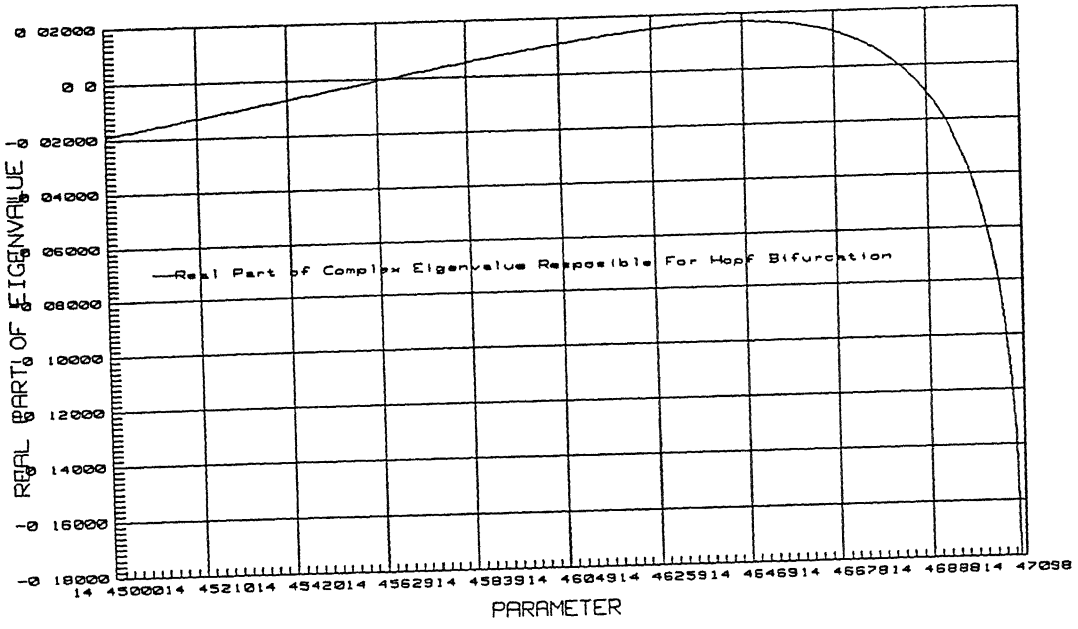

Figure 5 6 3-bus system with SVS movement of complex eigenvalue

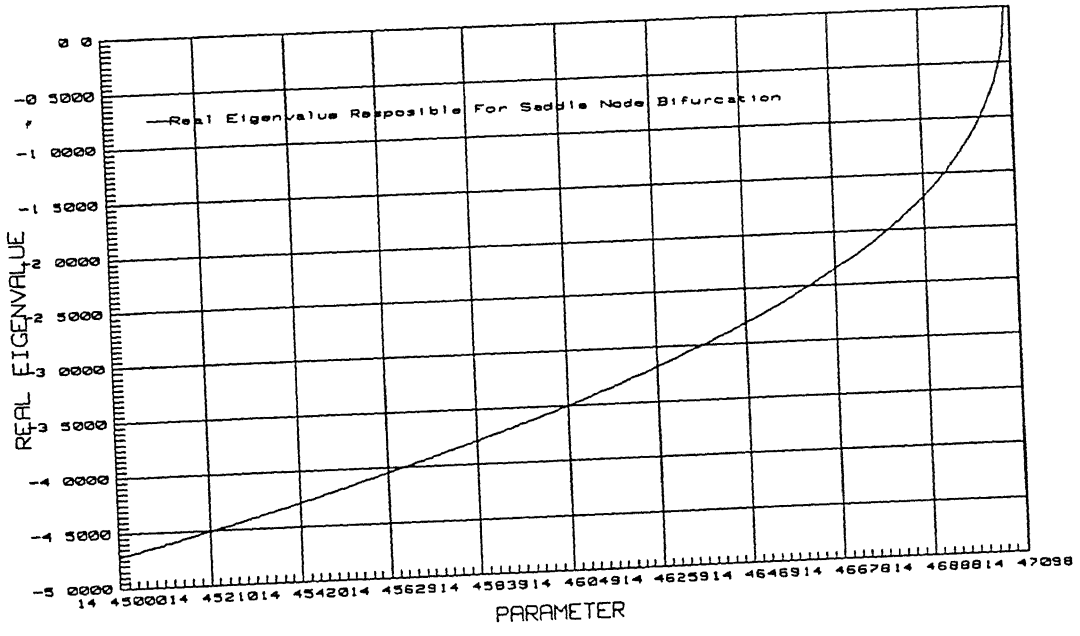

Figure 5 7 3-bus system with SVS movement of real eigenvalue

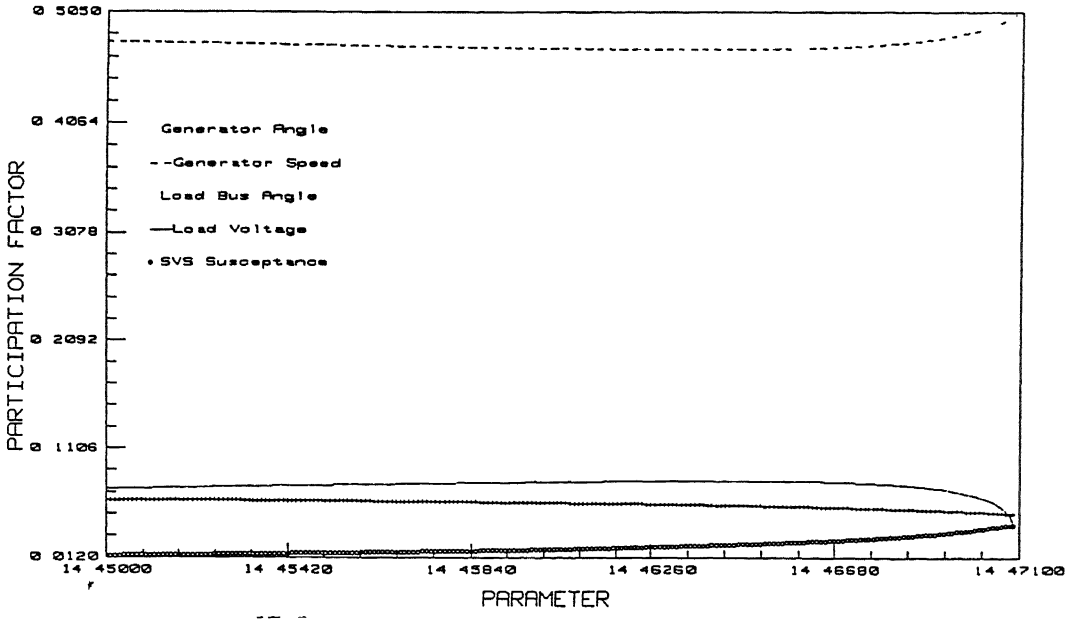

Figure 5 8 3-bus system with SVS participation factors of complex eigenvalue

The participation factors of these two eigenvalues are plotted in Figs 5 8 and 5 9 for different values of parameter It is seen from these figures that in the Hopf bifurcation window, the dynamics is dominated by the generator states (δ, ω) and for saddle-node bifurcation, the load bus voltage V dominates the dynamics

Fig 5 10 demonstrates the presence of two chaotic regions, one between $Q_1 = 14\ 44571$ and 14 45677 and the other between $Q_1 = 14\ 45818$ and 14 45930 For $Q_1 = 14\ 45592$, the Lyapunov exponents are found to be (0 267, 0 000, −2 529, −63 380, −63 388) For $Q_1 < 14\ 44521$, the chaotic attractor disappears as a result of boundary crisis (possibly because of collision with saddle kind object like the saddle fixed point or the unstable limit cycle) Since for $Q_1 <$ 14 44571, the fixed point is the only stable attractor, the trajectories settle down to this stable fixed point, for $Q_1 < 14\ 44571$ (Fig 5 10) It is important to notice that the inclusion of SVS dynamics causes the flow to be overall contracting in the Hopf bifurcation window and no collapse of voltage or angular instability is observed However, for $K_{svs} = 20$ and $\eta = 1\ 3$, $\xi = 1\ 6$ and $T_{svs} = 0\ 02$ see the dynamics of the system even after considering SVS dynamics is accompanied by voltage collapse due to boundary crisis Fig 5 11 shows the bifurcation diagram for this case, the system looses stability in the Hopf bifurcation window as a result of

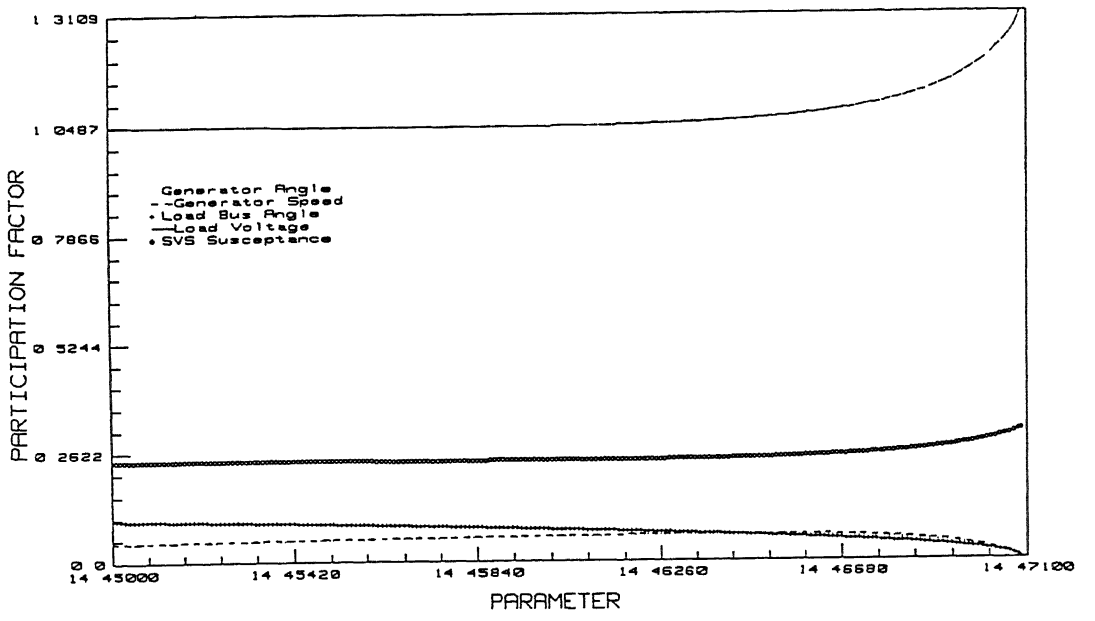

Figure 5 9 3-bus system with SVS participation factors of real eigenvalue

expanding flow The Lyapunov dimension of the attractor is 2 267 at $Q_1 = 14\ 45592$

5.5.2 4–Bus System

The model of generator at bus-1 and loads were taken same as in the study for 3-bus system with SVS The OLTC was modelled using equation (5 18) in section 5 4 1 The study on system shown in Appendix–D was carried out considering Q_1 (equation (5 20) as the bifurcation parameter while calculating the stationary points for the different values of Q_1, three critical points were observed as shown in the bifurcation diagram of Fig 5 12 These include two Hopf bifurcation points, subcritical HB at $Q_1 = 8\ 1650$ and supercritical HB at 8 3199 and a saddle-node bifurcation at $Q_1 = 8\ 3210168$ At $Q_1 = 7\ 8700$ the OLTC hits its minimum limit (0 9 p u) and remains constant for further increase in Q_1 Fig 5 13 shows the movement of the real part of the complex eigenvalue and Fig 5 14, the movement of the largest real eigenvalue It is seen from the Figs 5 13 and 5 14 that in the stable region before the saddle-node bifurcation point the real eigenvalue is critical, while in the stable region before subcritical HB, the complex eigenvalue is critical

The eigenvalue sensitivity analysis has been performed using the technique given in ref [72]

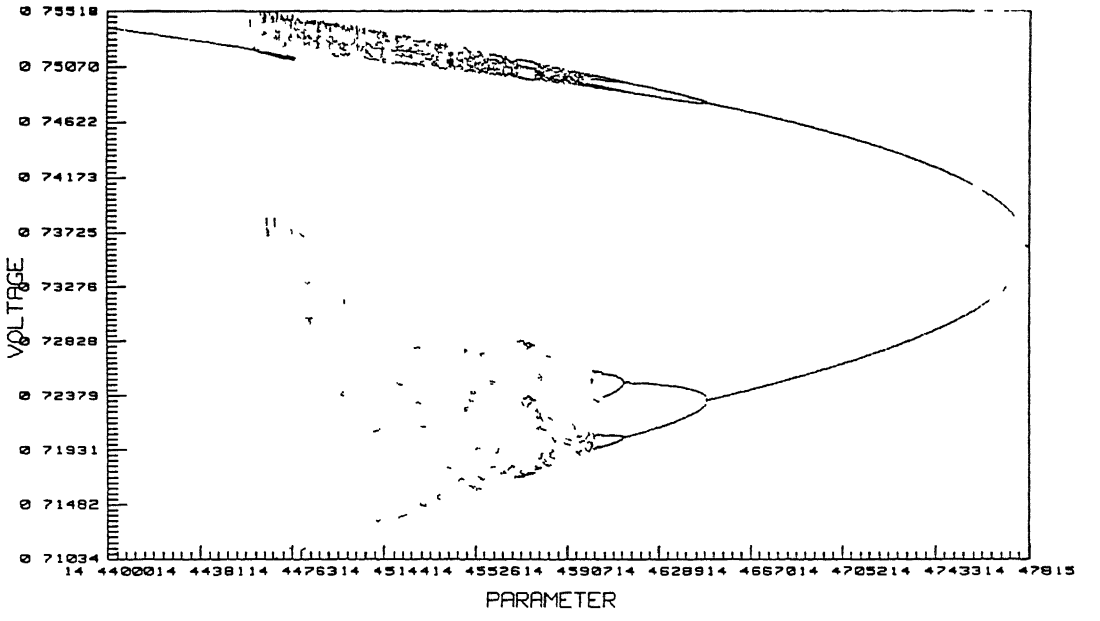

Figure 5 10. 3-bus system with SVS chaotic dynamics

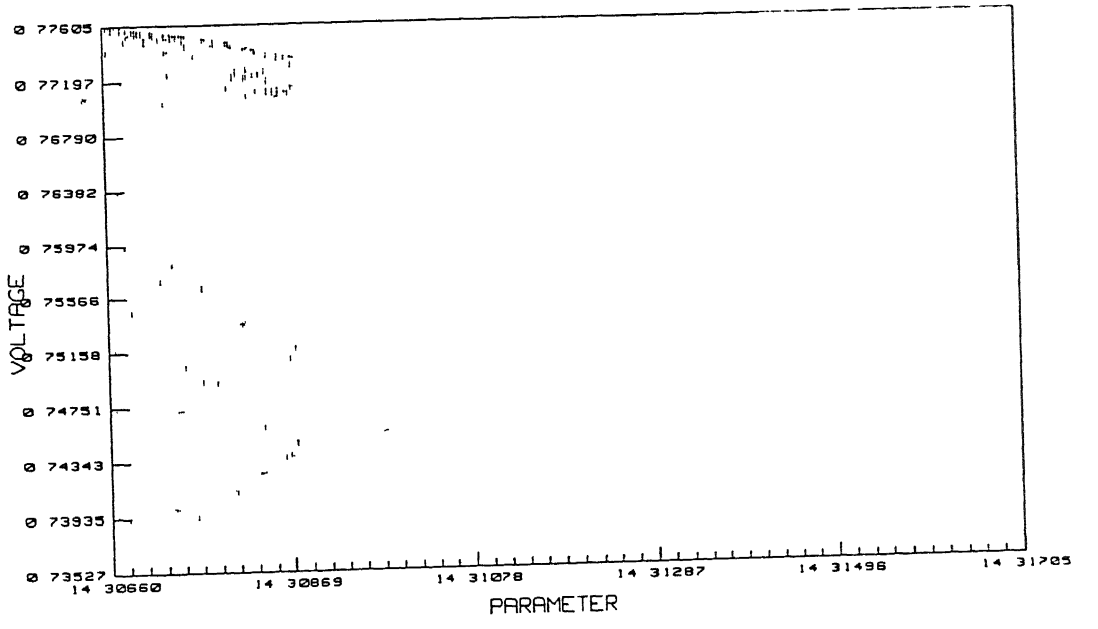

Figure 5 11 3-bus system with SVS boundary crisis

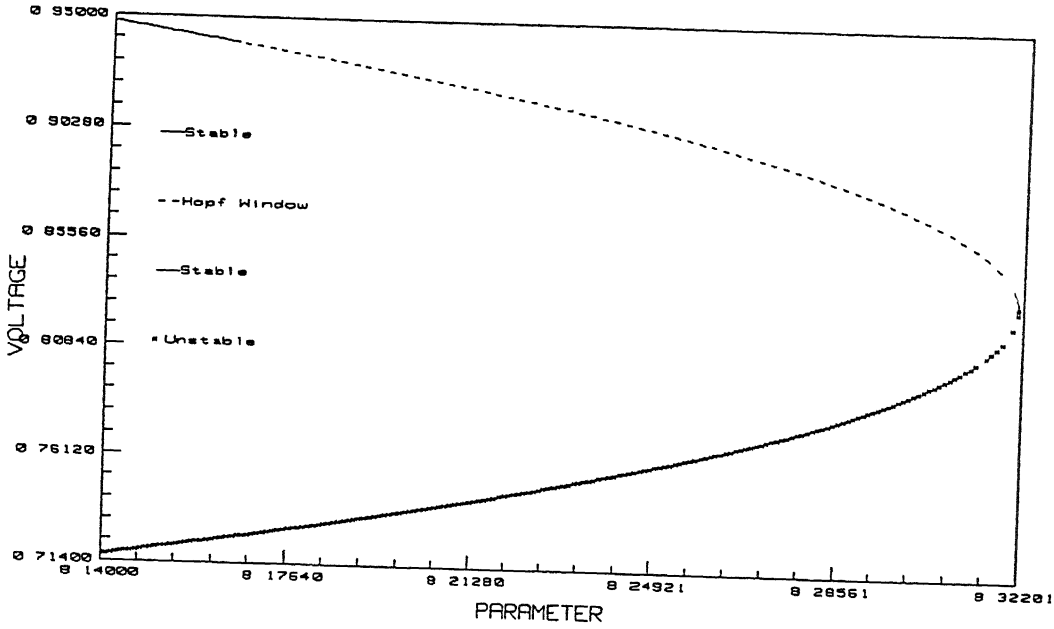

Figure 5 12 4-bus system with OLTC steady state bifurcation diagram

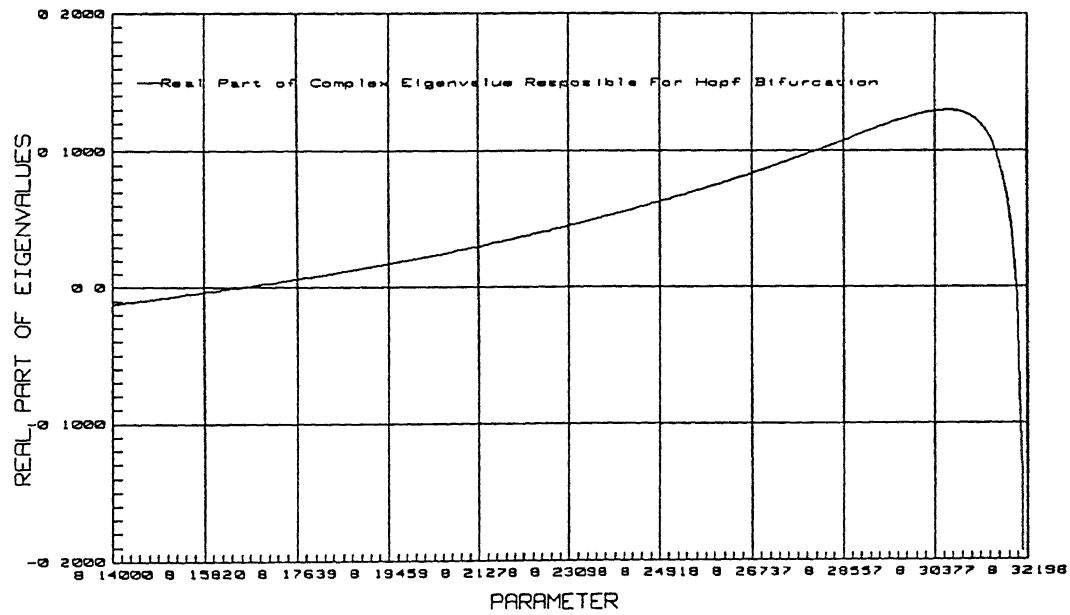

Figure 5 13 4-bus system with OLTC movement of complex eigenvalue

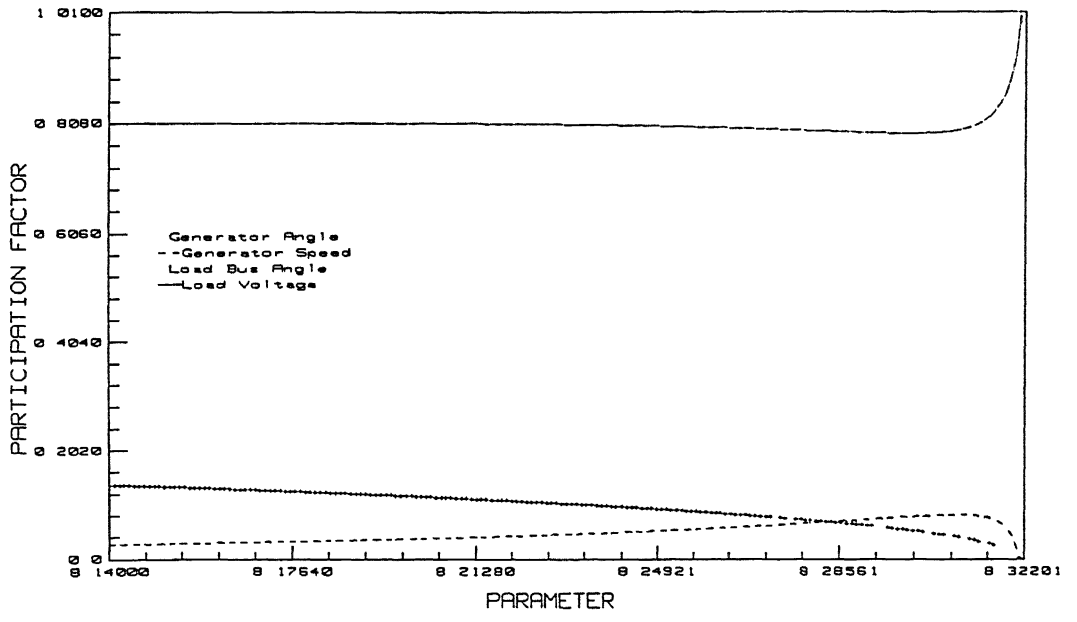

Figure 5 14 4-bus system with OLTC movement of real eigenvalue

and the participation factors for complex eigenvalues and real eigenvalue are shown in Figs 5 15 and 5 16 for different values of Q_1 It is interesting to note that the real eigenvalue is dominated by the load bus voltage V while the complex eigenvalue is mainly associated with (δ,ω) states

Through numerical simulation, it is observed from Fig 5 17 that at subcritical HB a unstable limit cycle is born which surrounds the stable fixed point until $Q_1 = 7\,9163$ The Floquet multipliers were computed and all of them were found to be within unit circle except one which was found to be outside the unit circle Thus, the periodic orbit is type-1 unstable It was observed during the numerical simulation, that the Floquet multiplier which was outside the unit circle enters the unit circle through $+1$, thus giving rise to a CFB at $Q_1 = 7\,9163$ The CFB arises when a stable and unstable limit cycle coalesce Thus it can also be called as saddle-node or fold bifurcation of the limit cycle Therefore, at $Q_1 > 7\,9163$, a stable periodic orbit exists The stable periodic orbit undergoes a PDB at $Q_1 = 7\,9165$ A Floquet multiplier crosses the unit circle through -1 The original stable periodic orbit becomes unstable and remains so until $Q_1 = 8\,31057$ At this point, a Floquet multiplier which was outside the unit circle enters the unit circle through -1 The periodic orbit gains stability at $Q_1 = 8\,31057$ and remains so until supercritical HB at $Q_1 = 8\,3199$ This periodic orbit undergoes further PDB leading to chaotic

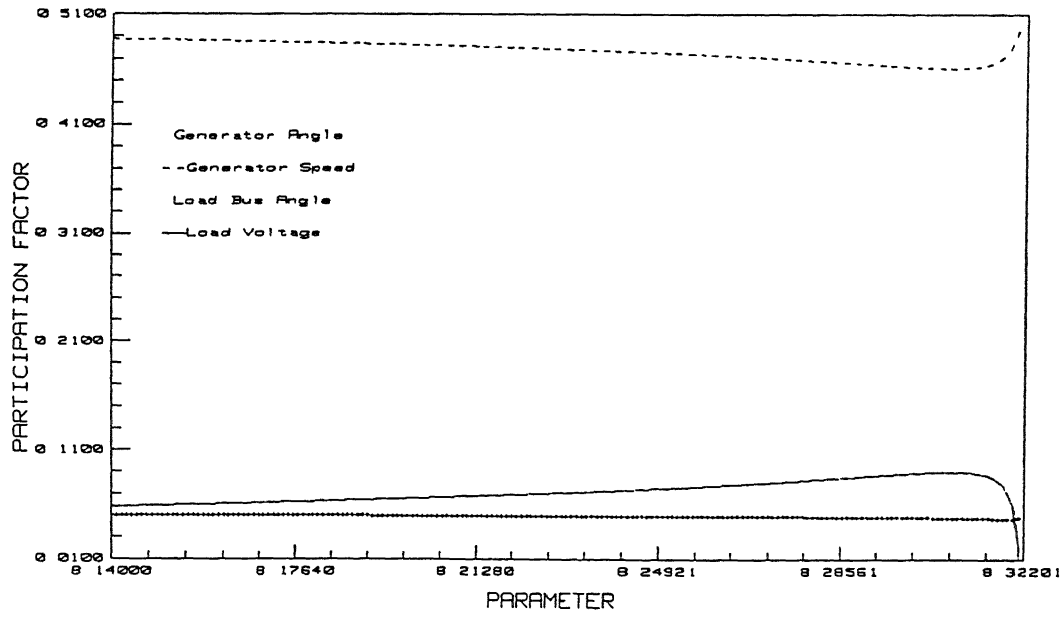

Figure 5 15 4-bus system with OLTC participation factors of complex eigenvalue

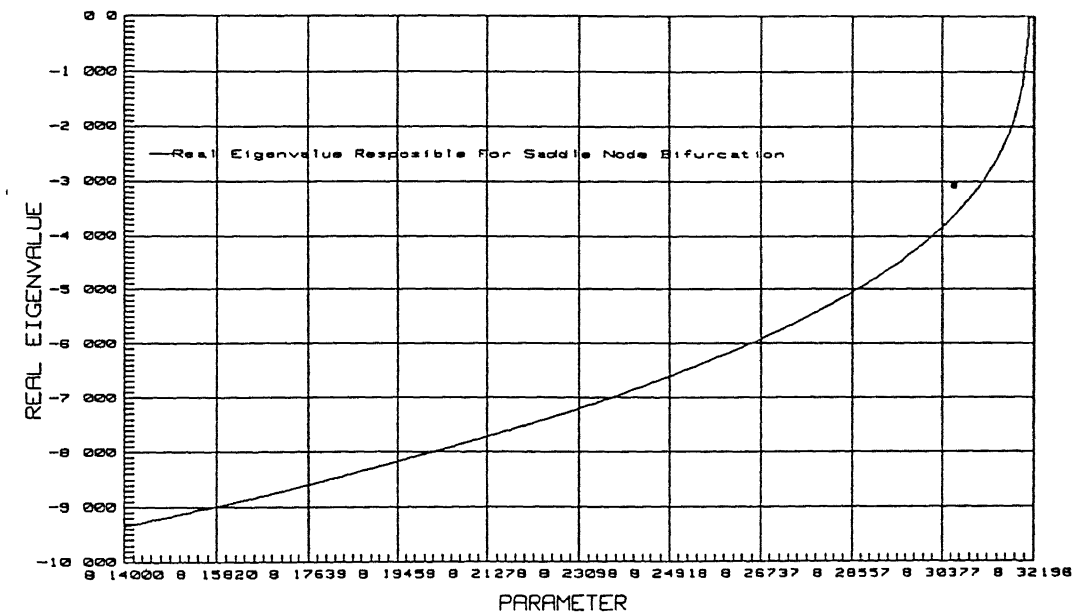

Figure 5 16 4-bus system with OLTC participation factors of real eigenvalue

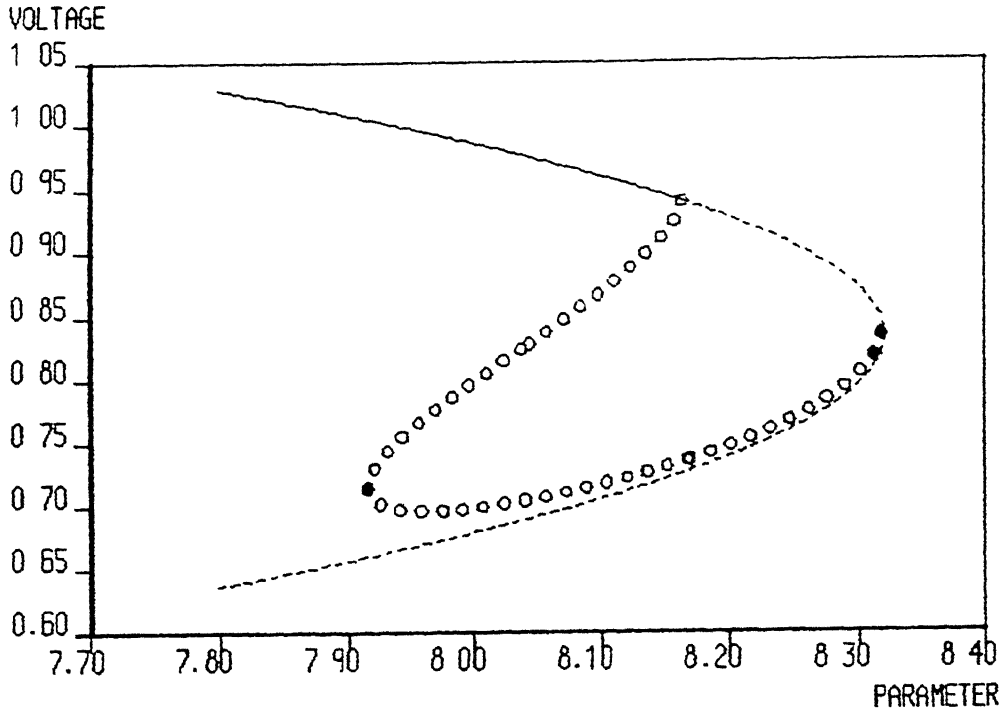

Figure 5 17: 4-bus system with OLTC bifurcation diagram

oscillations Starting from $Q_1 = 8\ 3199$ the bifurcation diagram using brute-force method (page 210, ref [59]) has been shown in Fig 5 18 At $Q_1 = 8\ 3067$, the system looses stability and the simulation halts as a consequence of expanding flow i e divergence of the vector field becomes positive Figs 5 19 to 5 21 depict a typical simulation for $Q_1 = 8\ 30567$ from the following initial conditions, ($\delta = 0\ 3149$, $\omega = 0\ 22016$, $\theta = -0\ 00187$, $V = 0\ 87188$) It is seen that the system voltage though oscillating remains fairly healthy for upto 27 6 seconds and then collapses as seen from Fig 5 19 The angle of load bus voltage shoots up at that point in time as shown in Fig 5 20 However, generator angle variation remains within acceptable range as shown in Fig 5 21

The collapse of voltage takes place due to boundary crisis (blue sky bifurcation) at $Q_1 = 8\ 30567$ In the boundary crisis, a strange attractor exists for parameter values upto the critical value, at which the collision takes place Subsequent to this value, the strange attractor no longer exists, but it leaves a signature of a transient chaotic motion The transient chaotic motion appears chaotic for a relatively long time (depending on the initial condition) and then suddenly experiences a sharp excursion either to another attractor or to infinity This excursion occurs through a tunnel in state space which necessarily follows the unstable manifold of the saddle

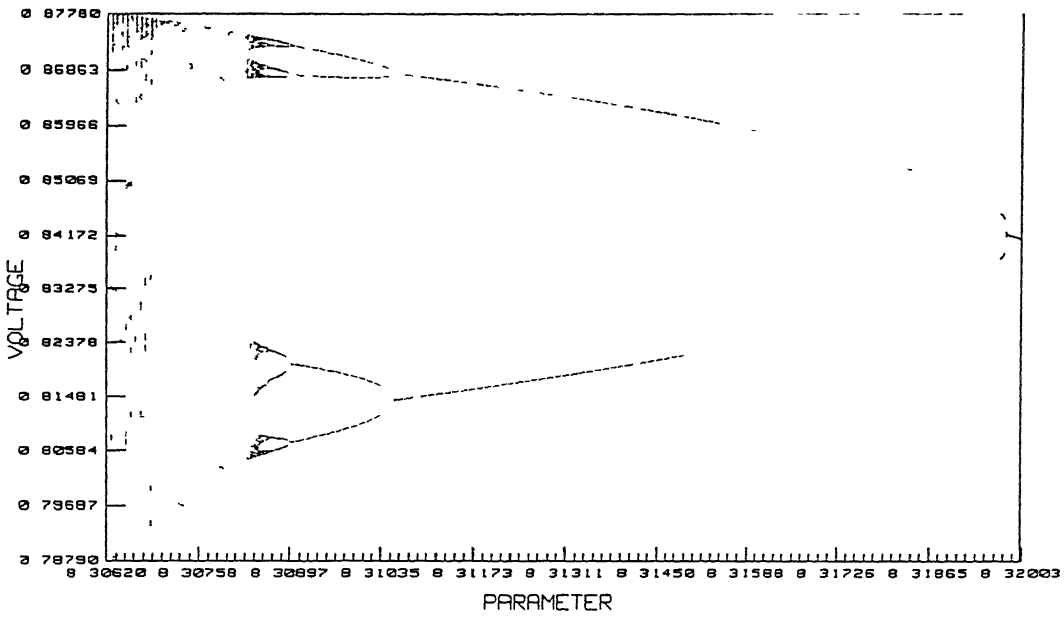

Figure 5 18 4-bus system with OLTC chaotic dynamics

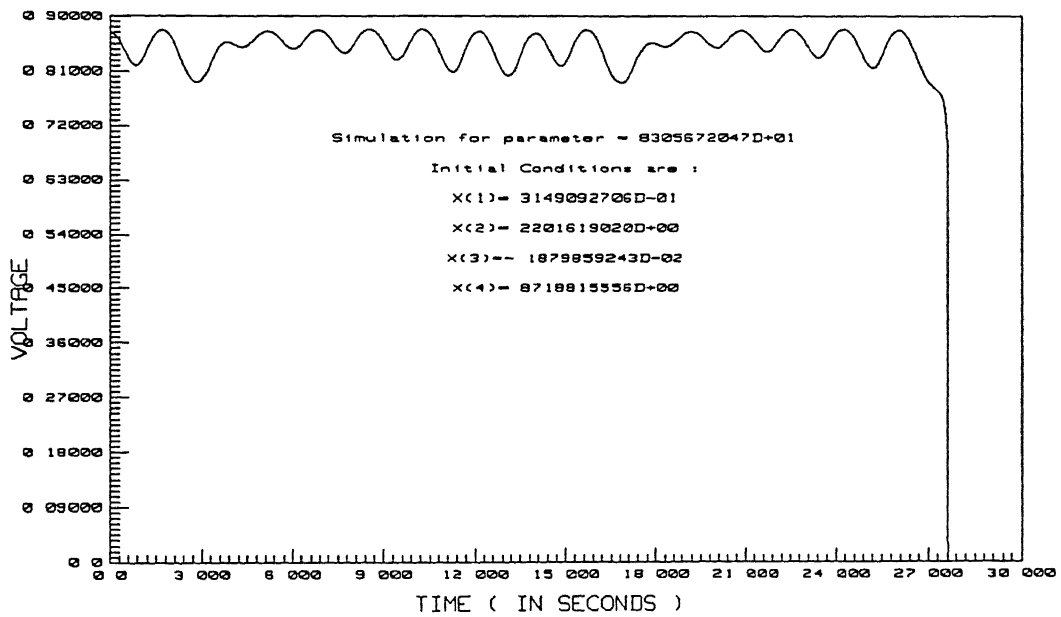

Figure 5 19 4-bus system with OLTC time variation of V

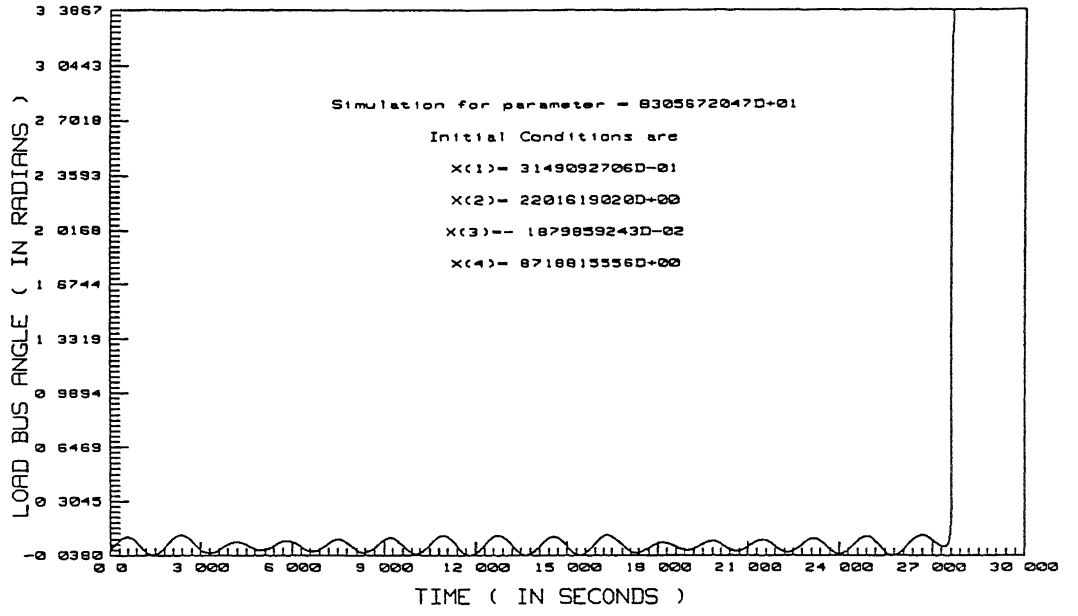

Figure 5 20 4-bus system with OLTC time variation of θ

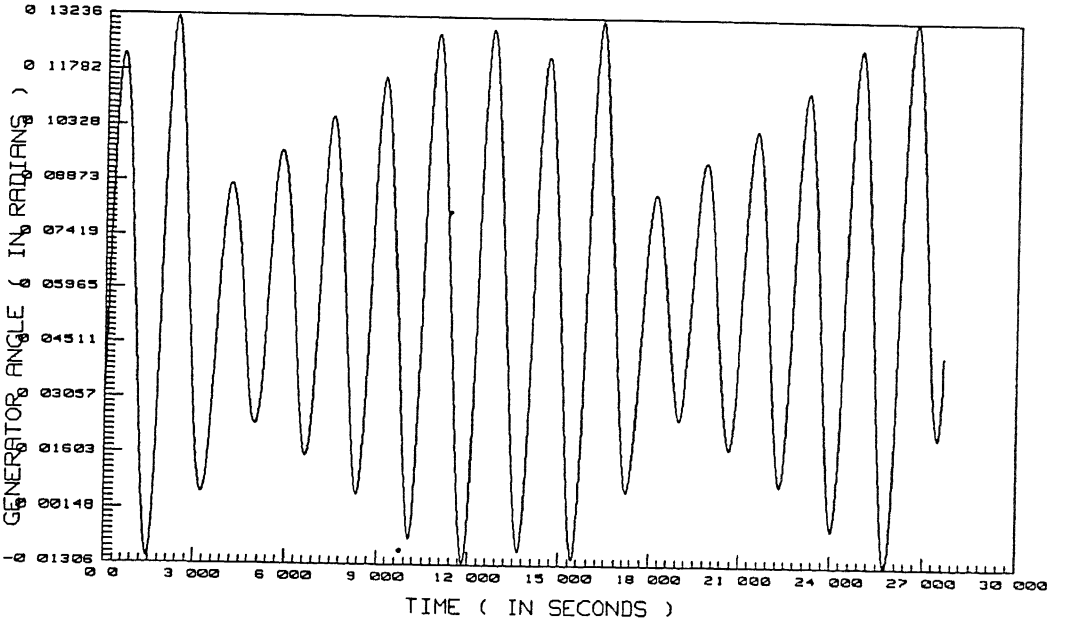

Figure 5 21 4-bus system with OLTC time variation of δ

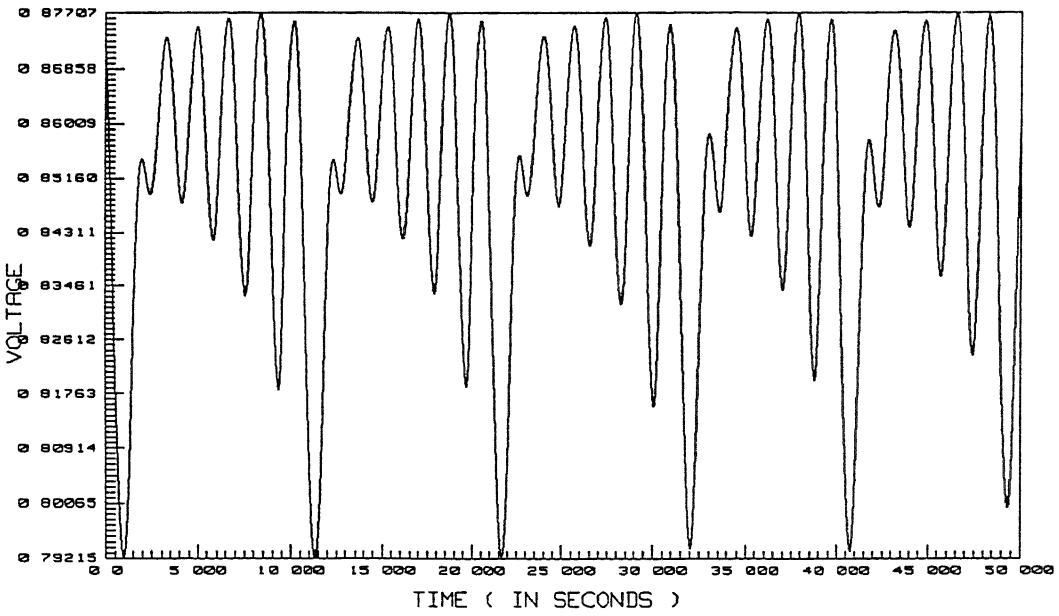

Figure 5 22 4-bus system with OLTC time variation of V in chaotic region

point or orbit with which the collision takes place The result is a discontinuous, catastrophic disappearance of the strange attractor

Lyapunov exponents have been computed for $Q_1 = 8\ 3067$ LEs are found to be (0 331, 0 000, −2 03, −33 615) One positive Lyapunov exponent confirms the presence of chaos Fig 5 22 depicts the time variation of voltage in the chaotic region for parameter $Q_1 = 8\ 3067$ Fig 5 23 shows the corresponding simulation projected in the phase onto load bus voltage and bus angle coordinates The Lyapunov dimension of the attractor was computed as 2 163

Further it was observed that for for $Q_1 > 7\ 916320$ (i e after CFB) a stable periodic orbit is born which undergoes PDB at $Q_1 = 7\ 916354$ The stable periodic emerging as a result of PDB undergoes further PDB at $Q_1 = 7\ 916370$ Another PDB occurs at $Q_1 = 7\ 916374$ Since the bifurcations took place in very narrow range, the simulation could not be carried out to trace further bifurcations

5.5.3 9–Bus System

The generator and load model for this system was taken same as those considered in studies presented section 4 5 1 2 of the Chapter 4 The dynamics was studied by varying MVA load ℓ

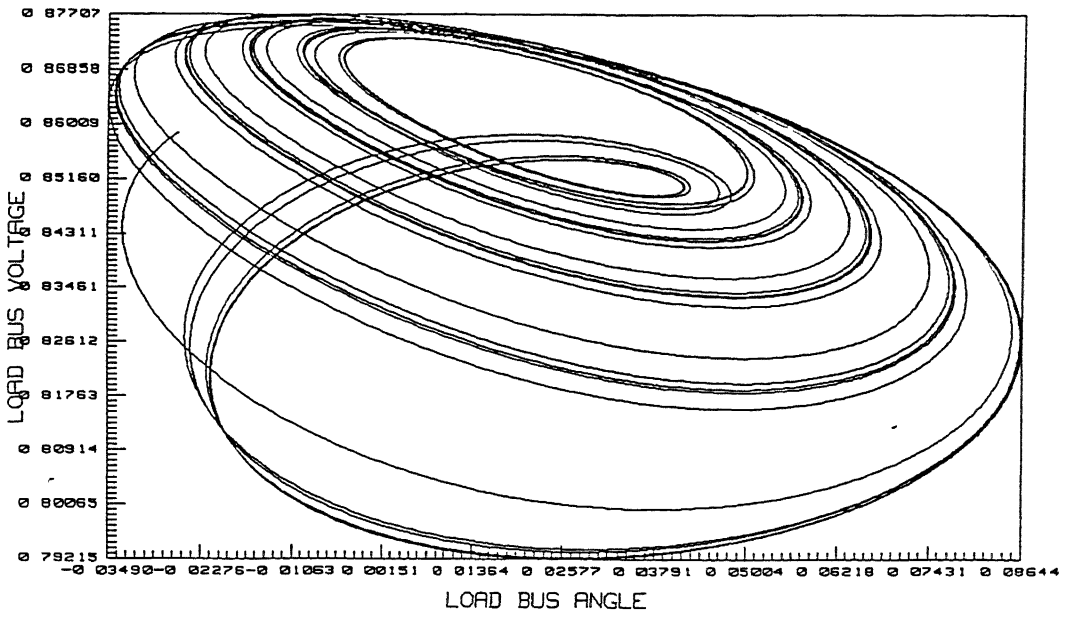

Figure 5 23 4-bus system with OLTC plot of trajectory projected on V, θ plane

at bus-5 and power factor pf was assumed to be unity Two sets of studies were performed, one at the base case condition and the other being a contingency case considering the outage of the line between buses-4 and 5

5.5 3.1 9–Bus System. Base Case

The bifurcation diagram has been drawn in Fig 5 24 Some of the important bifurcations has been observed as follows

- SNB at $\ell = 3\ 598273$ (point-3)
- Subcritical HB at $\ell = 3\ 577746$ and $3\ 588495$ (points-2 & 3)
- TRB at $\ell = 3\ 249934$ and $3\ 037992$ (points-6 & 13)
- PDB at $\ell = 3\ 135110, 3\ 235849, 3\ 042431$ and $3\ 558070$ (points-8, 9, 11 & 14)
- LP of periodic orbits at $\ell = 3\ 070598, 3\ 268290$ and $3\ 022379$ (points-7, 10 & 12)

The numerical investigations reveal that unstable periodic orbits emerging at $\ell = 3\ 577746$ and $\ell = 3\ 588495$ are of type-1 kind (i e one Floquet multiplier is outside unit circle) and at

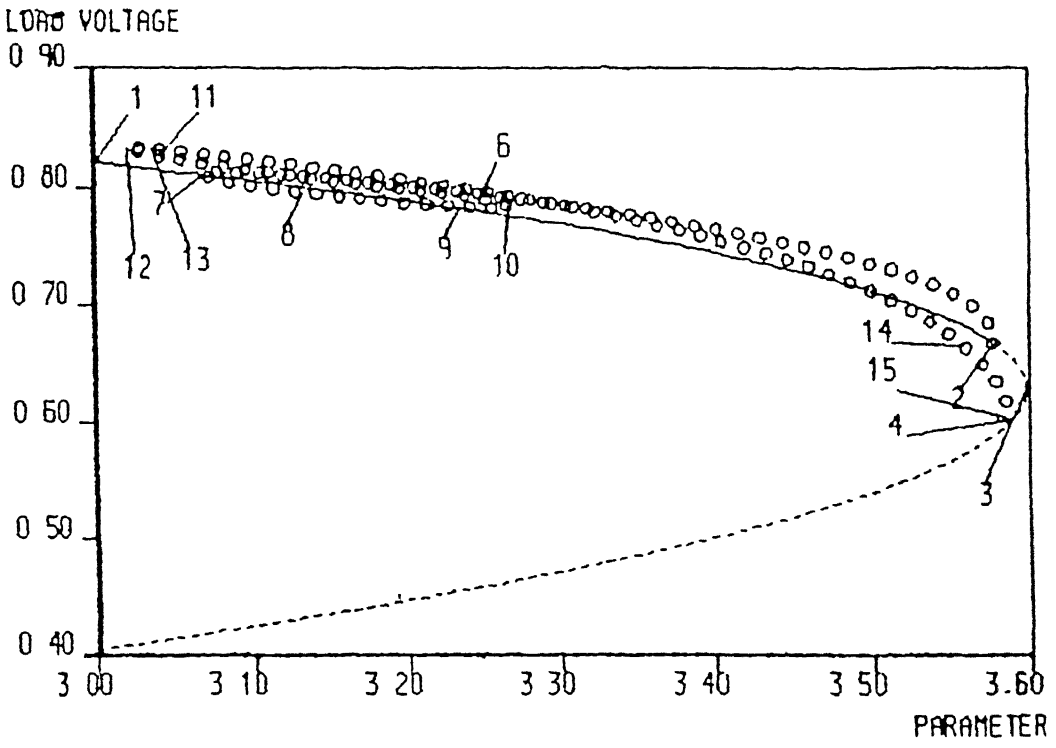

Figure 5 24 9-bus system (base case) bifurcation diagram

$\ell = 3\ 249934$ one periodic orbit bifurcates to unstable torus and the other one undergoes a PDB at $\ell = 3\ 558070$ For $3\ 249934 \leq \ell \leq 3\ 577746$ there exists a periodic orbit of type-1 kind Since the boundary of region of stability of the stable equilibrium point is given by the union of stable manifold of the type-1 unstable equilibria and closed orbit [45], the region will shrink in presence of unstable periodic orbit having one Floquet multiplier outside unit circle

The participation analysis was carried out to ascertain the participation of the states corresponding to the critical eigenvalue causing the Hopf bifurcation The eigenvalues along with the participation factors at $\ell = 3\ 577746$ are shown in Table 5 1 It is found that the states associated with generator # 2 are predominant in the critical mode Fig 5 25 shows a typical time variation of load voltage V_5 for $\ell = 3\ 58$ from initial condition ($\omega_2 = \omega_3 = 0$, $\delta_2 = -0\ 2154$, $\delta_3 = -0\ 26531$, $\theta_5 = -0\ 89383$, $V_5 = 0\ 71238$) This initial condition corresponds to stable operating point for $\ell = 3\ 50$ It is seen that on account of the subcritical Hopf bifurcation, the voltage at the load node will experience growing oscillations and collapses after about 135 36 seconds

Table 5 1 9-bus system eigenvalues and state participation factors

Eigenvalues	Participation Factors		
	δ_2, ω_2	δ_3, ω_3	θ_5, V_5
$-1\ 2802 \times 10^2$	$8\ 19 \times 10^{-4}$	$5\ 26 \times 10^{-4}$	$5\ 82 \times 10^{-1}$
			$4\ 19 \times 10^{-1}$
$-8\ 0958$	$1\ 26 \times 10^{-2}$	$4\ 99 \times 10^{-3}$	$4\ 16 \times 10^{-1}$
		$5\ 03 \times 10^{-3}$	$5\ 47 \times 10^{-1}$
$-3\ 5180$	$9\ 91 \times 10^{-2}$	$4\ 00 \times 10^{-1}$	$6\ 16 \times 10^{-4}$
$\pm j1\ 1823$			$3\ 94 \times 10^{-4}$
$3\ 2445 \times 10^{-7}$	$3\ 95 \times 10^{-1}$	$9\ 68 \times 10^{-2}$	$1\ 29 \times 10^{-2}$
$\pm j6\ 0707^*$			$1\ 63 \times 10^{-2}$

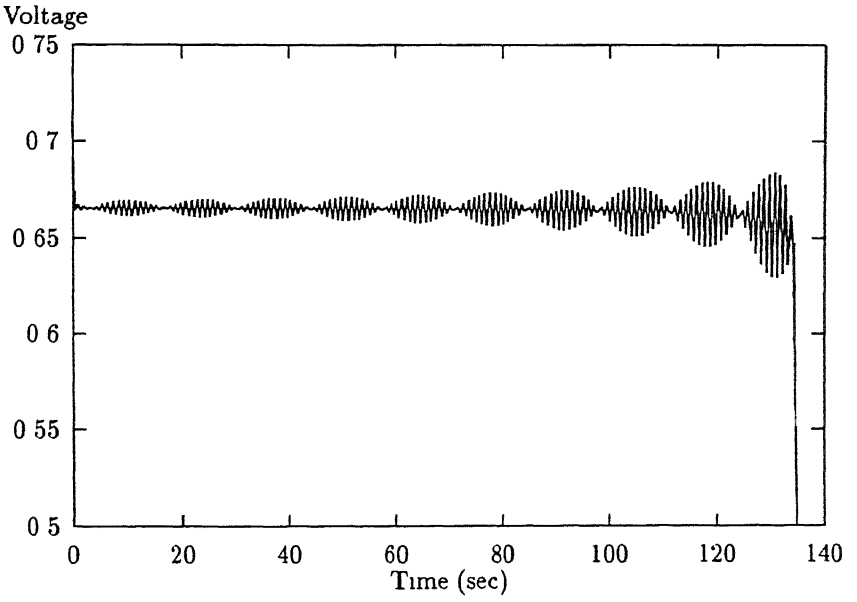

Figure 5 25 9-bus system (base case) time variation of V

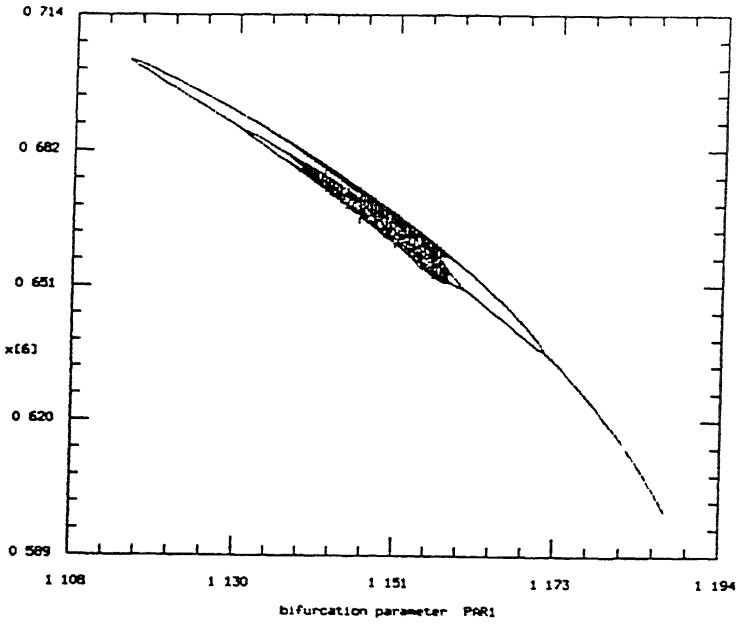

Figure 5 27 9-bus system (a contingency case). chaotic dynamics

The unstable periodic orbit, for 1 076371 $\leq \ell \leq$ 1 116463, has one Floquet multiplier outside the unit circle Though there is a stable fixed point (operating point) for 1 076371 $\leq \ell \leq$ 1 116463 the impact of this unstable periodic orbit is to decrease the stability region The stable periodic orbit emerging at ℓ = 1 076371 undergoes a series of PDB between ℓ = 1 115625 and ℓ = 1 171130 leading to chaotic oscillations as shown in Fig 5 27

For ℓ = 1 14, Lyapunov exponents were found to be (0 135, 0 000, −0 032, −0 38, −6 657 and −40 665) The presence of one positive LE confirmed the chaotic dynamics The Lyapunov dimension of the attractor is 3 284 Variation of the load voltage with time and its frequency spectrum are shown in Figs 5 28 and 5 29 The frequency spectrum in Fig 5 29 is continuous and broad band in nature

5.5.4 19–Bus UPSEB System

In this study, all the base case loads have been modelled as constant impedance type An additional load has been considered at bus-14 represented by load model-II described by the equations (4 36) and (4 37) in Chapter 4 The bifurcation diagram has been drawn as shown in Fig 5 30 considering ℓ as the parameter and keeping the power factor unity The other

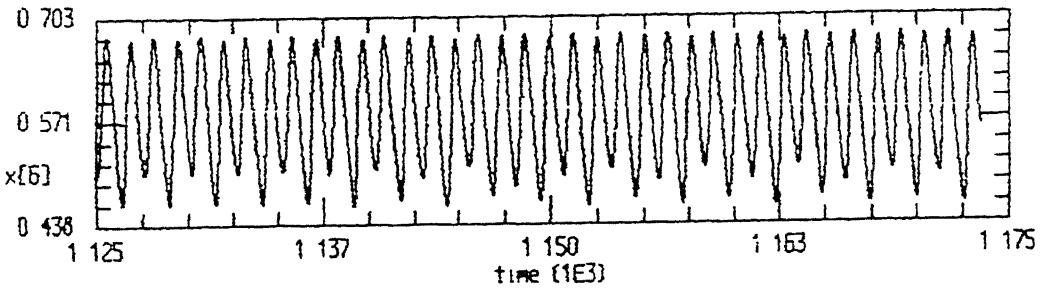

Figure 5 28 9-bus system (a contingency case) time variation of V_5

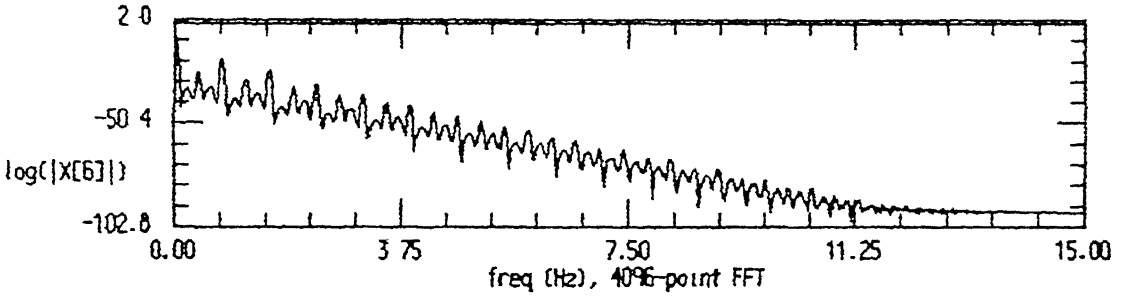

Figure 5 29 9-bus system (a contingency case) frequency spectrum

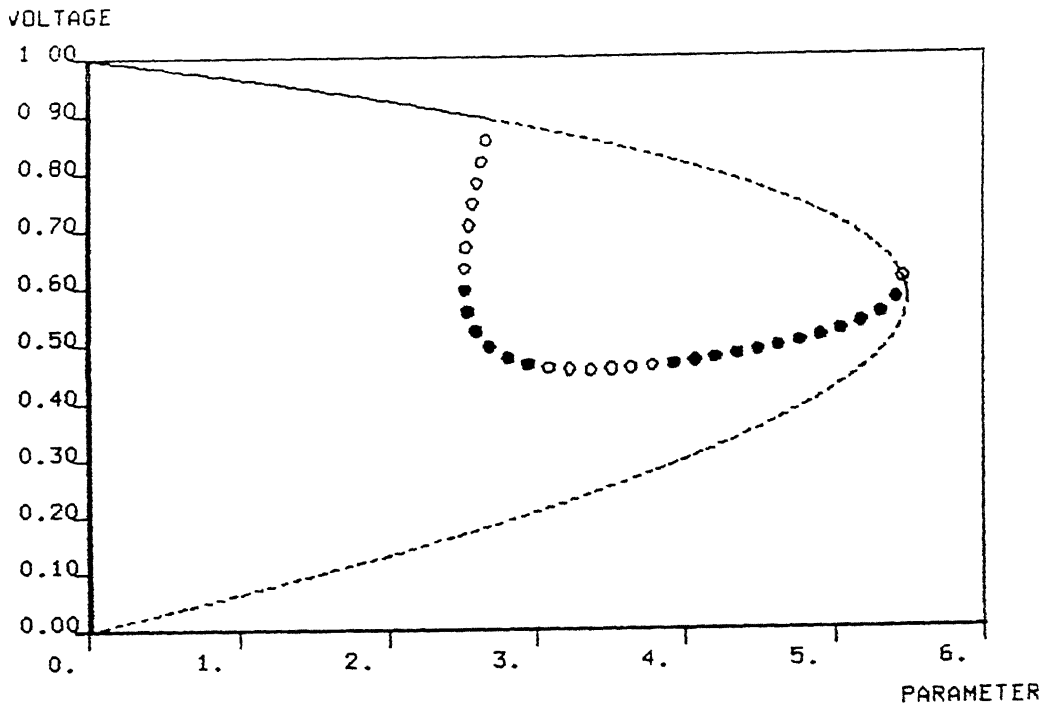

Figure 5 30 19-bus system bifurcation diagram

parameters of the dynamic load D, a, b and k were taken to be 0 05 (sec), 0 0, 0 0 and 0 1 (sec), respectively Some of the important points on the bifurcation diagram are given as below

- Subcritical HB at $\ell = 2\ 696254$
- Supercritical HB at $\ell = 5\ 454979$
- SNB at $\ell = 5\ 485668$
- CFB at $\ell = 2\ 519270$
- TRB at $\ell = 3\ 078993$ and $3\ 911500$

The unstable periodic orbit for $2\ 519270 \leq \ell \leq 2\ 696254$ is type-1 and will reduce the stability region of s e p At $\ell = 2\ 519270$, the Floquet multiplier which has been outside the unit circle enters the unit circle through $+1$, thus giving rise to a CFB The periodic orbit becomes stable and remains so until $\ell = 3\ 078993$ where a torus bifurcation occurs This torus breaks down into a chaotic attractor as ℓ is further increased which disappears at $\ell = 3\ 59421$ due to boundary crisis There is no attractor from $\ell = 3\ 59421$ to $3\ 911500$ where a complex pair of Floquet multiplier enters the unit circle, thus giving rise to a stable periodic orbit

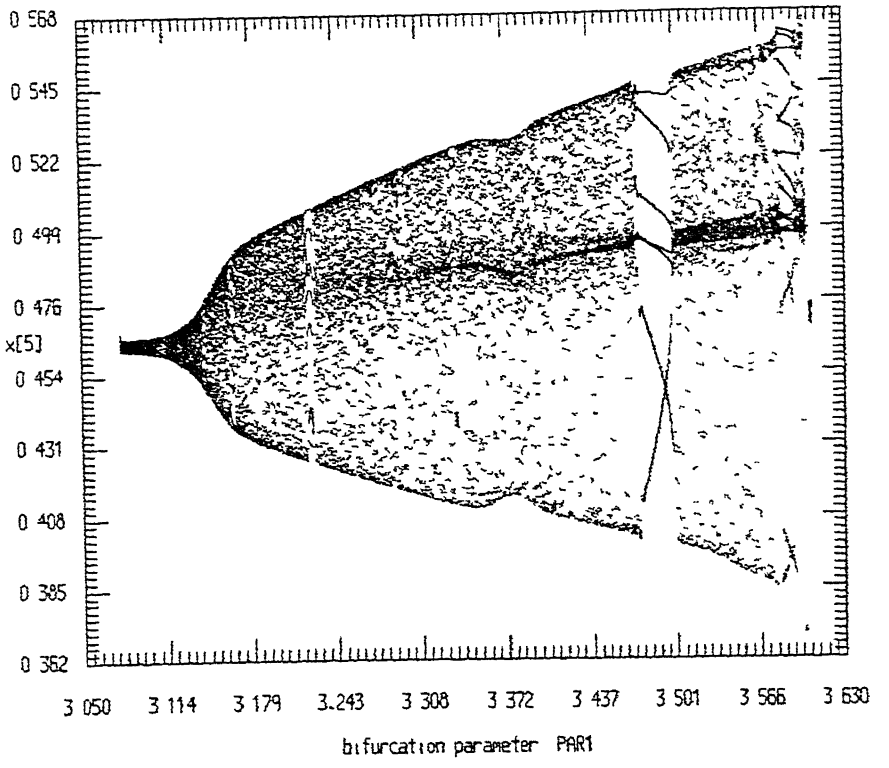

Figure 5.31 19-bus system chaotic dynamics

The bifurcation diagram for the chaotic region is shown in Fig 5 31 It is observed that at places along the parameter there exist few periodic windows This is called *mode-locking* or phase-locking and is due to the fact that the frequencies of oscillations become rational, resulting in periodic behaviour The Lyapunov exponents and dimension were computed and are shown in Table 5 2

Table 5 2 19-bus system Lyapunov exponents and dimension of chaotic attractor

Parameter ℓ	Lyapunov Exponents				Dimension
3 1	0 0306313	0 00	−0 001	−10 0378236	3 80984
	−0 0536428	−0 0617678	−183 165	−201 391	
3 14646	0 0300368	0 0145376	−0 00	−0 041033	4 06265
	−0 0565283	−0 126793	−168 523	−200 27	
3 36451	0 0237414	0 0156513	0 00	−0 0454897	3 86597
	−0 0473544	−0 223015	−165 617	−199 915	

5.6 Conclusion

From the studies carried out on the three sample systems, in this chapter, to explore the existence of various types of global bifurcations and chaos, following observations can be made

(i) Different types of dynamic bifurcations such as PDB, CFB, TRB, LP and chaos can exist in some of the power system networks for variation of the parameter even in their normal operating range

(ii) Some of the global bifurcations observed, possibly for the first time in power system model, include the bifurcation of periodic orbit to torus (TRB) and limit points of unstable to unstable periodic orbits

(iii) Chaos has been observed in all the three sample systems Chaos via PDB route has been observed in two of the systems and quasiperiodic route in one of the systems Chaos via torus breakdown has been observed for the first time in a practical 19-bus Indian system

(iv) The chaotic oscillations produce harmonics of all the frequencies with low frequencies (less than about 10 Hz) being dominant and a continuous broad band frequency spectrum is observed

(v) Boundary crisis (blue sky bifurcation) and subcritical Hopf bifurcation cause voltage collapse in some of the systems

(vi) By adjusting the SVS gain parameter the boundary crisis and hence the voltage collapse can be avoided

Chapter 6

Control of Dynamic Bifurcations and Chaos

6.1 Introduction

Presence of dynamic bifurcations and chaos has been shown to exist in several models of power system in Chapter 5 Though a chaotic oscillation is bounded, the system exhibits seemingly random behaviour and poses serious problems from operation view point Some of the implications of these nonlinear phenomena already observed are the reduction in stability margin/region of attraction especially due to subcritical Hopf bifurcation, introduction of harmonics especially low frequency harmonics during chaotic oscillation and system voltage collapse due to subcritical Hopf bifurcation and boundary crisis

Thus, these phenomena are unwanted in the system and need to be eliminated One of the easiest ways to remove these bifurcations in the system is by restricting the parameter to enter this region This may limit the transmission usable capacity resulting into reduced system loadability One of the efforts for stabilising unstable periodic orbit of a chaotic attractor is due to Ott et al [77], who applied the computed values of an externally manipulable system parameter This concept has been used by Bandyopadhyay et al [124] to stabilise a chaotic non isothermal CST reactor by controlling the bifurcation parameter or some other parameter to yield almost a periodic behaviour It has been demonstrated by Tan et al [154] that by varying the damping, the dynamic bifurcation and chaos can be controlled Wang et al [157] employed a feedback law to control the stability and amplitude of the bifurcated solution using generator speed deviation signal

With developments in high power electronics, recently new devices, popularly called FACTS (Flexible AC Transmission System) devices, for control of voltage and power have been developed [108,137,138] The prominent among them are controllable series capacitors (CSC), static phase angle regulator (PAR) and static VAR compensators (SVC)

In this Chapter, the studies have been conducted on the three sample systems consisting of 3-bus, 9-bus and 19-bus to explore the effectiveness of these new devices for controlling the dynamic bifurcations A first order model of these devices have been considered and the feedback control signal has been decided based on participation factor analysis

6.2 Control of Bifurcation

Bifurcation control deals with design of control inputs to modify the bifurcation characteristics of a parameterised system The control signal can take many forms, including open loop control or static or dynamic feedback The objective may be stabilisation and/or delay of a given bifurcation, reduction of the amplitude of bifurcated solutions, introduction of bifurcation at desired parameter values or a combination of these

Consider a one-parameter family of nonlinear control systems

$$x = f(x, u, \mu) \tag{6 1}$$

where $x \in R^n$ is the state vector, u is the scalar control and $\mu \in R^1$ is the bifurcation parameter The vector function f is assumed to be smooth in x, u, and μ Let equation (6 1), with the control set to zero undergoes either a subcritical or supercritical HB from a fixed point $x_0(\mu)$ at the critical parameter value $\mu = \mu_c$

Consider the case in which the HB is subcritical i e for $\mu < \mu_c$, the $x_0(\mu)$ is stable and a unstable periodic orbit surrounds it Then, for $\mu > \mu_c$ the system trajectory will diverge If the control u can be designed so as to render the HB to be supercritical, this situation will be remedied to a certain extent i e the same system trajectory will now converge to a small amplitude periodic solution Since this periodic solution is near the nominal equilibrium point, divergence of the system to a distant (and unacceptable) operating mode can thus be prevented Ref [123,161] present details of the laws

In general, a static state feedback using the control law

$$u = u(x - x_0(\mu)) \tag{6 2}$$

designed with reference to the nominal equilibrium path $x_0(\mu)$ of equation (6 2) will not only affect stability but also the location and stability of other equilibria The main disadvantage stems from the fact that system performance is often degraded by operating at an equilibrium which differs from the one at which the system is designed to operate

For these reasons, the dynamic state feedback is recommended [123, 161] This is achieved by incorporating high pass filters known as washout filters into the structure of the allowed controllers The use of washout filters is common in power system stabilisers A washout filter is stable high pass filter with transfer function

$$G(s) = \frac{s}{s+d} \tag{6 3}$$

Specifically, in equation (6 1), for each system feedback state variable x_i, $i = 1, . n$ a washout filter is introduced The value of d is a positive parameter This helps in preservation of equilibrium for variation of parameter in its operating range However, in the present study, only the static feedback is considered Equilibrium preservation is guaranteed since the feedback signals used are the generator speed deviation and generator acceleration power which are zero at equilibrium

There are many scenarios in which bifurcation can result into a chaotic invariant set Various routes to chaos have been discussed in Chapter 5 An important aspect in controlling chaos is that they may be suppressed by controlling a bifurcation in a given route to chaos The bifurcation control approach to this problem entails designing feedback control law which ensures a sufficient degree of stability for a primary bifurcation in such a scenario

In order to control dynamic bifurcation and chaos in the power system networks, the FACTS devices represented by a first order delay block has been utilised The participation analysis has been carried out to ascertain the appropriate error signal to these devices The generator speed deviation and acceleration power has been considered as error feedback signals because their steady state value would be zero and for this reason the washout filters have not been considered in this study

6.3 Model of FACTS Devices

The FACTS devices (CSC, PAR and SVC) have been represented in this study by a first order time delay model Their output Y is governed by the following differential equation

$$T_s \frac{dY}{dt} = K_s(X_r - X_m) - Y \tag{6 4}$$

and $Y_{min} \leq Y \leq Y_{max}$

where T_s is the time constant, K_s the gain of the controller, X_r is the reference value of the input quantity such as reference speed of the generator, or the mechanical power input to the generator X_m is the measured value of the feedback signal such as generator actual speed or real power output of the generator The output Y is the series capacitance X_{csc} for CSC, phase angle shift ϕ_p for PAR and the shunt sustenance b_{sh} for SVC

6.4 Case Study

The studies have been performed on HP-9000/735 computer system using AUTO86 software [34] The time constant T_s for all the three FACTS devices was taken as 0 01 sec in each of the studies The effect of controller gain variation was observed on the dynamic bifurcations As shown in subsequent sections, the generator states (δ, ω) were found to be dominant using participation analysis in the Hopf bifurcation window in each of the systems studied Hence, the generator speed deviation ω and the generator acceleration power P_a $(= P_M - P_{ge})$ was tried out as error signals to the controller of the FACTS devices These signals were also selected due to the fact that they do not affect the steady state performance and contribute to the damping of power system [147, 156, 171, 180] Participation of state variables in the critical mode were computed using the technique described in ref [72] to decide the input signal to the FACTS devices The studies were performed on the three sample systems namely 3-bus, 9-bus (base case and a contingency case) and 19-bus systems Results considering the effect of each of the FACTS devices at a time are presented below

6.4.1 3–Bus System

The data and network topology for this system have been shown in Appendix–B The generator at bus-3 was taken as infinite bus and the generator at bus-1 was modelled by its swing equation as described in section 4 4 1 of Chapter 4 A dynamic induction motor load model due to Walve [40] and as described in section 4 4 2 of Chapter 4 was considered along with constant static P and Q load at bus-2 Without considering the effect of FACTS devices, the bifurcation diagram has been drawn in Fig 6 1 treating (static) reactive load power Q_1 as the bifurcation parameter Some of the important bifurcation points observed in Fig 6 1 are listed below

- Subcritical HB at $Q_1 = 6\ 272709$

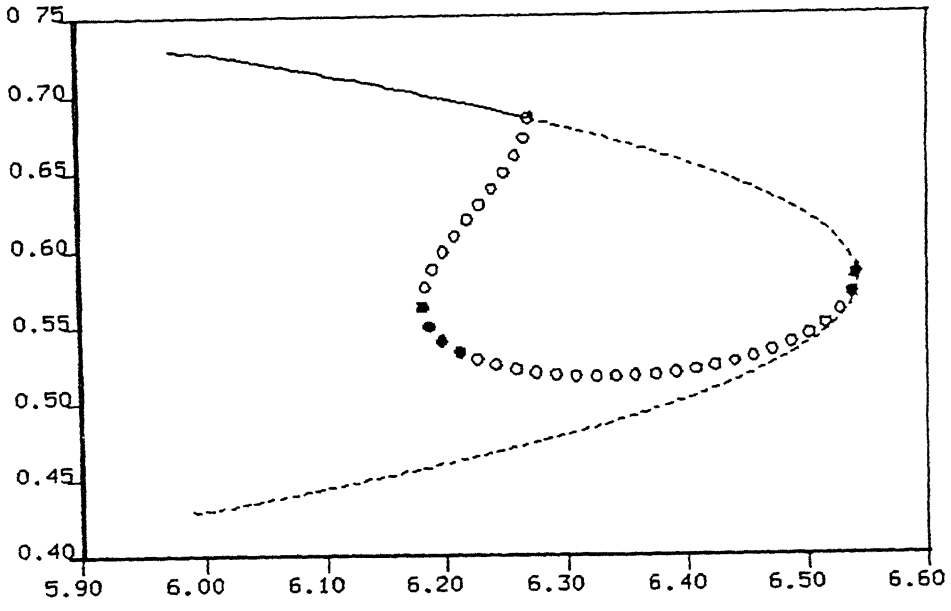

Figure 6 1 Bifurcation diagram for 3-bus system

- Supercritical HB at $Q_1 = 6\ 542023$
- CFB at $Q_1 = 6\ 181948$
- PDB at $Q_1 = 6\ 215310$ and $6\ 538772$
- SNB at $Q_1 = 6\ 543211$

The locus of HB points under variation of mechanical input power to the generator P_M is shown in Fig 6 2 Fig 6 2 reveals that if P_M is reduced, the two HB points move closer and for $P_M = 0\ 425$, they coalesce and disappear This, however, results into under utilisation of generator and transmission capacity

Six sets of studies were conducted to observe the effect of each controllable component, one at a time — three with the generator speed deviation as the error signal and the other three with generator acceleration power as the error signal

The CSC and PAR were sited in the line connecting bus-1 and 2 and the SVC was located at bus-2 as shown in Fig 6 3 Participation analysis was carried out to ascertain states predominant in the critical mode and it was found that the generator # 2 states (δ, ω) dominate the HB

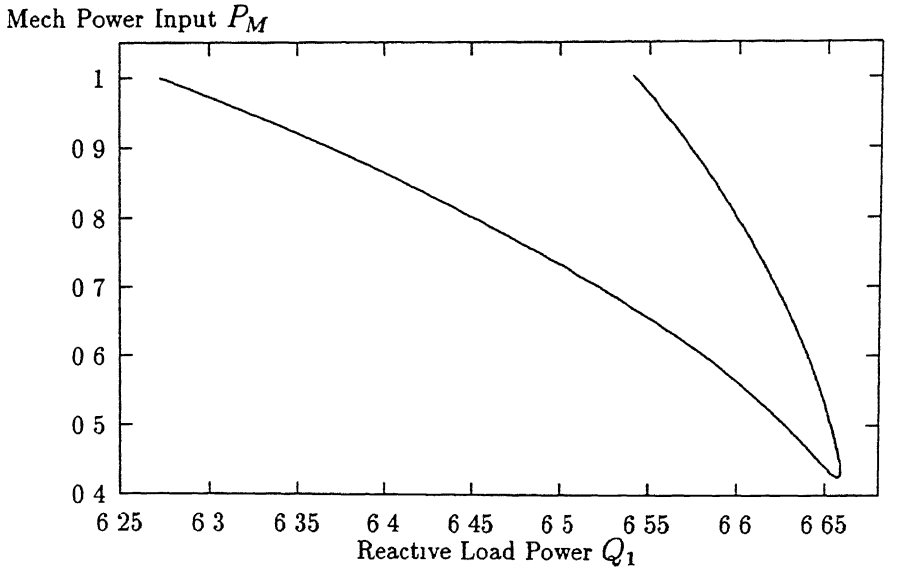

Figure 6 2 Effect of P_M on Hopf bifurcations

window Therefore, the error signals were derived from this generator The following limits were assumed for these devices These limits, however, will be encountered only in the time domain simulation studies involving disturbances

$X_{csc}^{max} = 0\ 1$ p u $\phi_p^{max} = 0\ 5$ rad $b_{sh}^{max} = 1\ 0$ p u
$X_{csc}^{min} = -0\ 1$ p u $\phi_p^{max} = -0\ 5$ rad $b_{sh}^{min} = -1\ 0$ p u

Figs 6 4 to 6 6 present the locus[1] of HB points considering CSC, PAR and SVC respectively with generator speed deviation Fig 6 4 shows the locus of CFB and HB points for gain variation of CSC When the gain of controller is increased from zero, the two HB points move closer Also the CFB moves closer to the HB point and for a gain value of 0 006, the CFB coalesces with the subcritical HB and disappears When the gain is further varied, the two HB points move closer and coalesce and disappear for a gain value of 0 0075 The strange attractor and HB window disappear and the dynamics become stable Similar effects of PAR and SVC were observed on the system dynamics From Figs 6 5 and 6 6, it is seen that HB window can be completely eliminated by PAR and SVC if the gain value of PAR is greater than 0 04725 and that of SVC is greater than 0 25

[1]It shows the position of the two Hopf bifurcations as the gain is varied

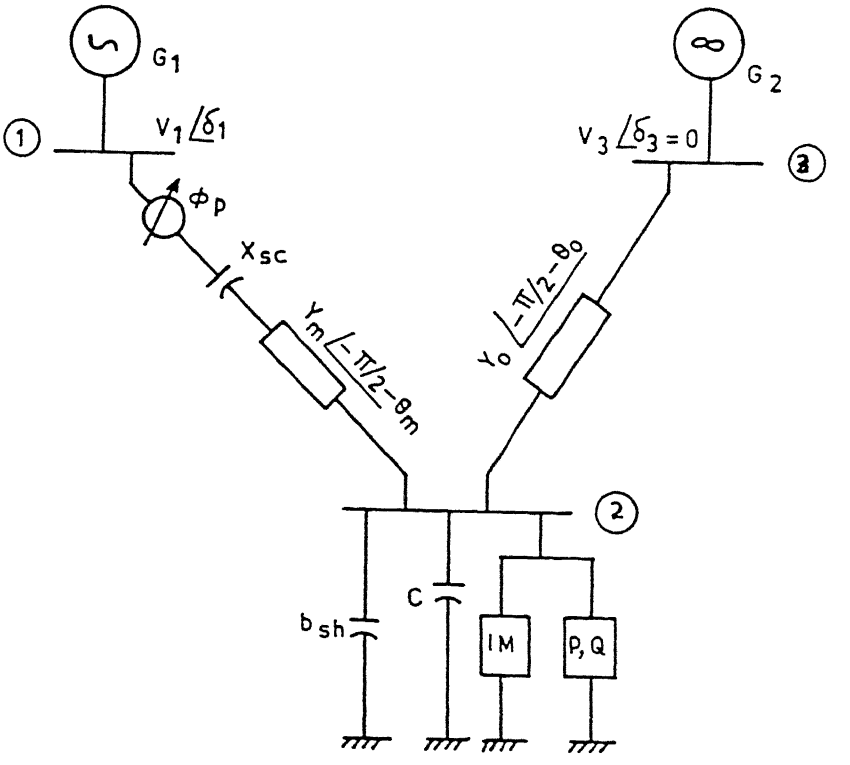

Figure 6 3 3-bus system with CSC, PAR and SVC

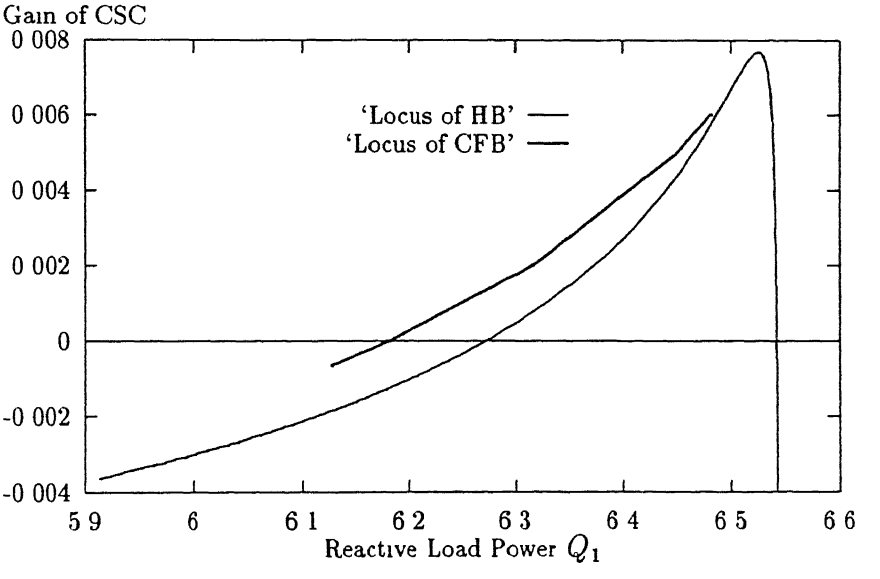

Figure 6 4 3-bus system CSC gain vs Q_1 with ω as error signal

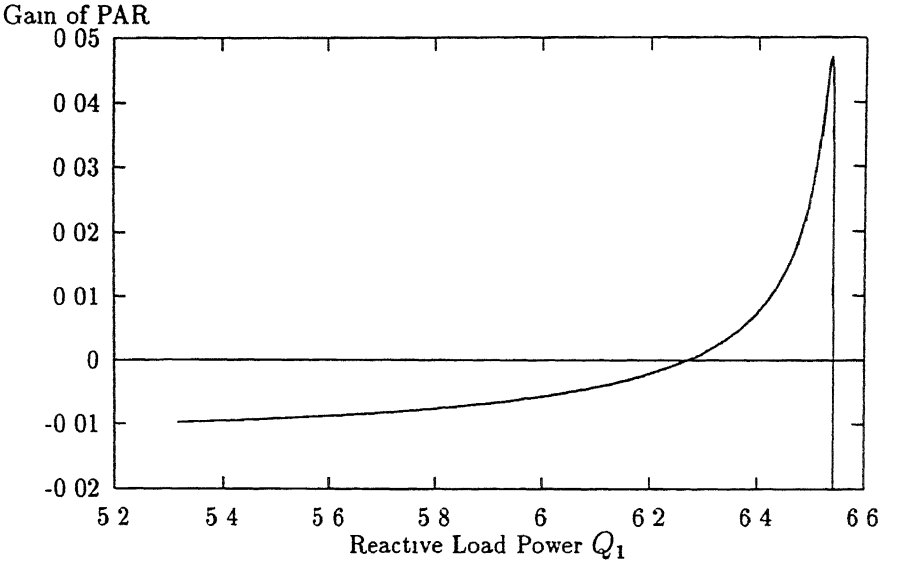

Figure 6 5 3-bus system PAR gain vs Q_1 with ω as error signal

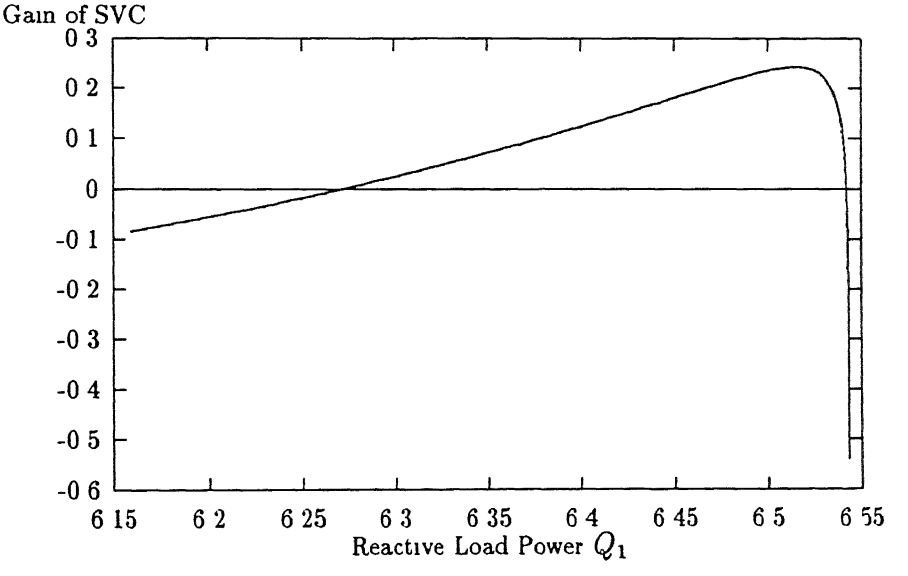

Figure 6 6 3-bus system SVC gain vs Q_1 with ω as error signal

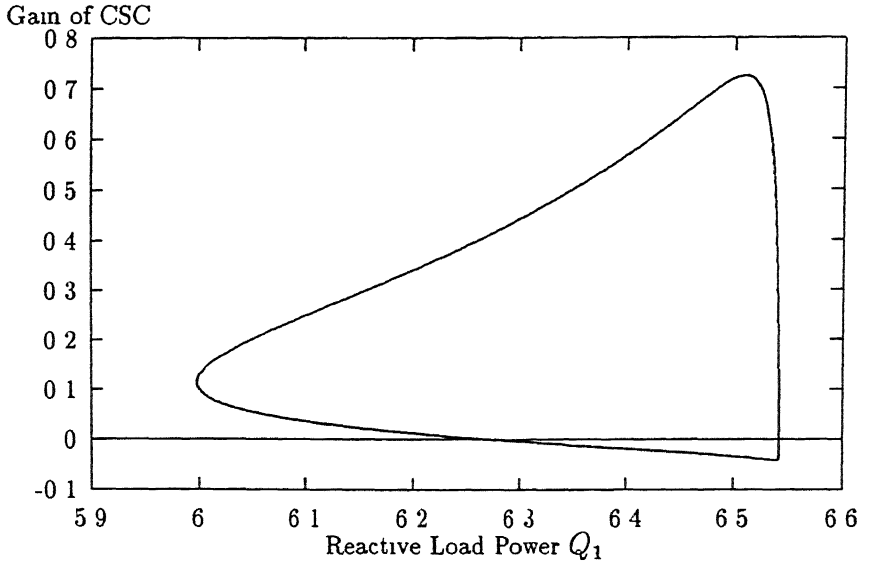

Figure 6 7 3-bus system CSC gain vs Q_1 with P_a as error signal

The studies were also conducted with generator acceleration power as error signal to these devices Figs 6 7 to 6 9 show the locus of HB points It can be seen from these these figures that if the gain of CSC or PAR is greater than 0 72 and 0 38 respectively or that of SVC is less than -0 7 the HB window and the strange attractor can be eliminated

6.4.2 9–Bus System

6.4 2.1 Base Case

The data and network topology for this system have been shown in Appendix–E The generator at bus-1 was taken as the infinite bus and the generators at bus-2 and 3 were represented by their swing equations (4 26) and 4 27) given in Chapter 4 The stator transients were ignored All the base case loads were represented by their constant impedance and in addition a dynamic load model as considered in the study presented in section 4 5 1 2 of Chapter 4 was assumed to be present at bus-5 The dynamics were studied by varying loading parameter ℓ and power factor pf was assumed to be unity Some of the important bifurcations observed from the bifurcation diagram in Fig 5 24 of Chapter 5 are listed below

- SNB at $\ell = 3\ 598273$

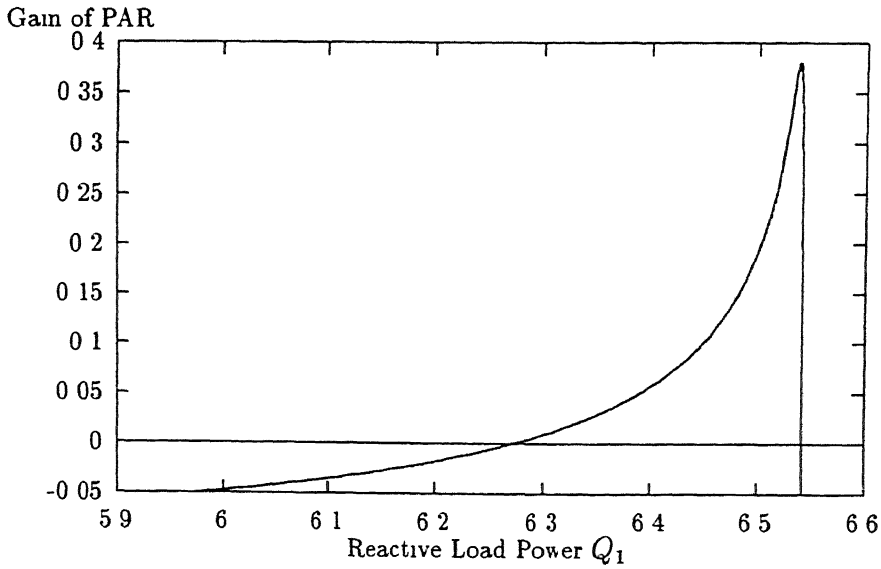

Figure 6 8 3-bus system PAR gain vs Q_1 with P_a as error signal

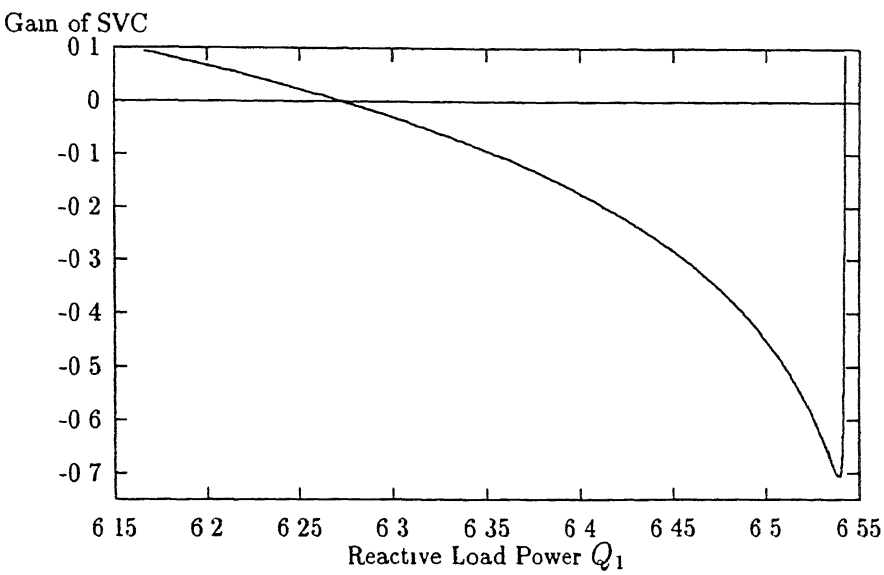

Figure 6 9 3-bus system SVC gain vs Q_1 with P_a as error signal

- Subcritical HB at $\ell = 3\ 577746$ and $3\ 588495$
- TRB at $\ell = 3\ 249934$ and $3\ 037992$
- PDB at $\ell = 3\ 135110, 3\ 235849, 3\ 042431$ and $3\ 558070$
- LP of periodic orbits at $\ell = 3\ 070598, 3\ 268290$ and 3.022379

From participation analysis carried out in the studies presented in section 5 5 3 1 in Chapter 5 (Table 5 1), it is observed that the states predominantly responsible for causing Hopf bifurcations were the states associated with generator # 2 It is seen from Table 5 1 in section 5 5 3 1 of Chapter 5 that critical mode is extremely sensitive to (δ_2, ω_2) states (i e Generator # 2) Hence, the input quantity to the controller was derived from Generator # 2 Accordingly the CSC and PAR were placed in line between buses-7 & 5 and SVC at load bus-5 The following limits were assumed for these devices

$X_{csc}^{max} = 0\ 1$ p u $\quad \phi_p^{max} = 0\ 5$ rad $\quad b_{sh}^{max} = 1\ 0$ p u
$X_{csc}^{min} = -0\ 1$ p u $\quad \phi_p^{max} = -0\ 5$ rad $b_{sh}^{min} = -1\ 0$ p u

Fig 6 10 shows the locus of Hopf bifurcation for variation of the controller gain with ω_2 as input signal to CSC It is found that for $K_{csc} \geq 0\ 0125$ with ω_2 signal the Hopf bifurcation come closer, coalesce and disappear A similar study was made with P_a signal and it was found (Fig 6 11) that for $K_{csc} \geq 0\ 1$, it is possible to eliminate the Hopf bifurcations completely. With the application of ω_2 signal to PAR, it turned out (Fig 6 12) that for $K_{par} \leq -0.125$, the Hopf bifurcation phenomena could be eliminated while the application of P_a signal to PAR did not help as is evident from Fig 6 13

The study was also performed with P_a signal to SVC at bus-5 and it was found that Hopf bifurcations could be eliminated (Fig 6 14) if $K_{svc} \geq 1\ 25$ However, with ω_2 signal, it was found that the two Hopf bifurcations are persistent and SVC could not eliminate them as shown in Fig 6 15

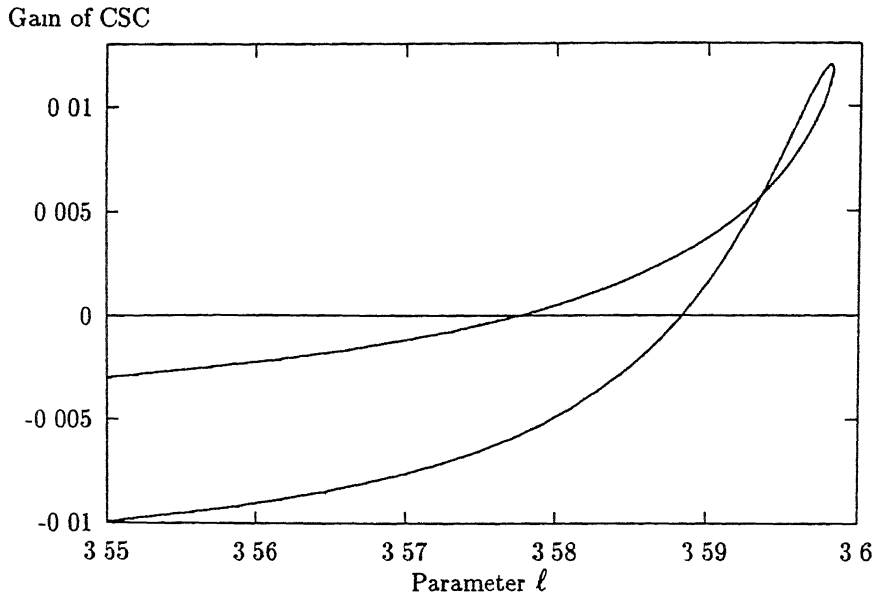

Figure 6 10 9-bus system (base case) CSC gain vs ℓ with ω_2 as error signal

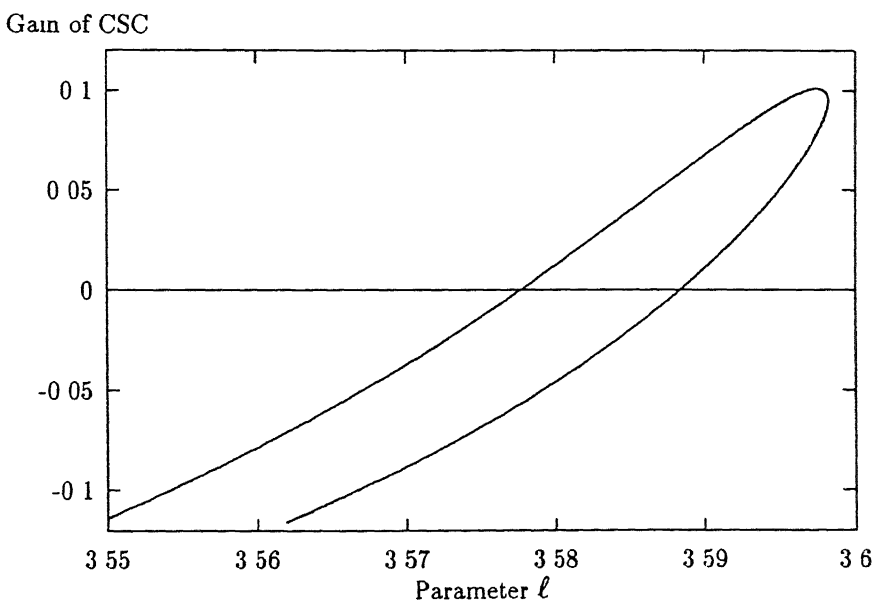

Figure 6 11 9-bus system (base case) CSC gain vs ℓ with P_{a_2} as error signal

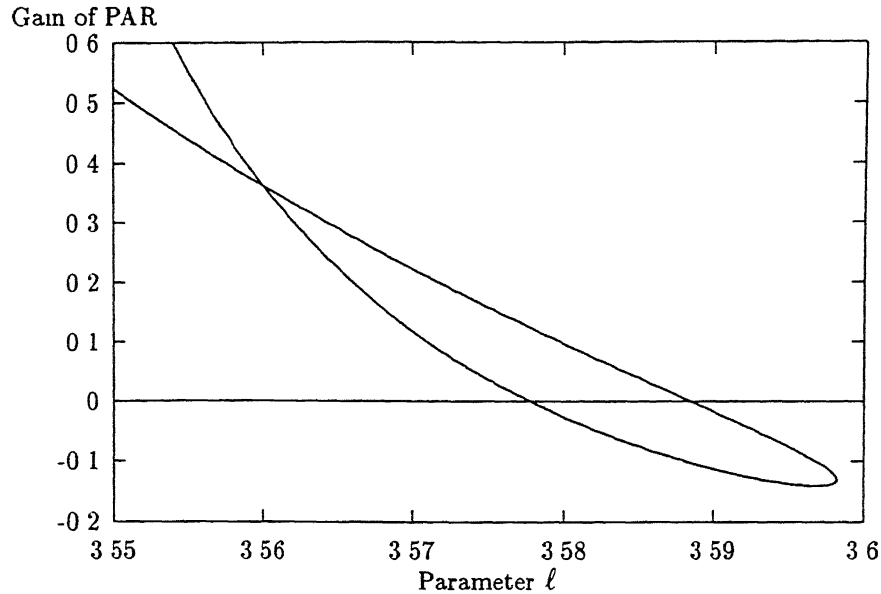

Figure 6 12 9-bus system (base case) PAR gain vs ℓ with ω_2 as error signal

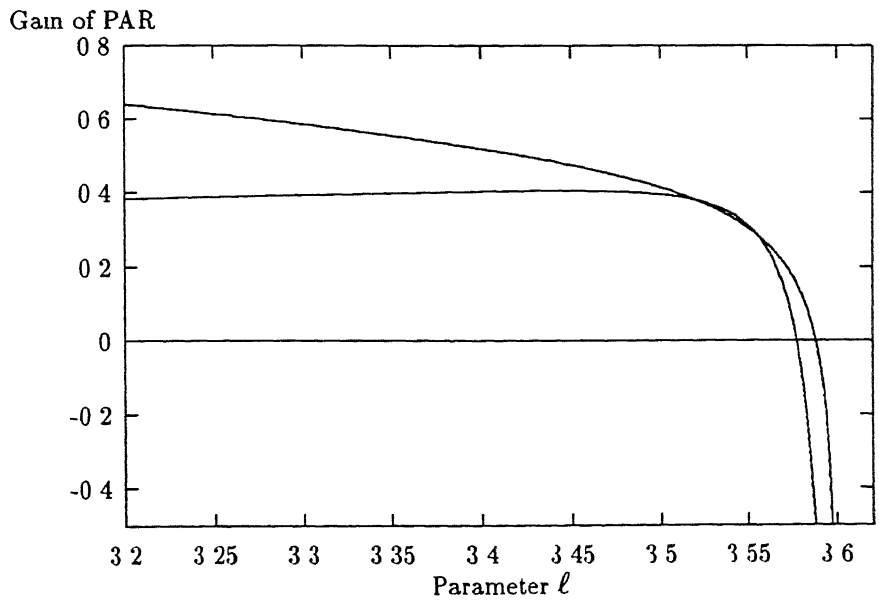

F gure 6 13 9-bus system (base case) PAR gain vs ℓ with P_{a_2} as error signal

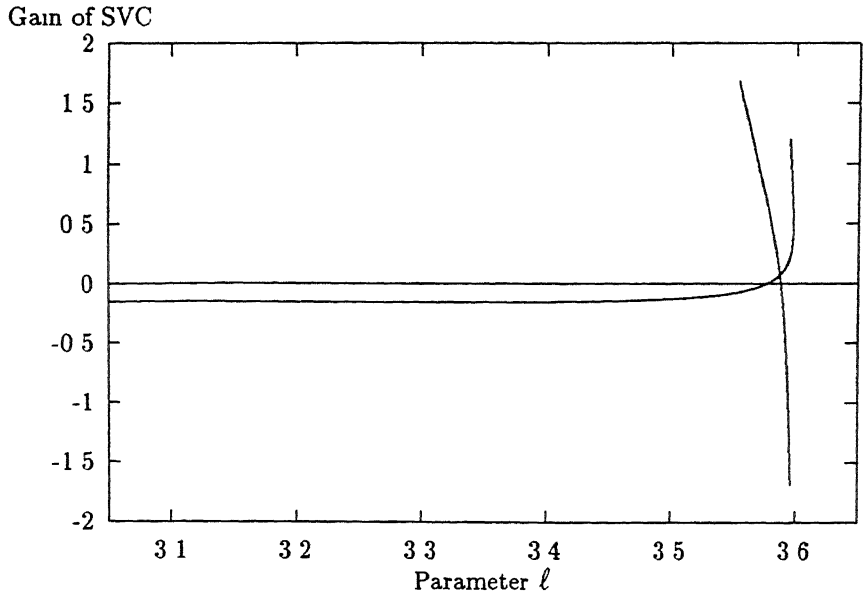

Figure 6 14 9-bus system (base case) SVC gain vs ℓ with ω_2 as error signal

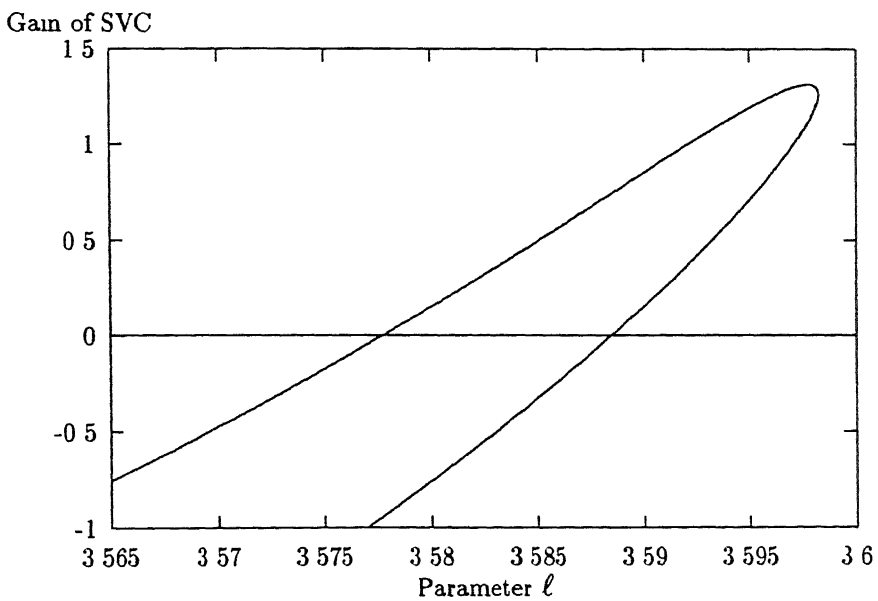

Figure 6 15 9-bus system (base case) SVC gain vs ℓ with P_{a_2} as error signal

Fig 6 16 shows a typical time variation of load voltage V_5 for $\ell = 3\ 58$ from initial condition ($\omega_2 = \omega_3 = 0$, $\delta_2 = -0\ 2154$, $\delta_3 = -0\ 26531$, $\theta_5 = -0\ 89383$, $V_5 = 0\ 71238$) This initial condition corresponds to stable operating point for $\ell = 3\ 50$ The simulation has been performed for two cases, one without considering the effect of CSC and the other with CSC present in the line with a gain (K_{csc}) setting of 0.15 In this case, P_a was used as input signal to CSC It was found that the application of CSC could avert the system voltage collapse

6.4.2.2 A Contingency Case

In this study the line 5-4 was taken out and the existing static load of $(125 + j50)$ MVA was reduced to $(100+j30)$ MVA This change in loading was done as the load flow for the contingency case was not converging

Without considering the effect of controllable components, the bifurcation diagram for variation in parameter ℓ has been drawn as shown in Fig. 5 26 in Chapter 5 Some of the important points on the bifurcation diagram are as below

- SNB at $\ell = 1\ 195323$
- Subcritical HB at $\ell = 1\ 116463$
- Supercritical HB at $\ell = 1\ 192705$
- CFB at $\ell = 1\ 076371$
- PDB at $\ell = 1\ 115625$ and $1\ 171130$
- LP of fixed points at $\ell = 0\ 2351554$ and $0\ 6105376$

From the participation analysis, it was found that the states predominantly responsible for causing Hopf bifurcations in this case also were the states associated with the generator # 2 The CSC and PAR were placed in line 7-5 and SVC at bus-5 The working limit of these components are assumed to be the same as given for the base case study

The speed deviation and acceleration power of generator # 2 have been taken as the input signal to the controller of FACTS devices The locus of HB points are plotted in Figs 6 17 to 6 22 It is found that by suitable choice of gains for these devices, the strange attractor and the HB window can be eliminated by either of the two signals

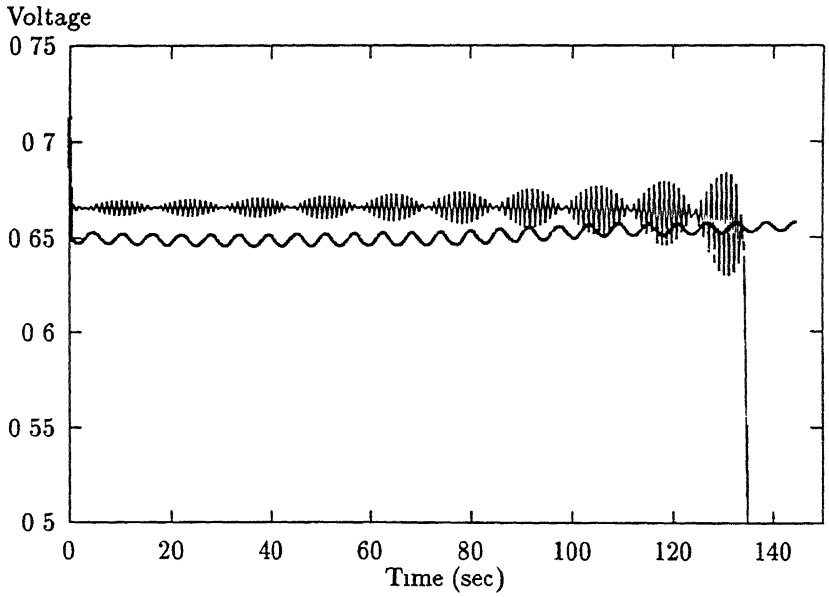

Figure 6 16. 9-bus system (base case) time variation of V_5

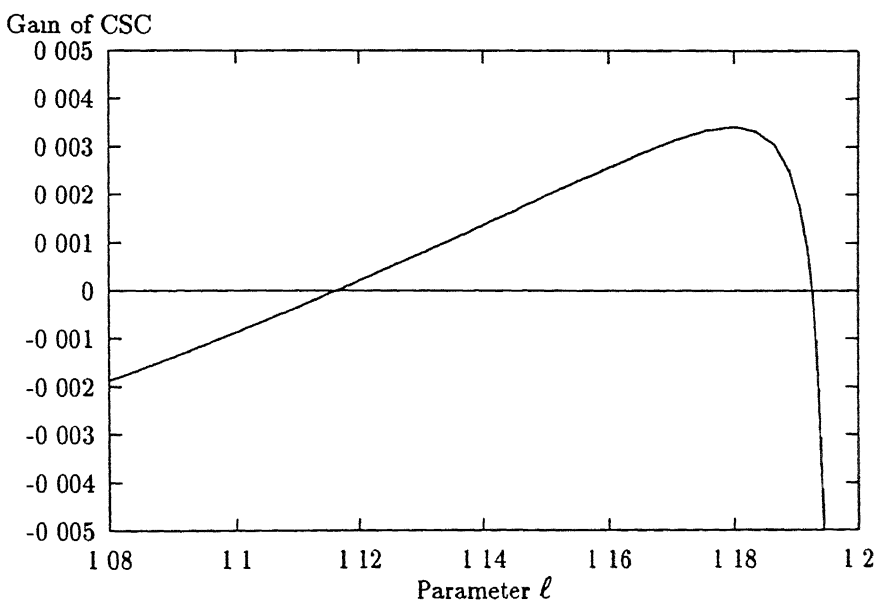

Figure 6 17 9-bus system (a contingency case) CSC gain vs ℓ with ω_2 as error signal

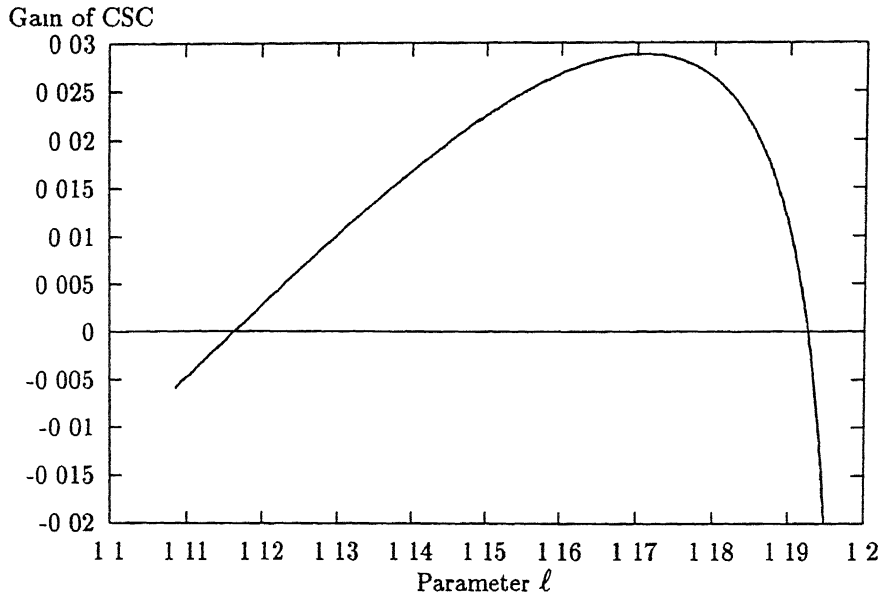

Figure 6 18 9-bus system (a contingency case) CSC gain vs ℓ with P_{a_2} as error signal

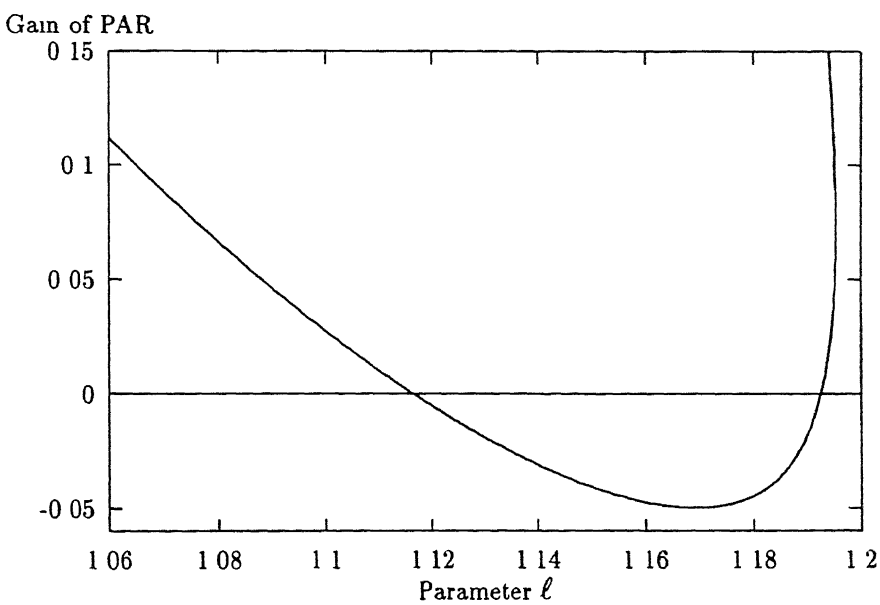

Figure 6 19 9-bus system (a contingency case) PAR gain vs ℓ with ω_2 as error signal

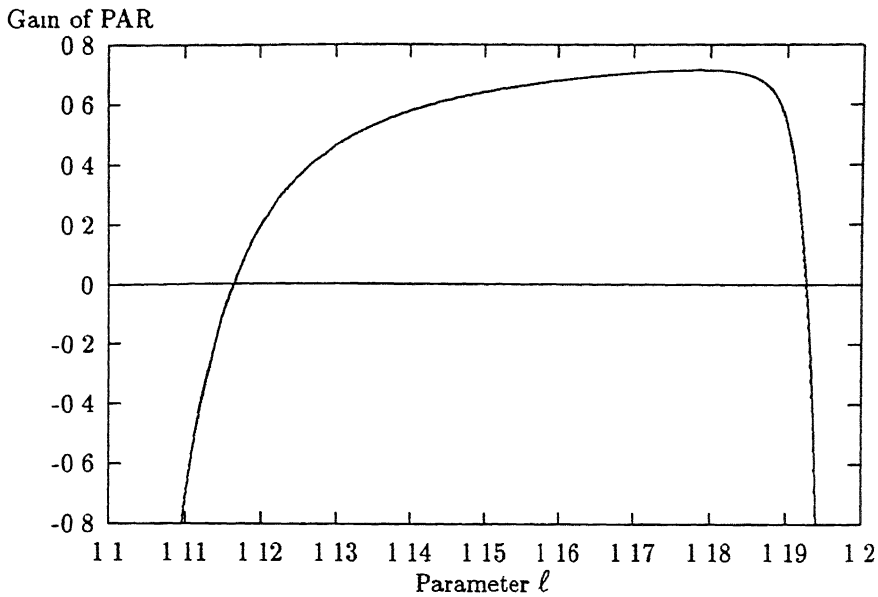

Figure 6 20 9-bus system (a contingency case) PAR gain vs ℓ with P_{a_2} as error signal

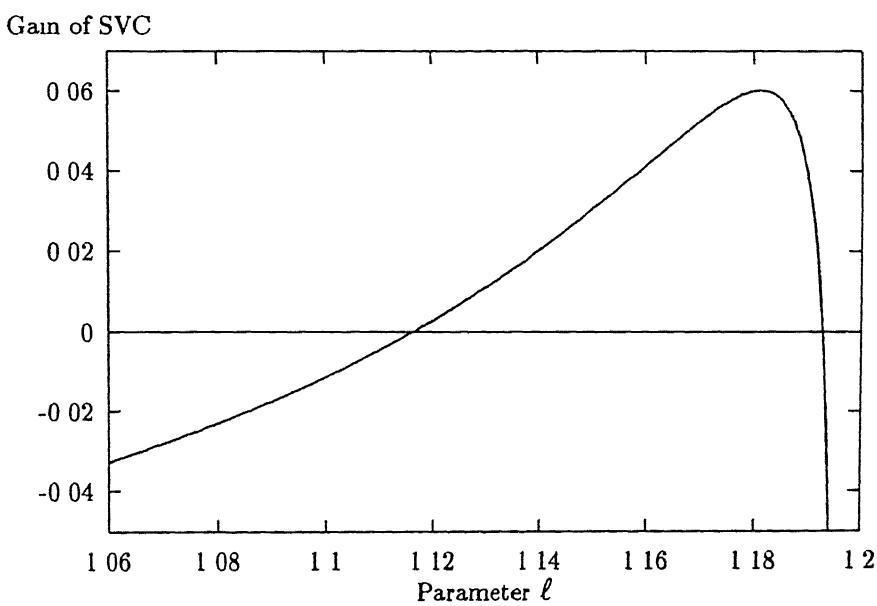

Figure 6 21 9-bus system (a contingency case) SVC gain vs ℓ with ω_2 as error signal

6.4.3 19–Bus UPSEB System

This system is described in Appendix–H The generator at bus-1 was treated as infinite bus and those at buses-2, 3 and 4 were represented by swing equations (4 26) and (4 27) as described in Chapter 4 All the base case loads were assumed to be constant impedance type In addition, a dynamic load model as described by equations (4 36) and (4 37) in Chapter 4 was assumed to be present at bus-14 The nominal MVA demand ℓ was taken as bifurcation parameter and the power factor was assumed to be unity The other parameters of the dynamic load was taken to be the same as in section 5 5 4 of Chapter 5 The bifurcation diagram as shown in Fig 5 30 of Chapter 5 was drawn considering ℓ as the bifurcation parameter, and the important bifurcation points as given in section 5.30 of Chapter 5 are

- Subcritical HB at $\ell = 2\ 696254$
- Supercritical HB at $\ell = 5\ 454979$
- SNB at $\ell = 5\ 485668$
- CFB at $\ell = 2\ 519270$
- TRB at $\ell = 3\ 078993$ and $3\ 911500$

The CSC and PAR were sited in the line between buses-5 and 7 and SVC at bus 14 The following limits were assumed for these devices

$X_{csc}^{max} = 0\ 002$ p u $\quad \phi_p^{max} = 0\ 5$ rad $\quad b_{sh}^{max} = 1\ 0$ p u
$X_{csc}^{min} = -0\ 002$ p u $\quad \phi_p^{min} = -0\ 5$ rad $\quad b_{sh}^{min} = -1\ 0$ p u

The participation analysis was carried out and the results are presented in Table 6 1 for $\ell = 3\ 0793$ It is observed that the states predominantly responsible for causing the HB is associated with generators # 2 and 3 The CSC and PAR were placed on the line between buses-5 and 7 and SVC at bus-14 The error signals have been taken as the sum of the generator speed deviations of generator # 2 and 3 and the sum of acceleration powers of the generator # 2 and 3

Fig 6 23 shows the locus of Hopf bifurcation for variation of the controller gain with generator speed deviation as error signal to CSC It is found that for $K_{csc} \leq -0\ 0012$ the Hopf bifurcation come closer, coalesce and disappear Control of dynamic bifurcations using CSC was tried with generator acceleration power as the error signal to the controller with its location

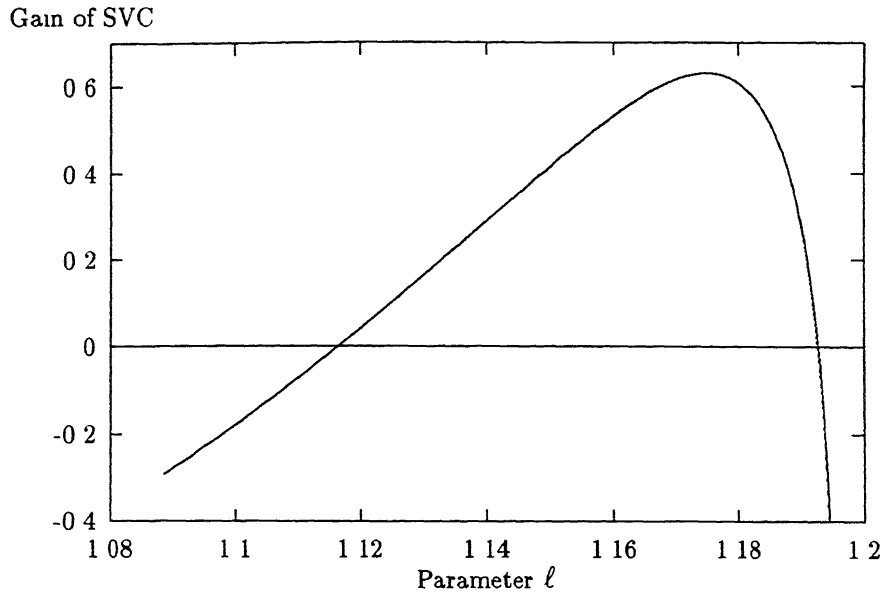

Figure 6 22 9-bus system (a contingency case) SVC gain vs ℓ with P_{a_2} as error signal

Table 6 1 19-bus system eigenvalues and state participation factors

Eigenvalues	Participation Factors			
	δ_2, ω_2	δ_3, ω_3	δ_4, ω_4	θ_{14}, V_{14}
$-2\ 3641 \times 10^{+02}$	$6\ 3782 \times 10^{-05}$	2.9551×10^{-05}	$3\ 2744 \times 10^{-05}$	$5\ 0361 \times 10^{-01}$
$\pm j1\ 3122 \times 10^{+02}$	$6\ 3784 \times 10^{-05}$	$2\ 9552 \times 10^{-05}$	$3\ 2748 \times 10^{-05}$	$5\ 0372 \times 10^{-01}$
$-1\ 6098 \times 10^{-02}$	$5\ 1885 \times 10^{-02}$	$5\ 2224 \times 10^{-03}$	$4\ 4289 \times 10^{-01}$	$2\ 3651 \times 10^{-05}$
$\pm j1\ 5169 \times 10^{+01}$	$5\ 1885 \times 10^{-02}$	$5\ 2224 \times 10^{-03}$	$4\ 4289 \times 10^{-01}$	$3\ 3128 \times 10^{-06}$
$-7\ 2877 \times 10^{-03}$	$2\ 0340 \times 10^{-01}$	$2\ 8736 \times 10^{-01}$	$9\ 2448 \times 10^{-03}$	$2\ 1481 \times 10^{-05}$
$\pm j1\ 2656 \times 10^{+01}$	$2\ 0340 \times 10^{-01}$	$2\ 8736 \times 10^{-01}$	$9\ 2447 \times 10^{-03}$	$7\ 3717 \times 10^{-06}$
$1\ 5435 \times 10^{-03}$	$2\ 4467 \times 10^{-01}$	$2\ 0740 \times 10^{-01}$	$4\ 7844 \times 10^{-02}$	$1\ 5211 \times 10^{-03}$
$\pm j7\ 3118$	$2\ 4467 \times 10^{-01}$	$2\ 0740 \times 10^{-01}$	$4\ 7843 \times 10^{-02}$	$2\ 2559 \times 10^{-04}$

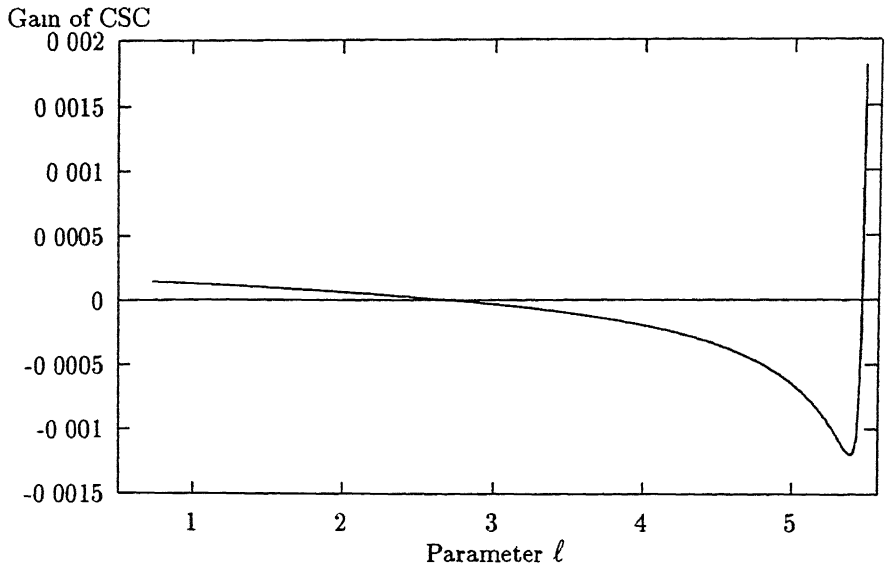

Figure 6 23 19-bus system. CSC gain vs ℓ with sum of ω_2 and ω_3 as error signal

considered at one of the lines between buses-5 and 7, 5 and 8 and 14 and 15 The study revealed that the HB window could not be eliminated in either of the cases

Figs 6 24 and 6 25 show the locus of HB points using PAR with generator speed deviation and acceleration power as error signals It is observed that the HB window can be eliminated for $K_{par} \leq -0\ 00175$ using speed deviation as the error signal and $K_{par} \leq -0\ 016$ for acceleration power as the error signal

Similarly Figs 6 26 and 6 27 reveal that SVC HB window can also be eliminated using SVC with either the speed deviation as error signal ($K_{svc} \geq 0\ 0225$ or the acceleration power as error signal ($K_{svc} \geq 0\ 125$

6.5 Conclusion

From the studies performed in this chapter, the following conclusions may be drawn

(i) On varying the controller gain, the subcritical HB becomes supercritical after a certain gain value with CFB disappearing Further variation of controller gain value may cause the other dynamic bifurcations to disappear yielding a stable steady state operating point, in the earlier Hopf bifurcation window

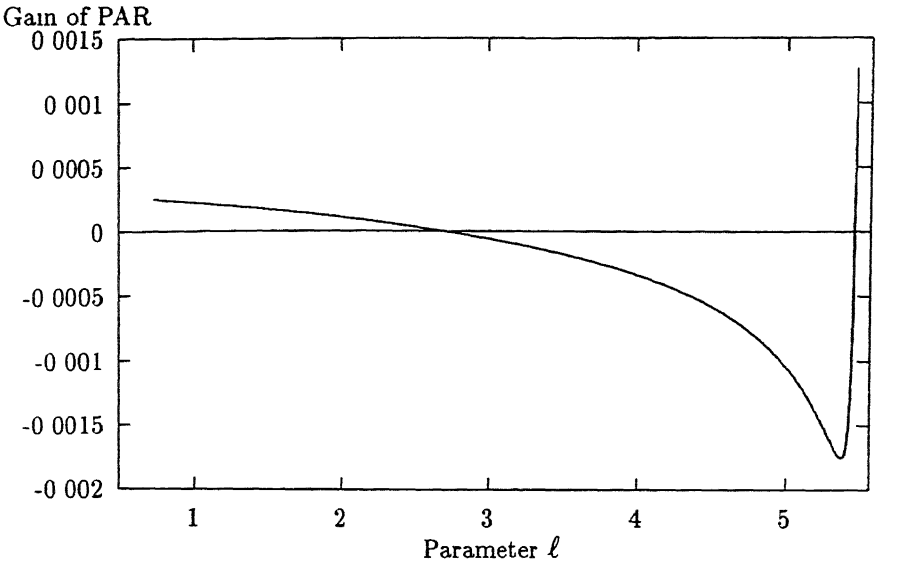

Figure 6 24 19-bus system: PAR gain vs ℓ with sum of ω_2 and ω_3 as error signal

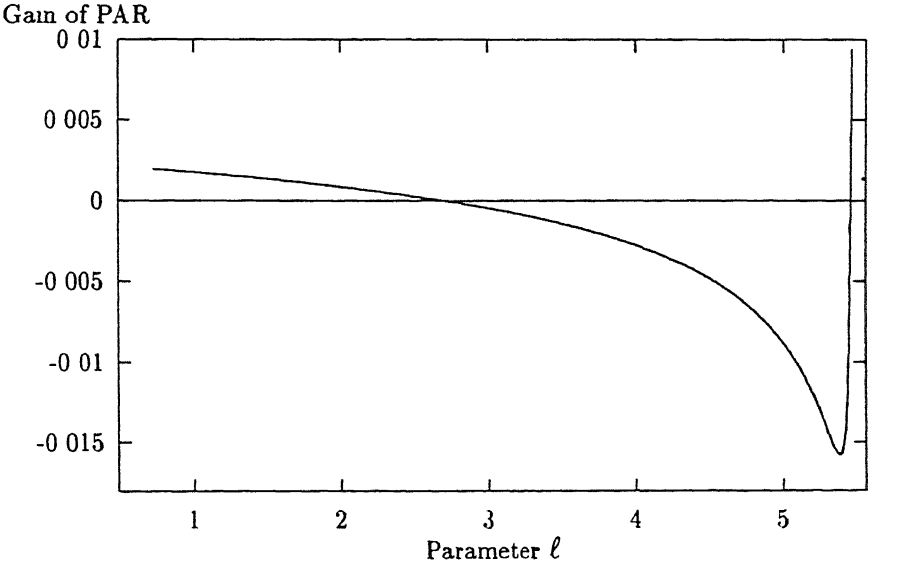

Figure 6 25 19-bus system PAR gain vs ℓ with sum of P_{a_2} and P_{a_3} as error signal

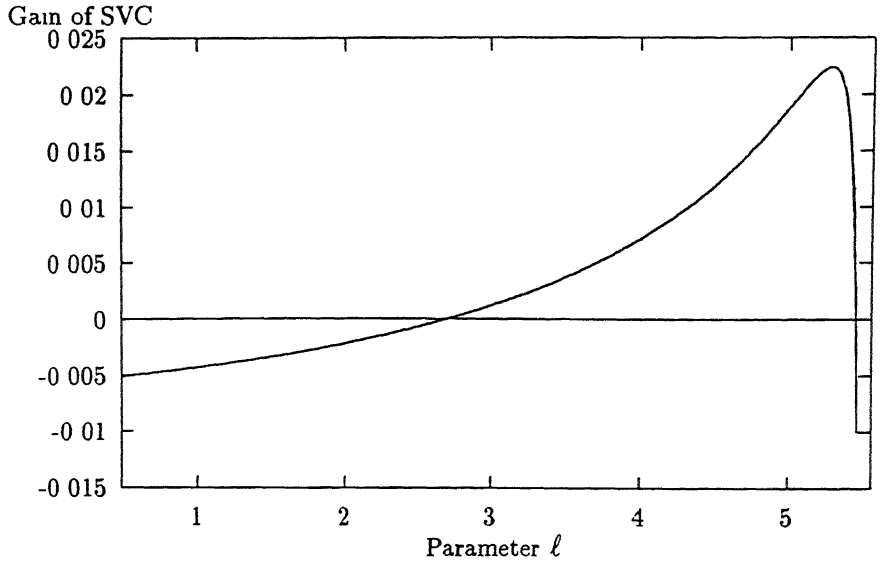

Figure 6 26 19-bus system SVC gain vs ℓ with sum of ω_2 and ω_3 as error signal

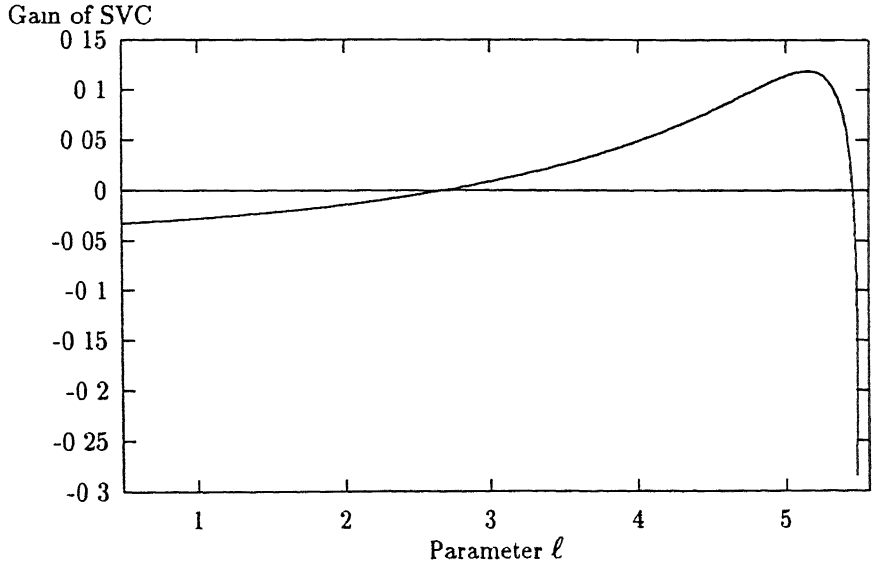

Figure 6 27 19-bus system SVC gain vs ℓ with sum of P_{a_2} and P_{a_3} as error signal

(ii) The CSC with generator speed deviation as error signal has been able to eliminate dynamic bifurcation and chaos in all the three base case system studies and also in the contingency case

(iii) The choice of appropriate input signal to the controller of FACTS devices is also very important as evident from the studies on 9-bus system (base case conditions) PAR could not eliminate the dynamic bifurcation and chaos with generator acceleration power (P_a) as error signal and the SVC could not eliminate the dynamic bifurcations with speed deviation as error signal However, PAR and SVC could eliminate the dynamic bifurcations when the choice of input signals was reversed Similarly, for 19 bus system, CSC did not work with P_a as error signal

(iv) The FACTS devices such as CSC, PAR and SVC can be effectively used for controlling the occurrence of dynamic bifurcation and chaos by proper choice of error signal and gain of the controller

Chapter 7

Conclusions

7.1 General

With growing interconnection along with economic and environmental pressures, the possible threat of voltage instability is becoming increasingly pronounced in power system networks Researchers and utilities, all over the world, are devoting efforts to understand, analyse and develop strategies to cope up with the menace of voltage instability/collapse This thesis has attempted to make an iota of contribution in this direction.

The thesis has addressed to both static and dynamic aspects of voltage stability Investigations considering static aspects include determining point of voltage instability in load parameter space for both AC and combined AC-DC systems (Chapter–2) and maximising the voltage stability margin through rescheduling of real and reactive power outputs of sources (Chapter–3) Dynamical studies have been conducted to explore the occurrence of various local bifurcations (Chapter–4), global bifurcations and chaos (Chapter–5) considering dynamical models of generators, composite loads, induction motors, SVS, OLTC etc and also the control of dynamic bifurcations (Chapter–6)

The aim of this chapter is to summarise the main findings of this thesis and provide suggestions for further research work Some of the main findings are given below

7.2 Summary of Important Findings

Chapter 2 has applied the concept of minimum singular value and condition number of load flow Jacobian for prediction of static voltage stability of integrated AC as well as AC-DC systems

From the works presented in this chapter, the following conclusions are drawn

(1) The concept of minimum singular value and condition number of power flow Jacobian can be effectively used to predict the static voltage instability of integrated AC-DC networks as well as the AC systems having polynomial type voltage dependent loads

(2) At static voltage instability point corresponding to system maximum loadability, the condition number approaches to infinity and the minimum singular value approaches to zero With increase in loading, an abrupt change in the minimum singular value and condition number of the load flow Jacobian is observed whenever a generator hits its reactive power limit or control mode changes in the DC link

(3) Considering the static model, it has been found that if the load is varied at only one bus in an integrated AC-DC system, the collapse of voltage takes at a bus where the load is being increased However, with simultaneous changes in the loadings at all the buses, all the bus voltages approach the nose point of the P-V curves simultaneously

(4) Consideration of reactive power output limits of synchronous machines reduces the loading at which the system becomes voltage unstable Thus, the maximum system loadability is reduced, whereas it is increased by considering the loads to be voltage dependent

Chapter 3 compares the effect of four different generation rescheduling schemes in increasing the voltage stability margin in reactive parameter space The four schemes of generation rescheduling has been formulated in view of minimising total fuel cost of generation (OBJ-I), minimising total system transmission loss (OBJ-II), maximising minimum singular value of the load flow Jacobian (OBJ-III) and minimisation of the slack reactive power injection (new scheme OBJ-IV) The main findings are as follows

(1) The generation rescheduling using any of the four objectives increases the voltage stability margin in stressed condition of system The stability margin can be measured in terms of Q-margin or the minimum singular value of the power flow Jacobian

(2) At light loading conditions, none of the schemes is able to increase the Q-margin The minimum singular value, however, is slightly improved with OBJ-III and IV In such cases, the correlation between minimum singular value of the power flow Jacobian and Q-margin is lost

(3) Amongst the four different objectives tried out, the new objective (OBJ-IV) has consistently resulted into better results than other objectives The results obtained are very close to the OBJ-III

(4) The new objective of minimising the slack bus reactive injection is computationally less expensive and can be effectively used for voltage stability margin enhancement

Chapter 4 has investigated certain aspects of local bifurcations and its implications on power system voltage stability Considering the detailed model of generators along with AVR, speed-governor control loop and induction motor loads Investigations reveal that·

(1) Power system models may exhibit static and dynamic bifurcations even for parameter values in their normal operating range.

(2) For the same value of bifurcation parameter, the system may become unstable either purely due to angle instability or purely due to the voltage instability or both may occur simultaneously, depending on the disturbance in the system.

(3) A system becomes unstable due to Hopf bifurcation and exhibits oscillatory behaviour for small perturbations It has been shown that for certain choices of induction motor load torque coefficients or AVR gain values, the power system may undergo oscillatory type instability that is essentially bifurcation of a fixed point into a periodic orbit

(4) Hopf bifurcation may occur both at low or high power factor loadings The effect of Hopf bifurcation is to further reduce the stable operating range of parameters

Chapter 5 has investigated various types of global bifurcations and its implications on voltage stability The main findings are as follows

(1) Different types of dynamic bifurcations such as PDB, CFB, TRB, LP and chaos can exist in the power system networks for variation of some of the parameters even in their normal range

(2) Some of the global bifurcations observed, possibly for the first time, in the power system networks include the bifurcation of periodic orbit to torus (TRB) and limit points of unstable to unstable periodic orbits

(3) Chaos has been observed in all the three sample systems, in two of the systems via PDB route. In one of the systems, quasiperiodic route to chaos has been observed for the first time in power system model The chaotic oscillations produce harmonics of all the frequencies and a continuous broad band frequency spectrum is observed

(4) Boundary crisis (blue sky bifurcation) and subcritical Hopf bifurcation cause voltage collapse in some of the systems By adjusting the SVS gain parameter, the boundary crisis and hence the resulting voltage collapse can be avoided

Chapter 6 has dealt with elimination of dynamic bifurcation and chaos using FACTS devices such as controllable series capacitors (CSC), static phase angle regulator (PAR), static VAR compensators (SVC) The important conclusions drawn from the studies presented in this chapter are as follows

(1) On varying the controller gain, the subcritical Hopf bifurcation becomes supercritical after a certain gain value with cyclic fold bifurcation disappearing Further variation of controller gain value causes other dynamic bifurcations to disappear yielding stable steady state operating point, in the earlier Hopf bifurcation window

(2) The choice of appropriate feedback control signal is very important In one of the systems studied, PAR could not eliminate the dynamic bifurcation and chaos with generator acceleration power (P_a) as the error signal and the SVC could not eliminate the bifurcation with generator speed deviation as the error signal However, they could eliminate the HB window when the choice of input signals was reversed Similarly in another system, CSC did not work with P_a as error signal

(3) The CSC with generator speed deviation as error signal has been able to eliminate dynamic bifurcation and chaos in all the sample systems studied

(4) The FACTS devices such as CSC, PAR, SVC can be effectively used for controlling the occurrence of dynamic bifurcations and chaos by proper choice of the error signal and gain of the controller

7.3 Scope for Further Research

As a consequence of investigations carried out in this thesis, the following aspects are being suggested as future research work to be carried out

(1) The static voltage stability margin in the present work and also by other researchers has been computed with respect to saddle node bifurcation in multidimensional parameter space. The studies may be extended to estimate the stability margin with respect to the Hopf bifurcation in multidimensional parameter space.

(2) More rigorous steady state model of synchronous machine may be considered to include the effect of machine saturation and under frequency operation, on the heating of the machine This will affect the static voltage stability margin

(3) In Chapter 4, it was observed that the dominant states at Hopf bifurcation considering excitation system model are the E'_q and E_{fd} Studies to eliminate dynamic bifurcation can be extended for such cases by utilising these variables variables as feedback control signals and incorporating washout filters to ensure preservation of steady state equilibrium The effect of power system stabilisers on control of dynamic bifurcation can also be studied

(4) In the present work, the location of FACTS devices were selected heuristically in the sample systems for control of dynamic bifurcations However, a more systematic approach need to be evolved for optimal siting of these devices

(5) Due to extensive computing requirements to study the global bifurcations and chaos, the research activities in this thesis and also in other works are confined to smaller systems only It will be worthwhile developing techniques and models for study of nonlinear dynamics of large size systems This may require exploring new methods to obtain network equivalents suitable for the voltage stability analysis

Bibliography

[1] O G C Dahl, *Electric Power Circuits, Vol II Power System Stability*, McGraw Hill, New York, 1938

[2] C Concordia, *Synchronous Machines*, Wiley, New York, 1951

[3] J Zaborszky and J W Rittenhouse, *Electric Power Transmission*, Ronald Press, New York, 1954

[4] R A Hore, *Advanced Studies in Power System Design*, Chapman and Hall, London, 1966

[5] Y Yoshida, *Development of a Calculation Model of AC Voltage Stability in HVDC Transmission System*, Electrical Engg in Japan, Vol 94, No 2, 1974, pp. 77-85

[6] V A Venikov, V A Stroev, V I. Idelchick and V.A. Torasov, *Estimation of System Steady State Stability in Load Flow Calculations*, IEEE Transactions on Power Apparatus and Systems, Vol 94, May/June 1975, pp 1034-1040

[7] P M Anderson and A A Fouad, *Power System and Stability*, The Iowa University Press, 1977.

[8] V A Venikov, *Transient Processes in Electrical Power Systems*, Mir Publishers, Moscow, 1977

[9] W R Lachs, *System Reactive Power Limitations*, Paper # A 79 015-9, presented at the IEEE PES Winter Meeting, New York, Feb 4-9, 1979

[10] Y Tamura, K Iba and S Iwamoto, *A Method of Finding Multiple Load Flow Solutions for General Power Systems*, Paper # A80043-OD, IEEE PES Winter Meeting, Feb 1980

[11] B D Hassard, N D Kazarinoff and Y H Wan, *Theory and Applications of Hopf Bifuication*, Cambridge University Press, Cambridge, UK, 1981

[12] T Hayashi, *Analysis of Voltage Instability of AC-DC Interconnected Systems*, Electrical Engg in Japan, Vol 101, No 4, 1981, pp 46-53

[13] J Jaris, F D Galiana, *Quantitative Analysis of Steady State Stability in Power Networks*, IEEE Trans on Power Apparatus and Systems, Vol PAS-100, Jan 1981, pp 318-326

[14] M A Pai, *Power System Stability Analysis by the Direct Method*, North Holland, New York, 1981

[15] S Abe, Y Fukunaga, A Isono and B Kondo, *Power System Voltage Stability*, IEEE Trans on Power Apparatus and System, Vol PAS-101, No 10, October 1982, pp 3830-3840

[16] C Grebogi, E Ott and J A. Yorke, *Chaotic Attractors in Crisis*, Physical Review Letters Vol 48, No 22, May 1982, pp 1507-1510

[17] N Kopell and R B Washburn Jr , *Chaotic Motions in the Two-Degree-of-Freedom Swing Equations*, IEEE Trans on Circuits and Systems, Vol CAS-29, No 11, Nov 1982, pp 738-746

[18] J Arrillaga, C P Arnold and B J Harker, *Computer Modelling of Electrical Power Systems*, Wiley, Chichester, UK, 1983

[19] G H Golub and C F Van Loan, *Matrix Computations*, the Johns Hopkins University Press, Baltimore, Maryland, 1983

[20] C Grebogi, E Ott and J A Yorke, *Crisis, Sudden Changes in Chaotic Attractors, and Transient Chaos*, Physica, Vol 7D, 1983, pp 181-200

[21] J Guckenheimer and P Holmes, *Nonlinear Oscillations, Dynamical Systems and Bifurcations of Vector Fields*, Springer-Verlag, New York 1983

[22] F M A Salam, *Chaos in the One Generator System with Excitation Feedback*, Proc 22nd IEEE Conf on Decision and Control, 1983, pp 360-364

[23] F M A Salam, J E Marsden and P P Varaiya, *Chaos and Arnold Diffusion in Dynamical Systems*, IEEE Trans on Circuits and Systems, Vol CAS-30, No 9, Sept 1983, pp 697-708

[24] Y Tamura, K Iba and S Iwamoto, *Relationship between Instability and Multiple Load Flow Solutions in Electric Power-Systems*, IEEE Trans on Power Systems, Vol 102, No 2, May 1983, pp 1115-1125

[25] Y N Yu, *Electric Power System Dynamics*, Academic Press, New York, 1983

[26] E H Abed and P Varaiya, *Nonlinear Oscillations in Power Systems*, Int Jr of Electric Power and Energy Systems, Vol 6, No 1, Jan 1984, pp 37-43

[27] P Borremans, A Calvaer, J P de Reuck, J Gooserens, E Van Geert, J Van Hecke and A Van Ranst, *Voltage Stability Fundamental Concepts and Comparison of Practical Criteria*, CIGRE report 38-11, August 1984

[28] J Carpentier, R Girard and E Scano, *Voltage Collapse Proximity Indicators Computed from an Optimal Power Flow*, Proc 8th Power System Computation Conference, Helsinki, Finland, 1984, Butterworth London, pp 671-678

[29] F.M A Salam, J E. Marsden and P P Varaiya, *Arnold Diffusion in the Swing Equations of a Power System*, IEEE Trans on Circuits and Systems, Vol 31, No 8, Aug 1984, pp 199-203

[30] A Hammad, K Sadek, H. Koelsch and G Gueth, *Advanced Scheme for Voltage Control at HVDC Converter Terminals*, IEEE Trans. on Power Apparatus and Systems, Vol 104, No 3, March 1985, pp 679-703

[31] W R Lachs, *Dynamic Study of Extreme System Reactive Power Deficit*, IEEE Trans on Power Apparatus and System, Vol 104, No 9, September 1985, pp 2420-2426

[32] C C Liu and F F Wu, *Steady State Voltage Stability Regions of Power Systems*, Systems & Control Letter, Vol 6, June 1985, pp. 23-31

[33] J C Alexander, *Oscillatory Solutions of a Model System of Nonlinear Swing Equations*, Int Jr of Electric Power and Energy Systems, Vol 8 , No 3, July 1986, pp 130-136

[34] E J Doedel, *AUTO Software for Continuation and Bifurcation Problems in Ordinary Differential Equations*, California Institute of Technology, USA, 1986

[35] A E Hammad and W Kuhn, *A Computation Algorithm for Assessing Voltage Stability at AC/DC Interconnections*, IEEE Trans on Power Systems, Vol 1, No 1, Feb 1986, pp 209-216

[36] H G Kwatny, A K Pasrija and L Y Bahar, *Static Bifurcation in Electric Power Networks Loss of Steady-State Stability and Voltage Collapse*, IEEE Trans on Circuits and Systems, Vol 33, No 10, October 1986, pp 981-991

[37] P Kessel and H Glavitsch, *Estimating the Voltage Stability of a Power System*, IEEE Trans on Power Delivery, Vol 1, No 3, July 1986, pp 346-354

[38] J M T Thompson and H B Stewart, *Nonlinear Dynamics and Chaos*, Chichester, UK, John Wiley and Sons, 1986

[39] Y Wallach, *Calculations and Programs for Power System Networks*, Prentice–Hall, Inc, Englewood Cliffs, New Jersey, 1986

[40] K Walve, *Modelling of Power System Components at Severe Disturbances*, CIGRE report 38-18, 1986

[41] F F Wu and C C Liu, *Characterization of Power System Small Disturbance Stability with Models Incorporating Voltage Variation*, IEEE Trans on Circuits and Systems, Vol CAS-33, No 4, April 1986, pp 406-417

[42] *Planning Against Voltage Collapse*, CIGRE Task Force report 38-01 03, Electra, No 111, March 1987

[43] C L DeMarco and A R Bergen, *A Security Measure for Random Load Disturbances in Nonlinear Power System Models*, IEEE Trans on Circuits and Systems, Vol 34, No 12, Dec 1987, pp 1546-1557

[44] J Medanic, M Ilic-Spong and J Christensen, *Discrete Models of Slow Voltage Dynamics for Under Load Tap-Changing Transformer Coordination*, IEEE Trans on Power Systems, Vol 2, No. 4, Nov 1987, pp 873-882

[45] H D Chiang and F F Wu, *Stability of Nonlinear Systems Described by a Second Order Vector Differential Equations*, IEEE Trans on Circuits and Systems, Vol 35, No 6, June 1988, pp 703-711

[46] H D Chiang, M W Hirsch and F F. Wu, *Stability Regions of Nonlinear Autonomous Dynamical Systems*, IEEE Trans on Automatic Control, Vol 33, No 1, Jan 1988, pp 16-27

[47] R L Chen and P P. Varaiya, *Degenerate Hopf Bifurcations in Power Systems*, IEEE Trans on Circuits and Systems, Vol 35, No 7, June 1988, pp 818-824

[48] F Mercede, J C Chow, H Yan and R Fischl, *A Framework to Predict Voltage Collapse in Power Systems*, IEEE Trans on Power Systems, Vol 3, No 4, Nov 1988, pp 1807-1813

[49] O O Obadina and G J Berg, *Determination of Voltage Stability Limit in Multimachine Power Systems*, IEEE Trans on Power Systems, Vol 3, No 4, Nov 1988, pp 1545-1554

[50] R Seydel, *From Equilibrium to Chaos Practical Bifurcation and Stability Analysis*, Elsevier Science Publishers, North-Holland, 1988

[51] A Tiranuchit and R J Thomas, *A Posturing Strategy against Voltage Instabilities in Electric Power Systems*, IEEE Trans on Power Systems, Vol 3, No 1, Feb 1988, pp 87-93

[52] A Tiranuchit, L M Ewerbring, R A Duryea, R J Thomas and F T Luk, *Towards a Computationally Feasible On-Line Voltage Instability Index*, IEEE Trans on Power System, Vol 3, No 2, May 1988, pp 669-675

[53] F L Alvarado and T H Jung, *Direct Detection of Voltage Collapse Conditions*, Proceedings Bulk Power System Voltage Phenomena—Voltage Stability and Security, EPRI EL-6183, pp 5 23-5 38, Jan 1989

[54] I Dobson and H D Chiang, *Towards a Theory of Voltage Collapse in Electric Power Systems*, Systems & Control Letters, Vol 13, 1989, pp 253-262

[55] A E Hammad and M Z El-Sadek, *Prevention of Transient Voltage Instabilities due to Induction Motor Loads by Static VAR Compensators*, IEEE Trans on Power Systems, Vol 4, No 3, Aug 1989, pp 1182-1190

[56] I A Hiskens and D J Hill, *Energy Functions, Transient Stability and Voltage Behaviour in Power Systems with Nonlinear Loads*, IEEE Trans on Power Systems, Vol 4, No 4, Oct 1989, pp 1525-1533

[57] C C Liu and K T Vu, *Analysis of Tap-Changer Dynamics and Construction of Voltage Stability Regions*, IEEE Trans on Circuit and Systems, Vol 36, No 4, April 1989, pp 575-590

[58] M A Pai and M G O' Grady, *Voltage Collapse Analysis with Reactive Generation and Voltage Dependent Constraints*, Journal of Electric Machines and Power Systems, Vol 17, No 6, 1989, pp 379-390

[59] T S Parker and L O Chua, *Practical Numerical Algorithms for Chaotic Systems*, Springer-Verlag, 1989

[60] C Rajagopalan, P W Sauer and M.A Pai, *Analysis of Voltage Control Systems exhibiting Hopf Bifurcation*, Proceedings of 28th IEEE Conference on Decision and Control, Tampa, FL, 1989, pp 332-335

[61] C Rajagopalan, P W Sauer and M A Pai, *An Integrated Approach to Dynamic and Static Voltage Stability*, Proc of 1989 American Control Conference, Pittsburg PA, Vol 3, June 1989, pp 1231-1235

[62] M Z El-Sadek and F N Abdelbarr, *Effects of Induction Motor Load in Provoking Transient Voltage Instabilities in Power Systems*, Electric Power System Research, Vol 17, No 2, Sept 1989, pp 119-127

[63] M M Begovic and A G Phadke, *Dynamic Simulation of Voltage Collapse*, IEEE Trans on Power Systems, Vol 5, No 4, Nov 1990, pp 1529-1534

[64] M M Begovic and D R Ostojic, *Determination of Critical Zones for Voltage Instability in Power Systems*, Proc of 29th IEEE Conference on Decision and Control, Honolulu, Hawaii, December 1990, pp 3011-3013

[65] M M Begovic and A G Phadke, *Voltage Stability Assesment through Measurement of a Reduced State Vector* IEEE Trans on Power Systems, Vol 5, No 1, Feb 1990, pp 198-203

[66] H D Chiang, Ian Dobson, R J Thomas, J S Thorp and L F Ahmed, *On Voltage Collapse in Electric Power Systems*, IEEE Trans on Power Systems, Vol 5, No 2, May 1990, pp 601-611

[67] J C Chow, R Fischl and H Yan, *On the Evaluation of Voltage Collapse Criteria*, IEEE Trans on Power Systems, Vol 5, No 2, May 1990, pp 612-620

[68] C L DeMarco and T J Overbye, *An Energy Based Security Measure for Assessing Vulnerability to Voltage Collapse*, IEEE Trans on Power Systems, Vol 5, No 2, May 1990, pp 419-427

[69] N Flatabo, R Ognedal and T Carlsen, *Voltage Stability Conditions in a Power System Calculated by Sensitivity methods*, IEEE Trans on Power Systems, Vol 5, No 4, Nov 1990, pp 1286-1293

[70] B Franken and G Andersson, *Analysis of HVDC Converters Connected to Weak AC Systems*, IEEE Trans on Power Systems, Vol 5, No 1, Feb 1990, pp 235-242

[71] R K Gupta, Z A Alaywan, R B Stuart and T A Reece, *Steady State Voltage Instability Operations Perspective*, IEEE Trans on Power Systems, Vol 5, No 4, Nov 1990, pp 1345-1352

[72] J F. Hauer, *Eigenvalue Analysis and Frequency Domain Methods for System Dynamic Performance*, IEEE publication # 90 TH 0293-3 PWR

[73] IEEE system dynamic performance subcommittee, *Voltage Stability of Power Systems Concepts, Analytical Tools and Industry Experience*, IEEE document 90TH0358-2-PWR-1990

[74] H G Kwatny and G E Piper, *Frequency Domain Analysis of Hopf Bifurcations in Electric Power Networks*, IEEE Trans. on Circuits and Systems CAS-37, No 10, Dec 1990, pp 1317-1321

[75] C Lemaitre, J P Paul, J M Tesseron, Y Harmand and Y S Zhao, *An Indicator of the Risk of Voltage profile Instability for Real-Time Control Applications*, IEEE Trans on Power Systems, Vol 5, No 1, Feb 1990, pp 154-161

[76] M A Nayfeh, A M A Hamdan and A H Nayfeh, *Chaos and Instability in a Power System — Primary Resonant Case*, Nonlinear dynamics 1, 1990, pp 313-339

[77] E Ott, C Grebogi and J.A Yorke, *Controlling Chaos*, Physical Review Letters, Vol 64, No 11, 1990, pp 1196-1199

[78] P W Sauer and M A. Pai, *Power System Steady-State Stability and the Load Flow Jacobian*, IEEE Trans on Power Systems, Vol 5, No 4, Nov 1990, pp 1374-1383

[79] Y Sekine and H Ohtsuki, *Cascaded Voltage Collapse*, IEEE Trans on Power Systems, Vol. 5, No. 1, Feb 1990, pp 250-256

[80] S Wiggins, *Introduction to Applied Nonlinear Dynamical Systems and Chaos*, Springer-Verlag, New York, 1990

[81] M Begovic, A Meliopoulos and X Chao, *Control of Voltage Stability via Optimal Power Flow*, Proc of International NSF Workshop 'Bulk Power System Voltage Phenomena Voltage Stability and Security', Deep Creek Lake, MD, August 1991, pp 321-332

[82] C Concordia, *Voltage Instability*, Int Jr of Electrical Power & Energy System, Vol 13, No 1, Feb 1991, pp 14-20

[83] N Fernandopulle and R S Ramshaw, *Analysis of Synchronous Motor Stability using Hopf Bifurcation*, Electric Machines and Power Systems, Vol 19, 1991, pp 239-250

[84] I A Hiskens and D J Hill, *Failure Modes of a Collapsing Power System*, Proceedings of the Workshop on Bulk Power System Voltage Phenomena, Deep Creek, MD, Aug 1991

[85] M Huneault F D Galiana, *A Survey of the Optimal Power Flow Literature*, IEEE Trans on Power Systems, Vol 6, No 2, May 1991, pp 762-770

[86] K Iba, H Suzuki, M Egawa and T Watanabe, *Calculation of Critical Loading Condition with Nose Curve using Homotopy Continuation Method*, IEEE Trans on Power Systems, Vol 6, No 2, May 1991, pp 584-593

[87] B H Lee and K Y. Lee, *A Study on Voltage Mechanism in Electric Power Systems*, IEEE Trans on Power Systems, Vol 6, No 3, Aug 1991, pp 966-973

[88] M A. Nayfeh, A M A. Hamdan and A H Nayfeh, *Chaos and Instability in a Power System Sub-Harmonic Resonant Case*, Nonlinear dynamics 2, 1991, pp 53-72

[89] H Ohtsuki, A Yokoyama and Y Sekine, *Reverse Action of On-Load Tap Changer in Association with Voltage Collapse*, IEEE Trans. on Power Systems, Vol 6, No 1, Feb 1991, pp 300-306

[90] T J Overbye and C L DeMarco, *Improved Techniques for Power System Voltage Stability Assessment using Energy Methods*, IEEE Trans on Power Systems, Vol 6, No 4, Nov 1991, pp 1446-1452

[91] T J Overbye and C L DeMarco, *Voltage Security Enhancement using Energy Based Sensitivities*, IEEE Trans on Power Systems, Vol 6, No 3, Aug 1991, pp 1196-1202

[92] *Survey of the Voltage Collapse Phenomenon*, North American Electric Reliability Council report, 1991

[93] R A Schlueter, I Hu, M W Chang, J C Lo and A Costi, *Methods for Determining Proximity to Voltage Collapse*, IEEE Trans on Power Systems, Vol 6, No 1, Feb 1991, pp 285-292

[94] A Semlyen, B Gao and W Janischewskyj, *Calculation of Extreme Loading Condition of a Power System for the Assessment of Voltage Stability*, IEEE Trans on Power Systems, Vol 6, No 1, Feb 1991, pp 307-315

[95] T Smed, G Andersson, G B Sheble and L L Grigsby, *A New Approach to AC/DC Power Flow*, IEEE Trans on Power Systems, Vol 6, 1991, pp 1238-1244

[96] S C Srivastava, P K Kalra, Ranjan Bose and Manu Agarwal, *Voltage Collapse in Electric Power System*, Proc of 1st IEE Int Conf on Advances in Power System Control, Operation and Management, HongKong, 1991

[97] T Van Cutsem, *A Method to Compute Reactive Power Margins with respect to Voltage Collapse*, IEEE Trans on Power Systems, Vol 6, No 1, Feb 1991, pp 145-156

[98] T Van Cutsem, *Voltage Collapse Mechanisms A Case Study*, Proc of the 1991 Workshop on Bulk Power System Voltage Phenomena Voltage Stability and Security, Mc Henry, USA, August 1991

[99] S A Zaid and M Taleb, *Structural Modeling of Small and Large Induction Machines using Integral Manifolds*, IEEE Trans on Energy Conversion, Vol 6, No 3, Sep 1991, pp 529-535

[100] V Ajjarapu and C Christy, *The Continuation Power Flow A Tool for Steady State Voltage Stability Analysis*, IEEE Trans on Power Systems, Vol 7, No 1, Feb 1992, pp 416-423

[101] V Ajjarapu and B Lee, *Bifurcation Theory and its Application to Nonlinear Dynamical Phenomena in an Electric Power System*, IEEE Trans on Power Systems, Vol 7, No 1, Feb. 1992, pp 424-431

[102] M M. Begovic and A G Phadke, *Control of Voltage Stability using Sensitivity Analysis*, IEEE Trans on Power Systems, Vol 7, No. 1, Feb 1992, pp 114-123

[103] C A Canizares, F L Alvarado, C L DeMarco, I. Dobson and W F Long, *Point of Collapse Methods Applied to AC/DC Power Systems*, IEEE Trans on Power Systems, Vol 7, No 2, May 1992, pp 673-683

[104] I Dobson, F Alvarado and C.L DeMarco, *Sensitivity of Hopf Bifurcations to Power System Parameters*, Proc 31st IEEE Conference on Decision and Control, Tucson, AZ, December 1992, pp 2928-2933

[105] I Dobson and L Lu, *Voltage Collapse Precipitated by the Immediate Change in Stability when Generator Reactive Power Limits are Encountered*, IEEE Trans on Circuits and Systems–I, Vol 39, No 9, Sept 1992, pp 762-766

[106] I Dobson, *Observations on the Geometry of Saddle Node Bifurcations and Voltage Collapse in Electrical Power System*, IEEE Trans Circuits and Systems–I, Vol 39, No 3, March 1992, pp 241-243

[107] I Dobson and L Lu, *Computing an Optimum Direction in Control Space to Avoid Saddle Node Bifurcation and Voltage Collapse in Electric Systems*, IEEE Trans on Automatic Control, Vol 37, No 10, October 1992, pp 1616-1620

[108] J Douglas, *FACTS the Delivery System of the Future*, EPRI Journal, 17(7), October 1992, pp 4-11

[109] A A Fouad and V Vittal, *Power System Transient Stability Analysis*, The Prentice Hall, New Jersey, 1992

[110] B Gao, G K Morison and P Kundur, *Voltage Stability Evaluation using Modal Analysis*, IEEE Trans on Power Systems, Vol 7, No 4, Nov 1992, pp 1529-1542

[111] I A Hiskens and C B McLean, *SVC Behaviour under Voltage Collapse Conditions*, IEEE Trans on Power Systems, Vol 7, No 3, Aug 1992, pp 1078-1087

[112] W R Lachs and D Sutanto, *Voltage Instability in Interconnected Power Systems A Simulation Approach*, IEEE Trans on Power Systems, Vol 7, No 2, May 1992, pp 753-761

[113] P A Lof, T Smed, G Anderson and D J Hill, *Fast Calculation of a Voltage Stability Index*, IEEE Trans on Power Systems, Vol 7, No 1, Feb 1992, pp 54-64

[114] M K Pal, *Voltage Stability Conditions considering Load Characteristics*, IEEE Trans on Power Systems, Vol 7, No 1, Feb 1992, pp 243-249

[115] C Rajagopalan, B Lesieutre, P W. Sauer and M A Pai, *Dynamic Aspects of Voltage/Power Characteristics*, IEEE Trans on Power Systems, Vol 7, No 3, Aug 1992, pp 990-1000

[116] M. Suzuki, S. Wada, M Sato, T Asano and Y Kudo, *Newly Developed Voltage Security Monitoring System*, IEEE Trans on Power Systems, Vol 7, No 3, Aug 1992, pp 965-973.

[117] P Varaiya, F Wu and H.D Chiang, *Bifurcation and Chaos in Power System A Survey*, EPRI TR-100834, August 1992, Final Report

[118] V Venkatasubramanian, H Schattler and J. Zaborszky, *Voltage Dynamics, Study of a Generator with Voltage Control, Transmission and Matched MW Load*, IEEE Trans Automatic Control, Vol 37, No 11, Nov 1992, pp 1717-1733

[119] K T Vu and C C Liu, *Shrinking Stability Regions and Voltage Collapse in Power System*, IEEE Trans on Circuits and Systems—I Fundamental Theory and Applications, Vol 39, No 4, April 1992, pp 271-289

[120] H O Wang, E H Abed and A M A Hamdan, *Bifurcations, Chaos and Crises in Power System Voltage Collapse*, Technical Research Report # TR 92-72, University of Maryland, USA

[121] N Yorino, H Sasaki, Y Masuda, Y Tamura, M Kitagawa and A Oshimo, *An Investigation of Voltage Instability Problems*, IEEE Trans on Power Systems, Vol 7, No 2, May 1992

[122] E H Abed, H O Wang, J C. Alexander, A M A Hamdan and H C Lee, *Dynamic Bifurcations in a Power System Model Exhibiting Voltage Collapse*, International Journal of Bifurcation and Chaos, Vol 3, No 5, 1993, pp 1169-1176

[123] E H Abed and H O Wang, *Feedback Control of Bifurcation and Chaos in Dynamical Systems*, Technical Research Report # TR 93-74, University of Maryland, USA

[124] J K Bandyopadhyay, V R Kumar and B D Kulkarni, *Regulatory Control of a Chaotic Nonisothermal CSTR*, AIChE Journal, Vol 39, No 5, May 1993, pp 908-912

[125] M Brucoli, M La Scala, R Sbrizzai and M Trovato, *Voltage Stability Analysis of Electric Power Systems with Frequency Dependent Loads*, Proc IEE Pt-C, Vol-140, No 1, January 1993, pp 1-6

[126] C A Canizares and F L Alvarado, *Point of Collapse and Continuation Methods for Large AC/DC Systems*, IEEE Trans on Power Systems, Vol 8, No 1, Feb 1993, pp 1-8

[127] H D Chiang, C W Liu, P Varaiya, F F Wu and M G Louby, *Chaos in a Simple Power System*, IEEE Trans on Power Systems, Vol 8, No 4, Nov 1993, pp 1407-1417

[128] H D Chiang, Jianzhong Tong and Karen Nan Miu, *Predicting Unstable Modes in Power Systems Theory and Computations*, IEEE Trans on Power Systems, Vol 8, No 4, Nov 1993, pp 1429-1437

[129] C Concordia (ed), *Special Issue on Voltage Stability and Collapse*, Int. Jr of Electrical Power & Energy Systems, Vol 15, No. 4, August 1993

[130] C Counan, M Trotignon, E Corradi, G Bortoni, M Stubbe and J Deuse, *Major Incidents on the French Electric System Potentiality and Curative Measures Studies*, IEEE Trans on Power Systems, Vol 8, No 3, Aug 1993, pp 879-886

[131] J Deuse and M Stubbe, *Dynamic Simulation of Voltage Collapse*, IEEE Trans on Power Systems, Vol 8, No 3, Aug 1993, pp 894-904

[132] I Dobson and L Lu, *New Methods for Computing a Closest Saddle Node Bifurcation and Worst Case Load Power Margin for Voltage Collapse*, IEEE Trans. on Power Systems, Vol 8, No 3, Aug 1993, pp 905-913

[133] I Dobson, *Computing a Closest Bifurcation Instability in Multidimentional Parameter Space*, Jr of Nonlinear Science, Vol 3, 1993, pp. 307-327

[134] N Flatabo, O B Fosso, R Ognedal, T Carlsen and K R Heggland, *A Method for Calculating of Margins to Voltage Instability Applied on the Norwegian System for Maintaining Required Security Level*, IEEE Trans on Power Systems, Vol 8, No 3, Aug 1993, pp 920-928

[135] A M A Hamdan, *Modes, State Variables and Local Bifurcations in Power System Dynamics*, Electrical Machines and Power Systems, Vol 21, 1993, pp 241-255

[136] D J Hill, *Nonlinear Load Models with Recovery for Voltage Stability Studies*, IEEE Trans on Power Systems, Vol 8, No 1, Feb 1993, pp 166-176

[137] N G Hingorani, *Flexible AC Transmission*, IEEE Spectrum, Vol 30, No 4, April 1993, pp 40-45

[138] N G Hingorani and K E Stahlkopf, *High Power Electronics*, Scientific American, Vol 269, No 5, November 1993, pp 78-85

[139] B Lee and V Ajjarapu, *Period-doubling Route to Chaos in an Electric Power System*, Proc IEE Pt-C, Vol-140, No 6, November 1993, pp 490-496

[140] B H Lee and K Y Lee, *Dynamic and Static Voltage Stability Enhancement of Power Systems*, IEEE Trans on Power Systems, Vol 8, No 1, Feb 1993, pp 231-238

[141] P A Lof, G Andersson and D J Hill, *Voltage Stability Indices for Stressed Power Systems*, IEEE Trans on Power Systems, Vol 8, No 1, Feb 1993, pp 326-335

[142] P A Lof, G Andersson and D J Hill, *Generator Modelling for Static Voltage Stability Studies*, Proc of the 11th Power System Computation Conference, Avignon, France, Aug/Sept 1993, pp 923-929

[143] P A Lof, D J Hill, S Arnborg and G Andersson, *On the Analysis of Long-Term Voltage Stability*, Int Jr of Electrical Power and Energy Systems, Vol 15, No 4, 1993, pp 229-237

[144] F K Mak and M D Ilic, *Classification of Voltage Problems in Electric Power Systems*, Int Jr of Electrical Power and Energy Systems, Vol. 15, No 6, 1993, pp 377-385

[145] J D McCalley, J F Dorsey, J F Luini, R P Mackin and G H Molina, *Subtransmission Reduction for Voltage Instability Analysis*, IEEE Trans on Power Systems, Vol 8, No 1, Feb 1993, pp 349-356

[146] N W. Miller, R D Aquila, K.M. Jimma, M T Sheehan and G L Comegys, *Voltage Stability of Puget Sound System under Abnormally Cold Weather Conditions*, IEEE Trans on Power Systems, Vol 8, No 3, Aug 1993, pp 1133-1142

[147] A Roman-Messina and B J Cory, *Enhancement of Dynamic Stability by Coordinated Control of Static VAR Compensators*, Int Journal of Electrical Power and Energy Systems, Vol 15, No 2, 1993, pp 85-93

[148] G K Morison, B Gao and P Kundur, *Voltage Stability Analysis using Static and Dynamic Approaches*, IEEE Trans on Power Systems, Vol 8, No 3, Aug 1993, pp 1159-1171

[149] C O Nwankpa and R M Hassan, '*A Stochastic based Voltage Collapse Indicator*, IEEE Trans on Power Systems, Vol 8, No 3, Aug 1993, pp 1187-1194

[150] M K Pal, *Voltage Stability Analysis Needs, Modelling Requirement and Modelling Adequacy*, Proc IEE Pt-C, Vol 140, No 4, July 1993, pp 279-286

[151] M A Pai, P W Sauer, B L Lesieutre and R Adapa, *Structural Stability in Power Systems - Effect of Load Models*, Athens Power Tech Conference, Athens Greece, Sept 1993

[152] V Veera Raju and A Kuppurajulu, *A Closed Loop Controller for Voltage Stability*, Int J of Electrical Power and Energy Systems, Vol-15, No 5, 1993, pp 283-292

[153] P W Sauer, B C Lesieutre and M A Pai, *Maximum Loadability and Voltage Stability in Power Systems*, Int. Jr of Electrical Power and Energy Systems, Vol 15, No 3, 1993, pp 145-154

[154] C W Tan, M Varghese, P. Varaiya and F Wu, *Bifurcation and Chaos in Power Systems*, Sadhana Proceedings in Engineering Sciences of the Indian Academy of Sciences, Bangalore, India, Vol 18, Part 5, Sept 1993, pp 761-786

[155] T J Overbye, *Use of Energy Methods for On-Line Assessment of Power System Voltage Security*, IEEE Trans on Power Systems, Vol 8, No 2, May 1993, pp 452-458

[156] L Wang, *A Comparative Study of Damping Schemes on Damping Generator Oscillations*, IEEE Trans on Power Systems, Vol 8, No 2, 1 1993, pp 613-619

[157] H O Wang and E H Abed, *Control of Nonlinear Phenomena at the Inception of Voltage Collapse*, Proc 1993 American Control Conference, San Francisco, June 1993, pp 2071-2075

[158] W Xu and P G Harrington, *Planning Methodologies for Voltage Stability Limited Power Systems*, Electrical Power and Energy Systems, Vol 15, No 4, 1993, pp 221-228

[159] L. Vargas and V H Quintana, *Clustering Techniques for Voltage Collapse Detection*, Electric Power System Research, Vol. 26, No. 1, Jan. 1993, pp 53-59.

[160] C D Vournas and N D. Krassas, *Voltage Stability as Affected by Static Load Characteristics*, Proc IEE pt-C, Vol 140, No 3, May 1993, pp. 221-228

[161] E H Abed, *Bifurcation-Theoretic Issues in the Control of Voltage Collapse*, IMA Volumes in Mathematics and its Applications, Vol. 64, Springer-Verlag, 1994, pp. 1-22

[162] V Ajjarapu, Ping Lin Lau and S Battula, *An Optimal Reactive Power Planning Strategy Against Voltage Collapse*, IEEE Trans on Power Systems, Vol 9, No 2, May 1994, pp 906-917

[163] F Alvarado, I Dobson and Y. Hu, *Computation of Closest Bifurcations in Power Systems*, IEEE Trans on Power Systems, Vol 9, No 2, May 1994, pp 918-928

[164] M M Begovic and Roger Q Mills, *Load Identification and Voltage Stability Monitoring*, IEEE/PES Winter Meeting New York, January 30 - February 3, 1994, paper no. 94WM 213-9 PWRS

[165] C A Canizares and Stene Hranilovic, *Transcritical and Hopf Bifurcation in AC/DC Systems*, Bulk Power System Voltage Phenomena — III Seminar, NSF/ECC INC, DAVOS, Switzerland, August 22-26, 1994

[166] C A Canizares, Autonio Z de Souza and Victor H Quintana, *Improving Continuation Methods for Tracing, Bifurcation Diagrams in Power Systems*, Bulk Power System Voltage Phenomena - III Seminar, NSF/ECC INC, DAVOS, Switzerland, August 22-26, 1994

[167] C A Canizares, *On Bifurcations, Voltage Collapse and Load Modeling*, IEEE/PES 1994 Summer Meeting, San Francisco, CA, July 24-28, 1994, Paper no 94SM 578-5 PWRS

[168] *Modeling of Voltage Collapse Including Dynamic Phenomena*, CIGRE Task Force # 38 02 10

[169] *Indices of Prediction of Voltage Collapse Including Dynamic Phenomena*, CIGRE Task Force # 38 02 11

[170] M L Crow, *Dynamics of Voltage Instability and Collapse* International Journal of Electrical Power & Energy System(UK) Vol 16, No 4, Aug 1994, pp 235-242

[171] F P DeMello, *Exploratory Concepts on Control of Variable Series Compensation in Transmission Systems to Improve Damping of Intermachine/System Oscillations*, IEEE Trans on Power Systems, Vol 9, No 1, Feb 1994, pp 102-119

[172] A Gebreselassie and J H Chow, *Investigation of the Effects of Load Models and Generator Voltage Regulators on Voltage Stability*, Int Jr of Electrical Power & Energy System, Vol 16, No 2, 1994, pp 83-89

[173] T Guo and R A Schlueter, *Identification of Genetic Bifurcation and Stability Problems in Power System Differential Algebraic Model*, IEEE Trans on Power Systems, Vol 9, No 2, May 1994, pp. 1032-1044

[174] D J Hill, I A Hiskens and D H Popovic, *Stability Analysis of Power System Loads with Recovery Dynamics*, International Journal of Electrical Power & Energy System(UK) Vol 16, No 4, Aug 1994, pp 277-286.

[175] Y Y Hong and C H Gau, *Voltage Stability Indicator for Identification of the Weakest Bus/Area in Power Systems*, Proc IEE pt-C, Vol 141, No 4, July 1994, pp 305-309

[176] P Kundur, *Power System Stability and Control*, the EPRI Power System Engineering Series, McGraw-Hill, New York, 1994

[177] C W Liu, J S Thorp, J Lu, R J Thomas and H.D Chiang, *Detection of Transiently Chaotic Swings in Power Systems Using Real Time Phasor Measurement*, IEEE Trans on Power Systems, Vol 9, No 3, Aug 1994, pp 1285-1292.

[178] J Lu, C W Liu and J.S Thorp, *New Methods for Computing a Saddle Node Bifurcation Point for Voltage Stability Analysis*, IEEE/PES 1994 Summer Meeting, San Francisco, CA, July 24-28, 1994, Paper no 94SM 514-0 PWRS

[179] P A Lof, G Andersson and D J Hill, *Voltage Dependent Reactive Power Limits for Voltage Stability Studies*, IEEE/PES Winter Meeting, New York, Jan /Feb 1994, Paper # 94WM 248-5 PWRS

[180] M Noroozian and G Andersson, *Damping of Power System Oscillations by use of Controllable Components*, Paper # WM94 064-6-PWRD, IEEE PES 1994, Winter Meeting, New York

[181] T J Overbye, I Dobson and C L DeMarco, *Q-V Curve Interpretations of Energy Measures for Voltage Security*, IEEE Trans on Power Systems, Vol 9, No 1, Feb 1994, pp 331-340

[182] T J Overbye, *Computation of a Practical Method to Restore Power Flow Solvability*, IEEE/PES Winter Meeting, New York, Jan/Feb 1994, Paper # 94WM 245-1 PWRS

[183] T J Overbye, *A Power Flow Measure for Unsolvable Cases*, IEEE Trans on Power Systems, Vol 9, No 3, Aug 1994, pp 1359-1365

[184] T J Overbye, *Effects of Load Modelling on Analysis of Power System Voltage Stability*, International Journal of Electrical Power & Energy System(UK) Vol 16, No 5, 1994, pp 329-338

[185] M A Pai, P W Sauer, B Lesieutre and R K Ranjan, *Structural Stability in Power Systems*, EPRI final report, TR-103870, April 1994

[186] V H Quintana and L Vargas, *Voltage Stability as Affected by Discrete Changes in the Topology of Power Networks*, Proc IEE pt-C, Vol 141, No 4, July 1994, pp 346-352

[187] R A Schlueter and I Hu, *Types of Voltage Instability and the Associated Modelling for Transient/Mid Term Stability Simulation*, Electric Power System Research, Vol 29, No 2, March 1994, pp 131-146

[188] K S Smith and L Ran, *Voltage Stability Assesment of Isolated Power Systems with Power Electronic Converters*, Proc IEE pt-C, Vol 141, No 4, July 1994, pp 310-314

[189] C W Taylor, *Power System Voltage Stability*, the EPRI Power System Engineering Series, McGraw-Hill, New York, 1994

[190] C D Vournas, *Voltage Stability and Controllability Indices for Multimachine Power Systems*, IEEE/PES 1994 Summer Meeting, San Francisco, CA, July 24-28, 1994, Paper no 94SM 513-2 PWRS

[191] H O Wang, E H Abed and A M A Hamdan, *Bifurcation, Chaos and Crises in Voltage Collapse of a Model Power System*, IEEE Trans on Circuits and Systems—I Fundamental Theory and Applications, Vol 41, No 4, March 1994, pp 294-302

[192] W Xu and Y Mansour, *Voltage Stability using Generic Dynamic Load Models*, IEEE Trans on Power Systems, Vol 9, No 1, Feb 1994, pp 479-493

Appendix A

Data for 2 Bus Test System (at 100 MVA base)

This system is shown in Fig A 1 The relevant data are provided in the following tables

Table A 1 Generator Data

$X_d = 0\ 4025$	$X'_d = 0\ 13074$	$T'_{do} = 8\ 00$ sec	$H = 7\ 76$ sec	$X_q = 0\ 2987$
$X'_q = 0\ 2173$	$D_g = 1\ 00$ p u	$T'qo = 0\ 02$ sec	$R_a = 0\ 000909$	

Table A 2 Exciter Data

$K_a = 10\ 0$	$T_a = 0\ 06$ sec	$A_{ex} = 0\ 0237$	$K_f = 0\ 0648$	$T_f = 1\ 00$ sec
$K_e = -0\ 08$	$T_e = 0\ 405$ sec	$B_{ex} = 0\ 9227$	$V_a^{max} = 3\ 5$	$V_a^{min} = -3\ 5$

Table A 3 Governor Data

$T_1 = 124\ 47$	$T_2 = 8\ 590$	$T_3 = 0\ 250$	$T_4 = 0\ 000$	$T_5 = 0\ 740$	$R_{eg} = 0\ 050$
$F = -2\ 000$	$P_{max} = 2\ 670$				

Table A 4 Induction Motor Data

$X_1 = 3\ 5065$	$R_1 = 0\ 03057$	$H = 1\ 0$ sec	$X_2 = 3\ 5065$	$R_2 = 0\ 03596$	$X_m = 3\ 399$

Table A 5 Transmission Line Data

$R_{TL} = 0\ 0056$	$X_{TL} = 0\ 056782$

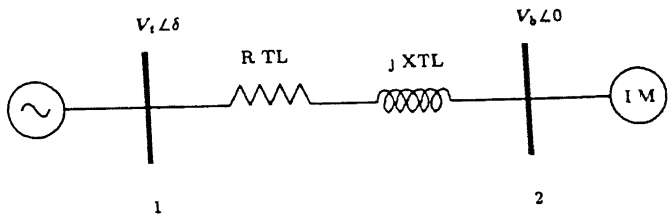

Figure A 1 2-bus system

Appendix B

DATA FOR 3 BUS TEST SYSTEM

The 3 bus system is shown in Fig B 1 The relevant data for this study system is given below

Table B 1 Generator Data

P_M	M_g	D	Voltage of Inf bus-1 and Gen bus-3 = 1 0
1 0	0 3	0 05	

Table B 2 Load Data

$P_1 = 0\,0$	$Q_1 = 0\,0$	$P_0 = 0\,6$	$K_{p\omega} = 0\,4$	$K_{pv} = 0\,3$	$T = 8\,5$	$Q_0 = 1\,3$
$K_{q\omega} = -0\,03$	$K_{qv} = -2\,8$	$K_{qv_2} = 2\,1$				

Table B 3 Line Data

Line no	From bus	To bus	Admittance	$y_{BUS/2}$
1	1	2	$20\angle -85$ deg	0
2*	2	3	$10\angle -85$ deg	0

$\star$ Bus 2 has compensation of 3 0 p u

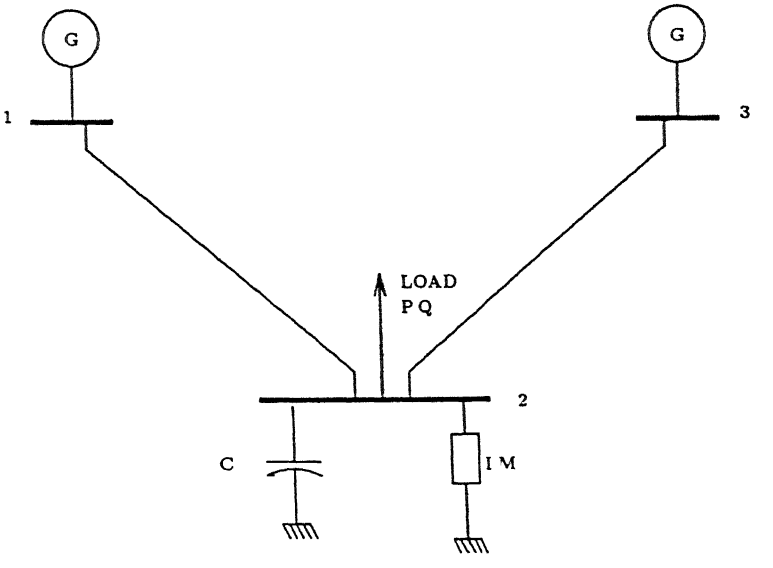

Figure B 1 3-bus system

Appendix C

DATA FOR 3 BUS TEST SYSTEM WITH SVS

The 3 bus system is shown in Fig C 1 The relevant data for this study system is given below

Table C 1 Generator Data

P_M	M_g	D	Voltage of infinite bus-1 and generator bus-3 = 1 0
1 0	0 5	0 05	

Table C 2 Load Data

$P_1 = 0\,0$	$P_V = 0\,4$	$Q_1 = 0\,0$	$Q_V = 1\,0$	$\eta = 1\,9$	$\xi = 1\,6$
$P_0 = 0\,3$	$K_{p\omega} = 0\,6$	$K_{pv} = 0\,6$	$T = 8\,5$	$Q_0 = 1\,3$	$K_{q\omega} = -0\,05$
$K_{qv} = -0\,8$	$K_{qv_2} = 2\,3$				

Table C 3 SVS Data

$V_{ref} = 1\,0$	$K_{svs} = 50\,0$	$T_{svs} = 0\,01$	$B_{min} = -15\,0$	$B_{max} = 15\,0$

Table C 4 Line Data

Line no	From bus	To bus	Admittance	$y_{BUS/2}$
1	1	2	$20\angle -82$ deg	0
2	2	3	$10\angle -85$ deg	0
3	3	1	$2\,8\angle -82$ deg	0

$\star$ Bus 2 has compensation of 10 0 p u

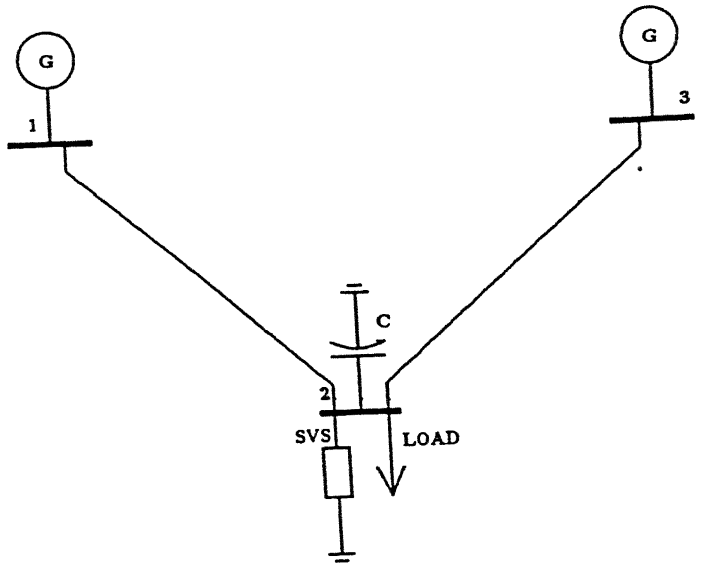

Figure C 1. 3-bus system with SVS

Appendix D

DATA FOR 4 BUS TEST SYSTEM

The 4-bus system is shown in Fig D 1 The relevant data for this study system is given below

Table D 1· Generator Data

$P_M = 1\,0$	$M_g = 0\,5$	$D = 0\,05$	Voltage of infinite bus-1 and generator bus-3 = 1 0

Table D 2 Load Data

$P_1 = 0\,0$	$P_V = 0\,1$	$Q_1 = 0\,0$	$Q_V = 1\,0$	$\eta = 2\,1$	$\xi = 1\,4$
$P_0 = 0\,3$	$K_{p\omega} = 0\,5$	$K_{pv} = 0\,3$	$T = 8\,5$	$Q_0 = 1\,3$	$K_{q\omega} = -0\,03$
$K_{qv} = -0\,8$	$K_{qv_2} = 2\,3$				

Table D 3 OLTC Data

$\Delta n = 0\,025$	$\Delta t = 10$ sec	$\epsilon = 0\,015$	$n_{min} = 0\,9$	$n_{max} = 1\,1$	$V^\circ = 1\,0$

Table D 4 Line Data

Line no	From bus	To bus	Admittance	$Y_{sh/2}$
1	1	4	$20\angle -82$ deg	0
2	4	3	$10\angle -85$ deg	0
3	3	1	$2\,8\angle -80$ deg	0
4*	4	2	$100\angle 0$ deg	0

⋆ Bus-4 has compensation of 12 0 p u

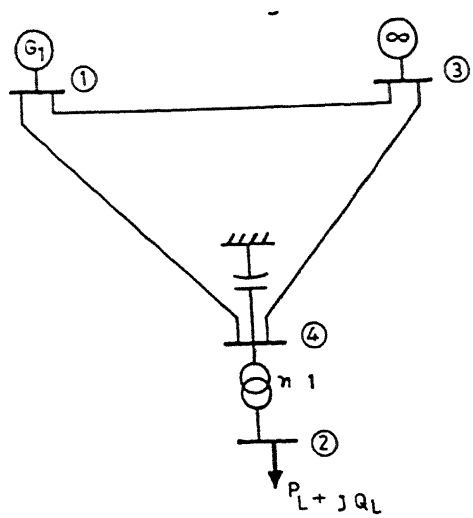

Figure D 1 4-bus system with OLTC

Appendix E

Data for 9 Bus Test System (at 100 MVA base)

The 9 bus system is shown in Fig E The system data is taken from ref [7] The relevant data are provided in following tables

Table E 1. Line Data

From bus	To bus	Series impedence		Shunt susceptance
		R(p u)	X(p u)	B(p u)
1	4	0 0000	0 0576	0 0000
4	6	0 0170	0 0920	0 1580
6	9	0 0390	0 1700	0 3580
9	3	0 0000	0 0586	0 0000
9	8	0 0119	0 1008	0 2090
8	7	0 0085	0 0720	0 1490
7	2	0 0000	0 0625	0 0000
7	5	0 0320	0 1610	0 3060
5	4	0 0100	0 0850	0 1760

Table E 2 Machine Data

Parameter	Machine–1	Machine–2	Machine–3
X_d(p u)	0 1460	0 8958	1 3125
X'_d(p u)	0 0608	0 1198	0 1813
T'_{do}(sec)	8 96	6 00	5 89
X_q(p u)	0 0969	0.8645	1 2578
X'_q(p u)	0 0608	0.1198	0 1813
T'_{qo}(sec)	0 310	0 535	0 600
H(sec)	23 64	6 40	3 01
D(p u)	1 0	1 0	1 0

Table E 3 Bus Data

Bus No	Bus Type	Generation(p u)		Load(p u)		Voltage Magnitude
		Real	Reactive	Real	Reactive	
1	Swing	—	—	0 00	0 00	1 0400
2	PV	1 63	—	0 00	0 00	1 0253
3	PV	0 85	—	0 00	0 00	1 0253
4	PQ	0 00	0 00	0 00	0 00	—
5	PQ	0 00	0 00	1 25	0 50	—
6	PQ	0 00	0 00	0 90	0 30	—
7	PQ	0 00	0 00	0 00	0 00	—
8	PQ	0 00	0 00	1 00	0 35	—
9	PQ	0 00	0 00	0 00	0 00	—

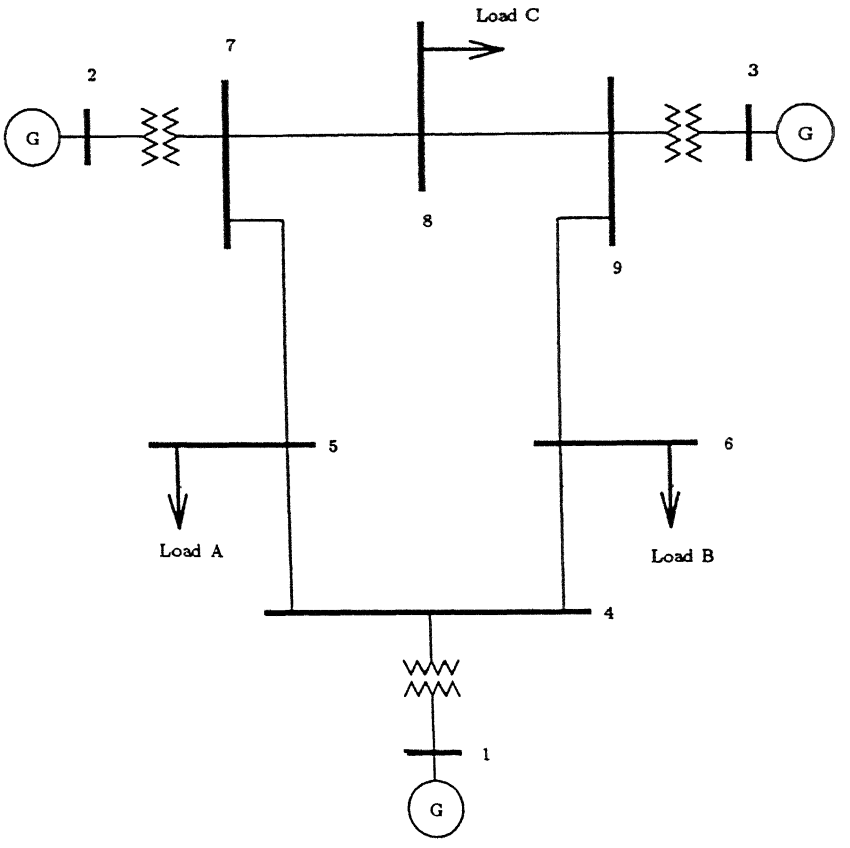

Figure E 1 9-bus system

Appendix F

Data for 10 Bus Test System (at 100 MVA base)

This system is derived from 9–bus system given in Appendix–E by connecting an induction motor load in addition to the existing load to bus 6 (Fig F.1) The data for excitation system and speed governing loop were taken from ref [7] in accordance with the capacity of the machines The relevant data are provided in following tables

Table F.1 Excitation System Data

Parameter	Exciter–1	Exciter–2	Exciter–3
K_a	10 00	10 00	10 00
K_f	0 0648	0 0910	0 1080
K_e	−0 0200	−0 0505	−0 0601
T_a(sec)	0 02	0 20	0 20
T_f(sec)	1 00	0 35	0 35
T_e(sec)	0 1000	0 5685	0 6758
A_{ex}	0 0096	0 0013	0 0016
B_{ex}	1 1461	1 3733	1 6349
V_a^{max}	2 00	2 00	2 00
V_a^{min}	−2 00	−2 00	−2 00

Table F 2 Speed Governor Data

Parameter	Governor–1	Governor–2	Governor–3
T_1(sec)	30 0	0 083	0 083
T_2(sec)	3 5	0 00	0 000
T_3(sec)	0 520	0.200	0 200
T_4(sec)	0 0	0 050	0 050
T_5(sec)	0 415	8 000	5 000
R_{eg}(p u)	0 050	0.050	0 050
F	−2 000	0.271	0 280
P_{max}	2 50	1 75	1 32

Table F 3 Induction Motor Data

X_1	R_1	H	X_2	R_2	X_m
3 5065	0 03057	1 0	3 5065	0 03596	3 399

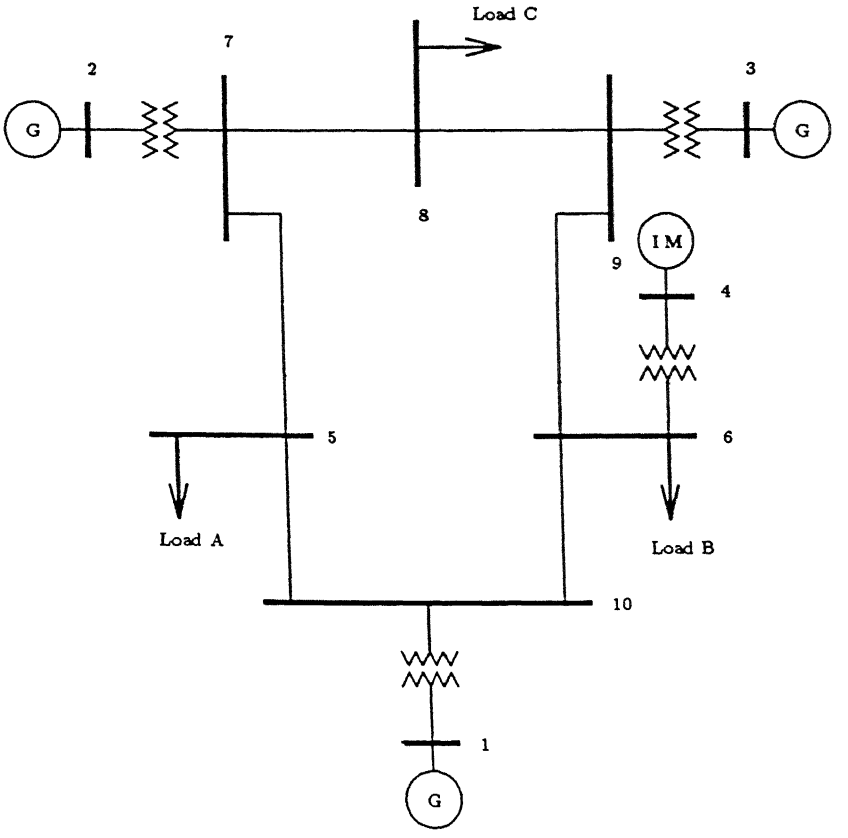
Load C
7
2
3
G
G
8
9
IM
4
5
6
Load A
Load B
10
1
G

Appendix G

Data for IEEE-14 Bus Test System (at 100 MVA base)

The IEEE-14 bus system is shown in Fig G 1 The system data is taken from ref [39] and buses renumbered The relevant data are provided in following tables

Table G 1 Generator Bus Data

Bus No	Scheduled real power generation P_G(MW)	Specified Voltage magnitude Vspec (p u)	Load	
			Real (MW)	Reactive (MVAR)
1(slack)	—	1 060	00 00	00 00
2	040 0	1 045	21 70	12 70
3	020 0	1 070	11 20	07 50
4	—	1 010	94 20	19 00
5	—	1 090	00 00	00 00

Table G 2 Generator Data

Gen no	Real generation limit		React generation limit		Cost characteristics*		
	Maximum (MW)	Minimum (MW)	Maximum (MVAR)	Minimum (MVAR)	a_i ($/MW^2-hr)	b_i ($/MW-hr)	c_i ($/hr)
1	200 0	050 0	100 0	−45 0	1 0	2 45	105 00
2	100 0	020 0	050 0	−40 0	1 0	3 51	044 40
3	100 0	020 0	024 0	−06 0	1 0	3 89	040 60
4	—	—	040 0	000 0	—	—	—
5	—	—	024 0	−06 0	—	—	—

$\star$ Fuel cost of i^{th} gen unit $F_i = (\frac{1}{2}a_i P_{G_i}^2 + b_i P_{G_i} + c_i)$\$/hr

Table G 3 Load Bus Data

Bus No	Load		Shunt compensation in(MAVR)	External shunt susceptance(p u)
	Real(MW)	Reactive(MVAR)		
6	00 0	00 0	000 0	0 00
7	29 5	16 6	−19 0	0 19
8	07 6	01 6	000 0	0 00
9	47 8	−3 9	000 0	0 00
10	09 0	05 8	000 0	0 00
11	03 5	01 8	000 0	0 00
12	06 1	01 6	000 0	0 00
13	13 5	05 8	000 0	0 00
14	14 9	05 0	000 0	0 00

Table G 4 Transformer Data

Transf no (Line no)	From bus	To bus	Series reactance X(p.u)	Tap settings (p u)(base case)
1	8	3	0 25202	0 962
2	9	6	0 20912	0 978
3	9	7	0 55618	0 969

Table G 5 Line Data

Line no	From bus	To bus	Series impedence		Shunt susceptance B(p u)
			R(p u)	X(p u)	
4	1	8	0 05403	0 22304	0 0246
5	2	8	0 05695	0 17388	0 0170
6	4	9	0 06701	0 17103	0 0173
7	9	8	0 01335	0 04211	0 0064
8	1	2	0 01938	0 05917	0 0264
9	2	4	0 04699	0 19797	0 0219
10	6	5	0 00000	0 17615	0 0000
11	2	9	0 05811	0 17632	0 0187
12	6	7	0 00000	0 11001	0 0000
13	7	10	0 03181	0 08450	0 0000
14	3	11	0 09498	0 19890	0 0000
15	3	12	0 12291	0 25581	0 0000
16	3	13	0 06615	0 13027	0 0000
17	7	14	0 12711	0 27038	0 0000
18	10	11	0 08205	0 19207	0 0000
18	12	13	0 22092	0 19988	0 0000
20	13	14	0 17093	0 34802	0 0000

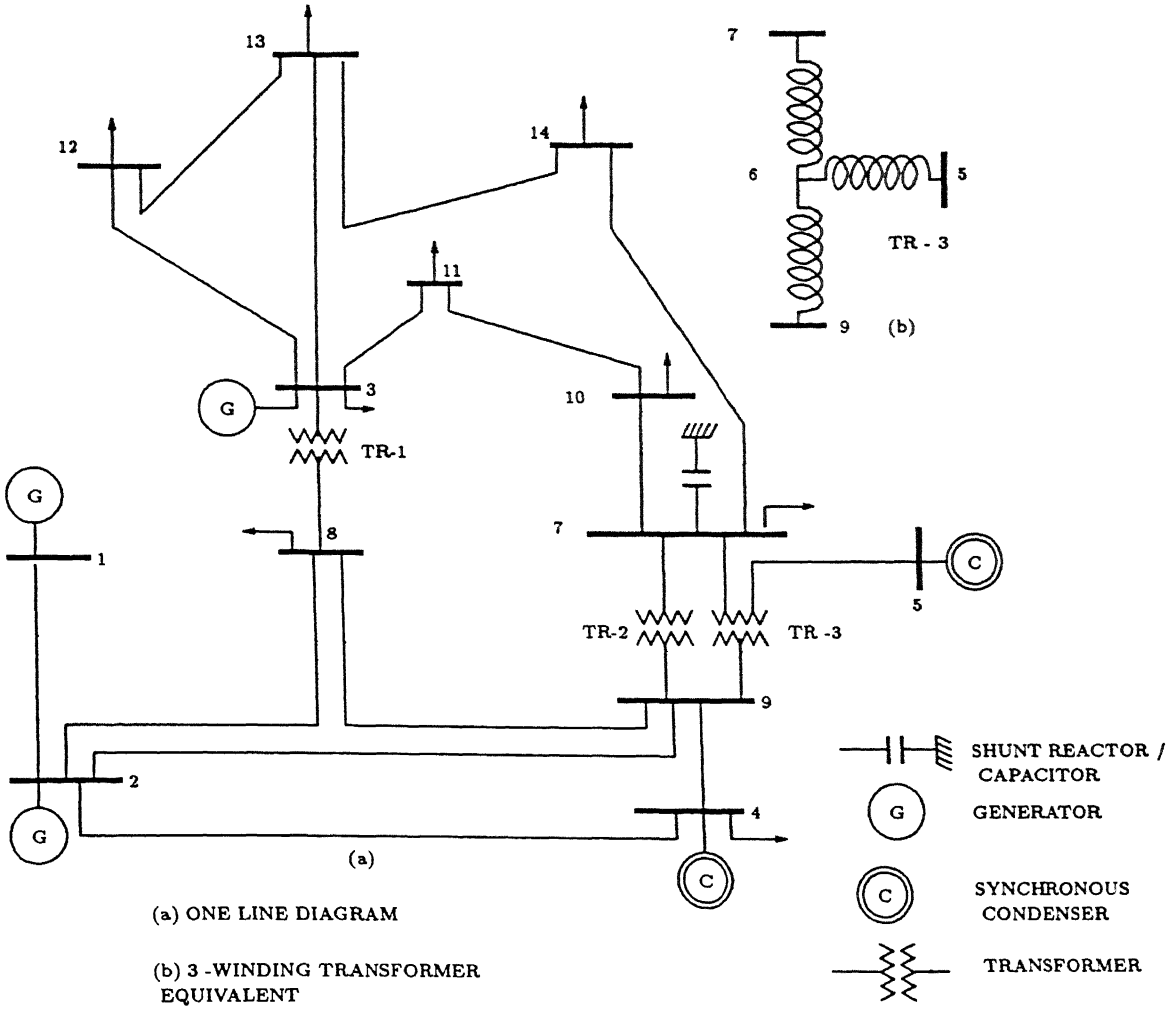

(a) ONE LINE DIAGRAM

(b) 3 -WINDING TRANSFORMER EQUIVALENT

Figure G 1· IEEE-14 bus system

Appendix H

Data for 19 Bus Test System (at 100 MVA base)

The UPSEB 19-bus system is shown in Fig H 1 The system data is taken from UP STATE ELECTRICITY BOARD STUDY CELL, IIT KANPUR and buses renumbered The relevant data are provided in following tables

Table H 1 Generator Bus Data

Bus No	Scheduled real power generation P_G(MW)	Specified Voltage magnitude Vspec (p u)	Load		React Generation	
			Real (MW)	Reactive (MVAR)	Maximum (MVAR)	Minimum (MVAR)
1(slack)	—	1 010	0 00	0 00	—	—
2	1600 0	1 058	0 00	0 00	960 0	−480 0
3	0900 0	1 056	0 00	0 00	540 0	−050 0
4	0550 0	1 057	0 00	0 00	330 0	−050 0

Table H 2 Transformer Data

Transf no (Line no)	From bus	To bus	Series resistance R(p u)	Series reactance X(p u)	Tap settings (p u)(base case)
1	5	2	00016	01991	1 000
2	6	1	.00073	01460	1 000
3	7	3	00030	03499	1 000
4	8	4	00049	04743	1 000

Table H 3 Load Bus Data

Bus No	Load		External shunt susceptance(p u)
	Real(MW)	Reactive(MVAR)	
5	00 0	00 0	−2 02269
6	191 0	16 0	−0 907029
7	1000 0	00 0	−0 571429
8	00 0	00 0	−0 453515
9	135 0	78 0	−0 453515
10	236.0	45 0	−0 453515
11	360 0	11 0	−1 02495
12	337 0	59.0	−0 453515
13	90 0	20.0	0 0
14	520 0	84.0	−0 453515
15	387 0	64 0	−0 907029
16	288 0	0 0	−2 6304
17	477 0	0 0	−0 453515
18	−151 0	69 0	0 0
19	−263 0	0 0	0 0

Table H 4 Line Data

Line no	From bus	To bus	Series impedence		Shunt susceptance B(p u)
			R(p u)	X(p u)	
5	5	7	00031	00310	04056
6	7	16	00918	09306	1 21680
7	16	5	00927	09429	1 23293
8	16	5	00833	08478	1 10855
9	8	5	00031	00310	04056
10	6	8	00051	00517	06760
11	8	9	00479	04880	63614
12	10	9	00254	02584	33798
13	6	10	00468	04770	62450
14	10	11	00294	02997	39206
15	11	5	00823	08375	1 09503
16	11	12	00650	06617	86521
17	13	12	00325	03307	43264
18	13	14	00370	03762	48870
19	14	12	00260	02646	34610
20	15	14	00806	08169	1 06808
21	6	15	00785	07990	1 04738
22	15	16	00015	00155	02704
23	16	17	00559	05686	74354
24	17	18	00121	01109	72815
25	14	19	00051	00517	06760

Table H 5 Machine Data

Parameter	Generator #2	Generator #3	Generator #4
M_g	0 266	0 178	0 084
X'_d	0 014	0 023	0 028
D	1 0	1 0	1 0

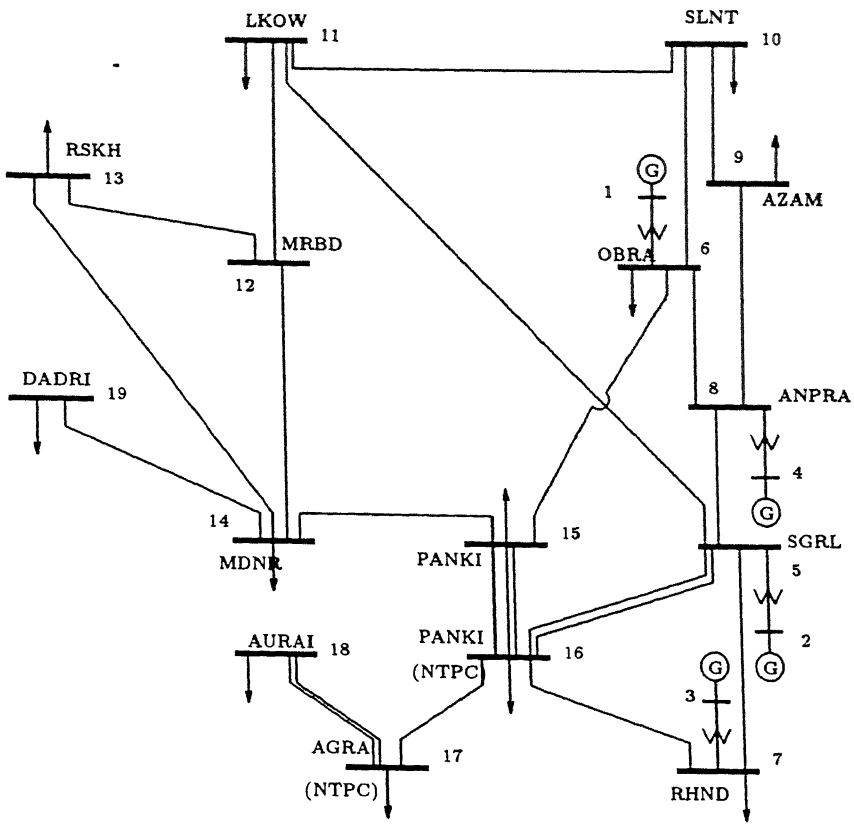

Figure H 1 19-bus UPSEB system

Appendix I

Data for IEEE-30 Bus Test System (at 100 MVA base)

The IEEE-30 bus system is shown in Fig I 1 The system data is taken from ref [39] and buses renumbered The relevant data are provided in following tables

Table I 1 Generator Bus Data

Bus No	Scheduled real power generation P_G(MW)	Specified Voltage magnitude Vspec (p u)	Load	
			Real (MW)	Reactive (MVAR)
1(slack)	—	1 060	00 00	00 00
2	040 0	1 045	21 70	12 70
3	020 0	1 010	00 00	30 00
4	—	1 082	30 00	00 00
5	—	1 010	09 42	19 00
6	—	1 071	00 00	00 00

Table I 2 Transformer Data

Transf no (Line no)	From bus	To bus	Series reactance X(p u)	Tap settings (p u)(base case)
1	13	07	0 2080	0 978
2	13	08	0 5560	0 969
3	11	09	0 2560	0 962
4	28	10	0 3960	0 968

Table I 3 Generator Data

Gen no	Real generation limit		React generation limit		Cost characteristics*		
	Maximum (MW)	Minimum (MW)	Maximum (MVAR)	Minimum (MVAR)	a_i ($/MW^2-hr)	b_i ($/MW-hr)	c_i ($/hr)
1	300 0	050 0	150 0	−100 0	1 0	2.45	105 00
2	150 0	020 0	050 0	−040 0	1 0	3 51	044 40
3	150 0	020 0	040 0	−010 0	1 0	3 89	040 60
4	—	—	024 0	−006 0	—	—	—
5	—	—	040 0	−040 0	—	—	—
6	—	—	024 0	−006 0	—	—	—

⋆ Fuel cost of i^{th} gen unit

Table I 4 Load Bus Data

Bus No	Load		Shunt compensation in(MAVR)	External shunt susceptance(p u)
	Real(MW)	Reactive(MVAR)		
7	00 0	00 0	000 0	0 00
8	05 8	02 0	000 0	0 00
9	11 2	07 5	000 0	0 00
10	00 0	00 0	−19 0	0 19
11	07 6	01 6	000 0	0 00
12	22 8	10 9	000 0	0 00
13	00 0	00 0	000 0	0 00
14	06 2	01 6	000 0	0 00
15	08 2	02 5	000 0	0 00
16	03 5	01 8	000 0	0 00
17	09 0	05 8	000 0	0 00
18	03 2	00 9	000 0	0 00
19	09 5	03 4	000 0	0 00
20	02 2	00 7	000 0	0 00
21	17 5	11 2	000 0	0 00
22	00 0	00 0	000 0	0 00
23	03 2	01 6	000 0	0 00
24	08 7	06 7	−04 3	0 043
25	00 0	00 0	000 0	0 00
26	03 5	02 3	000 0	0 00
27	02 4	01 2	000 0	0 00
28	00 0	00 0	000 0	0 00
29	02 4	00 9	000 0	0 00
30	10 6	01 9	000 0	0 00

APPENDIX I DATA FOR IEEE-30 BUS TEST SYSTEM (AT 100 MVA BASE)

Table I 5 Line Data

Line no	From bus	To bus	Series impedence		Shunt susceptance
			R(p u)	X(p.u)	B(p u)
5	2	5	0 0472	0 1983	0 0209
6	2	13	0 0581	0 1763	0 0187
7	11	13	0 0119	0 0414	0 0045
8	5	12	0 0460	0 1160	0 0102
9	13	12	0 0267	0 0820	0 0085
10	13	3	0 0120	0 0420	0 0045
11	1	2	0 0192	0 0575	0.0264
12	1	27	0 0452	0 1852	0 0204
13	7	4	0 0000	0 2080	0 0000
14	7	8	0 0000	0 1100	0 0000
15	2	11	0 0570	0 1737	0 0184
16	9	6	0 0000	0 1400	0 0000
17	9	14	0 1231	0 2559	0 0000
18	9	15	0 0662	0 1304	0 0000
19	9	16	0 0945	0 1987	0 0000
20	14	15	0 2210	0 1997	0 0000
21	16	17	0 0824	0 1923	0 0000
22	15	18	0 1070	0 2185	0 0000
23	18	19	0 0639	0 1292	0 0000
24	19	20	0 0340	0 0680	0 0000
25	8	20	0 0936	0 2090	0 0000
26	8	17	0 0324	0 0845	0 0000
27	8	21	0 0348	0 0749	0 0000
28	8	22	0 0727	0 1499	0 0000
29	21	22	0 0116	0 0236	0 0000
30	15	23	0 1000	0 2020	0 0000
31	22	24	0 1150	0 1790	0 0000
32	23	24	0 1320	0 2700	0 0000
33	24	25	0 1885	0 3292	0 0000
34	25	26	0 2544	0 3800	0 0000
35	25	10	0 1093	0 2087	0 0000
36	27	11	0 0132	0 0379	0 0042
37	10	29	0 2198	0 4153	0 0000
38	10	30	0 3202	0 6027	0 0000
39	29	30	0 2399	0 4533	0 0000
40	3	28	0 0636	0 2000	0 0214
41	13	28	0 0169	0 0599	0 0065

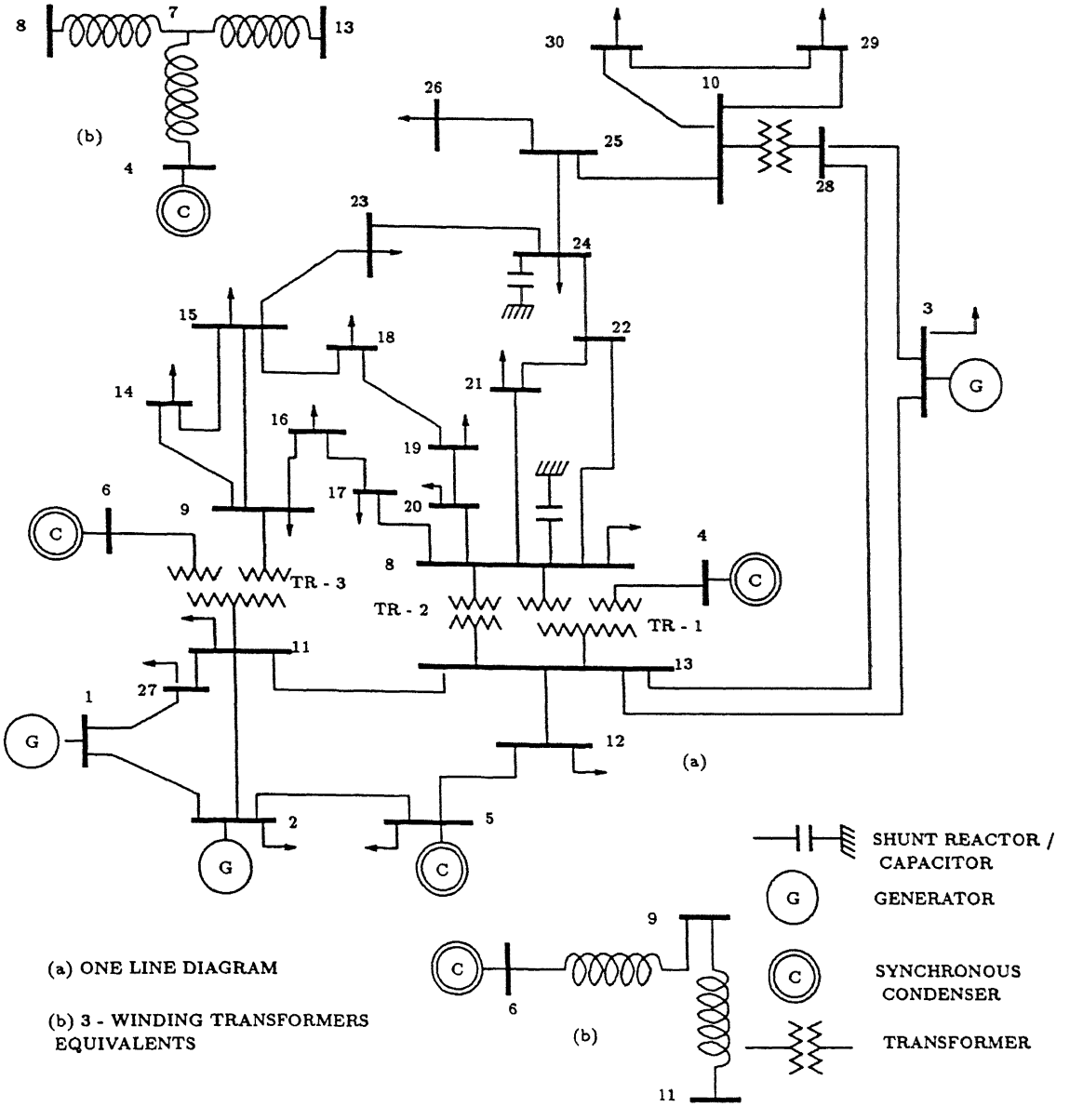

Figure I 1 IEEE-30 bus system

Appendix J

Data for UPSEB-156 Bus Test System (at 100 MVA base)

The UPSEB 156–bus system is shown in Fig J.1 The system data is taken from UP STATE ELECTRICITY BOARD STUDY CELL, IIT KANPUR and buses renumbered The relevant data are provided in following tables

Table J 1 Generator Bus Data

Bus No	Scheduled real power generation P_G(MW)	Specified Voltage magnitude Vspec (p.u)	Load		React. Generation	
			Real (MW)	Reactive (MVAR)	Maximum (MVAR)	Minimum (MVAR)
1(slack)	—	1 030	00 00	00 00	—	—
2	030 0	1 020	00 00	00 00	20.00	00 00
3	360 0	1 050	00 00	00 00	96 00	00 00
4	180 0	1 050	00 00	00 00	68.00	00 00
5	099 0	1 030	00 00	00 00	44 00	00 00
6	100 0	1 050	00 00	00 00	60 00	00 00
7	250 0	1 050	00 00	00 00	151 00	00 00
8	230 0	1 020	00 00	00 00	105 00	00 00
9	140 0	1 050	00 00	00 00	66 00	00 00
10	180 0	1 030	00 00	00 00	83 00	00 00
11	060 0	1 050	00 00	00 00	19 00	00 00
12	180 0	1 050	00 00	00 00	31 00	00 00
13	120 0	1 050	00 00	00 00	20 00	00 00
14	550 0	1 030	00 00	00 00	50 00	00 00
15	020 0	1 030	00 00	00 00	10 00	00 00

Contd

Table J.1 (Contd) ..

Bus No.	Scheduled real power generation P_G(MW)	Specified Voltage magnitude Vspec (p u)	Load		React Generation	
			Real (MW)	Reactive (MVAR)	Maximum (MVAR)	Minimum (MVAR)
16	018 0	1 020	00 00	00 00	04 00	00 00
17	032 0	1 020	00 00	00 00	08 00	00 00
18	020 0	1 020	00 00	00 00	09 00	00 00
19	1600 0	1 030	00 00	00 00	144 00	00 00
20	900 0	1 030	00 00	00 00	80 00	00 00
21	150 0	1 030	00 00	00 00	84 00	00 00
22	454 0	1 000	00 00	00 00	35.00	00 00
23	130 0	1 020	00 00	00 00	56 00	00 00
24	040 0	1.000	56 00	09 00	31 00	00 00
25	147 0	1 000	00 00	00 00	00 00	00 00
26	1000 0	1 000	00 00	00 00	00 00	00 00

Table J 2 Load Bus Data

Bus No	Load		Shunt compensation in(MAVR)	External shunt susceptance(p u)
	Real(MW)	Reactive(MVAR)		
26	735 0	00 0	000 0	0 00
27	00 0	00 0	000 0	0 00
28	05 8	02 0	00 0	0 00
29	11 2	07 5	000 0	0 00
30	00 0	−0 0	−19 0	0 19
31	07 6	01 6	000 0	0 00
32	22 8	10 9	000 0	0 00
33	00 0	00 0	000 0	0 00
34	06 2	01 6	000 0	0 00
35	08 2	02 5	000 0	0 00
36	03 5	01 8	000 0	0 00
37	09 0	05 8	000 0	0 00
38	03 2	00 9	000 0	0 00
39	09 5	03 4	000 0	0 00
40	02 2	00 7	000 0	0 00
41	17 5	11 2	000 0	0 00
42	00 0	00 0	000 0	0 00
43	03 2	01 6	000 0	0 00
44	08 7	06 7	−04 3	0 043
45	00 0	00 0	000 0	0 00
46	03 5	02 3	000 0	0 00

Contd

Table J.2 (Contd) ..

Bus No	Load		Shunt compensation in(MAVR)	External shunt susceptance(p u)
	Real(MW)	Reactive(MVAR)		
47	02 4	01.2	000 0	0 00
48	00 0	00.0	000.0	0 00
49	02 4	00 9	000 0	0 00
50	10 6	01 9	000 0	0 00
51	17 5	11 2	000 0	0 00
52	00 0	00 0	000 0	0 00
53	03 2	01 6	000 0	0 00
54	08 7	06 7	−04 3	0 043
55	00 0	00.0	000 0	0 00
56	03 5	02 3	000 0	0 00
57	02 4	01 2	000 0	0 00
58	00 0	00.0	000 0	0 00
59	02.4	00 9	000 0	0 00
60	10 6	01.9	000 0	0 00
61	07 6	01.6	000 0	0 00
62	22 8	10 9	000 0	0 00
63	00.0	00.0	000 0	0 00
64	06 2	01 6	000 0	0 00
65	08 2	02.5	000 0	0 00
66	03 5	01 8	000 0	0 00
67	09 0	05.8	000 0	0 00
68	03 2	00.9	000 0	0 00
69	09 5	03.4	000 0	0 00
70	02 2	00 7	000 0	0 00
71	17 5	11 2	000 0	0 00
72	00 0	00 0	000 0	0 00
73	03 2	01 6	000 0	0 00
74	08 7	06 7	−04 3	0 043
75	00 0	00 0	000 0	0 00
76	03 5	02 3	000 0	0 00
77	02 4	01 2	000 0	0 00
78	00 0	00 0	000 0	0 00
79	02 4	00 9	000 0	0 00
80	10 6	01 9	000 0	0 00
81	17 5	11 2	000 0	0 00
82	00 0	00 0	000 0	0 00
83	03 2	01 6	000 0	0 00

Contd

Table J 2 (Contd) ..

Bus No.	Load		Shunt compensation in(MAVR)	External shunt susceptance(p.u)
	Real(MW)	Reactive(MVAR)		
84	08 7	06 7	−04.3	0.043
85	00 0	00 0	000 0	0 00
86	03 5	02 3	000 0	0 00
87	02 4	01 2	000 0	0 00
88	00 0	00 0	000 0	0.00
89	02 4	00 9	000 0	0 00
90	10 6	01 9	000 0	0 00
91	07 6	01 6	000 0	0 00
92	22 8	10 9	000 0	0 00
93	00 0	00 0	000 0	0 00
94	06 2	01 6	000 0	0 00
95	08 2	02 5	000 0	0.00
96	03 5	01 8	000 0	0 00
97	09 0	05 8	000 0	0.00
98	03 2	00 9	000 0	0 00
99	09 5	03 4	000 0	0 00
100	02 2	00 7	000 0	0 00
101	17 5	11 2	000 0	0 00
102	00 0	00 0	000 0	0.00
103	03 2	01 6	000 0	0 00
104	08 7	06 7	−04 3	0 043
105	00 0	00 0	000 0	0 00
106	03 5	02 3	000 0	0.00
107	02 4	01 2	000 0	0 00
108	00 0	00 0	000 0	0 00
109	02 4	00 9	000 0	0 00
110	10 6	01 9	000 0	0 00
111	07 6	01 6	000 0	0 00
112	22 8	10 9	000 0	0 00
113	1021	00 0	000 0	0 00
114	06 2	01 6	000 0	0 00
115	08 2	02 5	000 0	0 00
116	03 5	01 8	000 0	0 00
117	09 0	05 8	000 0	0 00
118	03 2	00 9	000 0	0 00
119	09 5	03 4	000 0	0 00
120	02 2	00 7	000 0	0 00

Contd

Table J 2 (Contd)

Bus No	Load		Shunt compensation in(MAVR)	External shunt susceptance(p.u)
	Real(MW)	Reactive(MVAR)		
121	17 5	11 2	000 0	0.00
122	00 0	00 0	000.0	0.00
123	03 2	01 6	000 0	0 00
124	08 7	06 7	−04.3	0.043
125	00 0	00 0	000.0	0 00
126	03 5	02 3	000 0	0 00
127	02 4	01 2	000 0	0 00
128	00 0	00 0	000 0	0 00
129	02 4	00 9	000 0	0 00
130	10 6	01 9	000 0	0 00
131	07 6	01 6	000 0	0 00
132	22 8	10 9	000 0	0 00
133	00 0	00 0	000 0	0 00
134	06 2	01 6	000 0	0.00
135	08 2	02 5	000 0	0 00
136	03 5	01 8	000 0	0 00
137	09 0	05 8	000 0	0.00
138	03 2	00 9	000 0	0.00
139	09 5	03 4	000 0	0.00
140	02 2	00 7	000 0	0 00
141	17 5	11 2	000 0	0.00
142	00 0	00 0	000 0	0 00
143	03 2	01 6	000 0	0 00
144	08 7	06 7	−04 3	0 043
145	00 0	00 0	000 0	0 00
146	03 5	02 3	000 0	0.00
147	02 4	01 2	000 0	0 00
148	00 0	00 0	000 0	0 00
149	02 4	00 9	000 0	0.00
150	10 6	01 9	000 0	0 00
151	07 6	01 6	000 0	0 00
152	22 8	10 9	000 0	0 00
153	00 0	00 0	000 0	0 00
154	06 2	01 6	000 0	0 00
155	08 2	02 5	000 0	0 00
156	03 5	01 8	000 0	0 00

Table J 3 Transformer Data

Transf no (Line no)	From bus	To bus	Series resistance R(p u)	Series reactance X(p.u)	Tap settings (p.u)(base case)
1	42	54	.00170	04330	1 000
2	42	57	.03540	18180	1 000
3	42	3	00123	02469	1 000
4	93	16	01666	33333	1 000
5	86	10	00000	02917	1 000
6	50	42	00065	02604	1 000
7	50	1	00073	01460	1.000
8	90	88	00133	04660	1.000
9	29	71	00143	05000	1.000
10	30	29	00065	02604	1 000
11	28	27	00110	03770	1.000
12	32	31	00095	03330	1.000
13	97	46	00065	02604	1.000
14	33	32	00065	.02600	1.000
15	35	34	00090	03200	1 000
16	36	35	00065	02604	1 000
17	38	37	00286	.10000	1 000
18	40	39	00143	05000	1 000
19	46	45	00153	.05250	1.000
20	56	6	00306	.06135	1 000
21	56	55	00136	04760	1 000
22	60	59	00143	05000	1 000
23	63	62	00143	05000	1.000
24	64	63	00043	01736	1 000
25	66	65	00133	04644	1 000
26	69	68	00143	05000	1 000
27	73	72	00150	05160	1 000
28	76	9	00344	06875	1 000
29	78	77	00150	05160	1 000
30	80	79	00148	05200	1 000
31	82	81	00143	05000	1 000
32	89	12	00235	04710	1 000
33	95	17	01040	20800	1 000
34	85	18	01766	35313	1 000
35	99	2	00000	19034	1 000
36	91	13	00514	10285	1 000
37	87	11	00549	10978	1 000

Contd

Table J 3 (Contd) .

Transf no (Line no)	From bus	To bus	Series resistance R(p u)	Series reactance X(p u.)	Tap settings (p.u)(base case)
38	51	4	00000	.04860	1.000
39	92	14	00049	01943	1 000
40	112	108	00065	02604	1.000
41	74	73	00130	05208	1 000
42	94	96	00286	10000	1.000
43	58	44	00095	03333	1 000
44	57	7	00153	03600	1 000
45	54	5	00556	11110	1.000
46	31	15	01250	25000	1 000
47	32	23	00243	04860	1.000
48	108	107	00143	05000	1 000
49	129	105	00143	05000	1 000
50	126	104	00286	10000	1 000
51	124	8	00770	02720	1 000
52	103	102	00286	10000	1.000
53	109	19	00016	00591	1 000
54	113	20	00030	01199	1 000
55	123	41	00286	10000	1 000
56	61	21	00000	02841	1 000
57	127	22	00000	02273	1 000
58	128	127	00056	02222	0 950
59	155	140	00286	10000	1 000
60	26	154	00147	05830	1 000
61	133	153	00286	10000	1 000
62	51	152	00286	10000	1 000
63	124	131	00286	10000	1 000
64	67	156	00143	05000	1 000
65	118	130	00150	05160	1 000
66	119	125	00300	10320	1 000
67	43	122	00150	05160	1 000
68	84	121	00286	10000	1 000
69	52	151	00160	05600	1 000
70	116	114	00286	10000	1 000
71	111	53	00150	05160	1 000
72	120	47	00300	10320	1 000

Table J 4: Line Data

Line no	From bus	To bus	Series impedence		Shunt susceptance
			R(p.u.)	X(p.u.)	B(p.u.)
73	42	90	00810	03880	14030
74	42	28	00993	04746	38643
75	50	30	00468	04770	62450
76	50	33	00785	07990	1 04738
77	33	64	00806	08169	1 06808
78	54	57	01582	03777	.01735
79	54	75	01303	03102	01429
80	57	75	02606	06205	02857
81	75	88	03583	08532	03929
82	29	103	01830	09270	07390
83	55	59	04188	10518	01087
84	59	62	05584	14024	01449
85	30	36	00294	02997	39206
86	94	28	01093	05221	18892
87	94	118	00662	03164	11451
88	32	35	00505	02416	08730
89	32	52	01291	06171	22327
90	34	37	08000	20100	02080
91	35	38	01600	08100	06440
92	37	39	08560	21500	02220
93	38	40	01550	07940	06300
94	39	41	03820	09090	04180
95	41	45	04142	10490	04260
96	45	49	05680	14260	01470
97	45	77	03257	07756	03350
98	45	156	08000	20100	02080
99	156	62	04002	10051	01039
100	46	78	01660	08430	06720
101	46	61	01270	06410	05220
102	48	49	02280	05710	02370
103	48	77	02690	06420	02960
104	51	52	01770	08510	30260
105	52	56	01060	05060	18320
106	56	61	00580	02900	02370

Contd .

Table J 4 (Contd) .

Line no	From bus	To bus	Series impedence		Shunt susceptance
			R(p u)	X(p.u.)	B(p.u)
107	56	60	00370	01780	06440
108	60	63	00490	02370	08590
109	62	65	01120	02800	01160
110	63	66	00750	03840	03110
111	43	63	00679	03412	02782
112	43	80	00666	03390	02672
113	63	80	01440	07310	05850
114	66	67	00670	03390	02670
115	66	69	00583	02956	02346
116	68	79	04560	11450	01180
117	69	73	01410	07180	05700
118	70	77	04080	09640	04440
119	70	81	01440	03430	01580
120	70	24	01260	03160	01300
121	24	76	00791	01991	00820
122	24	72	02230	05620	00580
123	72	83	01860	04680	01930
124	73	91	.01440	.07250	.05900
125	73	87	00705	03590	11400
126	52	84	00990	05090	04010
127	58	84	00780	03980	03140
128	76	77	08100	20330	02100
129	80	82	01160	05830	04750
130	82	91	00690	03500	11260
131	89	91	00050	00253	00805
132	93	95	00460	01170	00120
133	83	95	03910	09840	01010
134	83	85	01950	04920	02020
135	85	95	01870	04700	00490
136	91	93	01031	11874	00193
137	92	112	00479	04880	63614
138	90	108	01732	08784	06973
139	30	112	00254	02584	33798
140	50	92	00051	00517	06760
141	29	124	00580	.02940	09420
142	71	131	.06978	17529	01817

Contd. .

Table J.4 (Contd.) .

Line no	From bus	To bus	Series impedence		Shunt susceptance
			R(p u)	X(p.u.)	B(p u.)
143	124	126	00830	04240	03340
144	92	109	00031	00310	04056
145	72	76	01390	03510	00360
146	117	109	00927	09429	1 23293
147	117	109	00833	08478	1 10855
148	117	110	00559	05686	.74354
149	36	97	00650	06617	86521
150	64	97	00260	02646	34610
151	36	109	00823	08375	1 09503
152	149	55	04560	11453	01183
153	149	44	04560	11450	01180
154	96	130	03723	.08863	.04082
155	130	31	00698	.01662	.00765
156	126	129	00930	04750	03740
157	129	124	01330	.06680	.05420
158	74	64	00370	03762	48870
159	74	97	00325	.03307	.43264
150	101	102	05030	12620	.01300
161	88	98	04372	.08520	03352
162	98	106	24980	.04714	01915
163	88	98	08744	.17040	.01676
164	98	106	04996	09428	00957
165	105	106	04930	11750	05410
166	104	105	05960	14960	01550
167	101	104	06140	15460	01590
168	71	101	05490	13790	01430
169	41	100	08470	21320	02190
170	49	100	05360	13560	01400
171	141	99	01163	02770	01276
172	86	94	00437	02552	09399
173	106	107	02050	04880	02250
174	63	111	00248	01186	04294
175	109	113	00031	00310	04056
176	113	117	00918	09306	1 21680
177	88	115	02311	04361	01772
178	29	116	01325	06667	05416

Contd

Table J 4 (Contd.) .

Line no.	From bus	To bus	Series impedence		Shunt susceptance
			R(p u)	X(p u)	B(p u.)
179	115	153	05956	14959	.01546
180	33	117	00015	.00155	02704
181	32	118	00124	00593	.02147
182	125	71	05119	12856	05332
183	86	119	00336	01963	.01808
184	86	120	01344	07852	.07230
185	35	119	01344	07852	07230
186	35	120	00336	01963	01808
187	46	123	01598	08108	06436
188	61	67	.01315	06696	05278
189	61	60	00499	02397	08523
190	58	127	.00998	04794	17046
191	110	128	00121	01109	72815
192	64	26	00051	00517	06760
193	108	133	01212	06100	04956
194	136	134	10889	27347	02826
195	136	31	09307	23370	02415
196	134	135	06140	15460	01590
197	34	47	02327	05840	00600
198	47	138	02327	05840	00600
199	34	137	09307	22670	02340
200	139	34	04188	10518	01087
201	140	39	09307	22670	02340
202	140	150	02280	05725	02360
203	141	41	02792	07012	02898
204	142	37	04188	10518	01087
205	143	100	04467	11219	01159
206	100	49	05380	12840	01480
207	100	41	08560	21500	02220
208	144	151	04560	11450	01100
209	145	151	04188	10518	01087
210	146	151	05680	14260	01470
211	147	149	03510	08440	00910
212	147	44	04188	10518	01087
213	148	45	02880	06860	00790
214	150	45	02094	05254	02174
215	152	134	01115	02810	.01429

Contd

Table J 4 (Contd)

Line no	From bus	To bus	Series impedence		Shunt susceptance
			R(p u)	X(p u)	B(p u)
216	155	123	00878	04430	03580
217	132	59	04002	.10051	.01039
218	132	156	04188	10518	01087
219	122	79	03723	09349	00966
220	151	121	05960	1496	0155
221	71	114	08000	20100	0208
222	114	27	01440	03430	.01580
223	62	53	01440	0343	0158
224	25	111	00083	00396	01431
225	25	63	00695	03500	02843

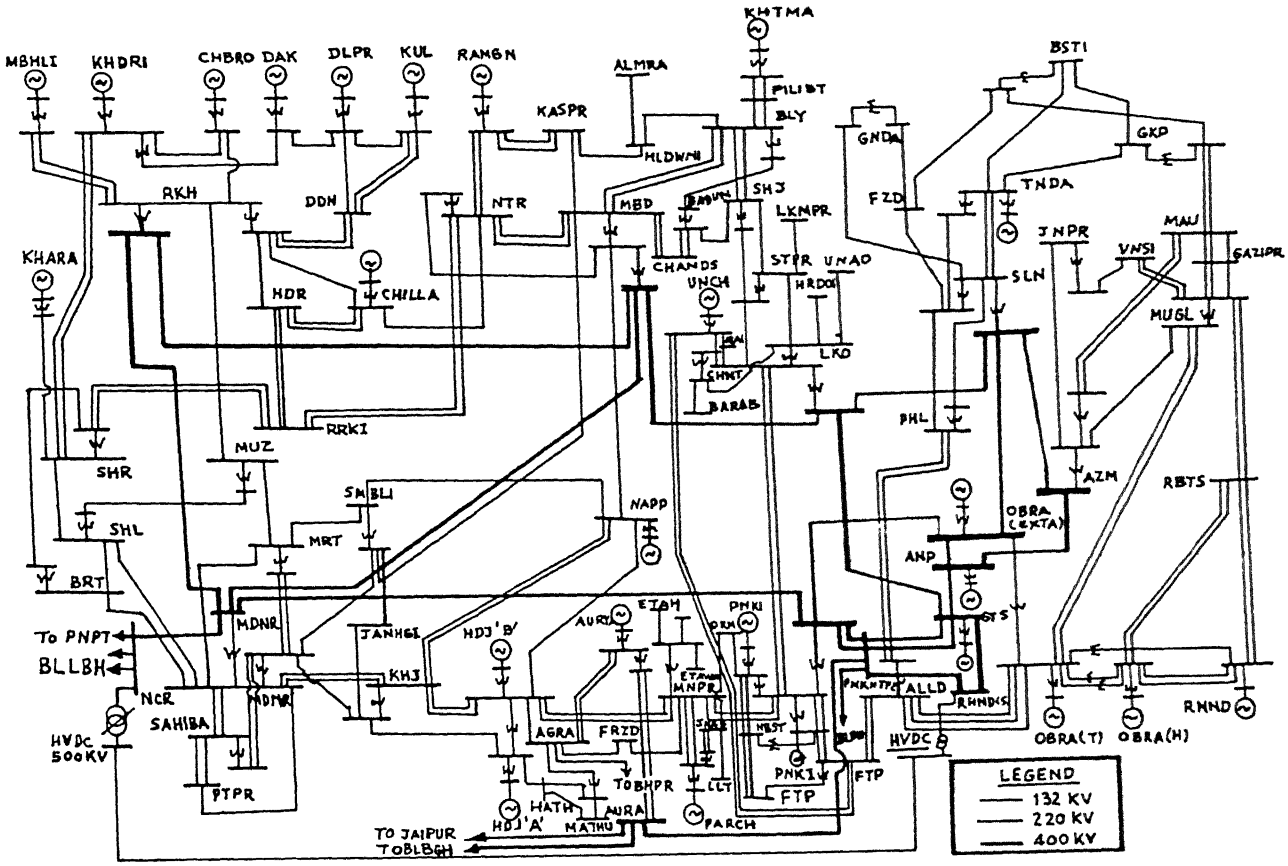

Figure J 1 156-bus Indian system

Curriculum–Vitae

Kailash N. Srivastava

Senior Research Associate(CSIR)
Department of Electrical Engineering
Indian Institute of Technology
KANPUR - 208016 INDIA

Academic Background

INDIAN INSTITUTE OF TECHNOLOGY, KANPUR, UP
M Tech in Power System January 85
UNIVERSITY OF GORAKHPUR, GORAKHPUR, UP
B E in Electrical Engineering June 83

Research Papers (Published/Accepted)

(1) *Economic Load Scheduling of Hydro-Thermal System Including Transmission Losses*, Journal of Institution of Engineers (India) Vol-67, Part EL-3, Dec 1986

(2) *Transient Residual Voltage Analysis During Isolated Operation of a Group of Induction Motor Loads*, Electric Machines and Power Systems Vol-22 No-2 March/April 1994, pp289-309.

(3) *Prediction of Voltage Collapse in an Integrated AC/DC Network Using Singular Value Decomposition Concept*, Electric Power System Research (USA), Vol-28, No-2, Nov 1993, pp111-112

(4) *Application of Hopf Bifurcation Theory for Determining Critical Value of a Generator Control or Load Parameters*, International Journal of Electrical Power & Energy System(UK) to appear

(5) *Dynamical Nonlinear Behaviour of Power System Exhibiting Chaos*, Proc. of 7th National Power System Conference, Calcutta (India) Dec 19-22,1992, pp 247-252

(6) *Fast Prediction of Voltage Stability Margin and Control Actions*, Proc of 7th National Power System Conference, Calcutta (India) Dec 19-22,1992, pp253-258.

(7) Chaotic Oscillation in Power System Under Disturbances, Proc. of IEE sponsored International Conference on Advances in Power System Control, Operation and Management, Hong-Kong Dec7-10, 1993, pp705-711.

(8) *Voltage Instability in Power System - An Overview and Key Issues*, Proc of IEEE sponsored International Symposium on Electricity Distribution and Energy Management, Singapore, Oct 27-29, 1993, Vol-2, pp 676-683

(9) *Damping Chaotic Oscillations Using Controllable Components*, Proc. of 8th National Power System Conference, New Delhi(India), Dec 14-17, 1994 to appear.

(10) *Bifurcation, Chaos and Voltage Stability in Power System*, Proc. of Central Power Research Institute sponsored Workshop on Voltage Stability, Bangalore(India), Aug 11-12, 1994

(11) Discussion of IEEE paper # 92 SM 395-5 PWRS titled *A Method for Calculation of Margins to Voltage Instability Applied on the Norwegian System for Maintaining Required Security Level*, IEEE T-PWRS Aug 1993 pp 920-928

(12) Discussion of IEEE paper # 93 SM 535-5 PWRS titled *An Optimal Reactive Power Planning Strategy Against Voltage Collapse*, IEEE T-PWRS May 1994

(13) Discussion of IEEE paper # 94 WM 064-6 PWRD titled *Damping of Power System Oscillations by Use of Controllable Components*, IEEE T-PWRD Oct 1994

(14) Discussion of IEEE paper # 93 SM 515-7 PWRS titled *A Generation Rescheduling Method to Increase the Dynamic Security of Power System*, IEEE T-PWRS Feb 95 to appear

(15) Discussion of IEEE paper # 94 WM 245-1 PWRS titled *Computation of a Practical Method to Restore Power Flow Solvability*, IEEE T-PWRS Feb 95 to appear.

(16) Discussion of IEEE paper # 94 WM 248-5 PWRS titled *Voltage Dependents Reactive Power Limits for Voltage Stability Studies*, IEEE T-PWRS Feb 95 to appear

(17) Discussion of IEEE paper # 94 WM 219-6 PWRS titled *Static Security in Power System Operation in Fuzzy Real Load Conditions*, IEEE T-PWRS Feb 95 to appear